UNDERSTANDING AIR INFILTRATION IN HOMES

By

Andrew Persily

Report PU/CEES #129

February 1982

A dissertation presented to the faculty of Princeton University in candidacy for the degree of Doctor of Philosophy.

Center for Energy and Environmental Studies
The Engineering Quadrangle
Princeton University
Princeton, NJ 08544

ABSTRACT

Air infiltration rates in homes are generally higher than necessary, and account for roughly one-third of their space conditioning energy demands. Infiltration rates are being reduced to conserve energy, but the reduction of ventilation increases the concentration of many airborne substances, possibly to hazardous levels. Techniques for evaluating the airtightness of homes are needed to determine if a home is too leaky from an energy point of view or too tight from the perspective of occupant health.

This thesis is a study of the techniques and issues related to evaluating the airtightness of homes. The first section reviews the background to the problem by discussing the physics of air infiltration and the techniques used to measure infiltration rates. An alternative to direct infiltration measurements, pressurization testing, is also discussed. Pressure testing is a fast and inexpensive measure of a home's tightness, and its relation to infiltration is an important problem in the field.

The second section of this thesis presents experimental work aimed at several questions raised in the background section. A long term experiment involving weekly pressurization testing of a home reveal the short-term reproducibility of the test results and the seasonal variation in a home's tightness. A small experimental building, the Test Chamber, was used to study the rela-

tion of pressurization to infiltration. In these experiments, pressurization test results were used to predict infiltration rates in the Test Chamber. Experiments were also conducted in fourteen identical homes to study the relation of pressurization to infiltration without the confounding effects of different housing styles and different weather conditions during the tests. Another experiment was done in the Test Chamber to evaluate the efficiency of an air-to-air heat exchanger. Such a device induces mechanical ventilation while recovering some of the heat (or cold) from the outgoing air. The efficiency of heat recovery was carefully measured and several aspects affecting the performance were studied.

ACKNOWLEDGEMENTS

Being the product of four years at Princeton University, this thesis reflects the assistance and influence of many people. Among those I would like to thank, there is only space to mention a small number. Special thanks are extended to Roy Crosby and Ken Gadsby for indispensable technical assistance and an enjoyable work climate, both of which made my time at Princeton successful. In addition, frequent, insightful and realistic discussions with Gautum Dutt are gratefully acknowledged. Contact with people at the Center for Energy and Environmental Studies and the Department of Mechanical and Aerospace Engineering helped my education to be worthwhile and to proceed smoothly.

Expressions of thanks go out to my advisor, Prof. Robert Socolow, for helping me develop my ability to work independently and then to report on my successes with confidence and authority. Links with the air infiltration research community were essential in my work, and I thank David Harrje for keeping me in touch with the international research effort and for other assistance. My dissertation readers, Prof. Antony Jameson and Prof. Howard C. Curtiss Jr., are gratefully acknowledged for their comments and criticism. Offering one's home for building research can be trying at times, and I would like to thank the Lavine family for allowing me to pressure test their home every week for one year.

Little of my professional success would have been possible without help, academic and otherwise, from friends at work and at play. Including all the names would be impossible but thanks are extended to everyone who helped carry things up on the roof, went on a Blower Door test, or just spent time hanging out. Very sincere thanks are extended to Greg Linteris, John Ford, Mike Lavine and Mimi Goldberg for answering and asking many questions over the years, and to the 2nd floor crowd for their soft room spirit. Extra special thanks go out to Steve R., Steve M., Jeff, Wes, Chris, John, Diane C., Diane H., the Bayshuns, and Elmos of the past, present and future, and to Shelly for friendship and support. Simply nobody will enjoy this thesis more than my parents, and I thank them for support over the years.

This thesis carries '1549-T' in the Records of the Department of Mechanical and Aerospace Engineering.

CONTENTS

APPENDICES

Chapter I

THE COMPLEXITIES OF REDUCING AIR INFILTRATION

About one-third of the 1977 U.S. energy consumption was used in residential and commercial buildings. Of these roughly 26 Quads* of energy, about 16 Q were consumed in residential buildings and almost 9 of these for space conditioning [1]. The fraction of space conditioning energy associated with air infiltration varies among homes, but is generally one-third of the total. Thus, about 3 Q of energy are used in the U.S. to condition outside air to desirable interior conditions.

The winter mean air infiltration rate in U.S. homes is roughly one house volume of air exchanged every hour [2]. This does not mean that all the air within the house is replaced each hour, but rather that one house volume of indoor air flows out of the openings in the house each hour. The outgoing air is a mixture of air that has been in the house since the beginning of the hour and air that entered during the hour. The interpretation of the infiltration rate of a house will be discussed later in this chapter. For a house with 2.4 m (8 ft) ceilings and a 110 m^2 (1200 ft^2) floor area, one exchange per hour corresponds to .076 m^3/s or 160 cubic feet per minute (cfm). This amount of ventilation is much larger than ASHRAE's recommendation of 10 cfm

---

1 Quad = 1 Q = 10^{15} Btu

per occupied room [3]. The reduction of excessive infiltration rates has the potential for saving significant quantities of energy. But lower limits on the infiltration rate of a home exist to avoid harm to occupants and building materials.

1.1 INFILTRATION REDUCTION AND HEALTH

While reducing the air infiltration rate of a house decreases the demand for space conditioning energy, it also increases the level of many airborne substances within the house. Whether these substances are found in hazardous concentrations depends on source strengths, house volume, and the infiltration rate. The increasing concern about the indoor environment is reflected in discussions by the international research community [4,5] and the popular press [6]. Several reviews on the subject of indoor air quality have been published, with some examples of pollutant levels measured in homes [7-9].

The sources of indoor pollutants include occupant activities, building materials and furnishings, the rocks, soil and ground water near the house, and the outside air. The smoking of tobacco within the home produces many substances including suspended particulates, carbon monoxide and formaldehyde. The indoor levels of these and other tobacco byproducts and the amount of ventilation necessary to avoid discomfort have been studied [10-12]. Gas cooking is another sources of carbon monoxide and formaldehyde, along with NO_x and hydrocarbons [13].

Formaldehyde and other organics are also released by resins in building materials and furniture [14,15]. The physiological effects of formaldehyde at low concentrations are not well known, and have been the source of controversy [16]. Radon gas is another source of concern in the environment, particularly because it is radioactive and the dose-response characteristics are not well known for the levels found in homes. The sources of radon include rocks, soil and ground water and sometimes the materials used to build the structure [17].

Moisture levels within the home depend on outdoor humidity levels and water vapor generation rates due to occupant activities such as cooking and showering. The effects of high moisture levels include degradation of building materials through condensation and eventual rotting of wood, especially in insulated attics and walls [18]. Excessively low levels of moisture are also undesirable, causing adverse physiological effects such as sinus problems. Excessive levels of bacteria [19] and airborne allergens [20] such as pollen, molds, animal hair and dust also cause health problems.

Various means have been proposed for the control of the indoor levels of these substances without necessarily resorting to excessive infiltration. Brundrett [21] and others recommend extraction of contaminants at their source before they spread throughout the house. He also points out that the air exchange that does occur should be well mixed with the interior air to be most effective. Lippmann [8] raises the possibility of cleaning

the air through chemical reactions, and physical transformations or depositions of pollutants. Berk and Hollowell [22], among others, recommend sealing off some contaminants at their sources. They also suggest using building materials with low emanation rates of undesirable substances. Another common recommendation is the use of mechanical ventilation coupled with heat recovery, or air-to-air heat exchangers. These devices are commercially available and have the potential for alleviating many indoor air quality problems and saving energy. As we learn more about the health effects of indoor pollutants, ventilation standards in homes will be formulated to reflect our understanding.

1.2 AN OVERVIEW OF THIS THESIS

This thesis is motivated by the problem of safely reducing infiltration rates in homes to save energy. The evaluation of the tightness, or leakiness, of a home is very important in dealing with this problem. We need to know the portion of the heating and cooling loads attributable to air infiltration in order to determine if the infiltration rates are indeed excessive and should be reduced. At present, there are no satisfactory means for calculating the infiltration rate of a home based on construction features. Nor can one determine the infiltration load by subtracting the calculated conduction load from the measured total. Techniques to calculate conduction losses are prone to error because they neglect obscure but important heat loss sites. On the other hand, we want to know if the infiltration rates are

so low that the house is overtight and potentially unhealthy. Tightness evaluation is also necessary for research into the effectiveness of particular retrofit techniques. Whether tightness evaluation should take the form of a direct measurement of air infiltration or some surrogate tightness measure is one of the questions addressed in this thesis. A reliable measure of tightness could be useful as a standard for homes for which the maximum leakiness will be set by energy considerations and the minimum by indoor air quality.

This thesis is divided into two basic sections. The first section discusses the background to the problem of evaluating the airtightness of homes, including reviews of past research. The second section presents original experimental work addressing several issues raised in the first section. The background section begins with a discussion of the physical causes of air infiltration in chapter II. Chapter III presents the methods used to directly measure infiltration rates in homes. We note that direct measurement of infiltration is a difficult and time-consuming procedure for characterizing the leakiness of a home, and may not be appropriate in all cases. Chapter IV discusses an alternative method of tightness evaluation which has been used in recent years. This technique of pressure testing a home provides a quick and inexpensive measure of a home's tightness, but there are questions concerning its accuracy and interpretation. Chapter V discusses the relation of pressurization test results to actual infiltration rates and some models of this relation. The

four chapters in the background section raise several important questions.

The next section contains the experimental work of this thesis and answers four specific questions in each of the chapters. Chapter VI presents our research into the accuracy and repeatability of pressurization testing in order to determine the usefulness and limitations of the technique. In chapter VII we show that pressurization test results can indeed be used to predict infiltration rates in a very simple and well-controlled test building. The next chapter describes a study of the relation of pressurization to infiltration in real homes. Most studies of this relation have considered a variety of housing types and ages, and the results have been erratic. In order to separate the effects of inappropriate models from the effects of variations due to building type, we conducted experiments in fourteen identical homes. These experiments are discussed in chapter VIII. The last chapter of experimental work, chapter IX, anticipates the situation when we have built or retrofit a home to be very airtight. In this case, mechanical ventilation is necessary to avoid deterioration of the indoor air quality, but this additional ventilation contradicts our original goal of saving energy. By combining heat recovery with this ventilation, we can keep interior air safe and comfortable without all of the energy use associated with desirable ventilation rates. An air-to-air heat exchanger is a device which performs this task, and chapter IX presents our experimental procedure for evaluating the per-

formance of one such device. By testing this heat exchanger with it operating in a building, we learned about facets of its performance that would not be apparent in a laboratory test. The final chapter presents our conclusions concerning the evaluation of building tightness.

1.3 NOTES ON INFILTRATION

The exchange of indoor and outdoor air is described by several different terms. Unfortunately, the terminology is not used consistently among the researchers in the field. To avoid confusion, mechanical or forced ventilation will refer to flow through intentionally installed ventilation devices powered by fans. Natural infiltration, natural ventilation, infiltration, ventilation and air exchange will refer to the net flow of air between inside and outside, i.e. weather induced air exchange plus mechanical ventilation.

There is some confusion regarding what we mean when we say a house has an infiltration rate of I house volumes per hour. We mentioned earlier that this does not mean that I volumes of air are replaced each hour. Instead, one may consider all the molecules in the house at some reference time to be tagged. The fraction of tagged molecules remaining at any later time decays exponentially with a time constant equal to $(I)^{-1}$. The air leaving the house at a given time is a mixture of tagged and untagged molecules. If the air within the house is perfectly and instantaneously mixed, then I house volumes of air flow in and out of

the house each hour. In the more general case of imperfect mixing, some air may flow in and then out without mixing at all with the "tagged" air. This unmixed flow is not included in the infiltration rate as defined above or as measured by the techniques described later. It does not contribute to the heating load nor to the maintainance of indoor air quality. The relation between the air flow in and out of the house and the infiltration rate in terms of tagged molecules is determined by the extent of mixing of the interior air.

REFERENCES

[1] von Hippel, F., "The Energy Demand of U.S. Buildings," Report No. 119, Center for Energy and Environmental Studies, Princeton University, 1981.

[2] Grot, R.A., Clark, R.E., "Air Leakage Characteristics and Weatherization Techniques for Low-Income Housing," DOE/ASHRAE Conference on Thermal Performance of Exterior Envelopes of Buildings, Orlando, Florida, December 1979.

[3] Ventilation for Acceptable Indoor Air Quality, Standard 62-1981, American Society of Heating, Refrigerating and Air-Conditioning Engineers, 1981.

[4] Fanger, P.O., Valbjorn, O., eds., Indoor Climate, Effects on Human Comfort, Performance, and Health, Proceedings of First International Indoor Climate Symposium, Copenhagen, 1978.

[5] International Symposium on Indoor Air Pollution, Health and Energy Conservation, Amherst, Massachusetts, October 1981.

[6] Smay, V.E., "Plugging all those Heat Leaks Can Cause Home Pollution," Popular Science, Vol. 217, No. 4, October, 1980.

[7] Hollowell, C.D., Berk, J.V., Traynor, G.W., "Impact of Reduced Infiltration and Ventilation on Indoor Air Quality in Residential Buildings," ASHRAE Transactions, Vol. 85(I), 1979.

[8] Lippmann, M., "Generation and Decay of Indoor Air Contamination," in reference [4].

[9] Moschandreas, D.J., Stark, J.W.C., McFadden, J.E., Morse, S.S., "Residential Air Pollution Levels: Observation and Data Interpretation, " in Building Air Change Rate and Infiltration Measurements, eds., Hunt, C.M., King, J.C., Trechsel, H.R., ASTM STP 719, American Society for Testing and Materials, 1980.

[10] Yaglou, C.P., "Ventilation Requirements for Cigarette Smoke, " ASHAE Transactions, Vol. 61, 1955.

[11] Lundqvist, G.R., "The Effects of Smoking on Ventilation Requirements, " in reference [4].

[12] Repace, J.L., Lowrey, A.H., "Indoor Air Pollution, Tobacco Smoke, and Public Health, " Science, Vol. 208, May 1980.

[13] Melia, R.J.W., Florey, C. duV., Altman, D.G., Swan, A.V., "Association Between Gas Cooking and Respiratory Disease in Children," British Medical Journal, Vol. 2, 1977.

[14] Mølhave, L., "Indoor Air Pollution Due to Building Materials, " in reference [4].

[15] Andersen, I., "Formaldehyde in the Indoor Environment - Health Implications and the Setting of Standards, " in reference [4].

[16] "A Firing over Formaldehyde," Science, Vol. 213, 7 August 1981.

[17] Budnitz, R.J., Berk, J.V., Hollowell, C.D., Nazaroff, W.W., Nero, A.V., Rosenfeld, A.H., "Human Disease from Radon Exposures: The Impact of Energy Conservation in Buildings," Energy and Buildings, Vol. 2, 1980.

[18] "Moisture in Building Construction," Chapter 20, ASHRAE Handbook of Fundamentals, 1977.

[19] Lidwell, O.M., "Ventilation, Air-Movement and the Spread of Bacteria in Buildings, " in reference [4].

[20] Løwenstein, H., Gravesen, S., Schwartz, B., "Airborne Allergens - Identification Problems and the Influence of Temperature, Humidity and Ventilation, " in reference [4].

[21] Brundrett, G.W., "Requirements for Ventilation, " CIBS Symposium, Natural Ventilation by Design, London, 1980.

[22] Berk, J.V., Hollowell, C.D., Pepper, J.H., Young, R., "Indoor Air Quality Measurements in Energy-Efficient Residential Buildings, " Report No. 8894, Lawrence Berkeley Laboratory, University of California, 1980.

SECTION ONE

BACKGROUND AND LITERATURE REVIEW

In the next four chapters we present background and past research concerning the evaluation of the airtightness of homes. The first chapter of this section, chapter II, is a description of the physical causes of air infiltration. We discuss the driving forces which induce pressure differences across the shell of a home, i.e. wind and indoor-outdoor temperature differences. Weather induced pressure differences are in the range of 1 to 5 Pa*, attaining values as high as 10 Pa under extreme conditions. After discussing the pressure differences, we turn to the leakage functions for the openings in the shell of a house. The functions relating the flow through an opening to the pressure difference across it are determined by the opening geometry. But the openings in homes have many different geometries and are extremely numerous, making a detailed description of the leakage of a house an extremely cumbersome task.

In chapter III we review the techniques used to measure actual infiltration rates in homes. These tracer gas techniques have been used for several decades and are indispensable for determining infiltration rates. But characterizing the tightness of a home in this manner requires infiltration measurements over a range of weather conditions. Gathering this data takes a long

---

* These pressures, and all other pressures in this thesis, are in units of Pascals or Newtons per square meter. One atmosphere is about 10^5 Pascals and one inch of water is 250 Pa.

time and requires expensive equipment. Also, the length of time required for such an unbiased characterization is long compared to the time over which changes in building tightness occur. Chapter IV describes pressurization testing, an alternative to tracer gas measurement which is quick and inexpensive. To pressure test a home, one uses a fan to induce a pressure difference across the shell of a house and measures the air flow required to maintain that pressure difference. The induced pressures range from 10 to 100 Pa, and are therefore much larger than those induced by the weather. Pressurization testing gives no information on the distribution of leakage around the shell, although this distribution is important in determining infiltration rates. Also, the pressure differences during a test are constant and uniform over the shell of the house as opposed to naturally occurring pressures which vary in time and position. For these and other reasons, there are doubts as to whether one can relate pressurization test results to actual infiltration rates.

As part of our review, we are considering the relative appropriateness of methods for tightness evaluation of homes. While pressurization testing is faster and cheaper than tracer gas measurement, it does have the problems mentioned above. If pressurization is to serve as a tightness check on homes, its relation to natural infiltration rates must be demonstrated and modelled. Chapter V discusses several attempts to model the relation between pressurization and infiltration. It is difficult to assess the predictive capabilities of these models from

the validation attempts made by the developers of the models. Their tests have been extremely variable in the type and age of building considered, and it is impossible to separate predictive errors and successes due to the models from variability due to housing type. At the end of chapter V we will review the major conclusions of the previous four chapters and identify questions which are addressed by our experiments in the second section of the thesis.

Chapter II

THE PHYSICS OF AIR INFILTRATION

Our first step in discussing the background of evaluating the tightness of homes is an examination of the factors which cause the exchange of indoor and outdoor air. The air infiltration rate of a home is determined by a complex interaction of the outside weather, the building envelope, and the actions of the occupants. The wind and the inside-outside temperature difference induce pressure differences across the shell of the house which vary over position on the building surface and time. These pressure differences cause air flow in and out of the openings in the house. The sites of air leakage in a building's shell are numerous and varied. While some are easy to locate, such as openings around doors and windows, and exhaust fan vents, other leaks can be much more obscure, if they are identifiable at all [1]. The amount and location of leakage varies greatly among buildings, even for homes of common floor plan, vintage and builder.

2.1 THE PRESSURES ACTING ACROSS THE BUILDING SHELL

The pressure differences across the shell of a house are caused by the wind and the difference in temperature between inside and outside. The wind induces a pressure distribution on the exterior surface of the house. These surface pressures are

higher or lower than the outside static air pressure p_o by an amount p_w. Ignoring any temperature effects, the pressure difference due to wind is then

$$\Delta p_w = (p_o + p_w) - p_i, \tag{2.1}$$

where p_i is the internal air pressure. With a low wind speed and a significant temperature difference between inside and outside, the pressure difference across the walls is induced by the difference between the inside and outside air densities. The different densities cause the inside and outside to have different pressure gradients, and this leads to inside-outside pressure differences. Temperature or "stack" induced pressure differences are expressed as Δp_s. When both wind and stack effects are important, the total pressure difference at some position on the building surface is the sum of both effects,

$$\Delta p = \Delta p_w + \Delta p_s. \tag{2.2}$$

Wind Pressures

The wind induces a pressure distribution on the outside of a building which is determined by the wind speed and direction, the building shape and nearby obstructions. Defining the local wind speed is difficult especially over built-up terrain [2]. Wind speed is generally measured at a meteorological station at a reference height H_r. To determine the wind speed at the building location at a height H one generally uses a power or logarithmic relationship [3]. The power law has the form

$$u = u_r(H/H_r)^{\alpha} \qquad (2.3)$$

where u is the wind velocity at height H, and the subscript r denotes the reference height H_r. The exponent α depends on the terrain, e.g. in built-up urban areas $\alpha \simeq 0.3$ and in unobstructed fields of grass $\alpha \simeq 0.1$. The building in question and the wind measuring device should be in the same terrain class with no changes in terrain between the two sites.

Although equation (2.3) is used to find the wind velocity u at the building height H, Handa [3] points out that the wind speed is highly irregular below the average height of roughness elements on the ground (e.g. homes, trees). He states that it is " not feasible to prescribe any empirical or theoretical profile " at the heights in our typical region of concern. Thus, as in the case of relating the meteorological wind speed to the local wind, difficulties are encountered in reducing this wind to the building level.

The surface pressures induced by the wind speed u are greater than or less than the outside air pressure p_o by an amount p_w. p_w is related to the wind speed through the wind pressure coefficient C_p,

$$p_w = C_p \tfrac{1}{2} \rho_o u^2, \qquad (2.4)$$

where ρ_o is the outside air density. C_p, as defined in equation (2.4), is assumed to be roughly constant over the range of wind speeds near buildings. The pressure difference across the shell due to wind alone is then

$$\Delta p_w = p_o + C_p \tfrac{1}{2}\rho_o u^2 - p_i. \qquad (2.5)$$

C_p is a function of the shape of the building, the angle of attack of the wind and the position on the building surface. Values of C_p are obtained from wind tunnel research and full-scale tests of buildings [3-5]. For windward walls, the wind pressure coefficients are on the average positive. On leeward walls and walls parallel to the wind, C_p is generally negative. Local exceptions to these signs of C_p do exist at corners and edges. Figure (2.1) shows typical values of C_p averaged over each wall of a building [3]. The sign and magnitude of C_p on the roof depends on the pitch angle of the roof. Figure (2.2) shows contours of C_p for a roof surface from measurements on a full-scale experimental building with adjustable roof pitch [4]. Note that at low roof pitches, there is significant suction on the roof ($C_p<0$). As the pitch increases, the wind pressure coefficient becomes positive over most of the roof. The values in figure (2.1) are averages of C_p over each surface, while figure (2.2) shows contours over the surface. For some purposes average values contain sufficient information, but sometimes the variation in C_p with position is important.

The determination of values of C_p for homes in the field is crucial for understanding wind-induced infiltration, and is also an area of weakness in the field. Most of the wind tunnel measurements of C_p are for isolated structures as opposed to real homes which are shielded by trees, bushes, fences and other

homes. Because the wind exposure of each house is different, the values of C_p will also be different. The effect of shielding on C_p and infiltration has only been studied in simple cases. Wise [6] has reported that C_p is reduced by as much as a factor of 10 due to shielding effects of other buildings. But he also pointed out anomalous experiments in which C_p was larger for a building on the leeward side of a home than for the windward home itself. The effect of shielding on C_p depends on the distance from the building in question, the density of the sheltering objects, and their heights, widths and lengths in relation to the building.

The effect of shielding on values of C_p has been studied only for special cases, and the effects of these changes in actual infiltration rates is not clear. In their attempts to predict infiltration rates due to wind in real homes, Warren and Webb [7] found that they were overpredicting these rates. Since they were using values of C_p obtained from wind tunnel tests on isolated buildings, they reduced C_p by 50% to account for shielding. These reductions in C_p translated into a 50% reduction in the predicted infiltration rates. Another series of wind tunnel tests on the effects of trees on air infiltration has shown reductions of infiltration rates from 30 to 75% depending on the number and density of the trees, along with the distance from the house [8-9]. The great variety for the wind shielding of homes creates a difficult situation in the determination of values of C_p for particular structures. Also, the magnitudes of the changes in infiltration rate due to changes in C_p are not clear. More

research is needed in this subject, both in wind tunnels and on full-scale buildings.

When measuring C_p in a wind tunnel, there are other factors to consider besides wind shielding and local topography to obtain a proper simulation. The Reynolds number of the model must equal that of the full-scale building. One must also carefully reproduce the wind profile as a function of height, and the turbulence of the approaching wind. It is difficult to construct a complete simulation, especially the scale, intensity and frequency of the turbulence, and therefore there is often considerable variation between models and full scale tests. In most cases, average values of C_p are found from average wind speeds, neglecting turbulence. The significance of turbulence in the wind is not well understood, but it has been suggested as an important factor in air infiltration [10-11]. At present, only a few models of infiltration consider the effects of turbulence [12-13], and some wind tunnel work includes these effects [12,14].

The wind impinging on a building is turbulent due to thermal and mechanical mixing of the atmosphere and due to the wake created by the building itself. The effect of turbulence on the infiltration rate depends on the frequencies and scales of the turbulence. There are basically three categories of turbulence. The first is in the approaching flow and is governed by thermal and mechanical mixing of the atmosphere. In this case the length scale is large and the pressures around the building are highly correlated with each other. The second category includes fluctu-

ations due to the body itself, or nearby buildings, and is called "wake flow turbulence." In this case, the pressures over the building are correlated only over small areas. The last type of turbulence includes high frequency fluctuations in the flow and is due to the attachment of the boundary layer to the building surface. The air exchange of a building is affected by all three types of turbulence. The low frequency, large scale fluctuations induce infiltration similar to that caused by steady wind. High frequency fluctuations cause air exchange due to small scale turbulence at the openings. The net airflow is made up of contributions from all frequencies and thus an accurate understanding of air exchange requires consideration of all frequencies in the wind spectrum [3].

Stack Pressures

Pressure differences also arise from stack or " chimney " effects due to differences in temperature and hence density between inside and outside a building. The density differences lead to the inside and outside having different pressure gradients with height. The slope of pressure as a function of height is $-\rho g$ where g is the acceleration of gravity. Thus, the stack pressure difference Δp_s has a derivative of $-g(\rho_o - \rho_i)$ with respect to height z. For winter conditions of T_i = 20°C and T_o = -10°C, the stack pressure difference increases by 1.3 Pa with each meter of height.

When no wind is blowing and the inside temperature is higher than outside, the inside air is less dense and tends to leak out close to the ceiling, and the heavier outside air flows in near the floor. In other words, the pressure difference between outside and inside is positive near the base of the building and negative near the ceiling (see figure 2.3). When the inside is cooler than the outside, the pressure differences and flows change direction. The height at which the outside and inside pressures are equal is called the "neutral zone" or the "neutral pressure level" [13]. The position of a building's neutral zone depends on the vertical distribution of leakage sites, and can be influenced by the presence of a chimney.

Pressure differences due to the stack effect may be written in terms of the distance from the neutral zone and the difference between the inside and outside air densities. In terms of densities, the pressure difference is

$$\Delta p_s = -gh(\rho_o - \rho_i), \qquad (2.6)$$

where g is the acceleration of gravity, h is the vertical distance from the neutral zone (positive being above the zone), and ρ_i is the internal air density. Equation (2.6) is written in terms of temperature as

$$\Delta P_s = -(gp_o h/R_A)[(1/T_o)-(1/T_i)] \simeq -3500h[(1/T_o)-(1/T_i)]$$
$$= -3500h(\Delta T/T_i T_o), \qquad (2.7)$$

where p_o is in atmospheres, h in meters, R_A is the gas constant of air, Δp_s is in Pascals, T_o and T_i are the outside and inside temperatures in °K, and $\Delta T = T_i - T_o$. One can also write Δp_s as a function of the distance above ground level z.

An Example of the Pressures Acting on a Home

It is enlightening to apply the above equations to a building and calculate the pressure differences. Consider a two-story home with a height H = 6.0 m, and a square floor area of 75 m^2. For simplicity we assume there is no basement and neglect the pressures existing at the roof.

The pressure differences due to the wind p_w are calculated using equation (2.5). The wind is assumed to strike directly against one wall of the home, and the values of the wind pressure coefficients C_p are taken from figure (2.1) [3]. Table (2.1) lists the wind pressures $C_p \frac{1}{2}\rho_o u^2$ in Pascals for the front, back and sides of the home for wind speeds from 0 to 5 m/s. We are neglecting effects due to local shielding by trees, shrubs and adjacent buildings.

In order to calculate the actual pressure differences across each wall due to the wind, one must know the magnitude of p_i relative to p_o. The internal pressure p_i adjusts itself such that the inflow and outflow are equal. Assuming that the leakage is uniformly distributed among the four walls of the house and that the flow through these leakage sites is directly proportional to Δp_w, one equates the inflow through the front wall to the flow out of the side and back walls and obtains,

$$p_i = p_o - 0.75u^2. \qquad (2.8)$$

Thus, when u=2.0 m/s, the internal air pressure is 3 Pascals less than the static pressure in the free wind $p_o \simeq 10^5$ Pa. For u=4 m/s, $p_o - p_i = 12$ Pa.

The pressure differences due to the stack effect Δp_s are calculated using equations (2.6) or (2.7), and are a function of the vertical distance along the structure. In the absence of wind effects the neutral zone is at one-half the building height for a home with a uniform leakage distribution. Δp_s is then a linear function of the distance from the neutral zone h. For winter conditions with an interior temperature of 20 °C and an outside temperature of 0 °C, $\Delta p_s = -0.88h$. Therefore, at the ceiling of the home, the inside pressure is 2.6 Pa higher than the outside pressure. If the outside temperature is reduced to -12 °C, then the pressure difference at the ceiling is -5.4 Pa. During the summer, with the interior cooler than the outdoors, the signs of the stack pressures will be reversed. If it is 26 °C inside the house and 32 °C outside, then the stack pressure at the ceiling will be only +0.7 Pa.

The pressures due to the wind and stack effects have been shown to be of the same order of magnitude, but under certain conditions one dominates the other. The Archimedes number Ar is useful to characterize the relative importance of stack and wind effects,

$$Ar = \Delta T g H / \overline{T} u^2, \qquad (2.9)$$

where $\bar{T} = (T_i+T_o)/2$. The relative magnitudes of the wind speed and temperature difference which lead to one being dominant depends on the height, exposure to wind and leakage distribution of the particular house in question. When both effects are important, one must add the pressures at each location due to each and determine the flow induced by the sum.

2.2 FLOW THROUGH THE OPENINGS IN A HOUSE

The pressure differences discussed above induce air flow through the openings in the building shell. The flow through each leakage site is determined by the pressure difference at its position and the flow characteristics of the leak. These characteristics take the form of a leakage function relating the flow through the opening to the pressure difference across it.

Leakage Functions and the Fluid Mechanics of Openings

The fluid mechanics relevant to the flow through the openings in homes has been discussed by others [16-17]. The flow through a crack or opening may be described by a general leakage function

$$q = f(\Delta p) \qquad (2.10)$$

where q is in m^3/s and Δp is in Pa. The form of the function f depends on the geometry of the opening, and each opening in the shell is described by a different function f.

From dimensional analysis of the flow through an opening one arrives at a fundamental relation between q and Δp,

$$q = C_D A \sqrt{2\Delta p/\rho} \quad , \tag{2.11}$$

where

C_D = discharge coefficient
A = cross-sectional area of the opening (m^3)
ρ = density of the fluid (kg/m^3)

In general, the discharge coefficient C_D is a function of the opening geometry and the Reynolds number of the flow. The Reynolds number is defined as

$$Re = qd_h/A\nu, \tag{2.12}$$

where ν is the kinematic viscosity of the fluid in m^2/s. d_h is the "hydraulic diameter" of the opening given by

$$d_h = 4A/\text{wetted perimeter}. \tag{2.13}$$

For example, the hydraulic diameter of a circle is its diameter and for a square it is the length of a side. In the case of a long, thin crack, d_h is twice the thin dimension of the crack.

At sufficiently low Reynolds number, the steady flow through a constant area duct is well characterized. The fluid velocity varies only in the direction perpendicular to the flow, and one may visualize the flow as many sheets or laminae flowing parallel to the walls. This type of flow is referred to as "laminar." For "fully-developed" laminar flow through an infinitely long pipe ("Poiseuille flow") or between two infinitely long, parallel plates, one can solve for the velocity distribution and obtain an expression for $f(\Delta p)$. In these cases, and in laminar flow in general, C_D depends on the square root of the pressure difference. Thus, the flow q is proportional to Δp.

At large Reynolds numbers, the flow becomes "turbulent." The velocity at a given point fluctuates rapidly at random, even when the net flow rate is constant. Mixing within the stream is more intense than in laminar flow in which mixing is at the molecular level. In turbulent flow, the discharge coefficient C_D is constant for a sufficiently large Reynolds number, and therefore the flow q is proportional to $\sqrt{\Delta p}$. The transition from laminar to turbulent flow occurs at the so-called "critical" Reynolds number R_c. The value of R_c for a particular duct depends on the surface roughness of the duct walls and the approaching flow conditions.

The case of fully-developed flow impinging on a hole in a thin plate or an "orifice" is also described by equation (2.11). Again, for a sufficiently large value of Re the discharge coefficient is a constant. In general, C_D for an orifice depends on Re and the relative areas of the orifice and the duct in which the orifice lies. The Reynolds number for which C_D approaches a constant value is on the order of 10^3.

The above discussion of laminar and turbulent flow applies to constant area openings. The openings in a home are much less uniform in geometry. They have many bends and variable area, and the flow never becomes fully-developed thereby preventing the use of simple relations between q and Δp. Each opening in the building envelope can still be described by equation (2.11), where A is an average cross-sectional area and C_D is difficult to obtain.

Instead of using equation (2.11) to describe the leakage characteristics of an opening, some use the following expression

$$q = c(\Delta p)^n, \qquad (2.14)$$

where c is a flow coefficient in $m^3/s\text{-}Pa^n$ and n is the flow exponent. From the discussion of equation (2.11), we expect equation (2.14) to only approximate the relation between q and Δp. In fact, the values of c and n will depend on the range of Δp used to obtain an approximation of the form of equation (2.14). Honma [18] conducted a series of experiments in which he measured q as a function of Δp for a large number of cracks and applied equation (2.14) to the data. He found that cracks with larger flow resistances, i.e. greater depths or narrower widths, tended to have an exponent n closer to 1 than did gaps with less resistance. A narrower width decreases the Reynolds number, thus moving one toward the laminar regime (n = 1). Increasing the depth makes the opening less like an orifice for which n = 1/2. Honma also found that n tended to decrease from 1 to 1/2 as the pressure difference, or flow, increased and that this transition occurred at lower flows for openings with lower flow resistances.

This transition from n=1 to n=1/2 as Δp increases (i.e., Re increases) also occurs in flow versus pressure relations for whole houses [19-20], and may be thought of as movement from laminar flow to turbulent. Kronvall [17] points out that while it is tempting to say that n = 1/2 corresponds to turbulent flow, there are other effects which exhibit this dependence. He mentions single resistances such as entrances, exits and bends. Kronvall also states that when there are large openings in the shell of a home, they dominate the q versus Δp relation. Since large openings are similar to orifices, n will be closer to 1/2

and will be relatively constant over the range of Δp instead of exhibiting a linear dependence at low Δp. Since much shell tightening in homes concentrates on large openings, one might expect the value of n for a whole house to increase upon retrofitting the home.

The Openings in a Real Building

The openings in the envelope of a real building are numerous and varied. There is a distinction between the air flow through purposely installed openings (e.g. vents) and the uncontrolled leakage through various cracks, gaps and joints. The second type of opening may be further divided into openings associated with building components (doors and windows) and the background leaks in the rest of the shell.

From consideration of the plans of a house, one would only expect the first two types of leaks, purpose-provided and building component. Both of these can be important, but they are only part of the leakage in a house. Background openings can account for one-half of the air leakage of a home. The sites of this leakage are quite obscure, and it is impossible to locate them all. These air leaks are very important in the heat loss of many homes, and are too often neglected in retrofitting efforts [1]. Because of the existance of this background leakage, attempts to determine the whole house leakage function or to predict infiltration rates from consideration of only "blueprint" leaks will not work. Actual measurements of home tightness are essential in accounting for the heat loss of a home.

We have discussed the driving forces of wind and temperature difference and the pressure differences they induce across the shell of a house. These pressure differences are on the order of 1 to 5 Pa, possibly as high as 10 Pa. The flow through each opening is related to the pressure difference across it through a leakage function. The most common form used for these functions is given in equation (2.14). Consideration of laminar and turbulent flow along with the experimental work of Honma [18] leads one to expect the exponent n in equation (2.14) to equal 1 at low pressure differences and change to 1/2 as Δp increases. The value of Δp at which this transition occurs depends on the geometry of the particular crack. Each opening in the house is described by a different leakage function depending on its geometry. The openings in a house include obvious leaks around windows and doors, and the much more obscure but equally important background leakage. Because the background leaks are so numerous and variable in geometry, their leakage functions are impossible to obtain. One can not determine the leakage function of a house by inspection, and therefore must employ measurements.

REFERENCES

[1] Harrje, D.T., Dutt, G.S., Beyea, J., "Locating and Eliminating Obscure but Major Heat Losses in Residential Housing," ASHRAE Transactions, Vol. 85(II), 1979.

[2] Evans, R.A., Lee, B.E., "Some Observations on the Problem of Defining Mean Wind Speeds Representative of Flow over Urban and Suburban Terrain," BS 52, Department of Building Science, University of Sheffield, 1980.

[3] Handa, K., Wind Induced Natural Ventilation, Report D10, Swedish Council for Building Research, Stockholm, Sweden, 1979.

[4] Eaton, K.J., Mayne, J.R., Cook, N.J., Wind Loads on Low-Rise Buildings-Effects of Roof Geometry, Current Paper 1/76, Building Research Establishment, Garston, Watford, 1976.

[5] "The Assessment of Wind Loads," Building Research Establishment Digest, No. 119, July 1970, revised 1974.

[6] Wise, A.F.E., "Ventilation of Buildings: A Review with Emphasis on the Effects of Wind," in Energy Conservation in Heating, Cooling, and Ventilating Buildings, eds. Hoogendoorn, C.J., Afgan, N.H., Series in Thermal and Fluids Engineering, Hemisphere Publishing Corp., 1978.

[7] Warren, P.R., Webb, B.C., "The Relationship Between Tracer Gas and Pressurization Techniques in Dwellings," First Symposium of the Air Infiltration Centre, Windsor, England, 1980.

[8] Mattingly, G.E., Peters, E.F., "Wind and Trees - Air Infiltration Effects on Energy in Housing," Journal of Industrial Aerodynamics, Vol. 2, 1977.

[9] Buckley, C.B., Harrje, D.T., Knowlton, M.P., Heisler, G.M., "The Optimum Use of Coniferous Trees in Reducing Home Energy Consumption," Report No. 71, Center for Environmental Studies, Princeton University, 1978.

[10] Malinowski, H.K., "Wind Effects on the Air Movement Inside Buildings," Proceedings of Third International Conference on Wind Effects on Buildings and Structures, Tokyo, 1971.

[11] Hill, J.E., Kusuda, T., "Dynamic Characteristics of Air Infiltration," ASHRAE Transactions, Vol. 81(I), 1975.

[12] Cockroft, J.P., Robertson, P., "Ventilation of an Enclosure Through a Single Opening," Building and Environment, Vol. 11, 1976.

[13] Warren, P.R., "Ventilation through Openings on one Wall Only," in Energy Conservation in Heating, Cooling, and Ventilating Buildings, eds., Hoogendoorn, C.J., Afgan, N.H., Series in Thermal and Fluids Engineering, Hemisphere Publishing Corp., 1978.

[14] Bilsborrow, R.E., Fricke, F.R., "Model Verification of Analogue Infiltration Procedures," Building Science, Vol. 10, 1975.

[15] Emswiler, J.E., "The Neutral Zone in Ventilation," ASHVE Transactions, Vol. 32, 1926.

[16] Sherman, M.H., "Air Infiltration in Buildings," Report No. 10712, Lawrence Berkeley Laboratory, University of California, 1980.

[17] Kronvall, J., "Air Flows in Building Components," Report TVBH-1002, Division of Building Technoloy, Lund Institute of Technology, Lund, Sweden, 1980.

[18] Honma, H., Ventilation of Dwellings and its Disturbances, Faibo Grafiska, Stockholm, Sweden, 1975.

[19] Nylund, P.O., Infiltration and Ventilation, Report D22, Swedish Council of Building Research, Stockholm, Sweden, 1980.

[20] Grimsrud, D.T., "Case Studies of Air Infiltration," Report No. 7830, Lawrence Berkeley Laboratory, University of California, 1978.

Table 2.1 Wind Pressures Exerted on Walls of a Home, $C_p \frac{1}{2} \rho_o u^2$*

Wind Speed (m/s)	Average Pressure (Pascals)		
	Front	Back	Side
0	0	0	0
1	0.42	-0.24	-0.42
2	1.68	-0.96	-1.68
3	3.78	-2.16	-3.78
4	6.72	-3.84	-6.72
5	10.50	-6.00	-10.50

*Values of C_p based on figure (2.1) from reference [3].

Figure 2.1 Values of Wind Pressure Coefficients from reference [3].

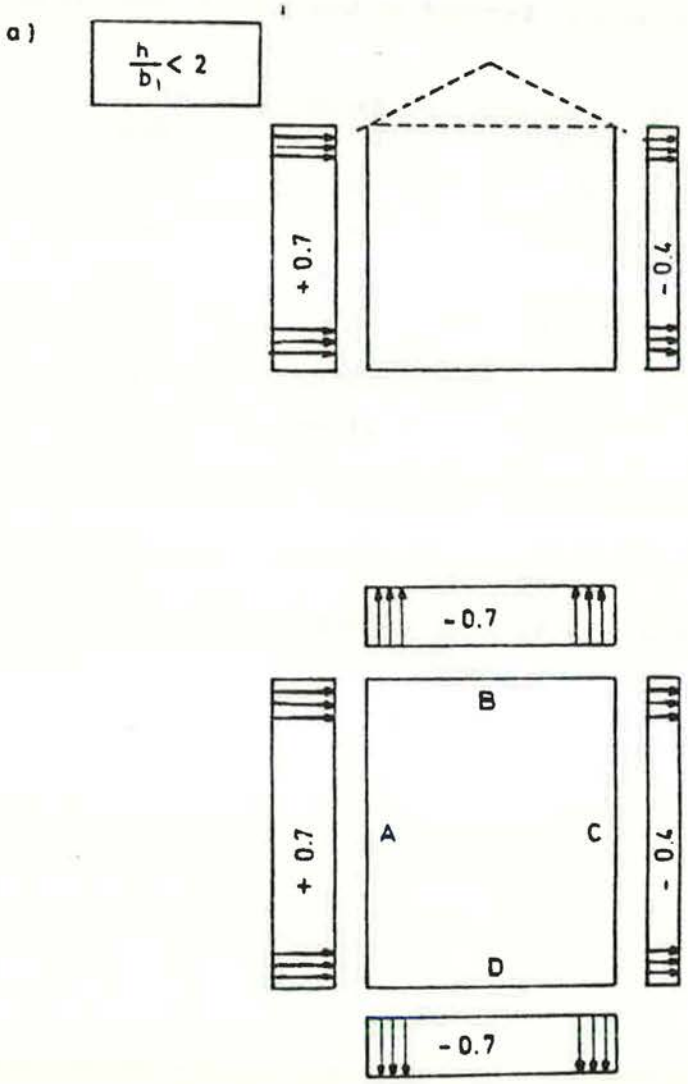

Figure 2.2 Values of C_p for Variable Roof Pitch, from reference [4].

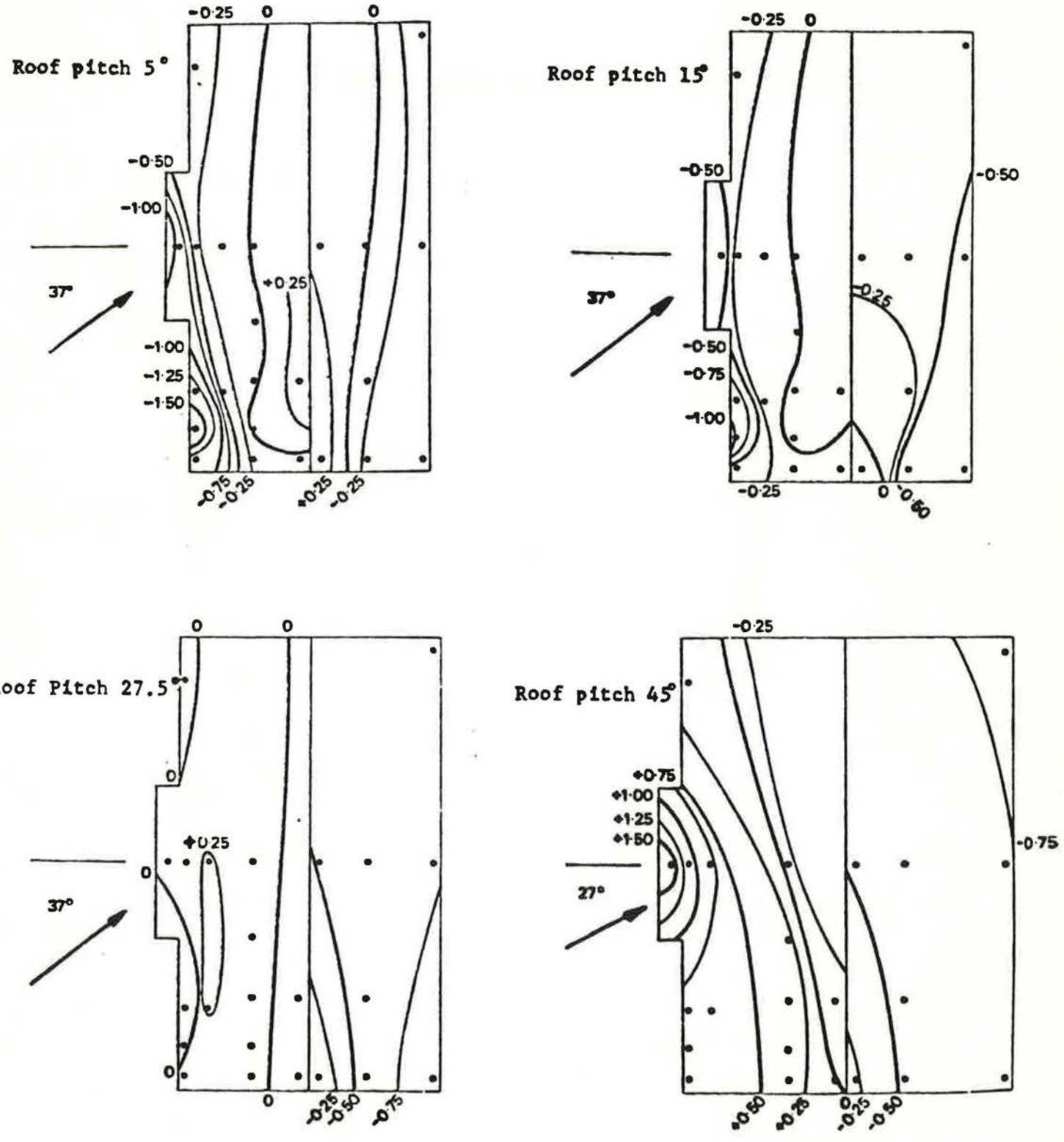

Figure 2.3 Pressures Due to the Stack Effect

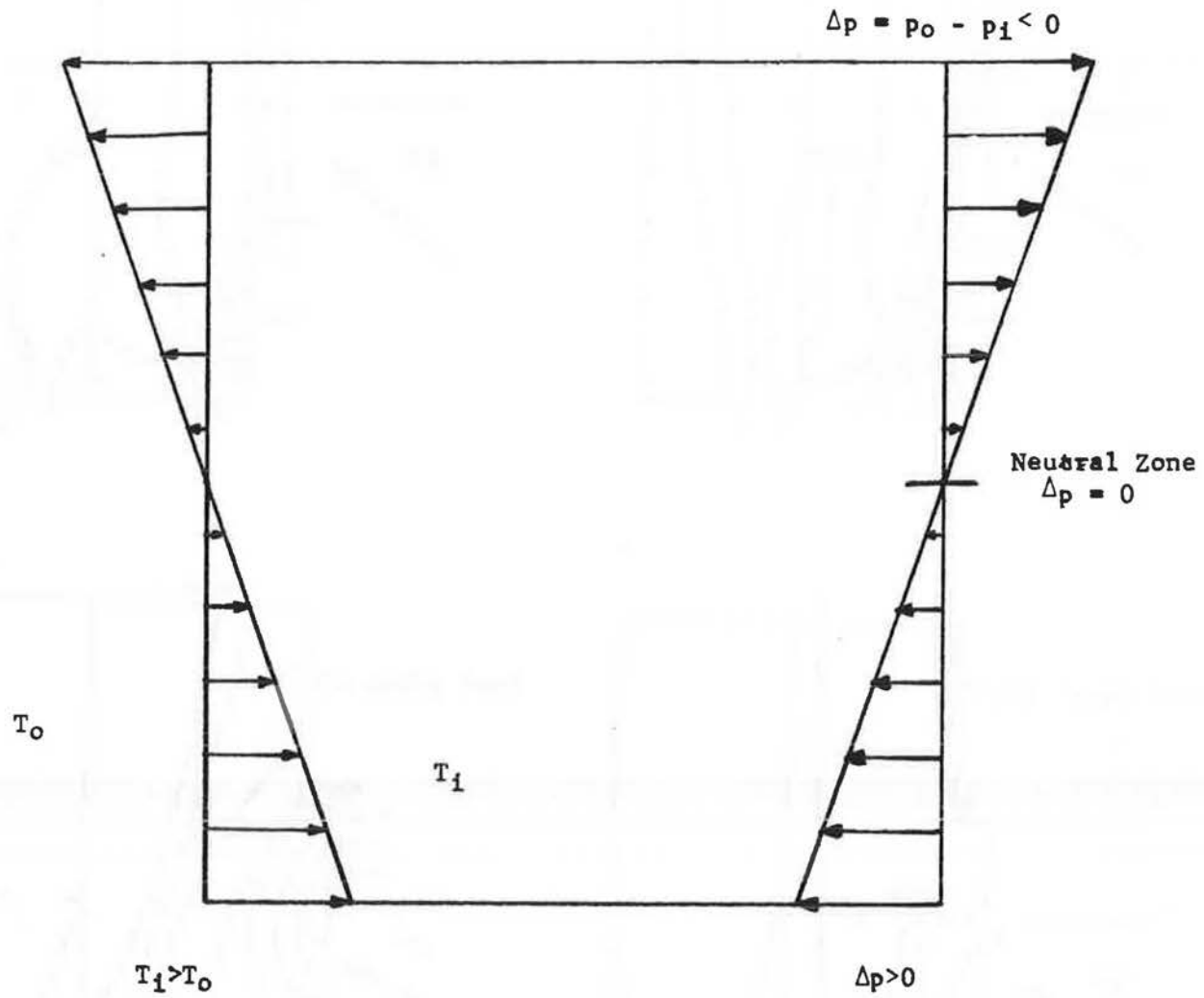

Chapter III

MEASURING AIR INFILTRATION USING THE TRACER GAS TECHNIQUE

Techniques have been developed to measure air infiltration rates because present methods to predict these rates are not accurate. Infiltration measurement using the tracer gas technique is one method of evaluating the tightness of a building, but it only gives the infiltration rate under the weather conditions during the measurement. Because of the complex dependence of infiltration on weather and occupant activities, a single infiltration measurement is only of limited use for characterizing the tightness of a home. Many measurements of infiltration under a wide variety of conditions are needed to evaluate the tightness of a home. There have been several reviews of infiltration measurement techniques [1-8]. The following review discusses specific measurement techniques and some related problems.

3.1 TECHNIQUES AND PROBLEMS

A tracer gas is used to measure the air infiltration rate of a building by releasing the gas into the structure and monitoring its concentration over time. The physics of this process are described by

$$d\bar{c}/dt = \bar{c}_o I + G - \bar{c}I, \qquad (3.1)$$

where

$\bar{c}$ = concentration of tracer in the ventilated space at time t
$\bar{c}_o$ = concentration of tracer in the outside air
I^o = infiltration rate (exchanges/hr)
G = rate of generation of tracer in the ventilated space.

The same infiltration rate I is used for the volumetric inflow and outflow of air, i.e. indoor and outdoor air density differences are being neglected. With values of $\bar{c}_o$, G, and $\bar{c}$ as a function of time, one can calculate the infiltration rate I using equation (3.1). $\bar{c}_o$ is usually zero, except when using water vapor or carbon dioxide as a tracer gas.

Various methods of tracer gas measurement exist. In tracer gas decay, one injects a volume of tracer into the building, allows it to mix throughout the structure and then monitors the decay in concentration over time. During the decay G = 0, and if the infiltration rate is constant the tracer concentration decays exponentially,

$$\bar{c} = \bar{c}_o e^{-It}. \qquad (3.2)$$

Thus, the rate of change of the natural logarithm of concentration equals the negative of the infiltration rate. The tracer gas decay technique is suseptible to errors if the interior air is imperfectly mixed [6]. Problems arise because the tracer gas concentration is different in different parts of the house. One may avoid these problems through multi-point injection and sampling, or by mixing the interior air.

In the constant concentration technique the injection rate is controlled to keep the tracer concentration constant [9]. This simplifies equation (3.1) to an expression for the infiltration rate I,

$$I = G/\bar{c}', \tag{3.3}$$

where $\bar{c}'$ is the constant concentration. This technique is less affected by imperfect mixing than decay, because the concentration is uniform within the house. Still, there are mixing problems because of the delay in the response of concentration to a change in the tracer injection rate G. The control system continues to increase G because $\bar{c}$ does not immediately attain $\bar{c}'$, resulting in an overshoot of the target concentration. An unstable oscillation can result if the system attempts to keep the concentration at $\bar{c}'$. There is disagreement between those who claim that a constant concentration system will be unstable [6,10] and those who have used it successfully [9]. The instability problem can be avoided if instead of aiming for a single concentration, one keeps the tracer concentration within a specific range through periodic updates of the injection rate. The time between updates must be long compared to the mixing times.

The third technique is constant injection or equilibrium concentration in which there is a steady rate of tracer injection. The infiltration rate is calculated from the injection rate and the equilibrium tracer gas concentration. This method is simple and a single concentration measurement yields the infiltration

rate if the mixing is perfect. But long time periods may be necessary to achieve equilibrium, and varying infiltration rates make a large measurement scale necessary and may lead to errors.

There are several considerations in choosing a tracer gas and many different gases have been used. The gas should be easily and inexpensively measurable over a wide range of concentration. There should be no sources of the tracer or any other gas within the house that will interfere with the measurement device. Also, a tracer gas should be nonflammable, unreactive and non-toxic, especially for experiments in occupied buildings. Early ventilation research used helium and hydrogen as tracers and katharometers to measure concentration through changes in thermal conductivity [11-13]. More recent work has employed nitrous oxide [14], ethane [15], carbon dioxide [16], methane [17], and sulfur hexafluoride [18-19]. Some of these tracers have undesirable qualities such as flammability and normal existence in the air, but they can be used with care.

As mentioned earlier, mixing of air within the structure is important in tracer gas measurements. If the indoor air is perfectly mixed, i.e. incoming air is instantaneously mixed throughout the entire building, then an accurate measurement of the infiltration rate will be straightforward. But mixing is never perfect, especially in buildings with several rooms, and this may introduce errors into infiltration measurements. Ideally, one would monitor every room and determine the flow rates between the rooms and the outdoors, but this is complicated and expensive.

Multi-chamber infiltration techniques have been discussed theoretically [5,20-21] and some measurements have been made [9].

Infiltration measurement systems are usually designed for unattended long term (roughly one week) measurements of hourly average infiltration rates. These systems include tracer injection and air sampling devices and a method of controlling them, a concentration measuring instrument, and some means of recording the data. Many systems using the tracer gas decay technique have been developed because of its simplicity [18-19,22].

One shortcoming of tracer gas measurement is that it gives the rate only for the weather conditions during the test. To average out effects of weather and occupant activity one could use the infiltration rate averaged over several days or weeks instead of one hour. A passive, long term technique is being developed at Brookhaven National Laboratory which employs several small devices about the size of cigarettes [23]. A perfluorocarbon tracer gas is released at a known rate by diffusion out of a polymer, and several of these capsules are distributed within a building. The tracer gas is collected by adsorption onto charcoal in another small capsule. When the adsorber is removed, the amount of collected tracer is determined and related to the injection rate to determine the average infiltration rate. This technique is so simple and the devices so small, that the sources and adsorbers may be sent through the mail to a large number of homes.

3.2 REVIEW OF RESEARCH

Using the measurement techniques described above, infiltration rates of buildings, their magnitudes and their relations to various conditions have been studied. Most research has involved infiltration measurements in one or more homes, usually hourly averages, and attempts to relate these rates to weather conditions and the state of the building [12,14-15,17-18,24-36].

The weather variables affecting infiltration are the wind speed and direction and the indoor-outdoor temperature difference. Our definition of the wind pressure coefficient in equation (2.4) leads one to assume that the wind induced pressures are proportional to the square of the wind speed. The relation of infiltration rate to wind speed then depends on the flow dependence on pressure difference. Generally the flow is assumed to depend on the pressure difference raised to either 0.5 or 1.0, and thus the wind induced infiltration will depend on the wind speed u or its square. The pressure differences due to temperature effects depends on the inside-outside temperature difference ΔT in equation (2.7), and therefore the stack induced infiltration is usually related to ΔT or $\sqrt{\Delta T}$.

In most infiltration research, measured infiltration rates are related to the wind speed and temperature difference, but the interaction of wind and stack effects are difficult to model. Because of the nonlinear relation between flow and pressure difference, one must add the two pressures before computing the net flow. In fact, the infiltration rate induced by a combination of

wind and stack effects may be less than the sum of the infiltration rates of the two forces acting separately [37]. Some have tried products of the wind speed and temperature difference in order to include combined effects of the two variables. The state (open or closed) of doors, windows and vents have also been considered, along with furnace on-time. Because of the strong dependence of the infiltration rate on weather and building state [30], many measurements over a range of conditions are necessary to characterize the leakiness of a home.

Infiltration research of the past thirty years has involved regressing measured infiltration rates against one or more of the above variables. The nonlinear dependence of infiltration on temperature difference and wind is usually modelled as a linear relation,

$$I = \bar{A} + \bar{B}\Delta T + \bar{C}u. \qquad (3.4)$$

Most infiltration research has involved multiple regressions of I against ΔT and u. Some have included u^2 and ΔT^2 [12,28,29] and door opening and furnace firing times [30]. Harrje and Mills [31] made measurements on several homes before and after a series of retrofits and noted the change in the coefficients $\bar{A}$, $\bar{B}$ and $\bar{C}$ in equation (3.4).

EPRI sponsored research at Ohio State University in which nine houses were studied for one year [24]. They attempted to analyze the data using equation (3.4) to obtain a unified model applicable to any house. When this linear approximation failed, they

tried a nonlinear and more physical approach. The resultant model of air infiltration is

$$I = \beta_o C_T (4\Delta p_T + \sqrt{2}\Delta p_u)^{\frac{1}{2}}. \qquad (3.5)$$

Δp_T is the pressure differnce due to stack effects at the building roof, based on equation (2.6). Δp_u is the pressure differnce due to wind, proportional to u^2. C_T is the measurable crack length over the building surface and β_o is a regression constant supposedly related to the construction quality of the building. For the nine homes tested, β_o varies from about 2.5 to 1.0 which is much less than the variability of $\bar{A}$, $\bar{B}$ and $\bar{C}$ in equation (3.3). Table (3.1) shows examples of $\bar{A}$, $\bar{B}$ and $\bar{C}$ for several homes from past research, and the spread is indeed quite large. $\bar{A}$ varies by almost 100 to 1, $\bar{C}$ by about 10 to 1, and $\bar{B}$ by 5 to 1.

Equation (3.4) is only an approximation to the nonlinear relation between infiltration rate and the wind and temperature difference. Because the relation is nonlinear, the values of $\bar{A}$,$\bar{B}$ and $\bar{C}$ depend on the values of u and ΔT for which the infiltration measurements are made. Thus, $\bar{A}$,$\bar{B}$ and $\bar{C}$ will vary among houses due to the weather conditions during the test as well as due to variations in building tightness and weather sensitivity. The nonlinearity in I as a function of u and ΔT is a source of the large variation of values in table (3.1). In order to obtain unbiased estimates of $\bar{A}$,$\bar{B}$ and $\bar{C}$, one needs many infiltration measurements over a large range of wind and temperature difference. This takes several months and ties up expensive equipment. Also,

the tightness of homes can change during the length of time required to collect this data. A small number of measurements give only limited information on the building leakiness and can not be extrapolated to other weather conditions. Thus, the use of tracer gas measurements for evaluating the tightness of homes, requires a large number of expensive and time-consuming measurements for each house. For this reason, tracer gas techniques are not appropriate for tightness evaluation of homes.

We have described tracer gas techniques for measuring infiltration rates in homes, and discussed possible measurement problems. The technique is indispensable for measuring infiltration rates because of our inability to calculate them. Most tracer gas measurements yield the average infiltration over an hour or so. These short term rates are sensitive to the weather conditions during the test and therefore give only limited information on the tightness of a home. To evaluate a home's tightness using tracer gas measurements requires many measurements under a wide variety of weather conditions to determine the sensitivity of infiltration to weather. It takes many months to obtain all of this data and this becomes quite expensive because of the costly equipment involved. Also, the tightness of a home can change significantly over this time period. Thus, tracer gas measurement is not appropriate for evaluating the tightness of homes. These factors also complicate the use of tracer gas measurements as a tightness standard for homes. The evaluation of tightness

should be done with some surrogate tightness measure such as that obtained from the pressurization technique described in the next chapter.

REFERENCES

[1] Hitchin, E.R., Wilson, C.B., "A Review of Experimental Techniques for the Investigation of Natural Ventilation in Buildings," Building Science, Vol. 2, 1967.

[2] Lagus, P.L., "Characterization of Building Infiltration by the Tracer Dilution Method," Energy, Vol. 2, 1977.

[3] Ross, H., Grimsrud, D., "Air Infiltration in Buildings: Literature Survey and Proposed Research Agenda," prepared for International Energy Agency by U.S. Department of Energy, Report No. 7822, Lawrence Berkeley Laboratory, University of California, 1978.

[4] Grimsrud, D.T., "Case Studies in Air Infiltration," Report No. 7830, Lawrence Berkeley Laboratory, University of California, 1978.

[5] Sherman, M.H., Grimsrud, D.T., Condon, P.E., Smith, B.V., "Air Infiltration Measurement Techniques," Report No. 10705, Lawrence Berkeley Laboratory, University of California, 1980.

[6] Hunt, C.M., "Air Infiltration: A Review of Some Existing Measurement Techniques and Data," Building Air Change Rate and Infiltration Measurement, eds., Hunt, C.M., King, J.C., Trechsel, H.R., ASTM STP 719, American Society for Testing and Materials, 1980.

[7] Lagus, P.L., "Air Leakage Measurements by the Tracer Gas Dilution Method - A Review," Building Air Change Rate and Infiltration Measurement, eds., Hunt, C.M., King, J.C., Trechsel, H.R., ASTM STP 719, American Society for Testing and Materials, 1980.

[8] Kronvall, J., Airtightness - Measurements and Measurement Methods, Report D8, Swedish Council of Building Research, Stockholm, Sweden, 1980.

[9] Etheridge, D.W., Alexander, D.K., "The British Gas Multi-Cell Model for Calculating Ventilation," ASHRAE Transations, Vol. 86(II), 1980.

[10] Condon, P.E., Grimsrud, D.T., Sherman, M.H., Kammerud, R.C., "An Automated Controlled-Flow Air Infiltration Measurement System," Building Air Change Rate and Infiltration Measurements, eds., Hunt, C.M., King, J.C., Trechsel, H.R., ASTM STP 719, American Society for Testing and Materials, 1980.

[11] Dick, J.B., "Measurement of Ventilation Using Tracer Gas Technique," Heating, Piping and Air Conditioning, Vol. 22, 1950.

[12] Bahnfleth, D.R., Moseley, T.D., Harris, W.S., "Measurement of Infiltration in Two Residences," ASHAE Transactions, Vol. 63, 1957.

[13] Coblentz, C.W., Achenbach, P.R., "Design and Performance of a Portable Infiltration Meter," ASHAE Transactions, Vol. 63, 1957.

[14] Howard, J.S., "Ventilation Measurements in Houses and the Influence of Wall Ventilators," Building Science, Vol. 1, 1966.

[15] Elkins, R.H., Wensman, C.E., "Natural Ventilation of Modern Tightly Constructed Houses," Proceedings of American Gas Association Conference on Natural Gas Research and Technology, Chicago, 1971.

[16] Hill, J.E., Kususda, T., "Dynamic Characteristics of Air Infiltration," ASHRAE Transactions, Vol. 81(I), 1975.

[17] Janssen, J.E., Glatzel, J.J., Torborg, R.H., Bonne, U., "Infiltration in Residential Structures," Heat Transfer in Energy Conservation, eds., Goldstein, R.J., Didion, D., Gopal, R., Kreider, K., Schoenhals, R., American Society of Mechanical Engineers, 1977.

[18] Hunt, C.M., Burch, D.M., "Air Infiltration Measurements in a Four Bedroom Townhouse Using SF_6 as a Tracer Gas," ASHRAE Transactions, Vol. 81(I), 1975.

[19] Harrje, D.T., Hunt, C.M., Treado, S.J., Malik, N.J., "Automated Instrumentation for Air Infiltration Measurements in Buildings," Report No. 13, Center for Environmental Studies, Princeton University, 1975.

[20] Sinden, F.W., "Theoretical Basis for Tracer Gas Measurements of Air Infiltration," Building and Environment, Vol. 12, 1978.

[21] Honma, H., Ventilation of Dwellings and its Disturbances, Faibo Grafiska, Stockholm, Sweden, 1975.

[22] Hartmann, P., Muhleback, H., "Automated Measurements of Air Change Rate (Decay Method) in a Small Residential Building without any Forced-Air-Heating System," First Symposium of the Air Infiltration Centre, Windsor, England, 1980.

[23] Dietz, R., Cote, E., Senum, G., Wieser, R., "An Inexpensive Perfluorocarbon Tracer Technique for Wide-Scale Infiltration Measurement in Homes," International Symposium on Indoor Air Pollution, Health and Energy Conservation, Amherst, Massachusetts, October 1981.

[24] Fuel Utilization in Buildings, Final Report, EA-894, Project 137-1, Electric Power Research Institute, 1978.

[25] Dick, J.B., "Experimental Studies in Natural Ventilation of Houses," JIHVE, Vol. 17, 1949.

[26] Dick, J.B., "The Fundamentals of Natural Ventilation of Houses," JIHVE, Vol. 18, 1950.

[27] Dick, J.B., Thomas, D.A., "Ventilation Research in Occupied Houses," JIHVE, Vol. 19, 1951.

[28] Laschober, R.R., Healy, J.H., "Statistical Analysis of Air Leakage in Split-Level Residences," ASHRAE Transactions, Vol. 70, 1964.

[29] Tamura, G.T. Wilson, A.G., "Air Leakage and Pressure Measurements," ASHRAE Transactions, Vol. 70, 1964.

[30] Malik, N., "Field Studies of Dependence of Air Infiltration on Outside Temperature and Wind," Energy and Buildings, Vol. 1, 1978.

[31] Harrje, D.T., Mills, Jr., T.A., "Air Infiltration Reduction Through Retrofitting," Building Air Change Rate and Infiltration Measurements," eds., Hunt, C.M., King, J.C., Trechsel, H.R., ASTM STP 719, American Society for Testing and Materials, 1980.

[32] Coblentz, C.W., Achenbach, P.R., "Field Measurements of Air Infiltration in Ten Electrically - Heated Houses," ASHRAE Transactions, Vol. 69, 1963.

[33] Jordan, R.C., Erickson, G.A., Leonard, R.R. "Infiltration Measurements in Two Research Houses," ASHRAE Transactions, Vol. 69, 1963.

[34] Luck, J.R., Nelson, L.W., "The Variation of Infiltration Rate with Relative Humidity in a Frame Building," ASHRAE Transactions, Vol. 83(I), 1977.

[35] Goldschmidt, V.W., Wilhelm, D.R., "Summertime Infiltration Rates in Mobile Homes," ASHRAE Transactions, Vol. 85(I), 1979.

[36] Wang, Sr., F.S., Sepsy, C.F., "Field Studies of the Air Tightness of Residential Buildings," Building Air Change Rate and Infiltration Measurements, eds., Hunt, C.M., King, J.C., Trechsel, H.R., ASTM STP 719, American Society for Testing and Materials, 1980.

[37] Sinden, F.W., "Wind Temperature and Natural Ventilation - Theoretical Considerations," Energy and Buildings, Vol. 1, 1978.

Table 3.1 Coefficients from Literature for $I^{*} = \bar{A} + \bar{B}\Delta T(^{\circ}C) + \bar{C}u(m/s)$

Reference	Building			$\bar{A}$	$\bar{B}$	$\bar{C}$
Bahnfleth [12]	2-story, hot water heat			.015	.0059	.029
	1-story, forced air			.015	.012	.027
Laschober [28]	Split level, hot water heat			0.11	.030	.19
	Split level, forced air			-	.019	.15
Dick [25]	Row houses			0.99	-	.27
	Various heating systems			1.03	-	.26
				1.29	-	.20
				0.63	-	.17
Dick [27]	Various heating systems			1.34	-	.29
Tamura [29]	1-story, forced air			-	-	.038
Malik [30]	Identical row houses, 2-story, forced air	low wind	#1	0.19	.027	-
			#2	0.26	.023	-
		high wind,	#1	0.21	-	.083
Wang [36]	2-story, forced air, identical homes	low wind	#2	.026	.015	-
			#3	.028	.021	-
			#4	.062	.017	-
		low T	#2	.026	-	.063
			#3	.028	-	.072
			#4	.062	-	.038

*The infiltration rate I is in units of exchanges per hour.

Chapter IV

THE TECHNIQUE OF PRESSURIZATION TESTING

In the previous chapter we stated that evaluating a building's tightness through tracer gas measurement requires many measurements under a wide variety of weather conditions. This process can take months, and involves expensive and sophisticated equipment. Pressurization testing of homes is an alternative tightness evaluation which is quick and less expensive. But the relation of pressurization test results to infiltration rates under natural conditions is not well established. Many models of this relation are being developed and tested. Pressurization (or depressurization) of homes is also useful for finding sites of air leakage when used in conjunction with smoke or infrared scanning [1].

Building components, such as windows, have been pressure tested for many years, but the application to whole houses is more recent. In whole house pressurization a large fan mounted in a door or window induces a large and roughly uniform pressure difference across the building shell. The leakier the house, the more air flow is necessary to induce a specific inside-outside pressure difference. Typically, one subjects the home to several inside-outside pressure differences and measures the flow through the fan. The test results are interpreted in various ways to yield a measure of the leakiness of the home.

Pressurization testing has been done with a variety of devices throughout the world [2-14]. The equipment for pressure testing is preferably portable and operable by two people without a high level of technical expertise. Keeping the device portable places limitations on its design. For example, there must be some way to measure the flow through the fan, and while orifice meters and nozzles are accurate, they usually involve large and awkward ducting. These flow measuring devices also cause a pressure drop which may make a larger capacity fan necessary, again increasing the weight of the device. Our research has employed the " Blower Door ," developed at Princeton University and used throughout North America, which is calibrated to yield the flow through the fan as a function of fan RPM and pressure difference [2]. While such an indirect flow measurement may be less accurate, it makes the Blower Door much less bulky.

4.1 INTERPRETING THE RESULTS

Several methods are used to convert pressurization test results to a measure of leakage. The most common leakiness standard is the flow rate required to induce a 50 Pa pressure difference between inside and outside. The 50 Pa flow rate is often divided by the volume of the house to yield the flow rate in exchanges per hour (X/hr). The 50 Pa flow rate is used in Sweden as a standard for building tightness. The pressurization test results are sometimes fit to a curve of the same form as that used for individual openings in chapter II,

$$q = c(\Delta p)^n. \qquad (4.1)$$

q is the flow rate in m^3/s. In most cases curve fits are based on tests at several pressure differences from about 10 Pa up to 60 or 75 Pa, but Orr and Figley [7] use pressures up to 100 Pa.

Pressurization data is also converted to an "effective leakage area" for the building using the fundamental equation for flow through an opening

$$q = C_D A \sqrt{2\Delta p/\rho} . \qquad (4.2)$$

A is the actual leakage area and C_D is the discharge coefficient related to the opening geometry and Reynolds number. A and C_D are then combined into the effective leakage area $A_o = AC_D$. Researchers at the Lawrence Berkeley Laboratories use equation (4.1) to find the flow at 4 Pa, i.e. Q(4). They then use equation (4.2) to compute the equivalent or effective leakage area A_o [13]. Tamura [14] uses a single measurement of q at Δp = 75 Pa and equation (4.2) to determine the equivalent leakage area. Since the dependence of C_D on Δp is generally unknown, one may assume a constant value for C_D. Because C_D changes with Δp, A_o is a function of the pressure difference.

Etheridge of the British Gas Corporation [15] objects to curve fits using equation (4.1) because it is not dimensionally homogeneous, i.e. the constant c depends on the system of units one uses. Instead, he uses equation (4.2). The discharge coefficient C_D depends on the Reynolds number Re and the opening geometry through the ratio of the distance through the crack y and the hydraulic diameter d_h (see equation (2.13)). From tests on

several crack types, empirical relations between C_D, and Re and y/d_h have been found [16]. While this technique is straightforward when applied to cracks around doors and windows, it is difficult to apply to the significant amount of background leakage for which the opening geometry is not known.

Choosing an appropriate method for converting the results of a pressurization test to a measure of leakage is one question addressed in this thesis. The flow rate at 50 Pa is indeed the most common measure, but others, such as the 4 Pa flow rate, are used. The bottom line in choosing among measures of tightness is their use in comparing the tightness of homes and in predicting ventilation rates under natural conditions.

4.2 PROBLEMS WITH THE TEST METHOD

Pressurization testing of homes is straightforward and fast as compared with infiltration measurements, but questions have been raised concerning this technique [4,17]. Basically, the conditions during a pressurization test differ in several respects from the conditions which induce infiltration. First, the test pressures are an order of magnitude larger than the pressures due to the wind and temperature differences. The flow through the leakage sites under these larger pressures may behave quite differently than the flows that occur naturally. A pressurization test may actually change the leakage characteristics of a home by pressing closed or pulling open building components. Also the pressure difference during a test is uniform and constant over

the entire envelope while it varies continually in time and space under normal conditions. Finally, a pressurization test determines the net leakage and gives no information on specific leakage locations which are crucial in determining infiltration rates.

The outside weather during a pressurization test, especially the wind speed, may effect the test results by inducing additional pressure differences across the shell. It is has been recommended that pressurization tests be conducted when the wind speed is less than 8.0 km/h = 2.2 m/s (= 5 mph). Confounding pressures will also be induced by stack effects, and therefore it is recommended that one conducts tests with inside-outside temperature differences of 11°C or less [18]. The effects of weather on pressurization test results have not been studied before and this prompted some experimental work in this thesis.

Many quantifications of pressurization tests involve normalizing the flow rate at some pressure difference by the house volume or the surface area of the building envelope. Ambiguities exist as to how one considers basements in these calculations. It is common to conduct separate pressurization tests on a home with the basement door closed and open. One might expect that closing the basement door would allow one to separate the basement leakage from that of the rest of the house. But there are usually other means for communication between the basement and the living space other than the basement door. Blomsterberg and Harrje [5] have shown that the relative ranking of the leakiness of homes is

different for tests with the basement door closed and its volume excluded from the normalization, and tests done with the basement door open and its volume included. This ranking change could be due to differences in the amount of communication between the basement and the living space, or differences in the amount of basement leakage to the outdoors.

Part of the problem with pressurization testing is that the real range of interest is in the lower pressure differences, and it is hard to measure small pressures and flows accurately. To overcome the problems of low pressure difference measurements, advanced pressurization techniques have been developed [19-20]. These so-called "AC" or alternating pressure methods involve inducing an alternating air flow into and out of a home and measuring the internal pressure response. The equipment and analysis are much more complex than in "DC" pressurization. Also, instead of measuring the flow rate, one relies on the measurement of very small changes in the internal pressure and this may be a source of error [4].

The results obtained through AC pressurization at the Lawrence Berkeley Laboratories do not show the expected linear relationship between pressure difference and flow rate in the low pressure range. Instead, they claim that the low pressure leakage is dominated by orifice flow, $n = 1/2$, rather than viscous flow. It is a suprising result that n starts at 1/2, increases to 1 and then returns back to 1/2 as the pressure difference increases. It is hard to think of any effect of fluid mechanics that would

eliminate the effects of viscosity at low pressure differences. While these results are confusing, AC pressurization techniques may be useful for determining the low pressure leakage function of a home.

4.3 REVIEW OF TIGHTNESS MEASUREMENTS ON HOMES

Many measurements have been made of the tightness of homes using the pressurization technique [3-12]. Most of these measurements are flow rates at 50 Pa in exchanges per hour (X/hr). Figure (4.1) compares the 50 Pa flow rate for many houses around the world. Kronvall's book on airtightness [24] contains pressurization test results for almost 400 Swedish homes, including some information on building type and construction details. Figure (4.1) shows the mean and one standard deviation of spread for the 50 Pa flow rate for single family homes made of wood and homes built with lightweigtht concrete. An earlier article by Kronvall [3] gives the leakage for 29 homes which are close to the tightness of his larger collection. The Swedish homes tend to have leakage rates of less than 5 X/hr at 50 Pa.

The U.S. homes are shown next in the figure [5,22,23] and tend to be leakier than the Swedish homes. A small sample of energy efficient homes is included which have exchange rates from about 10 to 15 X/hr at 50 Pa. The "low-income" houses are much leakier than the other U.S. homes, but the data is less reliable. Part of the reason for the difference between Swedish and U.S. whole house tightness is that the Swedes generally seal up all vents

and flues during their pressurization testing. The effect of this procedure on building tightness will vary among homes but is about 10%, and not enough to account for these differences. Finally, figure (4.1) shows several British homes of various construction and ages with exchange rates from 10 to 20 X/hr at 50 Pa [12]. Thus, while many homes exchange air at rates at or above 10 X/hr, the Swedes have shown us that homes can be built and/or retrofit to leakage rates of 5 X/hr or less.

We mentioned earlier that pressurization testing is criticized because it gives only a global leakage value with no information on the leakage distribution. By sealing up the separate components of a building during a pressurization test, one can find the distribution of leakage in a home. This is a tedious procedure and significantly increases the time required for a pressurization test. Tamura of the National Research Council of Canada [21] divided the leakage of six homes into the contributions of the ceiling, walls and the windows and doors. His findings are presented in table (4.1). Windows and doors account for from 15 to 24% of the leakage. The fraction attributable to the ceiling and walls is much more variable, 8 to 67% for the ceiling and 15 to 77% for the walls. This wide range of values is possibly due to the difficulty in completely separating the ceiling from the walls. Tamura's sample size is certainly too small to draw any conclusions about the leakage distribution except that it is variable from house to house. Caffey of Texas Power and Light [9] studied the leakage distribution of 50 homes and found that

on the average the sole plate around the base of a house accounts for 25% of the leakage, and the wall outlets for a suprisingly large 20%. The duct system and windows account for 14% and 12% respectively, but doubts have been expressed as to the accuracy of Caffey's numerical results. Warren and Webb of the Building Research Establishment of Great Britain [12] considered 19 homes and reported the precentage of background leakage for each. Background leakage, which includes all leakage other than purposely installed vents, windows and doors, ranged from 50 to 75% of the whole house leakage. The most important result of these measurements is that the obvious leakage sites, windows and doors, account for only about 15% of the whole house leakage. These leakage distributions have been given for the flows at Δp = 50 Pa. Little work has been done on how the leakage distribution changes as one approaches weather induced pressure differences, although Warren and Webb [12] have found that background leakage becomes a smaller percentage of the total at lower pressure differences.

Pressure testing of homes to evaluate their tightness is faster and less expensive than tracer gas measurements. It has disadvantages because it determines the leakage under test conditions which are much different than the conditions which actually induce infiltration. Also, a pressurization test gives no information on the leakage distribution, although limited information can be obtained with extra effort. The Blower Door is the most

common pressurization device used today in North America, but little work has been done concerning the repeatability and accuracy of the test results. Regardless of the particular device used, the most common measure of leakage is the flow rate required to induce a 50 Pa pressure difference between the inside and outside. A very tight home has a leakage rate of 5 X/hr or less at 50 Pa, while 5 to 10 X/hr is still somewhat tight. Leakage rates above 10 X/hr are associated with leaky homes. But the relation of these pressurization test results to actual infiltration rates must be understood before pressurization testing becomes an accepted measure of tightness.

REFERENCES

[1] Harrje, D.T., Dutt, G.S., Beyea, J., "Locating and Eliminating Obscure but Major Energy Losses in Residential Housing," ASHRAE Transactions, Vol. 85(II), 1979.

[2] Gadsby, K.J., Linteris, G.T., Dutt, G.S., Harrje, D.T., "The Blower Door," Report No. 124, Center for Energy and Environmental Studies, Princeton University, 1981.

[3] Kronvall, J., "Testing of Homes for Air Leakage Using a Pressure Method," ASHRAE Transactions, Vol. 84(I), 1978.

[4] Alexander, D.K., Ehteridge, D.W., Gale, R., "Experimental Techniques for Ventilation Research," Air Infiltration Centre Symposium, Instrumentation and Measuring Techniques, Windsor England, 1980.

[5] Blomsterberg, A.K., Harrje, D.T., "Approaches to Evaluation of Air Infiltration Energy Losses in Buildings," ASHRAE Transactions, Vol. 85(I), 1979.

[6] Stricker, S. "Measurement of Air-Tightness of Houses," ASHRAE Transactions, Vol. 81(I), 1975.

[7] Orr, H.W., Figley, D.A., "An Exhaust Fan Apparatus for Assessing the Air Leakage Characteristics of Houses," Division of Building Research, National Research Council of Canada, 1980.

[8] Wang, Sr., F.S., Sepsy, C.F., "Field Studies of the Air Tightness of Residential Buildings," Air Change Rate and Infiltration Measurements, eds., Hunt, C.M., King, J.C., Trechsel, H.R., ATSM STP 719, American Society of Testing and Materials, 1980.

[9] Caffey, G.E., "Residential Air Infiltration," ASHRAE Transactions, Vol. 85(I), 1979.

[10] Krinkel, D.L., Dickeroff, D.J., Casey, J., Grimsrud, D.T., "Pressurization Test Results: Bonneville Power Administration Energy Conservation Study," Report No. 10996, Lawrence Berkeley Laboratory, University of California, 1980.

[11] Stewart, M.B., Jacob, T.R., Winston, J.G., "Analysis of Infiltration by Tracer Gas Techniques, Pressurization Tests, and Infrared Scans," Owens Corning Fiberglas, Granville, Ohio, 1980.

[12] Warren, P.R., Webb, B.C., "Ventilation Measurements in Housing," CIBS Symposium, Natural Ventilation by Design, London, 1980.

[13] Sherman, M.H., Grimsrud, D.T., "Infiltration-Pressurization Correlations: Simplified Physical Modelling," ASHRAE Transactions, Vol. 86(II), 1980.

[14] Tamura, G.T., "Measurement of Air Leakage Characteristics of House Enclosures," ASHRAE Transactions, Vol. 81(I), 1975.

[15] Etheridge, D.W., "Crack Flow Equations and Scale Effects," Building and Environment, Vol. 12, 1977.

[16] Hopkins, L.P., Hansford, B., "Air Flow Through Cracks," Building Services Engineer, Vol. 12, 1977.

[17] deGids, W.F., "Problems and Consequences of the Pressurization Test for the Air Leakage of Houses," Air Infiltration Centre Symposium, Instrumentation and Measuring Techniques, Windsor, England, 1980.

[18] Standard Practice for Measuring Air Leakage by the Fan-Pressurization Method, Designation E 779-81, American Society for Testing and Materials.

[19] Sherman, M.H., Grimsrud, D.T., Sonderegger, R.C., "The Low Pressure Leakage Function of a Building," Reprt No. 9162, Lawrence Berkeley Laboratory, University of California, 1979.

[20] Card, W.H., Sallman, A., Graham, R.W., Drucker, E.E., "Infrasonic Measurement of Building Air Leakage: A Progress Report," in Building Air Change Rate and Infiltration Measurement, eds., Hunt, C.M., King, J.C., Trechsel, H.R., ASTM STP 719, American Society for Testing and Materials, 1980.

[21] Tamura, G.T., "The Calculation of Home Infiltration Rates," ASHRAE Transactions, Vol. 85(I), 1979.

[22] Grimsrud, D.T., Sherman, M.H., Blomsterberg, A.K., Rosenfeld, A.H., "Infiltration and Air Leakage Comparisons: Conventional and Energy Efficient Housing Designs," Report No. 9157, Lawrence Berkeley Laboratories, University of California, 1979.

[23] Grot, R.A., Clark, R.E., "Air Leakge Characteristics and Weatherization Techniques for Low-Income Housing," DOE/ASHRAE Conference on Thermal Performance of Exterior Envelopes of Buildings, Orlando, Florida, December 1979.

[24] Kronvall, J., Airtightness-Measurements and Measurement Methods, Report D8, Swedish Council of Building Research, Stockholm, Sweden, 1980.

Table 4.1

Leakage Distribution in Six Houses, from Tamura [14]

House #	Ceiling(%)	Walls(%)	Windows and Doors (%)
1	65	15	20
2	67	21	22
3	16	65	19
4	34	42	24
5	8	77	15
6	11	66	23

Figure 4.1

Comparison of Whole House Leakage

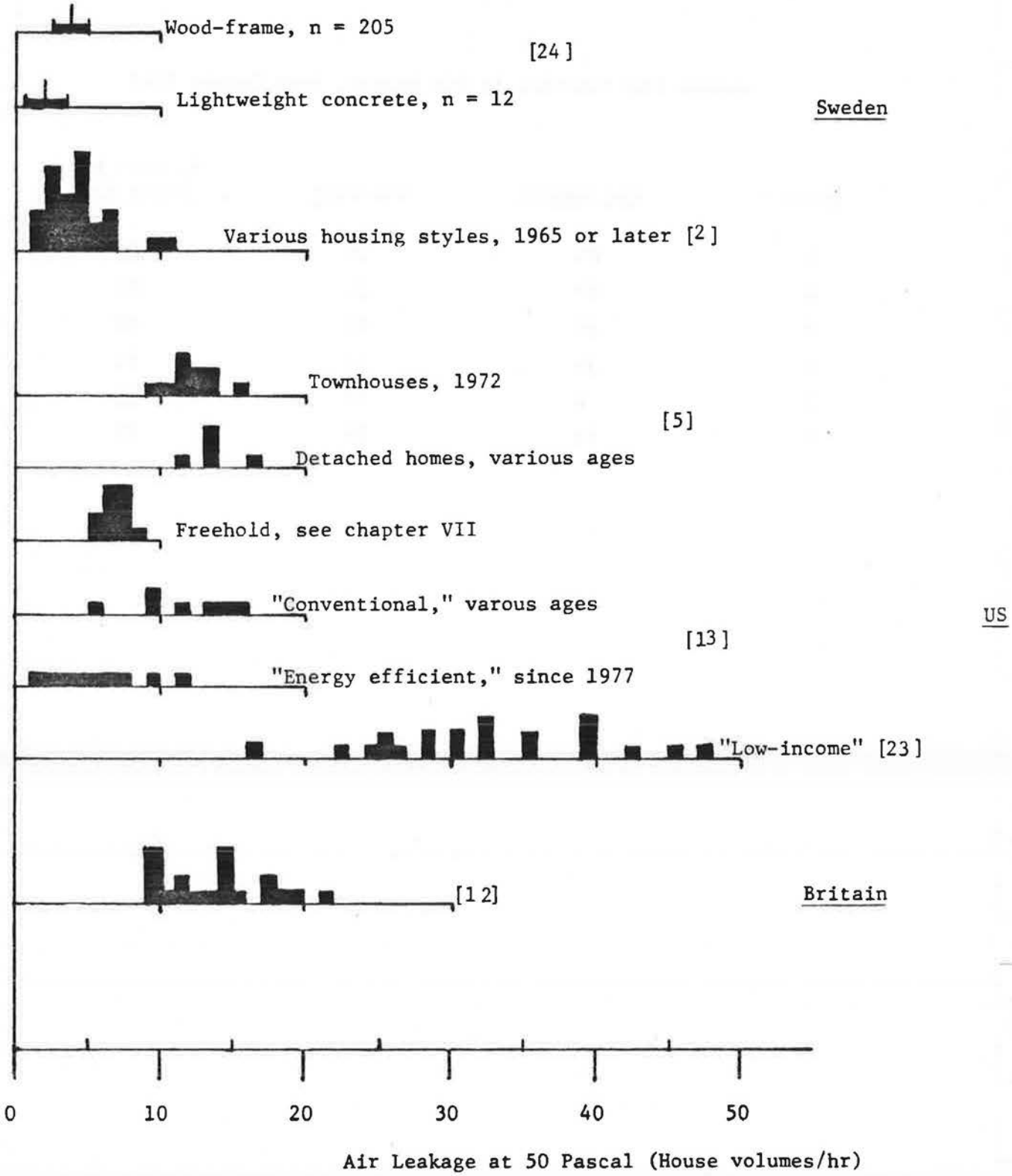

Chapter V

RELATING PRESSURIZATION TO INFILTRATION

Using tracer gas measurements of infiltration rates for evaluating the tightness of homes is expensive and time-consuming. Pressurization testing of homes is an alternative tightness check, but to be useful it must be related to natural infiltration rates. It may be difficult to establish this relation because of basic differences between the conditions during pressurization testing and the conditions induced by weather. The test pressures are large, constant and uniform as compared with those from weather which vary in time and position over the building envelope. Also, the location of leakage sites are important in determining air infiltration rates, and pressurization testing yields no information regarding this distribution.

Kronvall [1] suggests dividing models of the relation between pressurization and infiltration into "approximate" and "phenomenological" models. Approximate models are simplifications of a complete formulation of infiltration in a home. A detailed formulation is unusable because it requires many unknown inputs, but by making appropriate assumptions the model attains a useful form. Phenomenological models are based on less rigorous relations between pressurization and infiltration. In this chapter we present a general development of the infiltration-pressuriza-

tion relation, pointing out several sources of difficulty. A review of several models follow, with special attention paid to the assumptions made and attempts to validate the model in the field.

5.1 THE BASIC PROBLEM

Predicting the infiltration rate of a structure from the results of a fan pressurization test requires a physical model of air infiltration in buildings. Researchers use basically the same model, but they differ in the assumptions and the treatment of several unknowns. An infiltration model should predict a home's infiltration rate using the outside weather and the local terrain along with the building's geometry and leakage characteristics. The fan pressurization test is used to determine the leakage characteristics of the building.

Leakage Characteristics

The leakage characteristics of a building or a single opening relate the air flow through the opening(s) q to the pressure difference across the opening(s) Δp. These relations, discussed in chapter II, have the general form

$$q = f(\Delta p). \qquad (5.1)$$

There is a leakage function f for each opening in the shell of a building, although it may be difficult or impossible to determine. The leakage function for an entire building is the combination of the leakage for each opening in the shell. A common form used for the leakage function is

$$q = c\Delta p^n. \qquad (5.2)$$

To completely model the infiltration of a building one needs the leakage function for each opening.

Pressure Differences

Knowing the leakage characteristics for the openings in a building, one must then determine the pressure differences Δp acting across these openings. The pressure differences are induced by the wind, temperature differences and the action of mechanical ventilators. Weather induced pressure differences were discussed in detail in chapter II. The pressure distribution induced by the wind on the outside of a building is determined by the wind speed, wind direction, the building shape, and the objects surrounding the building. The pressure difference due to wind Δp_w at some location on the house is expressed in terms of the wind pressure coefficient C_p for that location, along with the inside and outside static pressures. A "stack" pressure difference Δp_s also exists when there is a temperature difference between the inside and outside.

Calculating the Flows

Knowing the leakage function for all the openings in the shell of a home and the pressure differences across these openings, one can calculate the flows through them. The only unknown in the problem is p_i, the static pressure at ground level within the house. This interior pressure adjusts itself to maintain a mass

balance of inward and outward flow. The difference between p_i and the outside pressure p_o depends on the wind and stack conditions along with the leakage distribution of the building.

In reality, the internal pressure distribution can be quite complex due to resistances to air flow between rooms and floors. Almost all infiltration models assume a house has no internal resistances so that the internal pressure at a height z is equal to $p_i - \rho_i gz$, where ρ_i is the internal air density and g is the acceleration of gravity.

To solve for p_i one may express the inflow q_i and the outflow q_o as integrals,

$$q_i = \int_S f(\Delta p)^+ ds \qquad (5.3A)$$

$$q_o = \int_S f(\Delta p)^- ds \qquad (5.3B)$$

The plus sign in equation (5.3A) means that only positive pressures are considered, i.e. if $\Delta p \leq 0$ then f=0. Similarly, the minus sign means that only negative values of Δp are considered. The integrals are computed over the surface of the building S. Both integrals may in theory be written as expressions in p_i. Flows due to mechanical ventilation also depend on p_i and may be written as q_{vo} and q_{vi}. q_{vo} is the outflow induced by mechanical means and q_{vi} is the inflow. Setting the mass flow in equal to the mass flow out,

$$\rho_o[q_i(p_i)+q_{vi}(p_i)] = \rho_i[q_o(p_i)+q_{vo}(p_i)]. \qquad (5.4)$$

Theoretically, equation (5.4) can be solved for p_i, whih can then be used to calculate the infiltration rate of the home.

This development could be used to calculate the infiltration rate of a building exactly if one knew the pressure difference and the leakage function for each opening. Of course, such detailed knowledge is impossible to obtain for a home in the field. To convert this formulation into a usable form, one must make assumptions concerning the leakage distribution and obtain values for the wind pressure coefficients. Also, the results from the pressurization test must be converted to a leakage function for the house. Several approximate models relating pressurization to infiltration have been developed which differ in the above respects.

5.2 APPROXIMATE MODELS

Table (5.1) summarizes several aspects of four approximate models of the relation between pressurization and infiltration. The second column describes the model developed by Warren and Webb of the Building Research Establishment in Great Britain [2]. In this model the pressurization data is fit to a curve of the form of equation (5.2), thus the flow exponent n is derived empirically. The measured leakage is assumed to be uniform over each surface, but may be distributed among the surfaces. The wind pressure coefficients are also assumed to be uniform over each surface and dependent on wind direction. No assumptions are made concerning the location of the neutral pressure level.

Warren and Webb compare calculated values and field measurements of nondimensionalized infiltration rates in the wind and stack regimes only. About fifteen homes of various ages and types were invloved in these validation tests. There is no distinction between the homes in the plots of calculated versus predicted infiltration, nor any information on the actual weather conditions or infiltration rates. The average of the predicted infiltration rates in the stack regime agrees with the average of the measured rates, but the individual predictions miss the measurements by ±15%. In the wind regime there is more scatter in the plot of measured versus predicted infiltration, on the order of ±30%, and a trend to overpredict by about 50%. The authors suggest that this overprediction is due to using wind pressure coefficients for isolated buildings. The homes in the experiments were sheltered by trees, fences and others structures. Warren and Webb reduced the wind pressure coefficients by 50% and obtained good average agreement in the wind regime. These problems of choosing appropriate values of wind pressure coefficients are indicative of the difficulties in obtaining values of C_p for homes in their particular wind environment.

Another pressurization-infiltration model was developed at the Lawrence Berkeley Laboratory as part of a long term study of pressurization and infiltration in homes [3-7]. This model, in the third column of table (5.1), also fits the pressurization data to equation (5.2). The curve is then used to predict the flow at Δp=4 Pa, and Q(4) is converted to an effective leakage

area A_o using the equation for the flow through an orifice, equation (2.11). Equation (2.11) is also used to determine the flows induced by the calculated pressure differences due to weather, thus n=1/2 in the model. The leakage coefficient A_o is determined using the 4 Pa flow because this pressure difference is closer to weather induced pressures and is therefore believed to be more realistic for quantifying the leakage of a home. But the 4 Pa flow is extrapolated out of range of the measured data and is therefore a questionable measure. The relative merits of the 4 Pa flow versus the more common 50 Pa flow rate have been discussed but never studied experimentally.

The LBL model assumes effects of wind direction are unimportant, and therefore neglects differences in leakage among the vertical surfaces. But, one still needs the leakage in the ceiling and floor. Also, the values of the wind pressure coefficients of the ceiling and floor are assumed equal to zero. This model requires a value for the height of the neutral pressure level and assumes it is approximately one-half of the building height. To use the LBL model, one must choose between five terrain classes and five shielding classes for the home in question to account for differences in these two factors.

The LBL model was tested on 15 homes. Each home was pressurized to find the effective leakage area A_o. The portion of this leakage in the ceiling and floor, along with the terrain and shielding classes, were estimated from inspections or descriptions of the homes. The average of the calculated infiltration

rates is close to the average of the measurements, but individual predictions are in error by as much as 50%. Most predictions are within ±25% of the measured rate, but some houses are consistently overpredicted and others underpredicted. Because the model averages out effects of wind direction, some of the predictive error may be due to directional effects. More recent validation work is showing that the LBL model predicts long term averages of infiltration better than short term values because over the long term wind direction becomes less important.

The next model in table (5.1) was developed by Tamura of the National Research Council of Canada [8] and is based on research done with Shaw and Wilson on two single-story homes [9-12]. The leakage of the homes was characterized by a single pressurization measurement at 75 Pa and the flow exponent n is set equal to 0.65. The distribution of leakage is assumed uniform and both the location of the neutral pressure level and the value of the wind pressure coefficient are based on measurements on the two houses.

Tamura checked the model's predictions against measured infiltration rates for the same houses used to develop the infiltration expressions. The measurements in the stack regime are within 25% of the predicted ventilation rates. The wind expression underpredicts, by as much as 50%, especially at low wind speeds. The model has not been tested on any houses besides those used to develop the predicitve expressions.

Recent work at the British Gas Corporation by Etheridge and Alexander has produced an infiltration model which includes several effects which are usually ignored [13]. First, this model treats the building as many cells instead of ignoring internal partitions. Also, it includes ventilation arising from turbulent flow reversals caused by the turbulent nature of the wind. The leakage characterization of the building employs the dimensionally homogeneous flow equations discussed earlier (see equation 2.11) [14]. This model considers three types of openings in characterizing the leakage of a building. "Purpose-provided" openings such as vents are assumed to have a constant discharge coefficient C_D. The second type of opening, "component cracks," are identifiable openings in doors and windows. All remaining leakage sites are classified as "background leakage." For flow through the last two types of openings, C_D depends on the Reynolds number and the ratio of the distance through the crack and the hydraulic diameter as discussed in chapter IV. Expressions relating C_D to Re and the above ratio describe steady flow through component cracks quite well, but are less accurate for background leakage due to its greater complexity.

The flow equations for a building can be determined from the geometry of the cracks, but greater accuracy results from using a pressurization test. Etheridge and Alexander used pressurization tests to determine the flow equations for purpose-provided openings and component cracks in a home used to validate their model. Determining the flow equations for background leakage is more

difficult. A pressurization test was carried out on each room, but this leakage had to be broken down into the proportions leaking into the adjacent volumes. The proportions were found indirectly by trying several distributions consistent with the pressurization measurements and using actual infiltration measurements to determine the most appropriate distribution. Etheridge and Alexander acknowledge the need for a more direct method. They point out that all distributions considered yield the same whole house pressurization test results, but different infiltration predictions. Thus, predictive methods considering only whole house leakage are neglecting important information.

This formulation is unique in including the effects of the fluctuating component of the wind pressure by making assumptions about the form of the fluctuating component of pressure. Despite the unknown aspects of fluctuating pressure differences, this first effort to include them in a whole-house infiltration model is encouraging. This model was tested on one relatively leaky home with eleven cells. The external pressure distribution due to wind was determined from a wind tunnel model carefully constructed to properly scale the turbulence. The predicted and measured infiltration rates for the whole house agree within roughly 25%. The multi-cell approach permits the prediction of infiltration rates for individual rooms. These results, while worse than the whole-house predictions, are unique.

The four models discussed above are approximations to a complete development of the relation between infiltration rates and

pressurization tests. Tamura's and Etheridge and Alexander's models have been developed from and for test homes, and cannot be applied to other buildings. Tamura's is unusual in requiring only a single pressurization measurement at a large pressure difference of 75 Pa. Using the leakage at such a large pressure difference may be unrealistic. The researchers at LBL believe that pressurization test results at lower pressures are still unrealistic and therefore they extrapolate their results to obtain the flow at 4 Pa. Using the 4 Pa flow rate to quantify the leakage of a home is also questionable since 4 Pa is out of range of the pressurization measurements.

The models include various amounts of detail on the leakage distribution. Etheridge and Alexander are the most detailed in considering three types of openings and pressure testing each room separately. Warren and Webb divide the leakage among the walls, ceiling and floor, but keep it uniform over each surface. LBL assumes the leakage in the vertical walls to be uniformly distributed among them. Neither LBL nor Warren and Webb propose straightforward means for determining this leakage distribution.

5.3 PHENOMENOLOGICAL MODELS

The approximate models are based on a complete formulation of air infiltration in homes which is too complex to use. To convert the complete formulation to a simpler form one makes assumptions, estimations and/or measurements concerning the leakage distribution, the relation of weather to pressure differences,

and the use of pressurization test results to calculate infiltration rates. Rather than beginning with a complex model and making simplifications, some researchers have chosen simple approaches to relating pressurization and infiltration. Several of these approaches are outlined below.

Kronvall of the Lund Institute of Technology in Lund, Sweden has developed a simple relation between pressurization test results and infiltration rates [1]. For the home under study, two pressurization tests at 25 and 50 Pa are made and fit to equation (5.2) to obtain values of C ($m^3/hr\text{-}Pa^n$) and n. Then two infiltration measurements are made on the home under winter and summer weather conditions and the constants C_1 and C_2 are determined in the following expression

$$I = C(C_1 \Delta T + C_2 u^2)^n. \qquad (5.5)$$

It is assumed that equation (5.5) can be used to predict infiltration rates for the house. Kronvall tested the approach in the field on nineteen one and one-half story homes. The values of C_1 and C_2 were obtained for each house and then averaged for all nineteen. The resultant expression to predict infiltration is

$$I = C(0.026 \Delta T + 0.010 u^2)^n. \qquad (5.6)$$

Infiltration rates calculated using equation (5.6) were compared with measured rates in the nineteen homes used to obtain the expression, and of course the average of the calculated and measured infiltration rates were close to each other. But the plot

of measured versus calculated infiltration shows considerable scatter, on the order of ±25% with some calculated rates 100% higher than the corresponding measurement.

Shaw of the National Research Council of Canada has developed another simple model from tests on two electrically heated, 2-story homes with the same floor plan [15-16]. Each house was pressure tested and the results were fit to a variation of equation (5.2),

$$\hat{q} = \hat{c}S\Delta p^n, \tag{5.7}$$

where $\hat{q}$ is in l/s (liters per second), $\hat{c}$ is in l/s-m^2-Pa^n and S is the surface area of the building envelope. The two test homes were relatively tight, having flow rates of about 6 exchanges per hour at 50 Pa. The values of $\hat{c}$ were found to be 0.110 for one house and 0.075 for the other. Both homes were found to have n equal to 0.71. Two additional homes tested by Shaw and Tamura [16] also had n = 0.71. The fact that all four homes had the same value of n is quite suprising.

Shaw examined measured air infiltration rates for the two houses in the wind, stack and combination regimes. The following expressions for the infiltration I were developed,

Stack
$$I = 0.32(S/V)\hat{c}(\Delta T)^n \tag{5.8}$$

Wind blowing from exposed side
$$I = 0.42(S/V)\hat{c}u^{2n} \tag{5.9}$$

Wind blowing from shielded side
$$I = 0.76(S/V)\hat{c}u^n \tag{5.10}$$

Combination $I = 4.53(S/V)\hat{c}$ (5.11)

Note that when both wind and stack effects are important, the data are best fit by a constant infiltration rate.

Shaw used these expressions to predict infiltration rates for 25 other relatively tight homes and compared these predictions with actual measurements. The calculated and predicted rates agree within roughly ±25%, but all the infiltration rates were very low, 0.1 X/hr or less. This range of infiltration rates is unique to very tight homes, and it is not clear how well this model would predict for leakier homes.

5.4 NONPRESSURIZATION MODELS

There are infiltration models which treat the leakage characteristics as given and therefore do not require a pressurization test. The model developed by the Institute of Gas Technology [17-18] assumes a form for the leakage function of a building and compares the output of the model to measured infiltration rates. From this comparison they calculate a permeability coefficient for the house in units of flow over pressure difference per length of measured crack. The measured crack length includes only obvious openings such as windows and doors, and neglects other obscure but important openings in the shell.

The infiltration models of Nylund [19], de Gids [20] and Jardinier [21] are other models of infiltration which make predictions without the input of a pressurization test. Nylund's model is unusual in that he considers mechanical ventilation in

detail because Swedish homes generally use more mechanical ventilation then U.S. homes. Most models treat such ventilation as a constant, but Nylund includes the dependence of this ventilation on the pressure difference across the fan and the fan setting. Of course, such specific knowledge for a fan installed in the field is just as hard to find as it is for other leaks in a home.

5.5 A SIMPLE RELATION BETWEEN PRESSURIZATION AND INFILTRATION

In earlier chapters we discussed the use of pressurization testing to evaluate and compare the tightness of houses through the 50 Pa flow rate. Figure (5.1) shows a plot of measured infiltration rate I against 50 Pa leakage in exchanges per hour Q for a large variety of homes. The data set includes twenty-six Swedish homes [22], fourteen homes in Freehold from chapter VIII, and other homes in the Princeton area. The infiltration rates were measured under different weather conditions for each house, and some houses have more than one measurement of I. The house denoted by F was tested under three different tightness conditions. The least squares fit to the data is $I = Q(X/hr)/18 - 0.08$ with $r^2=0.77$. Figure (5.2) shows the same infiltration rates plotted against the 50 Pa flow rate in m^3/hr divided by the envelope area of the house in m^2. One might expect this second predictor to work better because it accounts for the surface to volume ratio, but no improvement of fit is evident. The least squares fit to these data is $I = Q(m^3/hr\text{-}m^2)/28 + 0.002$ with $r^2=0.72$. While our data set is

limited, the 50 Pa flow rate is definitely related to natural infiltration rates. The scatter about the regression lines, on the average ±30%, is on the same order as the scatter exhibited by the predictive models of infiltration discussed earlier. Using the 50 Pa flow rate to predict infiltration yields only one value of a quantity which varies with weather and there is significant spread in the data, but this estimate may be adequate for some purposes.

5.6 DISCUSSION

Six models relating pressurization to infiltration have been discussed above. Two of these, Etheridge and Alexander's and Tamura's, are specific to the test homes studied and cannot be used for other homes. One may ask how the predictions of the other four models compare when applied to the same home. These calculations were made for a house with a square base of 75 m^2 and a height of 6 m. The volume is 450 m^3 and the envelope area is 283 m^2. The 50 Pa flow rate is 8 exchanges per hour, and the flow exponent n equals 0.7. Table (5.2) shows the predicted infiltration rates for three conditions of weather: (1) u=5 m/s, ΔT=0 °C; (2) u=2.5 m/s, ΔT=10 °C; and (3) u=0 m/s, ΔT=20° C. Also included in this table are the predicted infiltration rates from the least square fits to the data in figures (5.1) and (5.2). From this table, we see that the models make very different predictions of infiltration. The Kronvall and LBL model are less variable over the three types of weather than the other models.

The means of the three infiltration rates for each model are close to that obtained from the linear fit to figures (5.1) and (5.2). Kronvall's predictions are lower than the rest, possibly because it was developed from data on very tight Swedish homes.

The four models included in table (5.2) predict very different infiltration rates and it is not clear why. There are many differences in how the models deal with unknown leakage distributions, and with the pressures induced by the wind. The models are also different in how they use the results of a pressurization test to characterize the leakage of a home. Different assumptions about leakage distributions are made and we really do not know which work best. The models have different sources for their values of the wind pressure coefficients, and some allow one to input their own values. More measurements of C_p are needed on homes to determine the effect of wind direction and shielding by trees and other objects. It is not even clear how sensitive infiltration rates are to changes in C_p due to shielding.

Validation tests in real homes are the best way to test and develop these models. All six of the models mentioned above have been validated in some homes, though Etheridge and Alexander consider only a single home which they studied in detail. Tamura and Kronvall tested their models in the same houses used to develop their model. Shaw, LBL and Warren and Webb tested their predictive abilities in a wide variety of homes. Shaw considered 25 tight homes in Canada and Sweden of several different housing styles, with no mention of age. The 15 homes tested by LBL were

also variable in age, volume, number of stories, heating system and whether there is a basement of not. Warren and Webb also considered homes of various ages and housing types. There is significant scatter in the plots of predicted versus measured infiltration rates for all the models. This scatter is due to both the shortcomings of the models and variations due to differences in the homes tested. The two effects should be studied separately through experiments which test one model on a wide variety of housing types to study the differences in houses. Experiments are also needed which test many models on one or more identical homes. Both kinds of test will improve our understanding of the relation between pressurization and infiltration.

REFERENCES

[1] Kronvall, J., "Correlating Pressurization and Infiltration Rate Data - Tests of an Heuristic Model," Lund Institute of Technology, Division of Building Technology, Lund, Sweden, 1980.

[2] Warren, P.R., Webb, B.C., "The Relationship Between Tracer Gas and Pressurization Techniques in Dwellings," First Symposium of the Air Infiltration Centre, Windsor, England, 1980.

[3] Sherman, M.H., Grimsrud, D.T., "Measurement of Infiltration Using Fan Pressurization and Weather Data," First Symposium of the Air Infiltration Centre, Windsor, England, 1980.

[4] Grimsrud, D.T., Sherman, M.H., Diamond, R.C., Condon, P.E., Rosenfeld, A.H., "Infiltration-Pressurization Correlations: Detailed Measurements on a California House," ASHRAE Transactions, Vol. 85(I), 1979.

[5] Grimsrud, D.T., Sherman, M.H., Diamond, R.C., Sonderegger, R.C., "Air Leakage, Surface Pressures and Infiltration Rates in Homes," Report No. 8828, Lawrence Berkeley Laboratory, University of California, 1979.

[6] Sherman, M.H., Grimsrud, D.T., Diamond, R.C., "Infiltration-Pressurization Correlation: Surface Pressures and Terrain Effects," ASHRAE Transactions, Vol. 85(II), 1979.

[7] Sherman, M.H., Grimsrud, D.T., "Infiltration-Pressurization Correlation: Simplified Physical Modeling," ASHRAE Transactions, Vol. 86(II), 1980.

[8] Tamura, G.T., "The Calculation of Home Infiltration Rates," ASHRAE Transactions, Vol. 85(I), 1979.

[9] Tamura, G.T., Wilson, A.G., "Air Leakage and Pressure Measurements on Two Occupied Houses," ASHRAE Transactions, Vol. 70, 1964.

[10] Tamura, G.T., "Measurement of Air Leakage Characteristics of House Enclosures, " ASHRAE Transactions, Vol. 81(I), 1975.

[11] Tamura, G.T., Shaw, C.Y., "Studies on Exterior Wall Tightness and Air Infiltration of Tall Buildings, " ASHRAE Transactions, Vol. 82(I), 1976.

[12] Shaw, C.Y., Tamura, G.T., "The Calculation of Air Infiltration Rates Caused by Wind and Stack Action for Tall Buildings, " ASHRAE Transactions, Vol. 83(II), 1977.

[13] Etheridge, D.W., Alexander, D.K., "The British Gas Multi-Cell Model for Calculating Ventilation," ASHRAE Transactions, Vol. 86(II), 1980.

[14] Etheridge, D.W., "Crack Flow Equations and Scale Effects, " Building and Environment, Vol. 12, 1977.

[15] Shaw, C.Y., "A Correlation Between Air Infiltration and Air Tightness for Houses in a Developed Residential Area, " Draft submitted to ASHRAE Semi-annual meeting, Cincinnati, Ohio, June 1981.

[16] Shaw, C.Y., Tamura, G.T., "Mark XI Energy Research Project, Air-Tightness and Air-Infiltration Measurements, " Building Research Note, No. 162, Division of Building Research, National Research Council of Canada, 1980.

[17] Macriss, R.A., Cole, J.T., Zawacki, T.S., Elkins, R.H., "An Air Infiltration Model for Modern Single Family Dwellings," Paper No. 79-14.5, 72nd APCA Annual Meeting, Cincinnati, Ohio, June 1979.

[18] Cole, J.T., Zawacki, T.S., Elkins, R.H., Zimmer, J.W., Macriss, R.A., "Applications of a Generalized Model of Air Inifltration to Existing Homes," ASHRAE Transactions, Vol. 86(II), 1980.

[19] Nylund, P.O., Infiltration and Ventilation, Swedish Council of Building Research, D22, 1980.

[20] de Gids, W.F., "Calculation Method for the Natural Ventilation of Buildings, " in Indoor Climate Systems and Installations, 7th TNO/TVVL Seminar, TNO Research Institute for Environmental Hygiene, Delft, Netherlands, 1977.

[21] Jardinier, P., "Ventilation and Permeability of Dwellings, " Cahiers Techniques du Batiment, No. 27, 1980.

[22] Kronvall, J. "Testing of Homes for Air Leakage Using a Pressure Method," ASHRAE Transactions, Vol. 84(I), 1978.

Table 5.1

Comparison of Pressurization-Infiltration Models

	Warren/Webb	LBL	Tamura	Etheridge/Alexander
Pressure Test	Several measurements from 10 to 60 Pascals	Several; 10 to 60 Pa	Single: 75 Pa	Pressure test of each room
Exponent n.	Empirical	Empirical n to get Q(4), then n=½ to determine infiltration	0.65	Alternative flow
Leakage Distribution	Ceiling, floor and each wall	Ceiling, floor and total of all walls	Uniform	Very detailed
Wind Pressure Coefficients	Uniform over each surface, dependent on wind direction	Values for walls averaged over all wind directions, zero for ceiling and floor	Based on measure-ments	Based on wind tunnel model of test house
Neutral Pressure Level	Not required	Assumed close to one-half building height	Based on measure-ments	Variable neutral zone in each cell

Table 5.2 Comparison of Predictions on Sample House

Wind Speed (m/s)		5	2.5	0	
Temperature Difference (°C)		0	10	20	
Model					**Mean**
Warren and Webb		.69	.29	.42	.47
LBL		.45	.35	.38	.39
Kronvall		.20	.21	.33	.25
Shaw	Exposed .58	Shielded .34	.68	.38	.50

Curve fit to figure (5.1) .36

Curve fit to figure (5.2) .46

Figure 5.1

Infiltration Rate vs Leakage at 50 Pascal

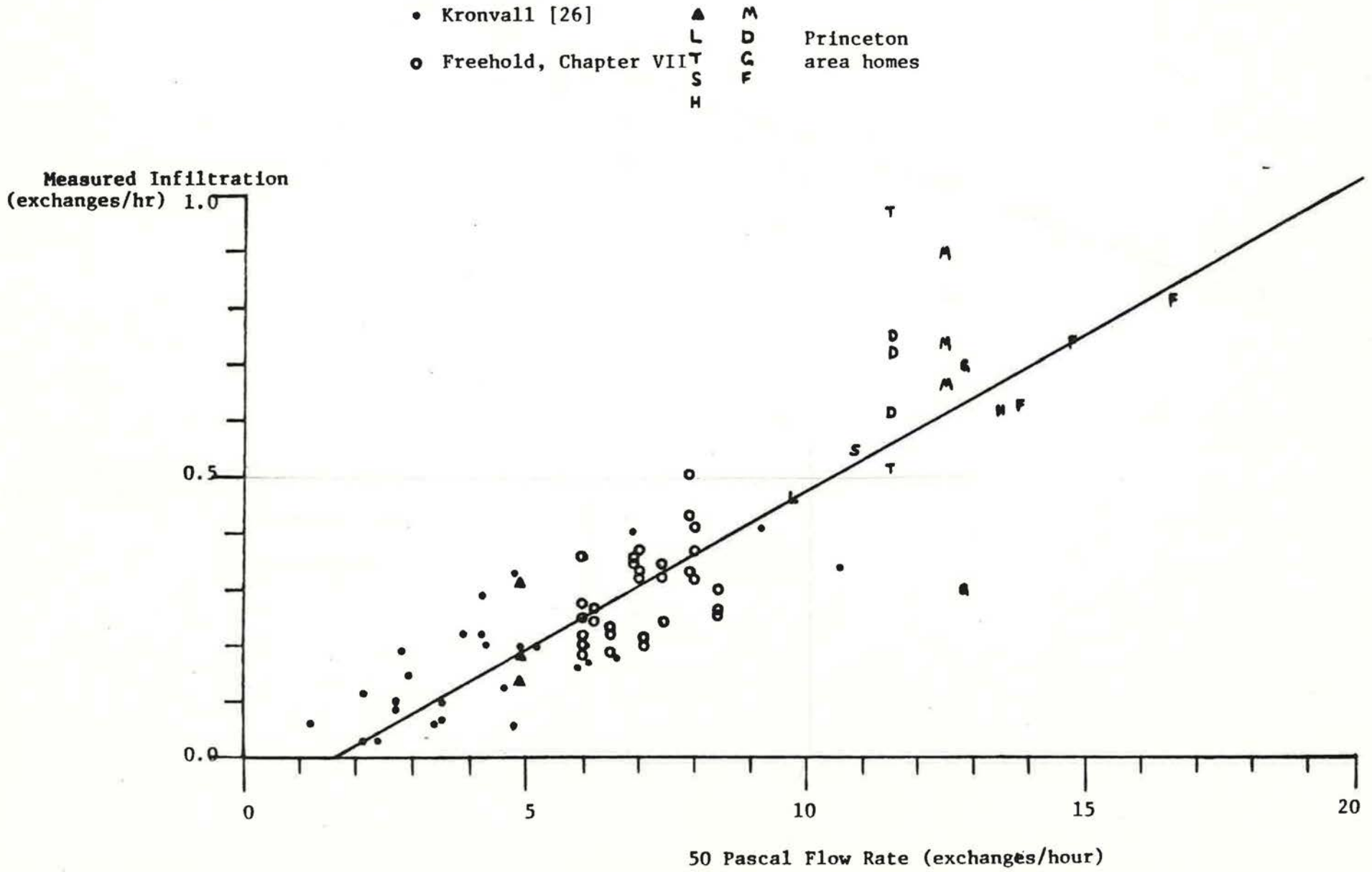

Figure 5.2

Infiltration Rate vs Area-Specific Leakage at 50 Pascal

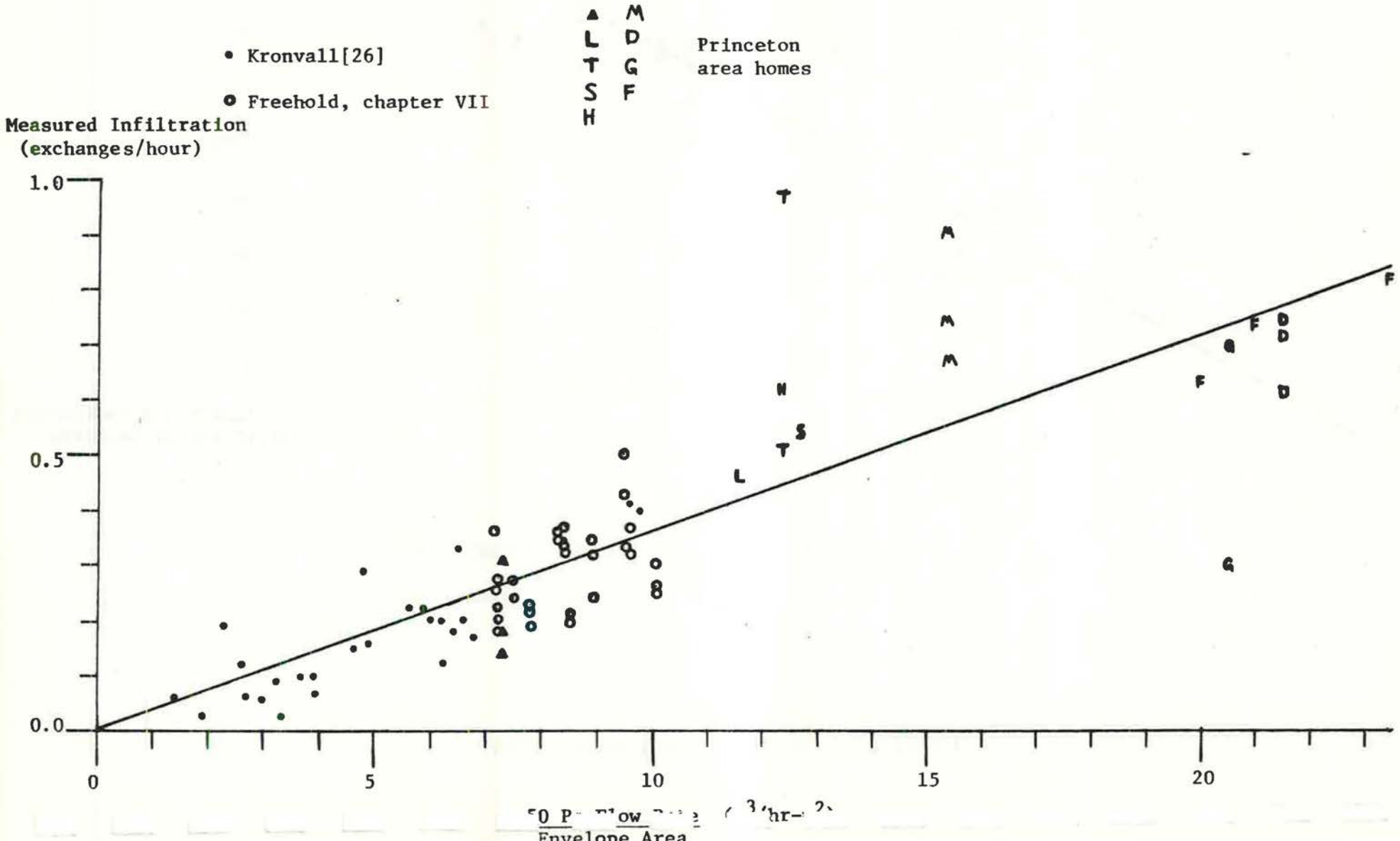

CONCLUSIONS OF BACKGROUND SECTION

We have reviewed the background and the present state of the art of tightness evaluation of bomes in the last four chapters. Chapter II's discussion of the physics of air infiltration showed that the pressure differences induced by the wind and inside-outside temperature differences are on the order of 1 to 5 Pa, possibly as high as 10. The leakage functions which describe the flow induced by these pressure differences through the shell of a home depend on the geometry of the individual openings. Because each opening is different and there are so many, one can not expect to determine the leakage function of an entire home from consideration of each opening.

Chapter III presented the technique of tracer gas measurement of infiltration rates as a means of evaluating the tightness of a home. Tracer gas measurement involves expensive and sophisticated equipment, and requires care to avoid errors due to imperfect mixing of the tracer gas within the house. But characterizing the leakiness of a house through this technique requires many measurements under different weather conditions and this increases the time and expense of such an evaluation. Also, as we will see later, the tightness of homes changes significantly over time periods on the order of months and it takes this long to obtain a good variety of weather conditions. In order to avoid the disadvantages of tracer gas testing, an alternative technique of tightness evaluation has been developed. This technique of pres-

surization testing was described in chapter IV. While pressure testing a home is indeed fast and inexpensive, there are problems in relating the test results to infiltration rates under natural conditions. Basically, the test conditions and those induced by weather are very different. The test pressures range from 10 to 100 Pa, and are constant in time and uniform in position. Weather induced pressure differences are much smaller and they vary in both time and position on the building surface. Also, pressurization testing gives no information on the distribution of leakage around the shell, and this distribution is important in determining the infiltration rate of a house. Pressurization could also be used as a building tightness standard, but it does not take into account effects of shielding on infiltration. Two homes with the same leakage rate but different wind exposures will have different infiltration rates under the same weather conditions. In addition to these problems, little attention has been paid to the accuracy and repeatability of pressurization test results in homes. Thus, there are well founded questions about the interpretation of a pressurization test and the relation to infiltration rates.

Chapter V reviewed models to predict infiltration rates from the results of pressurization testing and knowledge of building geometry and weather. A general development of the relation pointed out the need for several inputs and assumptions to make any model usable. One must input the leakage distribution of the home and the values of the wind pressure coefficients to relate

the wind speed to the induced pressures. Also, some relation between the flow and the calculated pressure differences must be derived from the results of the pressurization test. Different choices of these inputs and assumptions are used in the pressurization-infiltration models. It is impossible to tell which models work best because the attempts to validate the models have been on a wide variety of homes with no consideration given to the effects of housing style and age on infiltration. More research needs to be done on these pressurization-infiltration models to study separately the predictive ability of the models and the effects of housing style, construction materials and age on the pressurization-infiltration relation.

SECTION TWO

EXPERIMENTAL SECTION

The next four chapters present experimental work answering several questions raised in the previous section on background. These questions concern the use of pressurization as a tightness check on homes, and the relation of pressurization to infiltration rates under natural conditions. We have discussed the use of the Blower Door and other pressurization devices for the evaluation of tightness in homes. We have mentioned the lack of research into the accuracy and repeatability of Blower Door measurements, along with a need to study the effects of weather on the test results. Chapter VI presents experimental work designed to answer the question of how reproducible are pressurization test results and how are they affected by weather. In this and later chapters we compare the relative appropriateness of the 4 and 50 Pa flow rates for characterizing the leakiness of a building. Our results in chapter VI show that the 50 Pa flow rate is reproducible within 1 or 2%, and the 4 Pa flow within 5 or 6%. The wind speed during the test may affect the 50 Pa flow for speeds greater than 2.5 m/s, with the largest error induced by the wind on the order of 15%. We also found that the leakage of a home, as measured by pressurization, varies over the year as the moisture content of the air, and hence the wooden building materials, changes.

Chapter VII answers the question of whether pressurization test results can indeed be used to predict infiltration rates for a simple and well-controlled building. The experiments presented in this chapter study the pressurization-infiltration relation in a very simple structure for which we know the location of all the leakage. Pressurization tests were conducted to determine the leakage functions of the building in three conditions of tightness, and natural infiltration measurements were made under a variety of weather conditions. The pressure differences across the leakage sites were calculated from the weather and used in the measured leakage functions to calculate the infiltration rates. These calculated rates are compared to the measured rates and the agreement is quite good except for cases in which the wind blows parallel to the openings in the test structure.

In chapter VIII we deal with some of the shortcomings of past attempts to validate pressurization-infiltration models. As mentioned earlier, these models have been tested by their developers on many different homes with variable housing styles and ages. There is a need for more systematic validation of pressurization-infiltration models involving two types of tests. First, the various models' predictive abilities should be compared on one or more identical homes. Next, one model's predictions should be compared with measured infiltration rates on many different types of homes to study the effect of housing style, construction material and age on the relation of pressurization to infiltration. Chapter VIII presents experiments of the first type on fourteen

identical homes in Freehold, New Jersey. This experiment is exceptional also because the infiltration rates were measured simultaneously in all the homes to eliminate the effects of variation due to weather.

The last chapter of experimental work, chapter IX, anticipates the situation when we are able to determine that a home is too tight. In such cases, we need to ensure safe levels of indoor air quality. One may reconcile the apparently conflicting goals of saving energy through infiltration reduction and maintaining a healthy indoor environment through the use of mechanical ventilation with heat recovery, or air-to-air heat exchangers. As air-to-air heat exchangers are being developed, there are important questions on how to test the performance of these devices. In chapter IX we present a careful, experimental evaluation of one particular air-to-air heat exchanger. This device was tested in the same experimental building used in chapter VII and it was found to recover about 50% of the heat loss associated with the induced ventilation. Our careful studies of this air-to-air heat exchanger with it operating in a building revealed facets of its performance that would have been overlooked in laboratory tests.

Chapter VI

REPEATABILITY AND ACCURACY OF THE BLOWER DOOR

The Blower Door [1], and other pressurization devices, have been used for checking the tightness of homes for several years, and may be used as a standard for tightness. But questions exist concerning the repeatability of pressurization test results, and the effects of weather on the test results. In order to answer these questions a home in the Princeton area, the so-called BRAT house, was pressure tested about once a week for a year. Along with the above questions of repeatability and weather effects, we measured the distribution of leakage in the house and examined whether this distribution changes with pressure difference.

6.1 LEAKAGE DISTRIBUTION

The existing measurements of leakage distribution reviewed in chapter IV were made at 50 Pa with little indication of how they might vary with pressure difference. The leakage distribution of the BRAT house was measured at several pressure differences. The leakage of this two-story, wood frame building was divided between "vents" (fireplace, kitchen exhaust fan, and the furnace and water heater flues), windows and background. The house was first pressure tested with all windows closed and the vents in their normal state. The vents were then sealed and the tests re-

peated. The house was also tested with the primary windows open and the storm windows closed, and then with the storms open and the primaries closed. From the test results we determined the leakage distribution.

The results of these tests are presented in table (6.1). The percentage of leakage due to the three sources is given for both pressurization and depressurization at pressure differences of 12.5, 25, 37.5 and 50 Pa. The vents constitute about 5% of the leakage and the windows about 10%. This fraction of whole house leakage due to windows is similar to the percentages found by others as reported in chapter IV. The remaining background leakage of the BRAT house is about 85% of the total. We solved for the leakage distribution separately at each of the pressure differences and found no significant variation in the leakage distribution with pressure difference, nor any difference between pressurization and depressurization.

6.2 ACCURACY OF THE RESULTS

As the use of the Blower Door and other pressurization devices is expanding, we still do not know how repeatable are the measurements from a Blower Door, nor how the test results are affected by the outside weather during the test. To answer these questions about pressurization testing, experiments were performed on the BRAT home beginning in October of 1980. Blower Door tests were made on this house about once a week, and the results examined for repeatability and weather effects. The experiment is described in more detail in appendix E.

One source of inaccuracy for the Blower Door is error in the calibration which yields the volumetric flow rate through the fan as a function of the inside-outside pressure difference and the fan RPM [1]. This calibration is accurate within about 10%, with the largest uncertainties at low flow rates. The Blower Door was calibrated at only one air density and appendix C presents our calculation of a density correction. A new and more accurate calibration technique is necessary to verify the density correction. In the BRAT tests, the present Blower Door calibration is assumed to be correct and no density corrections are made except where noted.

We first considered the effects of weather, particularly wind, on pressurization test results. Operating a Blower Door is difficult under windy conditions because of wind induced pressures. Also, the turbulent nature of the wind causes the inside-outside pressure difference to fluctuate during the test. It is very difficult to induce a stable pressure difference with which to associate a fan RPM. Shielding the outside pressure tap is inadequate because the wind also interacts with the fan, affecting the flow rate. One could use inlet and exhaust ducts, but such an addition will reduce the flow capacity and increase the size and weight of the device, thus eliminating the Blower Door's advantage of being portable.

To study the effects of the wind on Blower Door tests, the local wind speed was recorded during each test. Figure (6.1) is a plot of the measured flow rate with the house pressurized to

50 Pa against the average wind speed during the test. Only tests done in 1980 are included because of changes in the home's tightness over time. The insert in this graph shows the same points plotted on a scale that contains the origin. As the local wind speed increases above 2.5 m/s the scatter in the data increases. Below this wind speed, the flow rate is relatively constant. Tests at wind speeds greater than or equal to 2.5 m/s lie in a region bounded below by the flow rate at low wind speeds. The upper bound of this region increases with the wind speed. Tests on windy days yield results both consistent with and significantly higher than tests under calm conditions because of the intermittancy of wind effects.

On days with high average wind speeds, the wind is not constantly strong; there are calm periods. Tests during these calmer periods do not exhibit the errors that exist when the wind blows strongly. The three tests conducted on the day with u=4.9 m/s in figure (6.1) are examples of this effect. Two of the tests have the same 50 Pa flow as the calm wind tests while one of the points is about 15% higher. The fact that wind effects on Blower Door tests are intermittent makes a meaningful wind correction improbable. The average of the predicted pressurization and depressurization flows at 4 Pa, $\bar{Q}(4)$, is plotted against wind speed in figure (6.2). The 4 Pa flows exhibit proportionally more scatter than the 50 Pa flows, but there is little systematic variation with the wind speed. The effect of wind direction on Blower Door test results was also considered, but no relation was evident.

From consideration of the plots of flow rate versus wind speed, we call tests with local winds less than 2.5 m/s calm. Winds equal to 2.5 m/s and not blowing into the front door in which the Blower Door is installed are also considered calm. Calm conditions occur at meteorological wind speeds less than about 6 m/s as measured by the U.S. Weather Service in Newark, New Jersey. Our "cutoff" speed is a local wind speed and is close to the ASTM recommendation of 2.2 m/s [2].

By considering only the calm tests in 1980, we can determine the variation in Blower Door results due to the instruments and the operator. Table (6.2) summarizes the variation of the measured flows and the flows calculated from curve fits to the test data for the calm tests in 1980. Means, standard deviations and their ratios are listed for the calculated flows at 4 and 50 Pa and the measured flows at 50 Pa for both pressurization and depressurization. The same quantities are given for the flows as calculated from all points together. Table (6.2) also includes the average of the pressurization and depressurization flows at 4 Pa. All of the 4 Pa flows have standard deviations of about 30 or 40 m^3/hr, about 5% of the mean. The 50 Pa flow rates have standard deviations from 40 to 80 m^3/hr, only 1 or 2% of the mean flows. Thus, the 50 Pa flow rate is more well defined than the extrapolation to 4 Pa.

One may also compare the stability of the 4 and 50 Pa flows by relating the flow coefficient C in $m^3/hr\text{-}Pa^n$ to the flow exponent n from curve fits to the pressurization data. Figure (6.3) is a

plot of C versus n for the pressurization curves of all the 1980 tests. The calm wind points lie very close to a straight line. Some of the windy points lie close to the line while others do not, and again we see the intermittancy of wind effects on the Blower Door.

Each point in figure (6.3) represents the curve fit to a pressurization test, and the leakage of a home is characterized by this family of curves. One may consider three points along the line in figure (6.3) which cover the range of calm test data,

$$Q_A = 283\Delta p^{.66} \qquad (6.2A)$$

$$Q_B = 252\Delta p^{.69} \qquad (6.2B)$$

$$Q_C = 220\Delta p^{.72}. \qquad (6.2C)$$

By setting pairs of these equations equal to each other, one finds the pressure difference at which they intersect. Q_A equals Q_B at a pressure difference of Δp = 49 Pa, $Q_B = Q_C$ at Δp = 93 Pa, and $Q_A = Q_C$ when Δp = 67 Pa. Thus, these curves intersect at about 70 Pa and the differences between the curves is minimized at large pressure differences. For Δp = 50 Pa, the average of the three flows is 3723 m^3/hr with a standard deviation of 38 m^3/hr, i.e. 1.0% of the mean. For Δp = 4 Pa, the mean of the three flows is 653 m^3/hr with a standard deviation of 55 m^3/hr or 8.4% of the mean flow. The flow extrapolated down to 4 Pa has a larger variation and is therefore less well suited as a measure for the leakiness of a home. The larger uncertainties in the

4 Pa flow rates is expected since it is an extrapolation out of the range of the actual measurements.

6.3 LEAKAGE IS SEASONAL

A distinction has been made between the 1980 and 1981 Blower Door tests on the BRAT house because of changes in the tightness of the house over time. One sees this change in figure (6.4) which shows the measured pressurization flow at 50 Pa plotted against the Julian date. The flow rate is roughly constant during most of 1980, although the lack of calm wind conditions during the last 60 days of the year obscure any changes. But during early 1981 the flow rate at 50 Pa is about 22% larger than it was in 1980. Around day 100, the flow begins to decrease as the house retightens. The last six points in 1981 are about 10% too high due to problems with the digital tachometer of the Blower Door. The 4 Pa flow rate exhibits the same seasonal variation, but because of the larger variation in the 4 Pa flows the changes are less striking. The maximum 4 Pa flow in 1981 is about 25% higher than the 1980 levels.

Contraction and expansion of building materials due to temperature alone is too small to account for the changes in the home's tightness. Instead, the change is believed to be caused by effects of moisture on the building materials. During winter weather the cold outside air does not hold much water and the wood in the structure dries and shrinks. This shrinkage increases the leakage area and hence the flow through the shell at a

given pressure difference. During the spring, warmer air and rain provide the structure with a moister environment. The wood absorbs the water and swells to close the openings in the shell.

Figure (6.5) is a plot of five day averages of the daily specific humidity against Julian date. The specific humidity is highest in the late summer then decreases to a minimum in early 1981. The moisture content of the air increases again in the spring. While the maximum flow rate in figure (6.4) is not clearly defined, it occurs at about day 25 of 1981. The minimum level of specific humidity occurs at about day 10. Thus, the minimum in tightness lags behind the minimum in air moisture by about two weeks. Luck and Nelson found a time constant of about 10 days for the moisture absorption of wood [3].

The seasonal variation of the moisture content of the outside air can explain the variation in the induced flow rate of the house. A seasonal variation in pressurization flow rates on the order of 40% has been measured by Warren and Webb [4]. Their data are shown in figure (6.6), but consists of only eight measurements over 1.5 years compared to roughly three dozen over one year in the BRAT house. Because the Warren and Webb house was unoccupied during the test period the lack of any internal moisture sources may have led to increased drying of the structure.

In discussing the seasonal variation of building leakiness, effects of outside temperature on the Blower Door results are very important. As presented in appendix C, the volumetric flow rate through the fan at a given pressure difference and fan speed

depends on the density, and hence the temperature, of the air. Because of differences in the inside and outside air densities, the flow out of the house during pressurization equals the flow through the fan times the ratio of the inside and outside temperatures in °K. Figure (6.7) shows the effects of these two corrections on the seasonal variation of the 50 Pa flow rate. Only tests made under calm wind conditions are included in this plot. The lower curve is the unadjusted 50 Pa flow rate. The middle curve is the flow rate through the fan with the density correction applied. The upper curve is the flow out of the house calculated by equating the mass flow into the house through the fan at T_o to the mass flow out of the house at an assumed inside temperature of 20°C. The unadjusted flow rate and the corrected flow rate through the fan both have seasonal variations of about 22%. The flow through the leaks in the house varies by about 36%.

Our pressurization experiments in the BRAT house have revealed useful information concerning this technique for evaluating the tightness of homes. We measured the effects of wind speed on the test results, and found that the results were unaffected by winds up to 2.5 m/s. This is close to the ASTM recommendation of testing at local speeds below 2.2 m/s, but other homes must be checked. Also, we found higher wind speeds lead to errors in the 50 Pa flow rate of at most 15%. But due to the fluctuating nature of wind, tests conducted at high average wind speeds may not

be in error. We found the distribution of the BRAT house leakage among the vents, windows and background to be independent of pressure difference. The fraction of leakage through windows, about 10% of the total, is similar to existing measurements which show that windows are not the most important source of leakage in homes.

The BRAT tests have also revealed the repeatability of Blower Door test results on a home. The 50 Pa leakage rate is reproducible by 1 or 2%, while the 4 Pa flow will vary by about 5%. The 4 Pa is less well-defined because it is an extrapolation outside of the range of measurements. By conducting the pressurization tests on the BRAT house over a year, we found and measured the seasonal variation of the leakage of a home. This variation is due to changes in the moisture content of the air which leads to drying and shrinking of the wood in the winter and swelling in the summer. The magnitude of this variation is about 25% for the BRAT house, but becomes larger if one accounts for density effects. The BRAT results are useful in developing the pressurization technique into a tightness standard, but similar research needs to be conducted in other homes.

REFERENCES

[1] Gadsby, K.J., Linteris, G.T., Dutt, G.S., Harrje, D.T., "The Blower Door," Report No. 124, Center for Energy and Environmental Studies, Princeton University, 1981.

[2] Standard Practice for Measuring Air Leakage by the Fan-Pressurization Method, Designation E 779-81, American Society for Testing and Materials.

[3] Luck, J.R., Nelson, L.W., "The Variation of Infiltration Rate with Relative Humidity in a Frame Building," ASHRAE Transactions, Vol. 83(I), 1977.

[4] Warren, P.R., Webb, B.C., "Ventilation Measurements in Housing," CIBS Symposium, Natural Ventilation by Design, London, 1980.

Table 6.1

Leakage Distribution in the BRAT House

Pressure Difference (Pascals)		Pressurization (% of total flow)	Depressurization (% of total flow)
	Vents	7	4
12.5	Windows	11	9
	Background	82	86
	V	7	3
25.0	W	14	7
	B	79	90
	V	5	4
37.5	W	9	10
	B	87	86
	V	6	3
50	W	12	12
	B	81	85

Table 6.2

Variation of Flow

Pressurization	Mean	Standard Deviation (σ)	σ/M
$Q_{calc}^{(4)}$	642	35	5.5%
$Q_{calc}^{(50)}$	3710	43	1.2%
$Q_{meas}^{(50)}$	3738	54	1.4%
Depressurization			
$Q_{calc}^{(4)}$	592	38	6.4%
$Q_{calc}^{(50)}$	4003	70	1.7%
$Q_{meas}^{(50)}$	4017	82	2.0%
All Points			
$Q_{calc}^{(4)}$	617	30	4.9%
$Q_{calc}^{(50)}$	3860	43	1.1%
$\frac{Q_p(4) + Q_D(4)}{2}$	617	28	4.5%

All flows in m^3/hr.

Figure 6.1

50 Pascal Flow vs Wind Speed

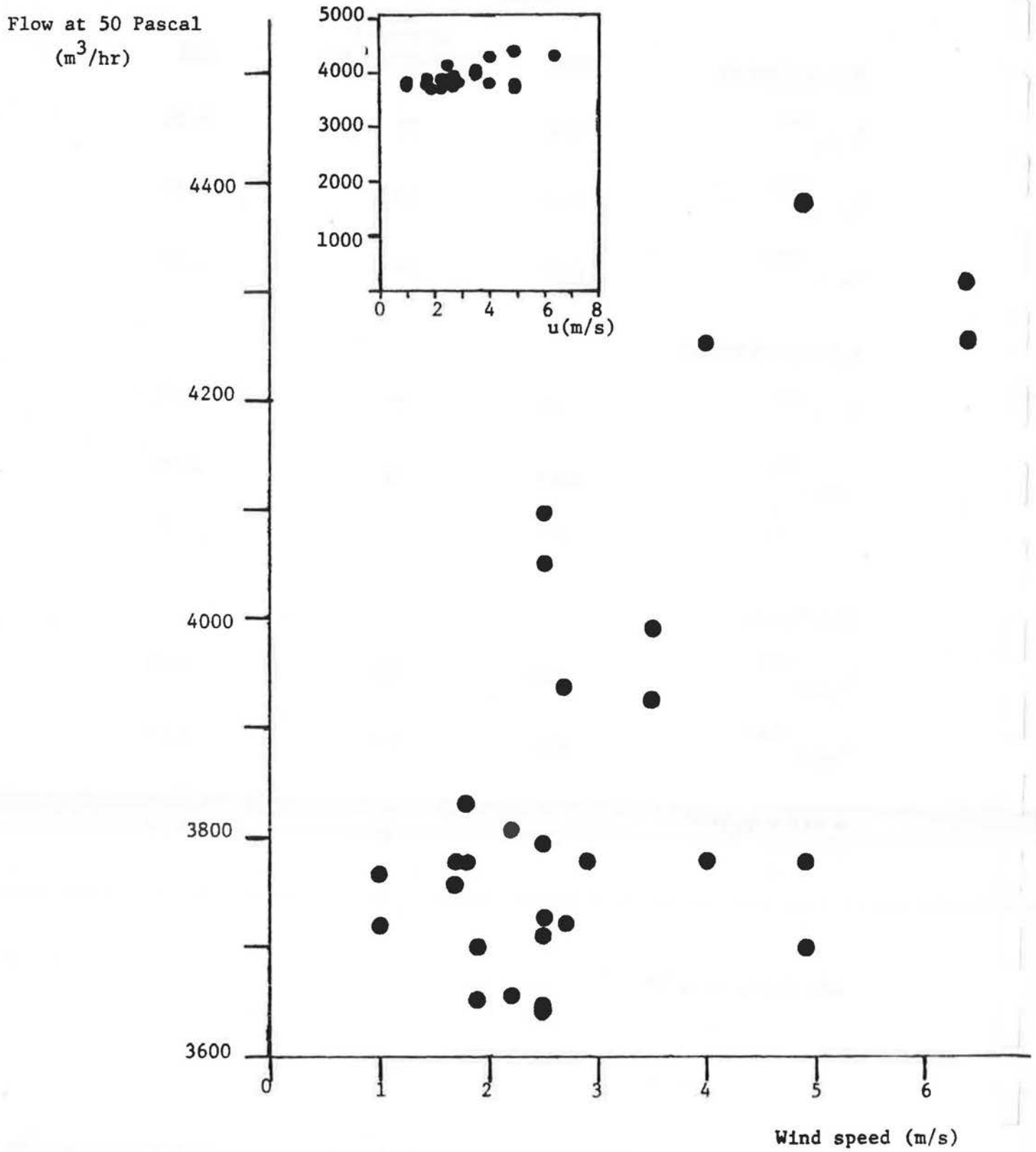

Figure 6.2

4 Pascal Flow vs Wind Speed

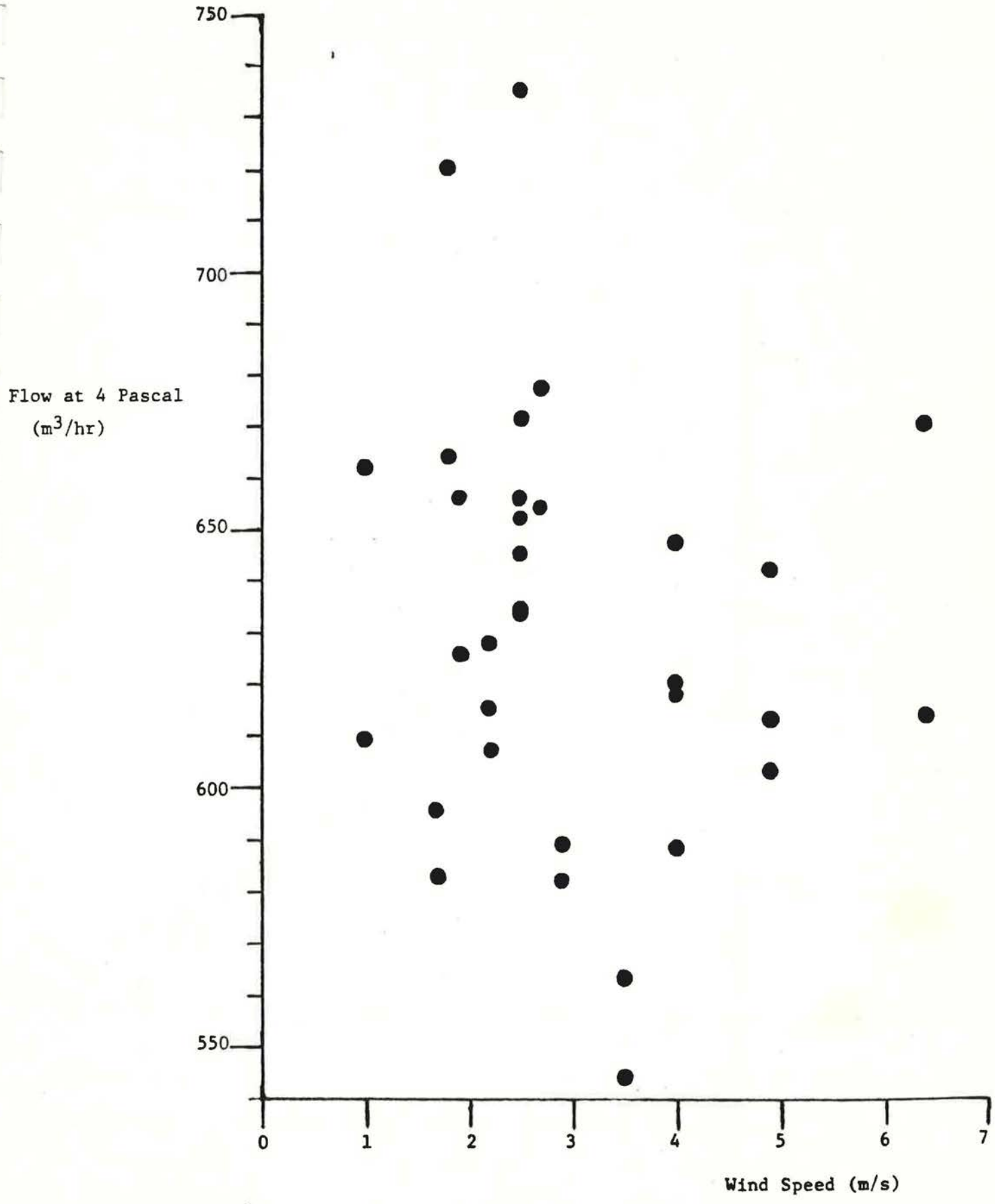

Figure 6.3

Coefficient vs Exponent for Curve Fits to Pressurization Points

Curve Fit: $Q = C\Delta p^n$

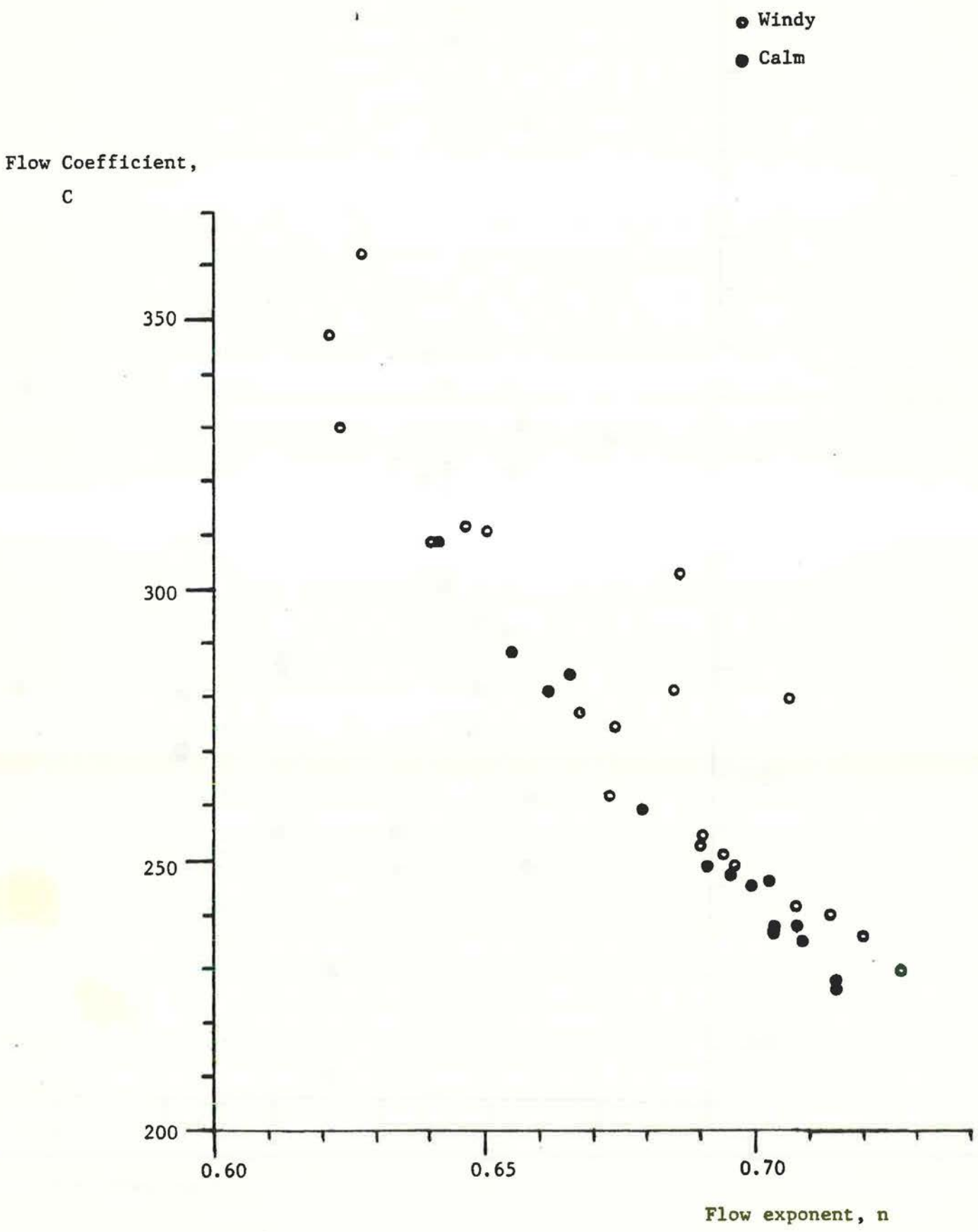

Figure 6.4

50 Pascal Flow vs Time

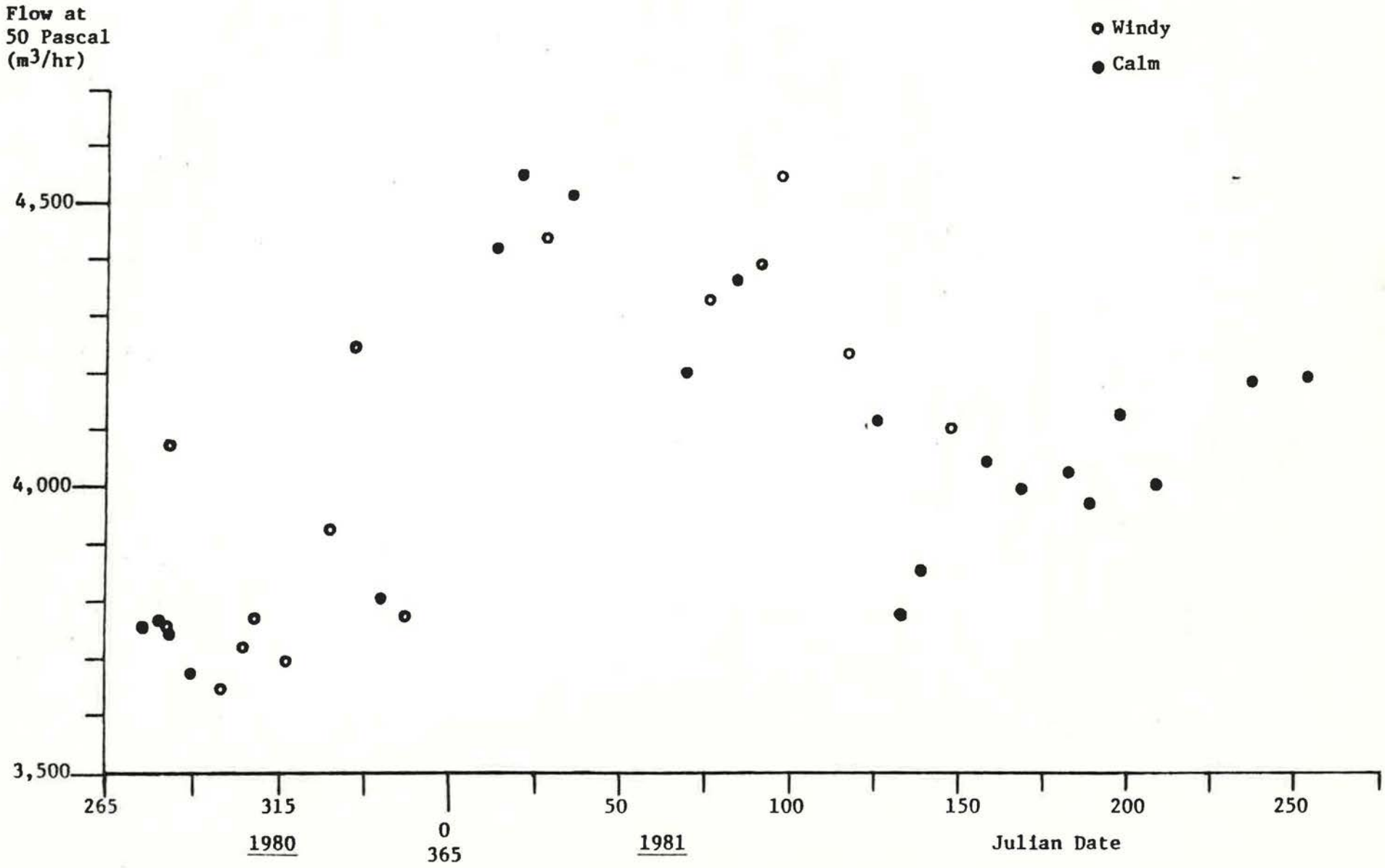

Figure 6.5

Five-Day Average Specific Humidity vs Time

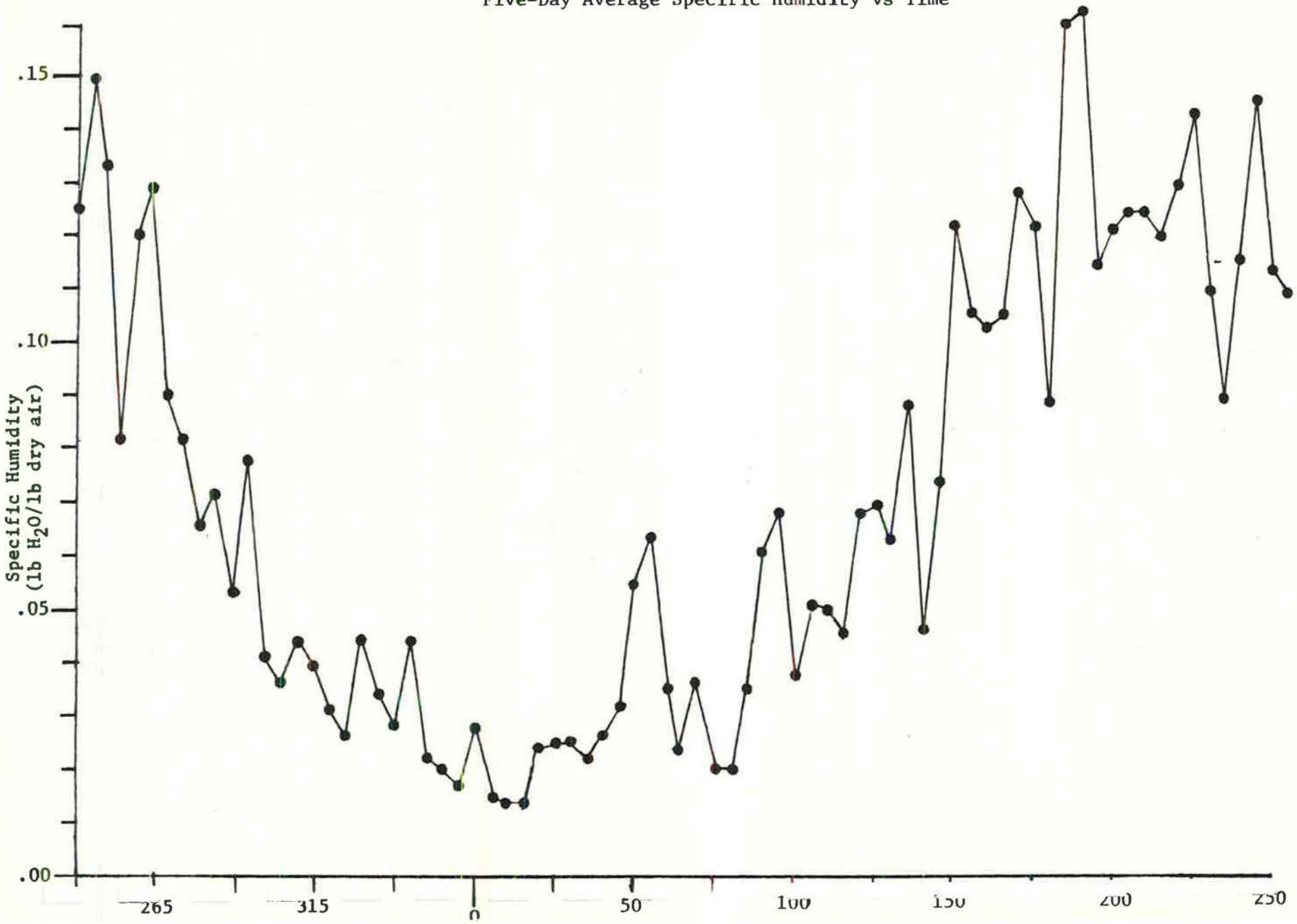

Figure 6.6

Seasonal Variation of 50 Pascal Flow Rate from reference [4]

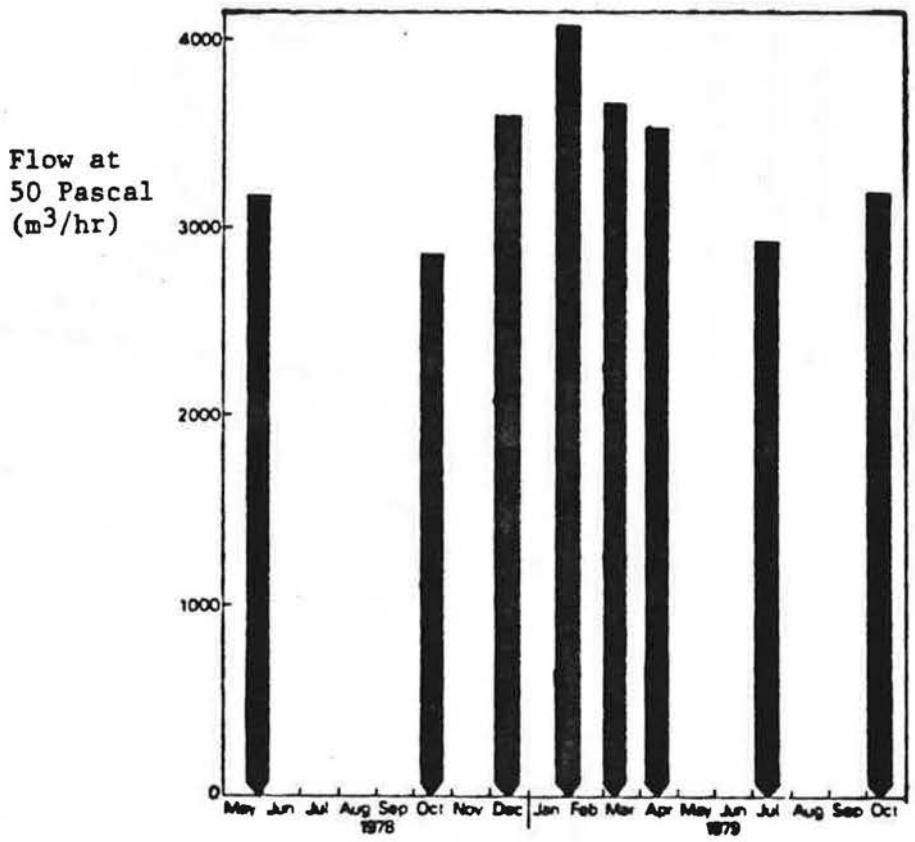

Figure 6.7

50 Pascal Flow vs Time with Density Considerations

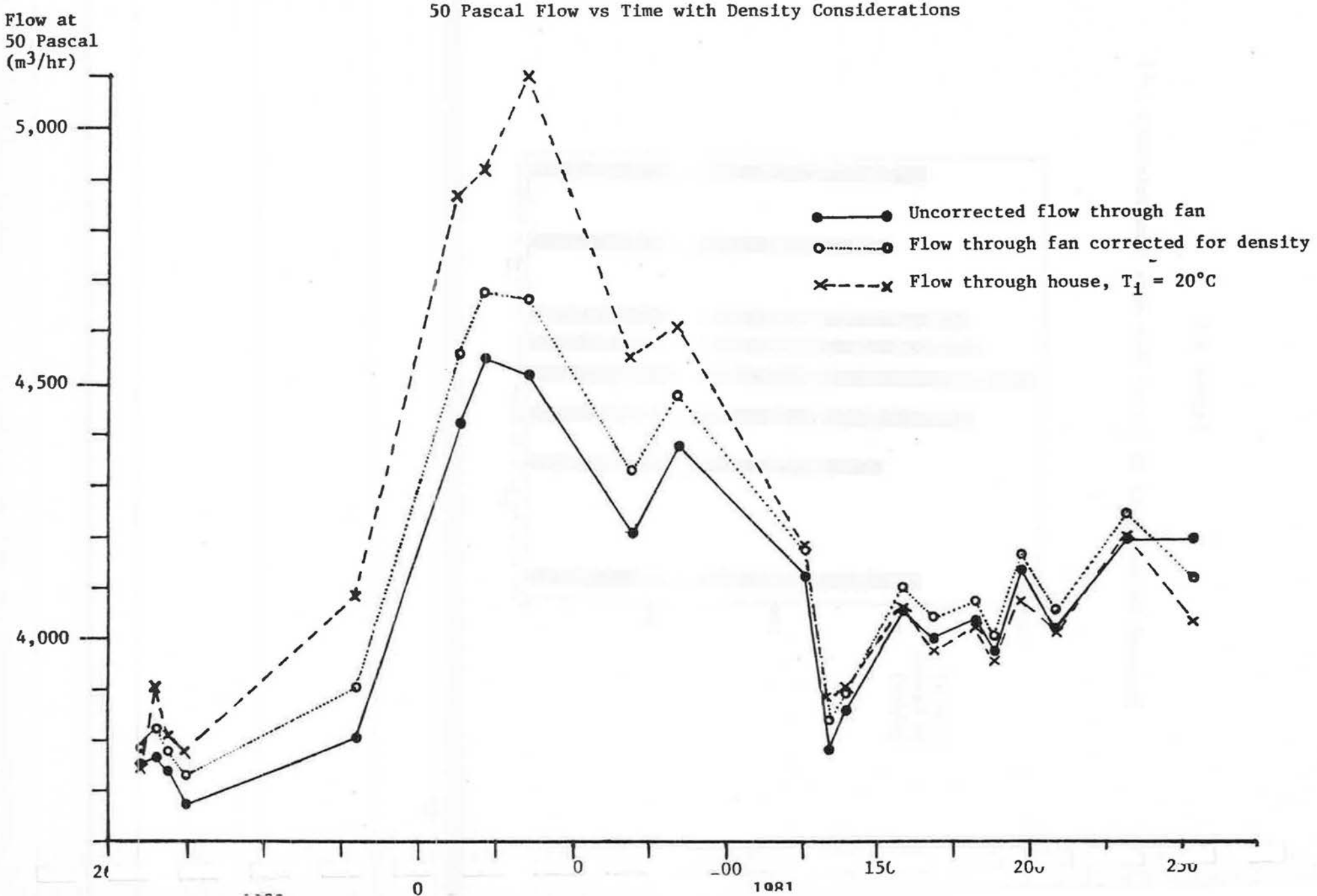

Chapter VII

RELATING INFILTRATION TO PRESSURIZATION IN A SIMPLE STRUCTURE

In discussing the relation of pressurization test results to natural infiltration in chapter V we pointed out differences between the test and the naturally induced conditions which might make a usable relation difficult to obtain. Among other differences, the test pressures are large, constant and uniform compared to the pressures induced by the weather. Studying the relation of pressurization and infiltration is difficult in real homes because of important unknowns such as their leakage characterisitics. It is not even clear if pressurization test results can be extrapolated to weather induced pressure differences to predict infiltration rates. Thus, we attempted to predict infiltration rates from pressurization test results in a very simple structure called the Test Chamber, a small building described in detail in appendix A. Because we know the location of all significant leakage in this building we have ideal conditions for predicting infiltration rates from pressurization.

7.1 PRESSURIZATION OF THE TEST CHAMBER

The pressurization tests were similar to Blower Door tests in homes, and used the device shown in figure (7.1) and described in appendix B. A centrifugal blower within the Test Chamber either blows out or draws air through the orifice meter extending out of the side of the structure. The Test Chamber was pressurized and evacuated to pressure differences from 7.5 to 60 Pa in increments of 7.5 Pa. Because the inside and outside temperatures were roughly the same during these tests, the flow through the meter equals the flow through the shell of the house.

The Test Chamber was tested under four conditions of leakage, the first being sealed as tightly as possible. The other leakage conditions were created through the use of carefully machined slits in aluminum sheets. Each of the four windows of the Test Chamber was fitted with one of the 1/16th inch thick aluminum sheets shown in figure (7.2). Each sheet contains a small and a large slit with dimensions shown in figure (7.3). The leakage characteristics of the small slits were found by taping the large ones during the pressurization test. The third leakage condition was with the large slits alone. In the fourth leakage condition, all the slits were open.

The pressurization tests were made under very calm conditions to avoid interference of wind induced pressures. In order to cover the entire range of pressure differences, four different orifices were used. In some cases, two windows were sealed and the pressurization test results for the two open windows were converted to the leakage if all four had been open.

Typical results of the pressurization tests on the Test Chamber are shown in figure (7.4) for the totally sealed case and in figure (7.5) for the large slits open. These figures are plots of the flow rate Q (m^3/hr) against the pressure difference Δp (Pa). Each set of points was fitted to a curve of the form

$$Q = C\Delta p^n \qquad (7.1)$$

The results of these curve fits are given in table (7.1), along with the predicted flow rates at Δp = 4 and 50 Pa. A curve is also fit to both the pressurization and the depressurization points together. When the Test Chamber is completely sealed, it has an exchange rate of 2.3 volumes per hour at 50 Pa. This is a low exchange rate, especially when one considers the high surface to volume ratio of the Test Chamber. If one divides the 50 Pa flow rate by the outside surface area of 48 m^2, one obtains 0.80 m^3/hr-m^2. This value of 0.80 is lower than any of the houses in figure (5.2). The tightest house in this plot has a leakage of about 1.4 m^3/hr-m^2 at 50 Pa.

The exponent n in the curve fits is about 1/2 for all leakage conditions except completely sealed. In the sealed case, n is significantly closer to 1.0. The Reynolds number for the sealed flows cannot be calculated because we do not know the crack geometry, but for the small slits Re varies from 750 to 1800. For the large slits the Reynolds number ranges from 1200 to 3000. Earlier discussion leads us to expect that turbulent flow through these slits will lead to an n close to 1/2. The leaks in the

sealed case are probably narrower and deeper than the slits, leading one to expect a value of n closer to 1.0.

By subtracting out the leakage for the completely sealed case and dividing the result by four, one obtains the leakage function for each individual window. These leakage functions are given in table (7.2) for the small slits, large slits and both slits together. Using these expressions we calculated the effective leakage areas A_o as discussed in chapter IV. The effective leakage areas were about 25% less than the physical leakage areas of the slits.

7.2 NATURAL VENTILATION MEASUREMENTS

The air infiltration rate of the Test Chamber was measured under all four leakage states using tracer gas decay. Ethane was used as the tracer and a Wilks Specific Vapor Analyzer (discussed in appendix B) was used to measure the ethane concentration. The measured rates are averages over one-half hour based on concentration readings every five minutes. The natural logarithm of concentration is linearly regressed against time, and the negative of the slope of the regression line is the infiltration rate. Few measurements were made with the Test Chamber completely sealed because these rates are very small, on the order of the uncertainty of the measurement technique, and they show little sensitivity to weather.

7.3 COMPARISON OF PRESSURIZATION AND INFILTRATION

The combination of precise pressurization test results and measured infiltration rates in such a simple structure presents an excellent opportunity for the comparison of the two measurement techniques. The first comparison is between infiltration measurements under roughly the same weather for all three leakage conditions. Three sets of such tests are plotted in figures (7.6) through (7.8) against the flow rates at 50 and 4 Pa. The infiltration rates are linearly related to either flow rate, with values of r^2 equal to about 0.99 from linear regressions of the data. In these plots, the slope of the infiltration rate against the 50 Pa flow rate is about 16, compared to roughly 18 for the homes in figure (6.1).

Stack Regime

Infiltration rates in the stack regime were predicted and compared to infiltration measurements with an average wind speed of 0.7 m/s or less, and a temperature difference of about 10°C or larger. The leakage functions in table (7.2) were used to predict the flow through each window as a function of the pressure difference across it.

The pressure differences were determined from the interior and exterior densities along with the location of the leakage sites. The pressure difference at a height z above the floor is

$$\Delta p(z) = (p_o - \rho_o g z) - (p_i - \rho_i g z), \qquad (7.2)$$

where p_o and p_i are the static pressures at z=0 outside and inside the structure, ρ_o and ρ_i are the outside and inside air densities, and g is the acceleration of gravity. This equation is rewritten as

$$\Delta p(z) = \Delta p_o + gz(\rho_i - \rho_o), \qquad (7.3)$$

where $\Delta p_o = p_o - p_i$. The air densities are determined by the temperatures measured during the infiltration measurement. z is the height from the floor to the middle of the windows, 0.54 m for the lower window and 3.14 m for the upper one. After inputting g,z and the densities into equation (7.3), one obtains $\Delta p(z)$ as a function of Δp_o for each of the four windows.

The infiltration rate is predicted through an iterative procedure for which Δp_o is the input. A value of Δp_o is chosen and the pressure difference at each window is calculated using equation (7.3). The flows through each window are calculated using the flow equations in table (7.2). If the inflows (Q<0) and the outflows (Q>0) are not the same, then additional values of Δp_o are input until the inflow and the outflow are equal. At this point, the flows are divided by the Test Chamber volume to yield the air infiltration rate in exchanges per hour.

The predicted and measured infiltration rates are compared in figure (7.9). The line of perfect agreement is shown in the plot. The predicted values are very close to the measurements, with a tendency to overpredict by about 15% when all slits are open. Our calculations of stack induced infiltration have re-

quired no assumptions except that the flow equations from the pressurization tests apply to the calculated pressure differences. The accuracy of our prediction shows that this assumption and our calculation method are appropriate.

Combination of Wind and Stack Regimes

The prediction of infiltration rates is more difficult when one includes wind effects, because one must obtain appropriate values for the wind pressure coefficients C_p. The pressure differences across the four openings are determinined using a variation of equation (7.2),

$$\Delta p(z) = (p_o + C_p \tfrac{1}{2} \rho_o u^2 - \rho_o g z) - (p_i - \rho_i g z). \qquad (7.4)$$

C_p is a function of wind direction and position on the building. We assume that C_p is constant over each face of the building. As in the case of stack prediction we determine $\Delta p(z)$ for each of the four openings for a particular value of Δp_o. The leakage functions from the pressurization tests are used to determine the flow through each window, and Δp_o is varied until the inflow equals the outflow. Either of these flows divided by the Test Chamber volume equals the air exchange rate.

Infiltration rates were first predicted for winds blowing roughly normal to the openings in the Test Chamber. This corresponds to wind directions from the east and west. Winds from the west are severely interferred with by a neighboring building, and therefore we tried to avoid measurements with winds from this di-

rection. In actuality, the wind direction, like the speed, is never constant and the average direction based on one-half hour of measurements includes other directions as well. Therefore, winds from the east-south-east and east-north-east are included with the east winds. Similarly, the west winds include WNW and WSW.

The values of C_p for the normal wind direction prediction are from figure (2.1) [1]. For the windward side $C_p = +0.7$ and for the leeward side $C_p = -0.4$. The results of these predictions are shown in figure (7.10) as a plot of the measured infiltration I_m versus the predicted infiltration I_p. The circled points denote winds from a westerly direction and show a tendency towards overprediction of the infiltration rate. This is caused by the neighboring building shielding the Test Chamber from west winds. The infiltration rates for the small and large slits are predicted very well. The rates for both slits are overpredicted by about 15%, as they were in the stack case.

Next we consider winds blowing across the openings in the Test Chamber, i.e. from the north or south. These also include winds from the NNW and NNE, and from the SSW and SSE, respectively. Again, the values of C_p come from Handa [1] and are the same for all four openings, -0.7. The measured I_m versus the predicted rates I_p are plotted in figure (7.11) and there is a strong tendency towards underprediction. Figure (7.12) shows I_m/I_p plotted against the Archimedes number Ar. Ar, as defined in chapter II, is a measure of the relative importance of stack and wind ef-

fects. Large values of Ar correspond to conditions dominated by stack effects, and small values correspond to wind dominance. The underprediction becomes worse as Ar decreases, i.e. for wind dominated infiltration.

It is not clear why we underpredict infiltration for winds blowing parallel to the walls with openings. Two explanations may account for this discrepancy. First, as mentioned earlier, the wind never blows just from the north or south. When the wind deviates significantly from blowing across the openings, one wall of openings will be pressurized and the other will be under negative pressure. This will lead to much different flow conditions than having negative pressures at all four openings. The other explanation for the underprediction is turbulence induced infiltration. With wind blowing across openings in a wall, small scale turbulence in the wind will cause more infiltration than expected from the simple, steady-state model used here [2,3].

It is difficult to tell which of the above explanations accounts for the underprediction, and both probably play a part. In considering the first explanation, we predict infiltration rates for a wind blowing from a direction 28° off from parallel to the wall. The values of the wind pressure coefficients come from full-scale measurements on an experimental building [4]. In this case we used $C_p = +0.4$ for the wall into which the wind blows, and -0.5 for the opposite wall. The measured infiltration rate is plotted against the predicted rate in figure (7.13) and the agreement is much better than in figure (7.11).

The improved infiltration prediction supports the hypothesis that directional effects cause underprediction for winds blowing across the openings. Infiltration prediction for these north and south winds should consist of a weighted average of the predictions in figures (7.11) and (7.13). This averaging would result in poorer prediction than in figure (7.13). Thus, we cannot fully explain the underprediction with this directional argument, and there are still the turbulent effects to consider. In fact, directional effects may be regarded as turbulence of a length scale on the order of the Test Chamber. Such large eddies will result in highly correlated pressures for the two faces, i.e. one will be pressurized while the other is under suction. Turbulence effects are very difficult to study, especially without well-defined values of the wind pressure coefficients.

The fact that our predictions were good in the stack and normal wind cases show that pressurization test results can be used to predict infiltration rates when we know where the leakage sites are. Our difficulties in prediction for winds blowing across the openings reflect the general difficulties in the field, a lack of knowledge of C_p as a function of direction and the problems of considering turbulence in the natural wind. Problems in obtaining values of C_p for a simple and exposed structure like the Test Chamber are worse for real homes which are in much more complex wind environments.

REFERENCES

[1] Handa, K., Wind Induced Natural Ventilation, Report D10, Swedish Council for Building Research, Stockholm, Sweden, 1979.

[2] Harris-Bass, J., Kavarana, B., Lawrence, P., "Adventitious Ventilation of Houses," Building Service Engineer, Vol. 42, 1974.

[3] Cockroft, J.P., Robertson, P., "Ventilation of an Enclosure Through a Single Opening," Building and Environment, Vol. 11, 1976.

[4] Eaton, K.J., Mayne, J.R., Cook, N.J., Wind Loads on Low Rise Buildings - Effects of Roof Geometry, Current Paper 1/76, Building Research Establishment, Garston, Watford, 1976.

Table 7.1 Test Chamber Pressurization Results

Leakage Conditions	Pressurization	Depressurization	All Points
Sealed	$Q = 1.44\Delta p^{.831}$ $Q(4) = 4.6 m^3/hr$ $Q(50) = 37.2 m^3/hr$ $= 2.2$ X/hr	$Q = 1.48\Delta p^{.840}$ $Q(4) = 4.7 m^3/hr$ $Q(50) = 39.6 m^3/hr$ $= 2.4$ X/hr	$Q = 1.46\Delta p^{.836}$ $Q(4) = 4.7 m^3/hr$ $Q(50) = 38.4 m^3/hr$ $= 2.3$ X/hr
Small Slits	$Q = 28.2\Delta p^{.520}$ $Q(4) = 58.0 m^3/hr$ $Q(50) = 216 m^3/hr$ $= 13.0$ X/hr	$Q = 31.2\Delta p^{.501}$ $Q(4) = 62.5 m^3/hr$ $Q(50) = 221 m^3/hr$ $= 13.3$ X/hr	$Q = 29.7\Delta p^{.511}$ $Q(4) = 60.3 m^3/hr$ $Q(50) = 219 m^3/hr$ $= 13.2$ X/hr
Large Slits	$Q = 74.4\Delta p^{.488}$ $Q(4) = 146 m^3/hr$ $Q(50) = 502 m^3/hr$ $= 30.2$ X/hr	$Q = 71.5\Delta p^{.492}$ $Q(4) = 141 m^3/hr$ $Q(50) = 490 m^3/hr$ $= 29.5$ X/hr	$Q = 73.0\Delta p^{.490}$ $Q(4) = 144 m^3/hr$ $Q(50) = 496 m^3/hr$ $= 29.9$ X/hr
All Slits	$Q = 109\Delta p^{.465}$ $Q(4) = 208 m^3/hr$ $Q(50) = 672 m^3/hr$ $= 40.5$ X/hr	$Q = 108\Delta p^{.468}$ $Q(4) = 207 m^3/hr$ $Q(50) = 674 m^3/hr$ $= 40.6$ X/hr	$Q = 109\Delta p^{.466}$ $Q(4) = 208 m^3/hr$ $Q(50) = 675 m^3/hr$ $= 40.7$ X/hr

Table 7.2 Leakage Functions for Individual Windows

	Pressurization	Depressurization
Small Slits	$Q = 7.1\Delta p^{.470}$	$Q = 8.0\Delta p^{.444}$
Large Slits	$Q = 18.8\Delta p^{.467}$	$Q = 18.0\Delta p^{.468}$
All Slits	$Q = 27.5\Delta p^{.449}$	$Q = 27.2\Delta p^{.450}$

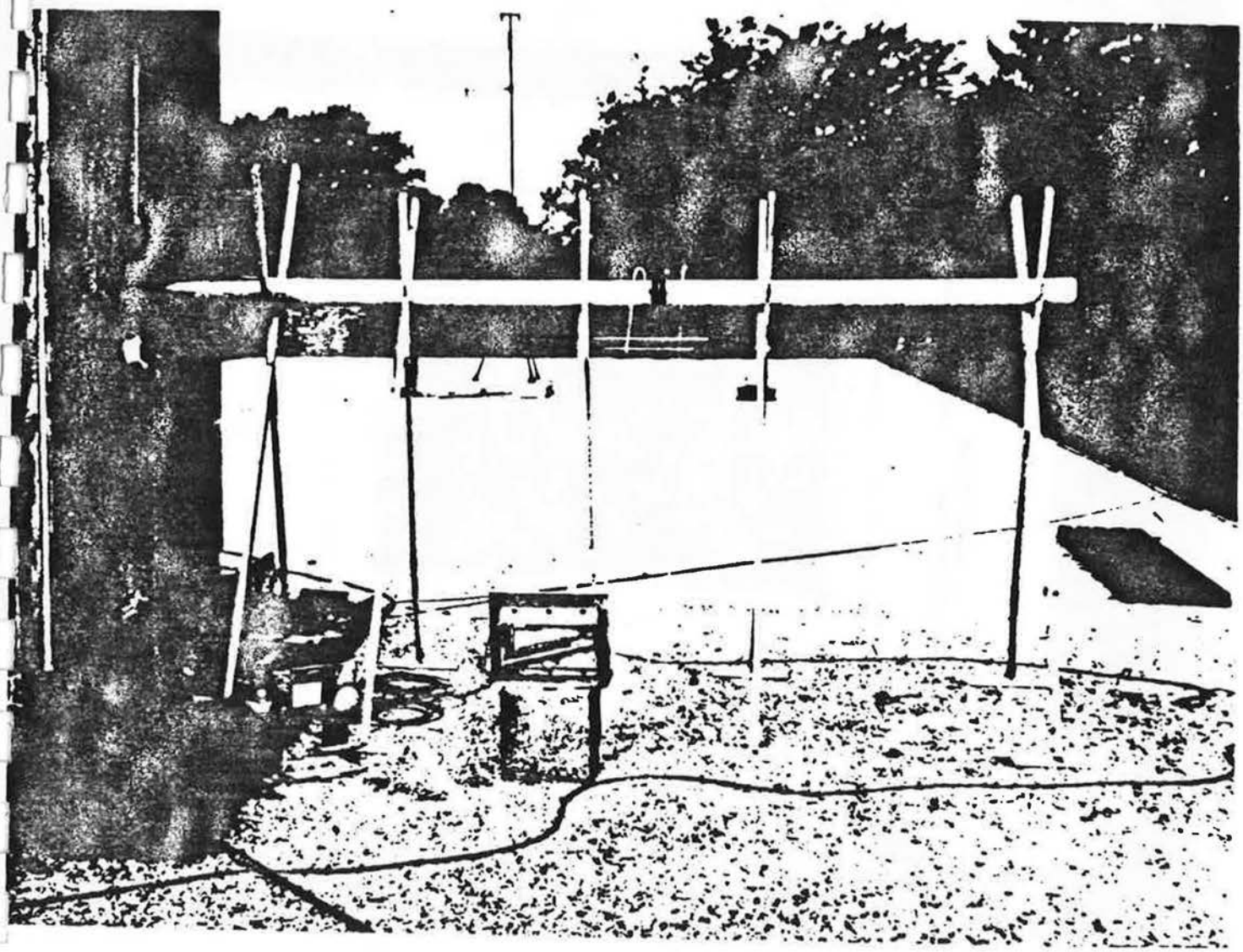

Figure 7.1 Pressurization Device for Test Chamber

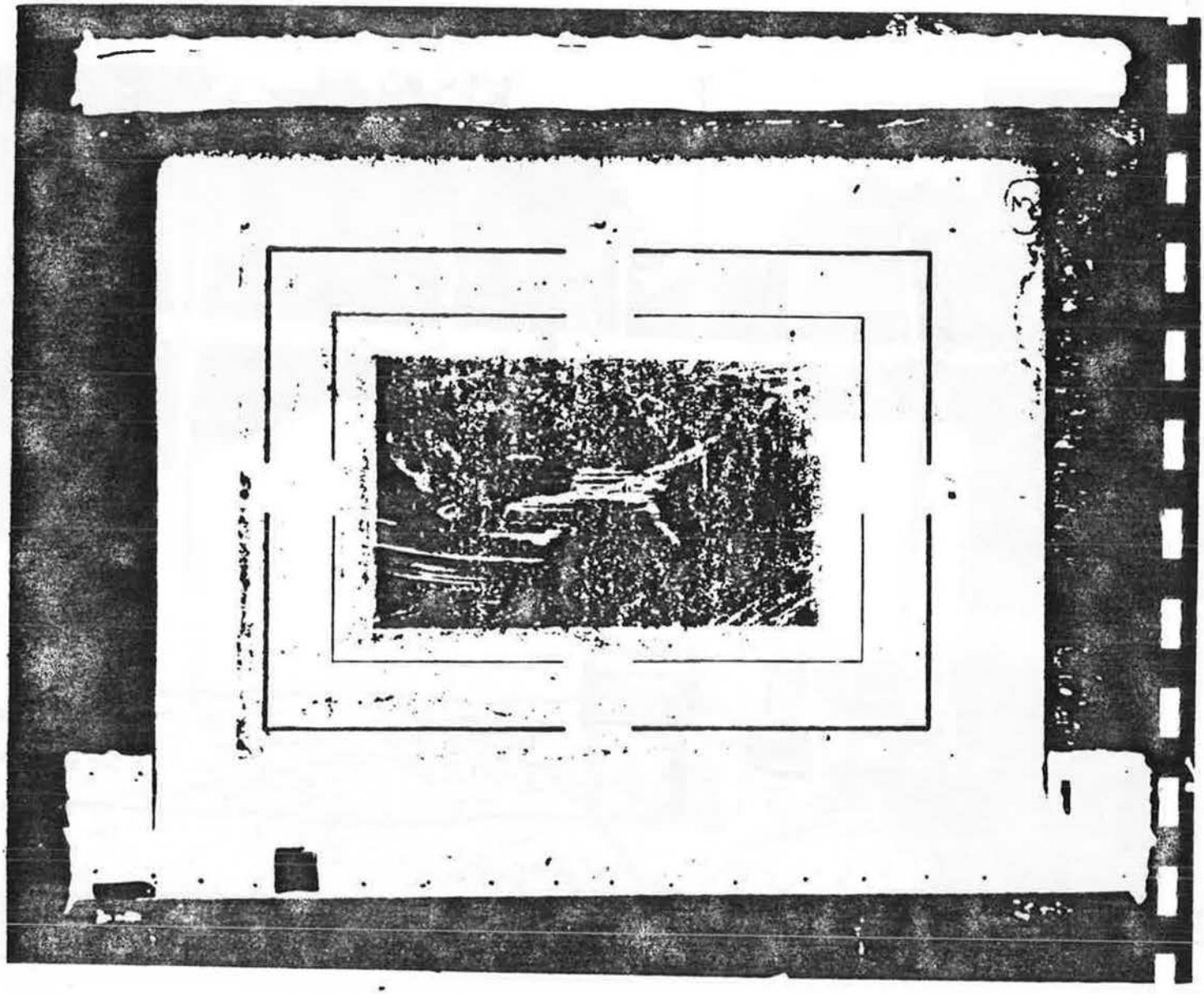

Figure 7.2 Aluminum Leakage Panels

Figure 7.3 Dimensions of Aluminum Leakage Panels

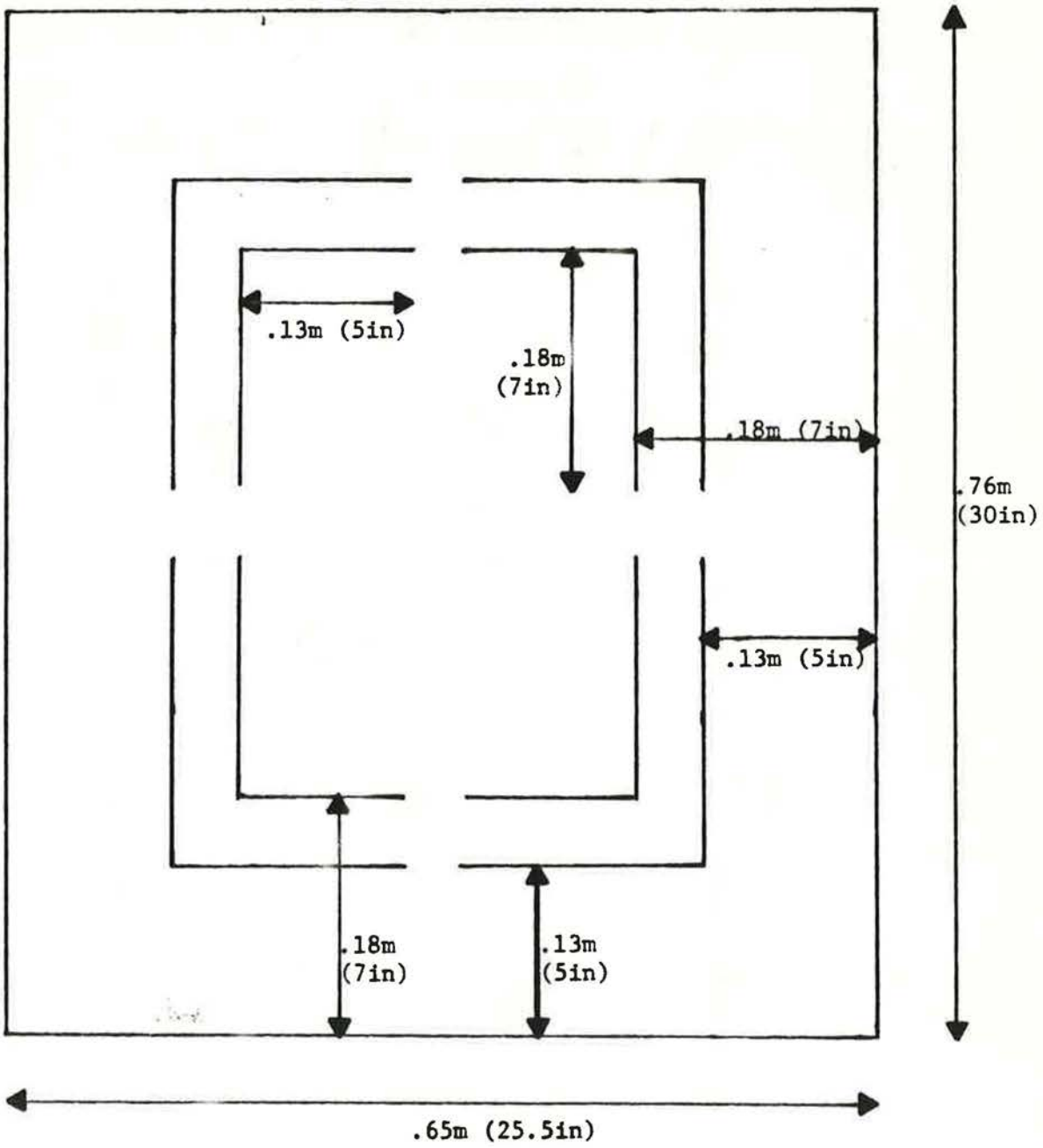

Outer Slit: 1/8th in thick. Crack length = 1.63m per window.

Inner Slit: 1/16th in thick. Crack length = 1.22m per window.

Figure 7.4

Test Chamber Pressurization Results, Sealed Condition

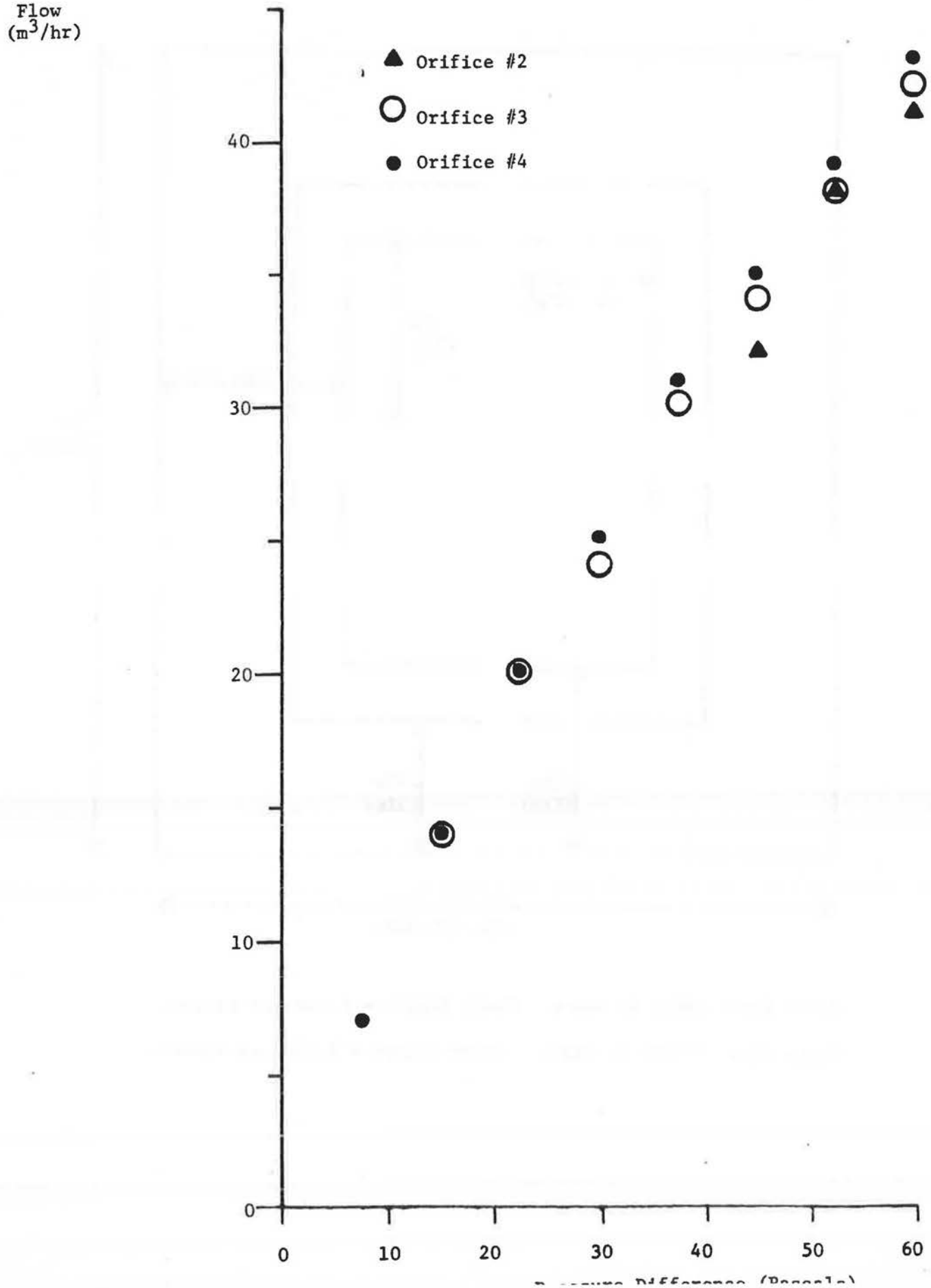

Figure 7.5

Test Chamber Pressurization Results, Large Slits Open

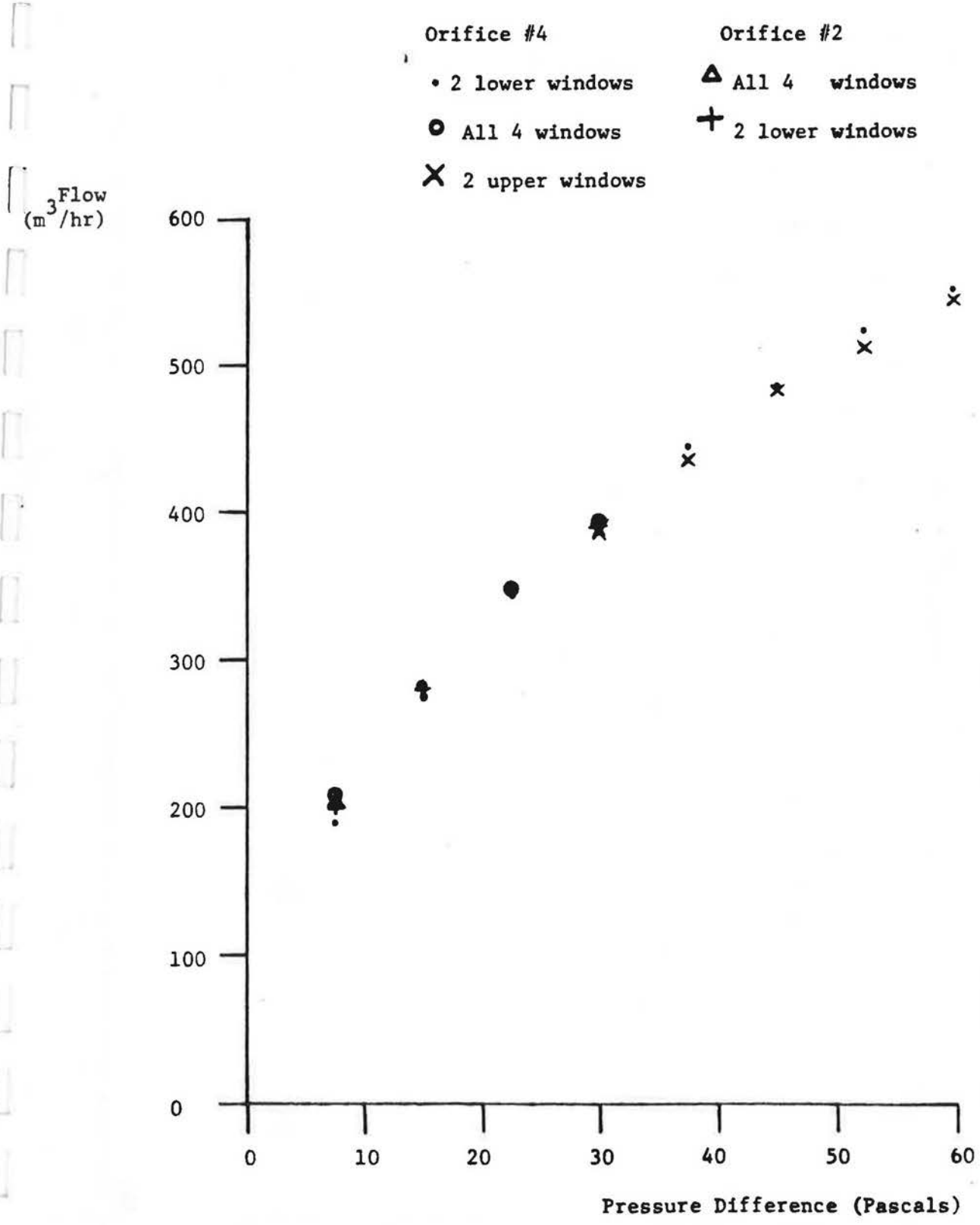

Figure 7.6

Infiltration Rate vs. Pressurization Flow Rate; Low Wind, ΔT = 10 to 15°C

Regression Lines

● 4 Pascal $I = -.012 + .012Q(4)$, $r^2 = .991$

▲ 50 Pascal $I = -.12 + .0037Q(50)$, $r^2 = .993$

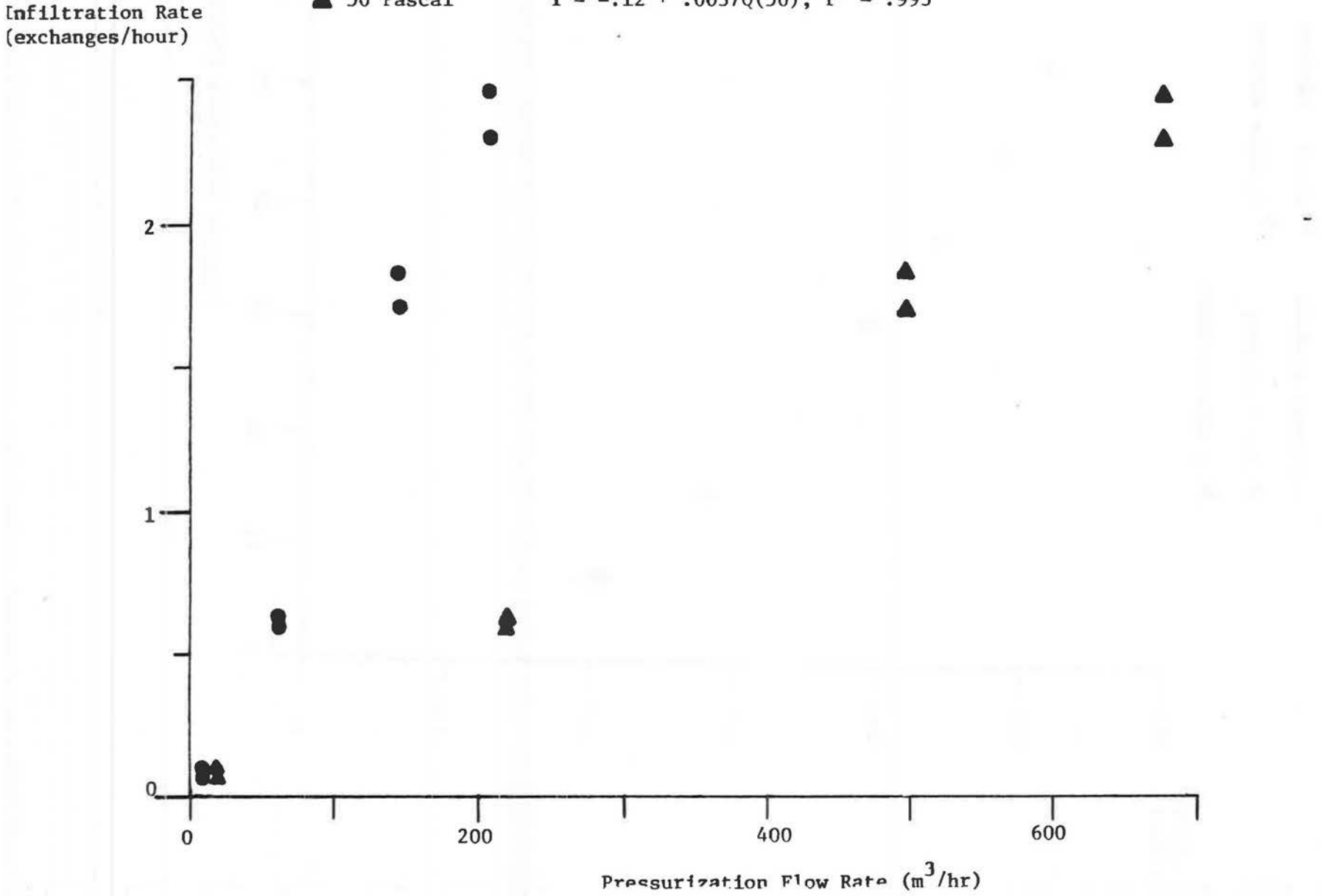

Figure 7.7

Infiltration Rate vs. Pressurization Flow Rate, u = 1.4 to 1.9 m/s, ΔT = 6.8 to 9.3°C

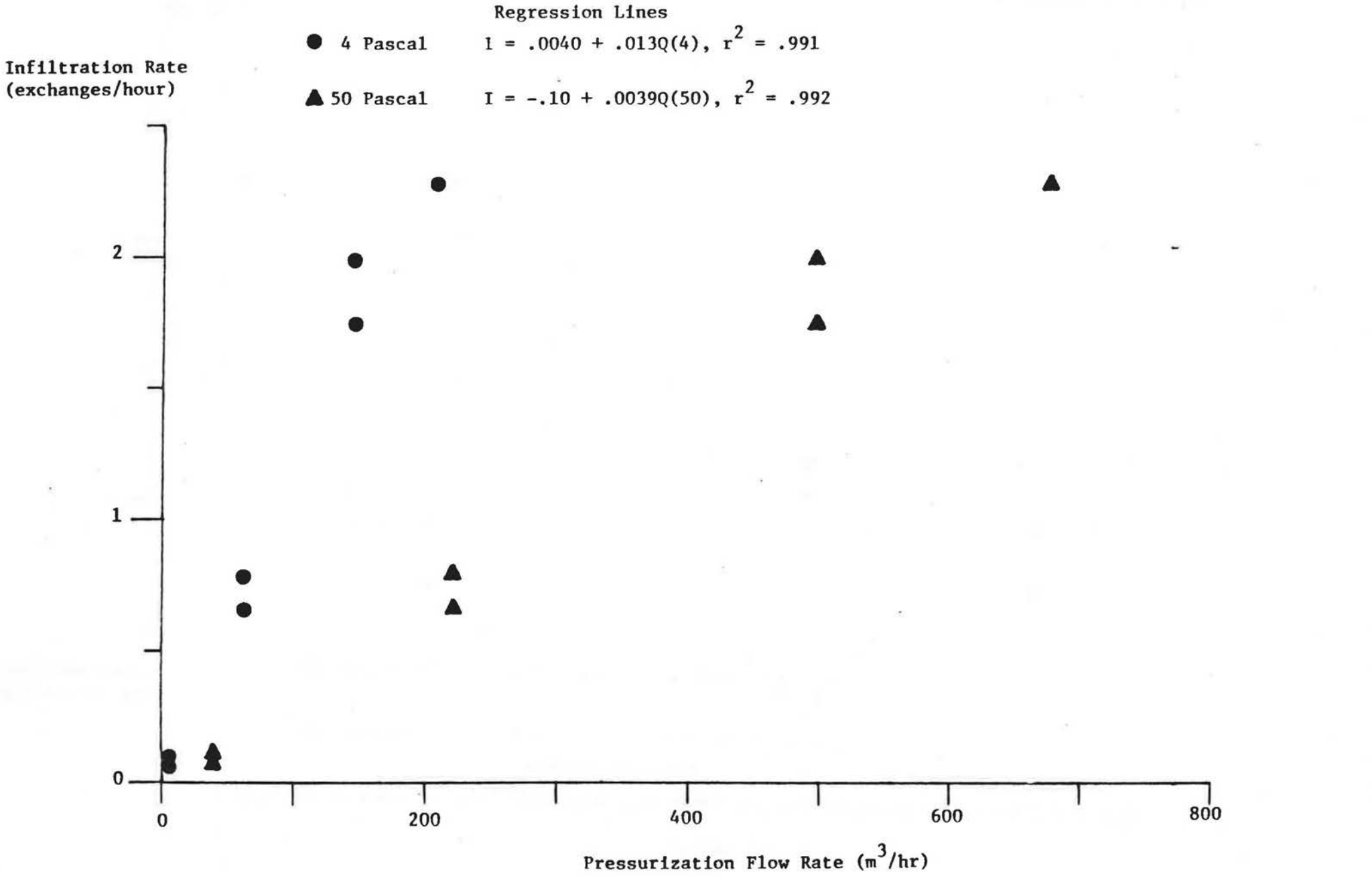

Figure 7.8

Infiltration Rate vs. Pressurization Flow Rate, u = 1.2 to 1.9 m/s, ΔT = 8.1 to 9.0°C

Regression Lines

● 4 Pascal $I = -.082 + .012Q(4)$, $r^2 = .914$

▲ 50 Pascal $I = -.20 + .0039Q(50)$, $r^2 = .924$

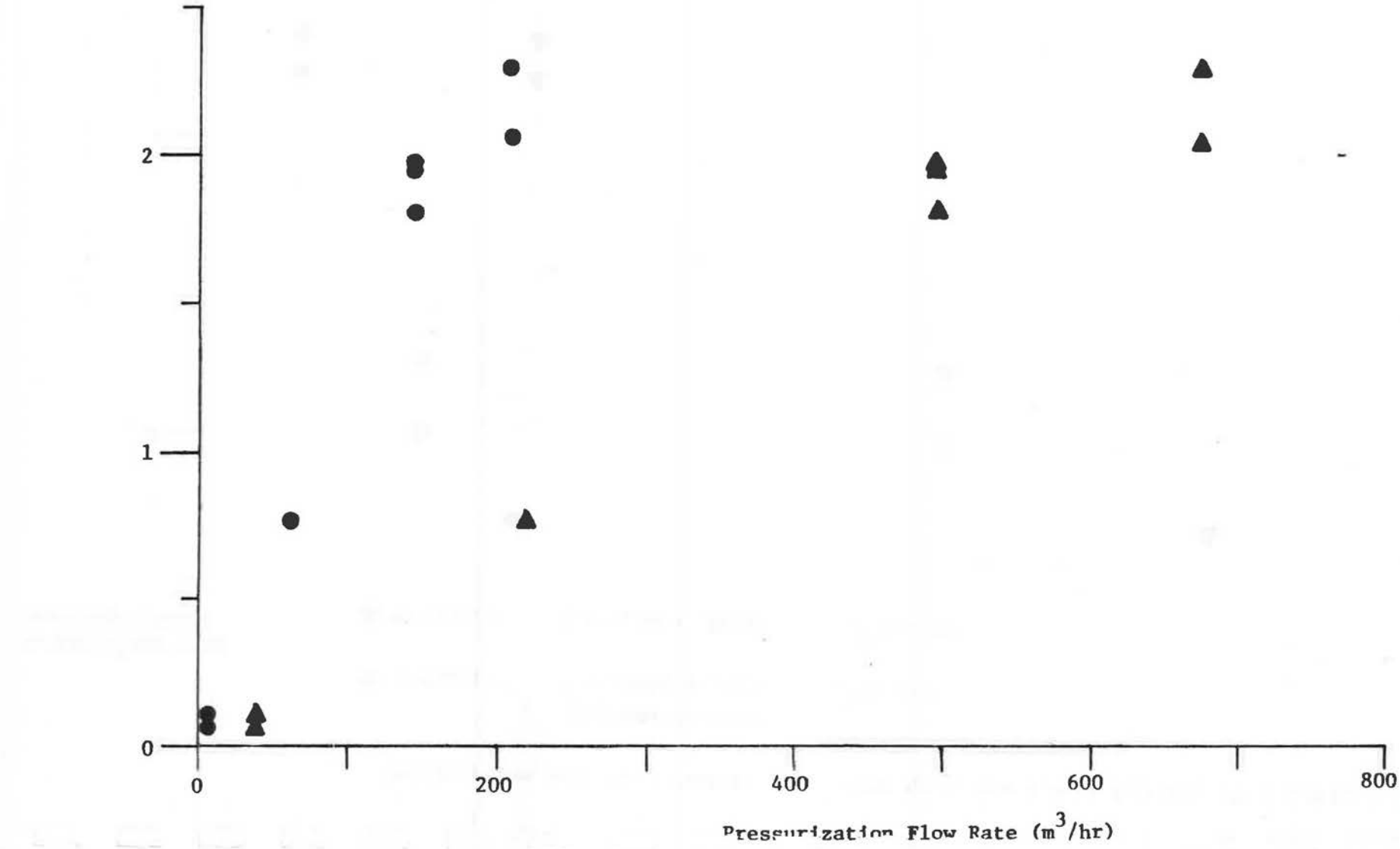

Figure 7.9

Measured v. Predicted Infiltration in Stack Regime

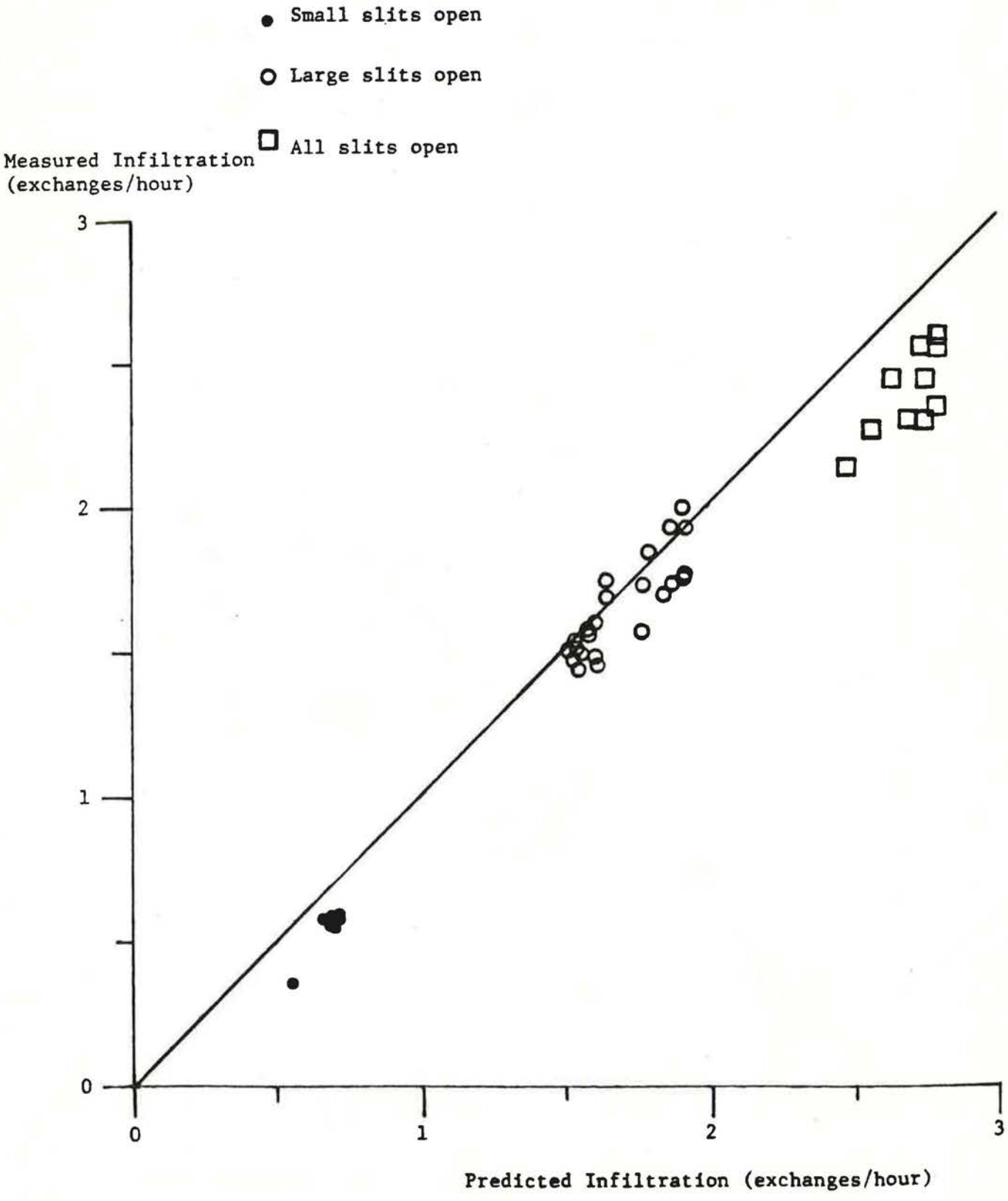

Figure 7.10

Measured vs. Predicted Infiltration, Normal Wind

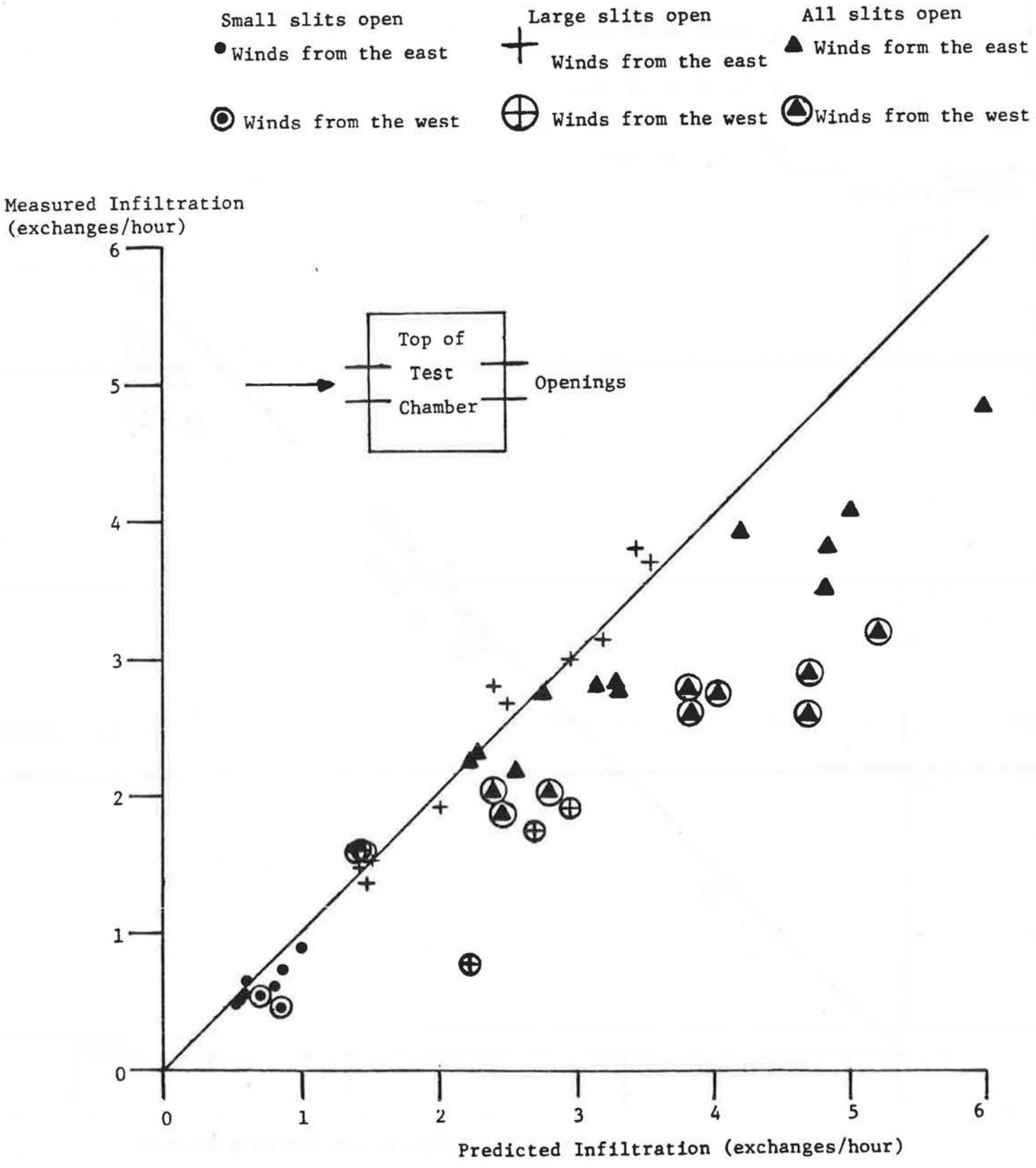

Figure 7.11

Measured vs Predicted Infiltration Parallel Wind

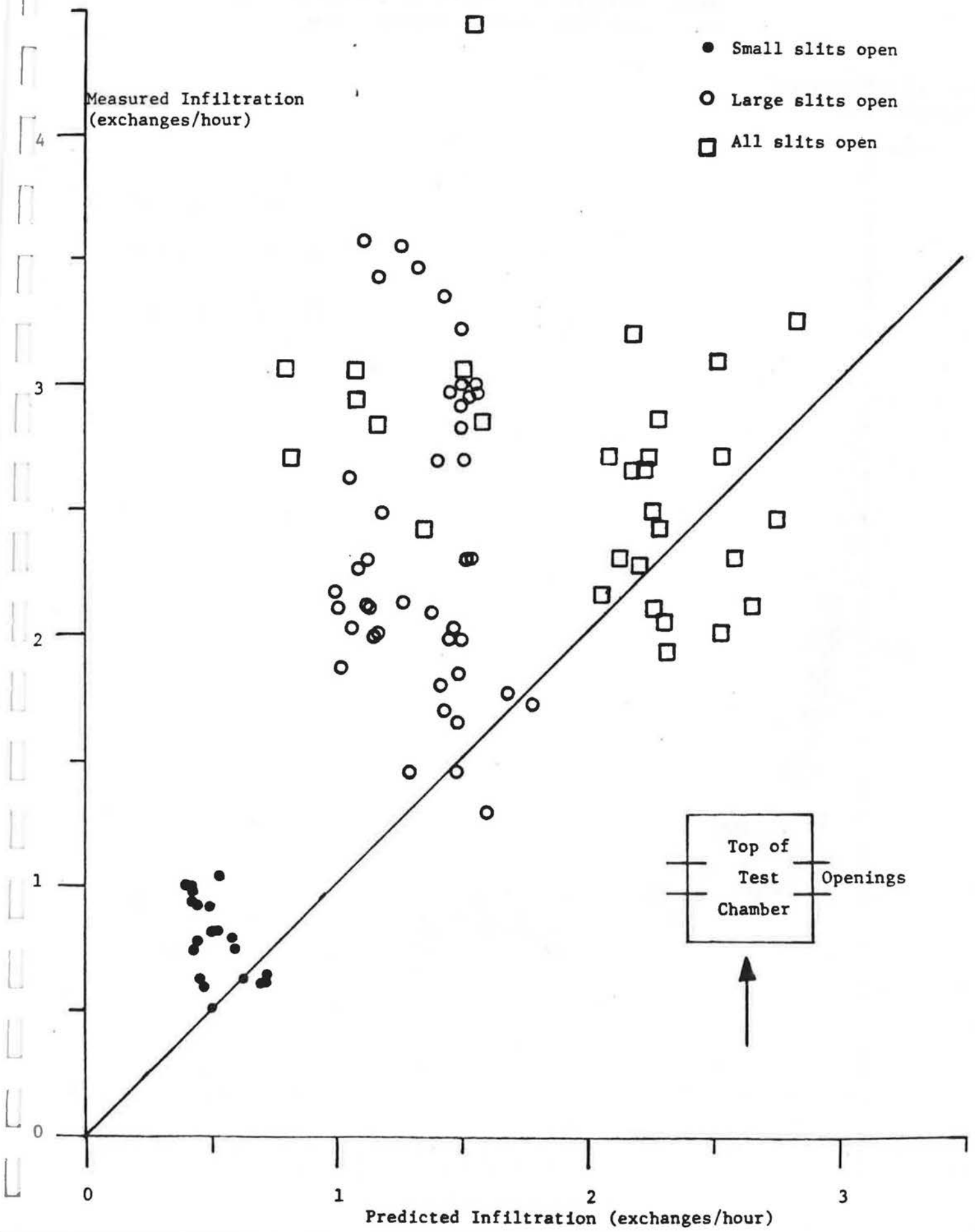

Figure 7.12

Ratio of Measured and Predicted Infiltration vs
Archimedes Number, Parallel Winds

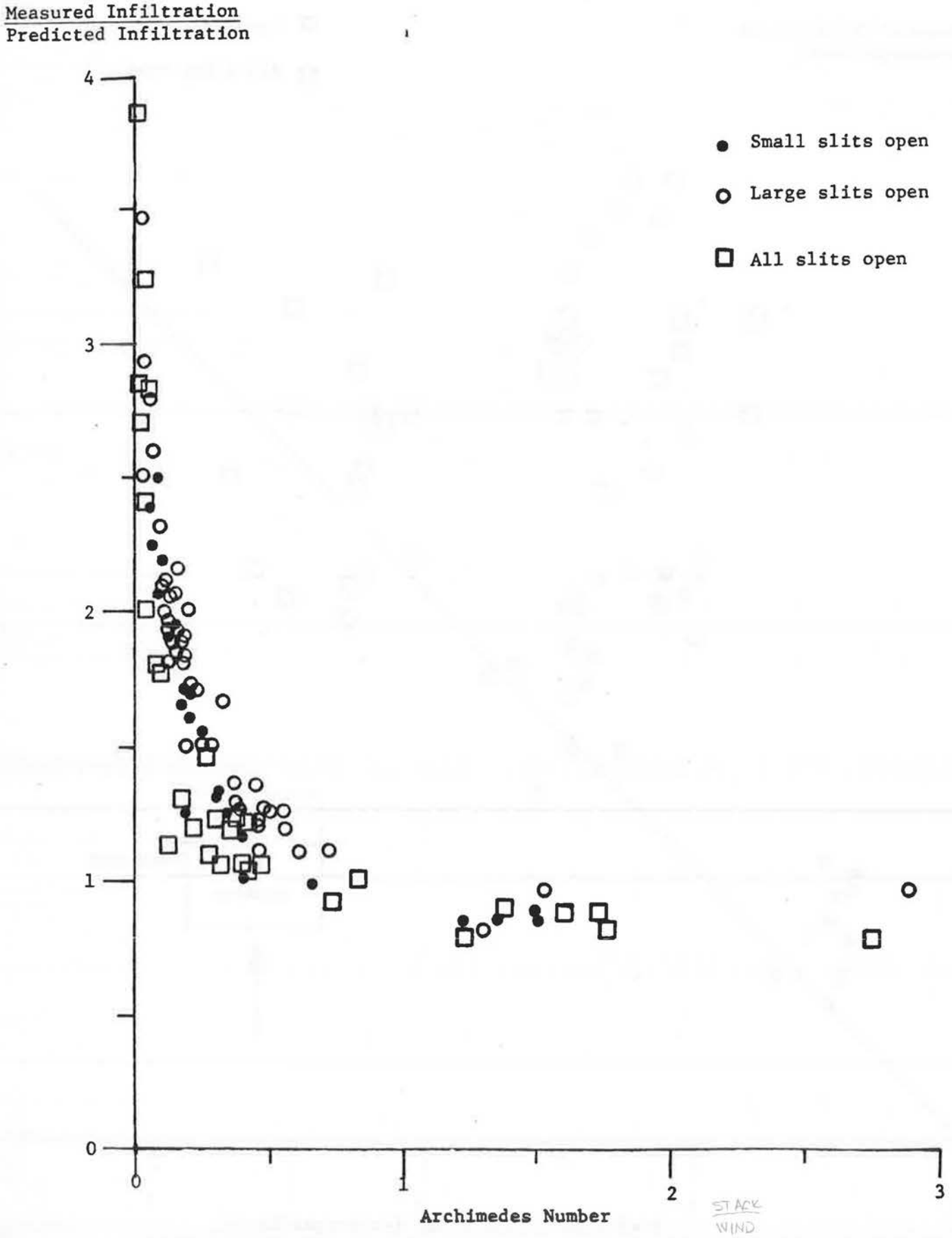

Figure 7.13

Measured vs. Predicted Infiltration, Off-Parallel Wind

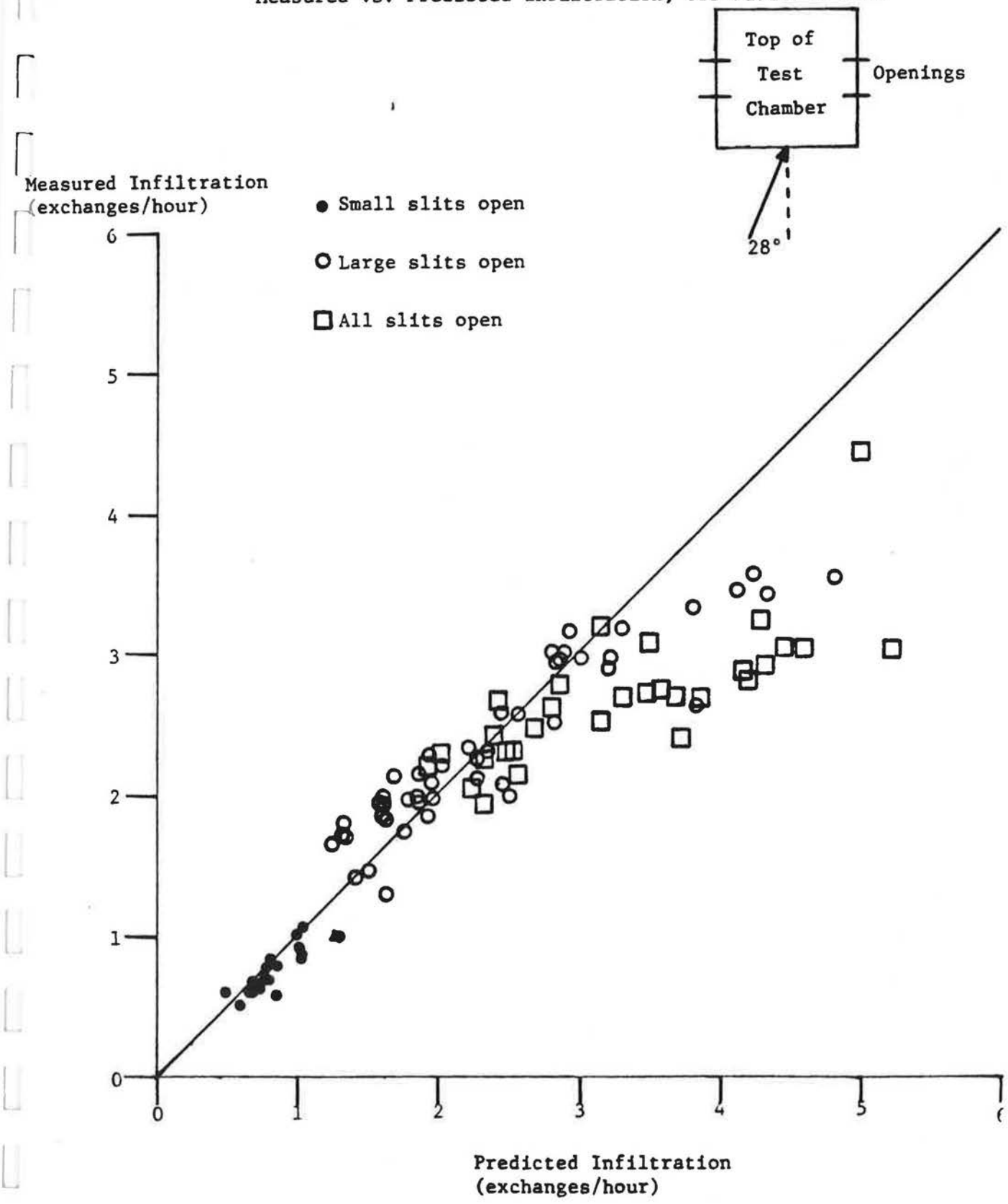

Chapter VIII

RELATING PRESSURIZATION AND INFILTRATION IN IDENTICAL HOMES*

We have shown in the previous chapter that pressurization can be used to predict infiltration rates successfully in a simple structure. Such prediction becomes more complicated in real homes because we do not know the distribution of leakage nor the leakage function of the openings. The models discussed in chapter V have been developed to make such predictions in real homes. But the attempts to validate these models have considered many different homes without consideration of housing style, construction materials and age. This chapter addresses this shortcoming of validation research by relating pressurization test results and measured infiltration rates in a group of identical homes.

8.1 DESCRIPTION

The fourteen homes in this experiment are identical two-story, wood frame colonials built in the late 1960's in Freehold, New Jersey. The floor area of the living space is 230 m^2, the envelope area above grade is 470 m^2, and the interior volume is roughly 565 m^3. All of the homes are within a half mile of one another. The local terrain consists of large lawns with some trees and shrubs scattered among the houses.

* The author acknowledges his indebtedness to Greg Linteris for extraordinary efforts in this project.

In May 1981 we pressure tested these homes on a day with relatively calm winds. Each house was pressurized and depressurized to pressure differences from 12.5 to 62.5 Pascals in increments of 12.5 Pa. It was not possible to pressurize some very leaky homes to 62.5 or even 50 Pa. Each house was tested twice to increase the reliability of the measurements.

We also made simultaneous air infiltration measurements on the houses on three consecutive nights in April 1981 using the tracer gas decay technique. The tests were performed by the homeowners after receiving written and verbal instructions. For each test the participants were supplied with a small polyethylene bottle containing about 30 cc of sulfur hexafluoride (SF_6). The homeowners released the tracer gas near the furnace return duct and ran the furnace fan for twenty minutes to ensure adequate mixing of the tracer with the interior air. Every half hour after the tracer gas release, the furnace fan was turned on for five minutes and a sample of interior air was collected from a central location in the house in a polyethylene bottle. Five such samples were collected for each tracer gas decay.

After each test, the sample bottles were exchanged for a new set the following morning. The bottles were returned to our laboratory where the SF_6 concentration in each bottle was determined using air infiltration monitoring equipment [1]. The infiltration rate I is related to the tracer gas concentration $\bar{c}$ through the following equation

$$\bar{c} = \bar{c}_o e^{-It}, \qquad (8.1)$$

where c_o is the initial tracer gas concentration. In order to determine I, the natural logarithms of the five concentration measurements are plotted against time and a least squares, linear regression is made to obtain the slope -I. The regression also yields a coefficient of determination r^2 which is a measure of the linearity of the fit. A low value of r^2 is a sign of an inaccurate infiltration measurement.

8.2 RESULTS

The results of the pressurization tests are presented in table (8.1) which lists the 50 Pascal leakage rate of the homes in m^3/hr and X/hr for both pressurization and depressurization, along with the average of the 4 Pa flow rates. At the bottom of the table, the means and standard deviations of these flows are given. In all three cases, the standard deviation is about 16% of the mean. All of the homes have similar leakage values except Y007 which is much leakier than the rest because of a louvered vent into the attic. Errors in pressure testing induced by building components which change during the test, such as this louvered vent, must be considered. Excluding this home, the 50 Pa pressurization flow rate varies from 5.9 to 8.2 X/hr a variation of 1.4 to 1. The depressurization flow rate ranges from 5.8 to 8.8 X/hr a variation of 1.5 to 1. These houses are relatively tight for N.J. frame homes of comparable vintage which range from about 10 to 15 X/hr at 50 Pa.

The results of the natural air infiltration measurements are presented in table (8.2). Only two nights of measurements were recorded for some houses when the homeowners were not available. Only eight out of forty measurements are noted as questionable for reasons such as one or two of the sample bottles being improperly sealed when received in the laboratory or low values of r^2. Figure (8.1) shows the infiltration rate for each house on the three nights plotted in order from lowest to highest average infiltration rate. The three values are very close to each other except for houses Y008 and Y013. In Y008, one test was done with the fireplace operating and shows a significantly larger infiltration rate than the other two nights. House Y013 has two similar infiltration rates, but the measurement on 7 April has an extremely low value. These two homes, along with Y007 which had an inaccurate pressurization test, are neglected in the following analysis. The means and standard deviations of the infiltration rates on the three nights are given at the bottom of table (8.2) for all homes except the three just noted. This large set of "bottle sample" measurements at Freehold is a demonstration of the usefulnesss of this technique. The high values of r^2 (only seven out of forty measurements had $r^2<0.95$) and the similarity of each home's measurements over the three nights show that this technique can be used to obtain reliable and inexpensive measurements of infiltration rates.

8.3 ANALYSIS

Prior to this work, no comparisons of pressurization and simultaneous infiltration measurements have been made on identical homes. The following section compares the two measurements and applies predictive models to the data. The analysis also involves standard linear regressions and the Spearman rank test [2] to compare the relative rankings of two sets of values. The Spearman rank test enables one to compare the ranks of two sets of n values ($x_1, x_2, \ldots, x_n$) and ($y_1, y_2, \ldots, y_n$). The rankings of these two sets are { $Rx_1, \ldots, Rx_n$ } and{ $Ry_1, \ldots, Ry_n$ }, which are both permutations of the integers 1 to n. The Spearman rank test is characterized by the parameter r_s, defined by

$$r_s = 1 - 6 \sum_{i=1}^{n} (Rx_i - Ry_i)^2 / n(n^2-1). \qquad (8.3)$$

If $r_s = 1$, then the sets x_n and y_n posess the same ranking. If $r_s = -1$, then the rankings are opposite.

Figure (8.2) is a plot of the infiltration rates for the three nights against the flow rate at 50 Pa of pressurization. Figure (8.3) is a plot of the infiltration rates against $\bar{Q}(4)$, i.e. the average of the expected pressurization and depressurzation leakage at 4 Pa. Table (8.3) lists the results of applying linear regressions and the Spearman rank test to the data. The linear regressions have correlations on the order of 0.30 for all cases. The Spearman ranks range from 0.43 to 0.65. Note that the slopes of the regression lines are similar for the three nights in the separate cases of 4 Pa and 50 Pa flow rates. There is little

difference between the predictive ability of the 4 Pa and 50 Pa leakage, although the Spearman ranks are larger for the 50 Pa flow rates. The scatter in figures (8.2) and (8.3) is due to the uncertainty in the measurements and due to variation among the houses in leakage distribution and wind exposure.

Predictive Models

Predictive models of air infiltration from chapter V were applied to the Freehold data. We used the model developed at the Lawrence Berkeley Laboratory [3] which parameterizes the leakiness of a house through the average of the expected flows under pressurization and depressurization at 4 Pa, $\overline{Q}(4)$. In order to calculate the infiltration rates from this model one must classify the local terrain and the shielding of the homes. There are five classes of each, and in both cases, class III is most appropriate for the Freehold homes. It is also necessary to input the leakage areas of the ceiling and floor.

For each night, the predicted infiltration rate was determined for the following cases:

1. Terrain and shielding are both class III.
2. Terrain is class III, shielding is IV.
3. Terrain and shielding are class IV.

Class IV corresponds to more obstructed terrain and more shielding than class III. Although the homes are in class III for both terrain and shielding, cases 2 and 3 are included to see the magnitude of their effects. Also, three cases of leakage distribution were used:

1. Uniform distribution of leakage.
2. All leakage in the walls.
3. Extra leakage in the ceiling.

Shaw's phenomenological model was also used to predict infiltration rates for the Freehold homes [4-5]. The model was developed from experiments on relatively tight homes, about 6 X/hr at 50 Pa. There are separate predictive equations for the stack and wind regimes, and for when both effects are important. But it is not clear how to determine within which regime a particular house lies for given weather conditions. We also tested the predictions of Kronvall's model [6] which is based on measurements on nineteen tight homes.

Table (8.4) shows the infiltration rates predicted by the models along with the weather and the average measured infiltration rates of all the houses for the three nights. The predictions from the curve fits to figures (5.1) and (5.2) are also given, and although they give only one infiltration rate for each house, this rate is close to the average of all the homes. In fact, the curve fits predict as well as any of the models employed. For the most realistic case of terrain and shielding both being in class III, the LBL model overpredicts by 25 to 100% depending on the leakage distribution. Assuming extra leakage in the ceiling provides the best prediction, but these values are still in error by up to 50%. For all asumptions of leakage distribution the overprediction becomes worse from 6 April to 8 April as the wind speed increases. Thus the model appears more sensitive to wind

than the homes. The other cases of shielding and terrain result in less sensitivity of the model to wind, and the predictions become somewhat better.

Shaw's stack expression predicts the average infiltration rate well for the first night, but as the weather moves out of the stack regime the model underpredicts. The shielded wind expression is a good predictor of the average infiltration rates, but like the LBL model, responds to the increasing wind speed more than the homes do. Kronvall's model predicts well, but also shows more sensitivity to wind than the homes.

The simultaneous infiltration measurements in the Freehold homes have enabled us to relate infiltration and pressurization without the confounding effects of differences among homes. The plots of measured infiltration rate versus pressurization flow rate exhibit a large amount of scatter, but a positive correlation is evident. The correlation coefficients show that the pressurization test results account for about one-third of the variation in the infiltration rates. The rest of the variation is due to differences in leakage distribution and wind exposure, as well as measurement errors.

The predictive models of infiltration presented in chapter V give mixed results. The LBL model is off by up to 100%, but can predict within 25% if one assumes unrealistic terrain and shielding classes. Making unverified assumptions about the leakage distribution also increases the accuracy of the predictions.

Shaw's model predicts within 25% if one makes the correct choices of stack or wind regimes, but there is no way of making this choice beforehand. Kronvall's model works well on these data, but is more sensitive to the increasing wind speed over the three nights than the houses, as are the other two models. The curve fits from figures (5.1) and (5.2) give only one infiltration rate independent of the weather, but it is closer to the measured rates than any of the models. Note that the Freehold data were included in these two figures. We have seen that the infiltration models are generally within 30% of the measured infiltration rates, but they are closer in the stack regime than for cases where wind plays an important role. This is the same result found in the previous chapter for the Test Chamber. Wind effects are difficult to model because of the great variability in the wind exposure of homes.

REFERENCES

[1] Harrje, D.T., Hunt, C.M., Treado, S.J., Malik, N.J., "Automated Instrumentation for Air Infiltration Measurement in Buildings," Report No. 13, Center for Environmental Studies, Princeton University, 1975.

[2] Popham, W.J., Sirotnik, K.A., Educational Statistics, Harper & Row, New York, 1973.

[3] Sherman, M.H., Grimsrud, D.T., "Infiltration-Pressurization Correlation: Simplified Physical Modelling," ASHRAE Transactions, Vol. 86(II), 1980.

[4] Shaw, C.Y., "A Correlation Between Air Infiltration and Air Tightness for Houses in a Developed Residential Area," ASHRAE Semi-annual Meeting, Cincinnati, Ohio, June 1981.

[5] Shaw, C.Y., Tamura, G.T., "Mark XI Energy Research Project, Air-Tightness and Air-Infiltration Measurements," Building Research Note, No. 162, Division of Building Research, National Research Council of Canada, 1980.

[6] Kronvall, J., "Correlating Pressurization and Infiltration Rate Data - Tests of an Heuristic Model," Lund Institute of Technology, Division of Building Technology, Lund, Sweden, 1980.

Table 8.1 Pressurization Data on the Freehold Homes

House	4 Pascal Flow Rate[1] (m^3/hr)	50 Pascal Flow Rates[2] Pressurization (m^3/hr)	Pressurization (exchanges/hour)	Depressurization (m^3/hr)	Depressurization (exchanges/hr
Y008	614	4125	7.3	4124	7.3
Y016	504	3499	6.2	3240	5.7
Y020	667	3830	6.8	3920	6.9
Y029	605	3417	6.0	3555	6.3
Y034	622	3422	6.1	3409	6.0
Y045	619	3551	6.3	3739	6.6
Y013	722	4435	7.8	3881	6.9
Y038	770	4711	8.3	4277	7.6
Y046	819	4527	8.0	5019	8.9
Y049	756	4225	7.5	4131	7.3
Y007	966	5353	9.5	5724	10.1
Y010	731	3817	6.8	4054	7.2
Y024	663	3843	6.8	4150	7.3
Y039	815	4235	7.5	4765	8.4
Mean	705	4042	7.2	4116	7.3
Standard Deviation	117	561		660	
Mean/S.D.	17%	14%		16%	

(1) Average of pressurization and depressurization flows from curve fits.

(2) Measured flow rates.

Table 8.2 Air Infiltration Measurements on the Freehold Homes

House	Average Infiltration Rate (exchanges/hour) 6 April	7 April	8 April
Y008	0.40*	0.51**	0.15
Y016	0.22	0.18*	0.25
Y020	0.36	---	0.35
Y029	0.20	0.36*	0.28
Y045	0.19	0.23*	0.22
Y034	0.20	0.36*	0.28
Y013	0.55	0.15	0.63
Y038	0.33	0.43	0.50
Y046	0.25*	0.26	0.30
Y049	0.34	0.32	0.24
Y007	---	0.32	0.30
Y010	0.32	0.37*	0.33
Y024	0.20	0.20	0.21
Y039	0.32	0.37	0.41
	Weather Data		
Wind Speed (m/s)	4.7	6.0	7.6
Temperature Difference (°C)	13.9	11.3	7.4

* Measurement problems.

** Fireplace in use.

Table 8.3

Infiltration Rate vs Pressurization Flow Rate

4 Pascal Flow Rate

6 April $I = 0.0053 + (.00038)\overline{Q}(4)$, $n = 10$, $r^2 = 0.33$, Spearman rank, $r_s = 0.52$

7 April $I = -0.055 + (0.0051)\overline{Q}(4)$, $n = 10$, $r^2 = 0.38$, Spearman rank, $r_s = 0.49$

8 April $I = -0.029 + (.00049)\overline{Q}(4)$, $n = 11$, $r^2 = 0.30$ Spearman rank, $r_s = 0.43$

50 Pascal Flow Rate

6 April $I = -0.064 + (.000085)Q(50)$, $n = 10$, $r^2 = 0.31$ Spearman rank, $r_s = 0.56$

7 April $I = -0.063 + (.000091)Q(50)$, $n = 10$, $r^2 = 0.26$ Spearman rank, $r_s = 0.65$

8 April $I = -0.18 + (.00012)Q(50)$, $n = 11$, $r^2 = 0.40$ Spearman rank, $r_s = 0.57$

Table 8.4

Comparison of Measured and Predicted Infiltration Rates

	6 April	7 April	8 April
Wind Speed (m/s)	4.7	6.0	7.6
Temperature difference (°C)	13.9	11.3	7.4
Infiltration rate* (exchanges/hr)	0.27	0.30	0.31
Predicted Infiltration Rates			
LBL Model Terrain = Shielding = III			
Uniform Leakage Distribution	0.43	0.48	0.55
All Leakage in Walls	0.47	0.66	0.67
Extra Leakage in Ceiling	0.34	0.38	0.46
Terrain = III, Shielding = IV			
Uniform Leakage Distribution	0.39	0.41	0.45
All Leakage in Walls	0.40	0.45	0.53
Extra Leakage in Ceiling	0.37	0.38	0.40
Terrain = Shielding = IV			
Uniform Leakage Distribution	0.36	0.37	0.39
All Leakage in Walls	0.34	0.38	0.43
Extra Leakage in Ceiling	0.35	0.35	0.34
Shaw Model			
Stack Regime	0.26	0.22	0.17
Shielded Wind Regime	0.29	0.34	0.40
Combination	0.59	0.59	0.59
Kronvall Model (see equation 5.6)	0.32	0.34	0.39
Curve Fit to Figure 5.1		0.31	
Curve Fit to Figure 5.2			

Average for all Freehold homes.

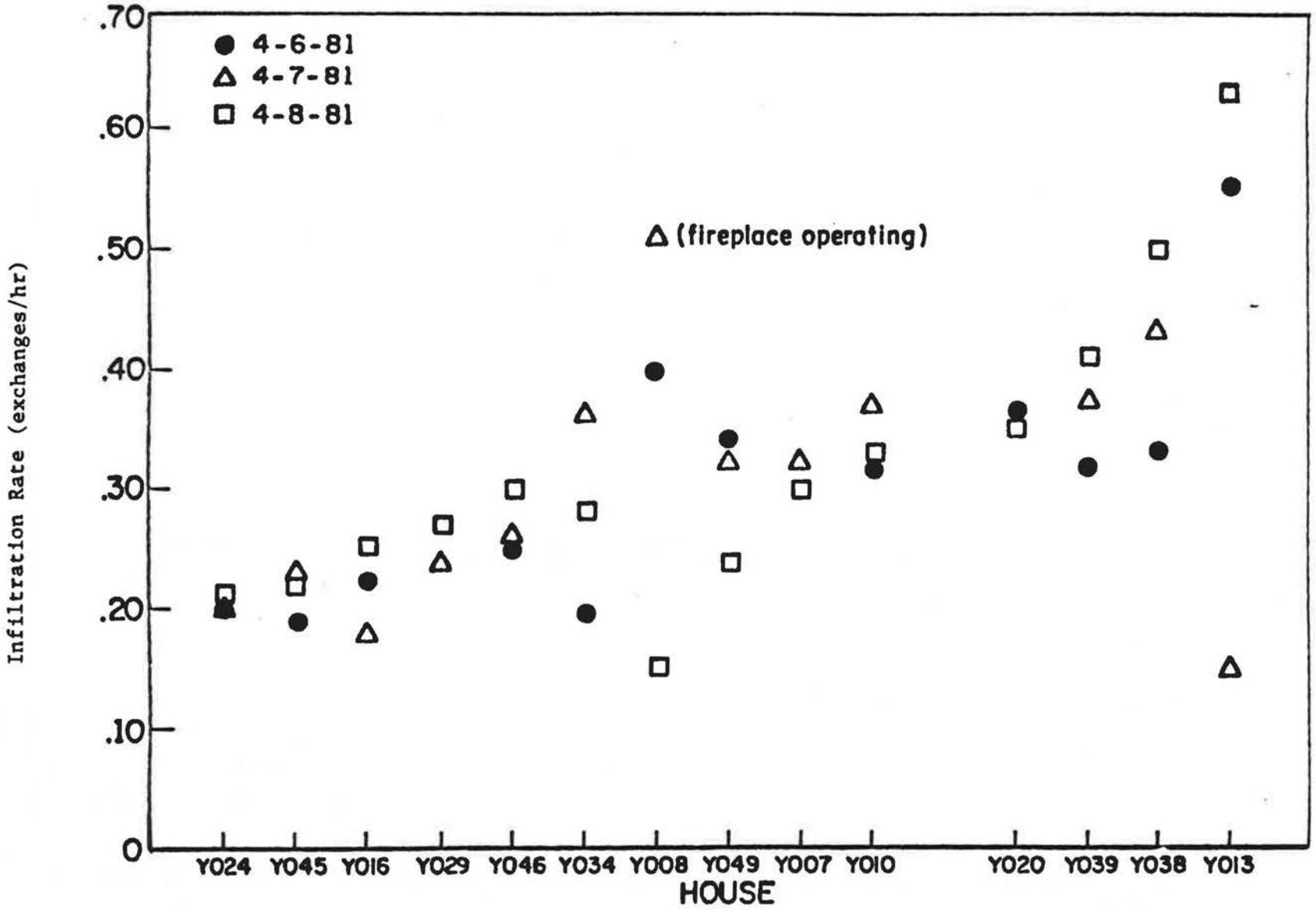

Figure 8.1

Infiltration for each Freehold House (in order from lowest to highest average infiltration rate)

Figure 8.2

Infiltration vs 50 Pascal Flow Rate for the Freehold Homes

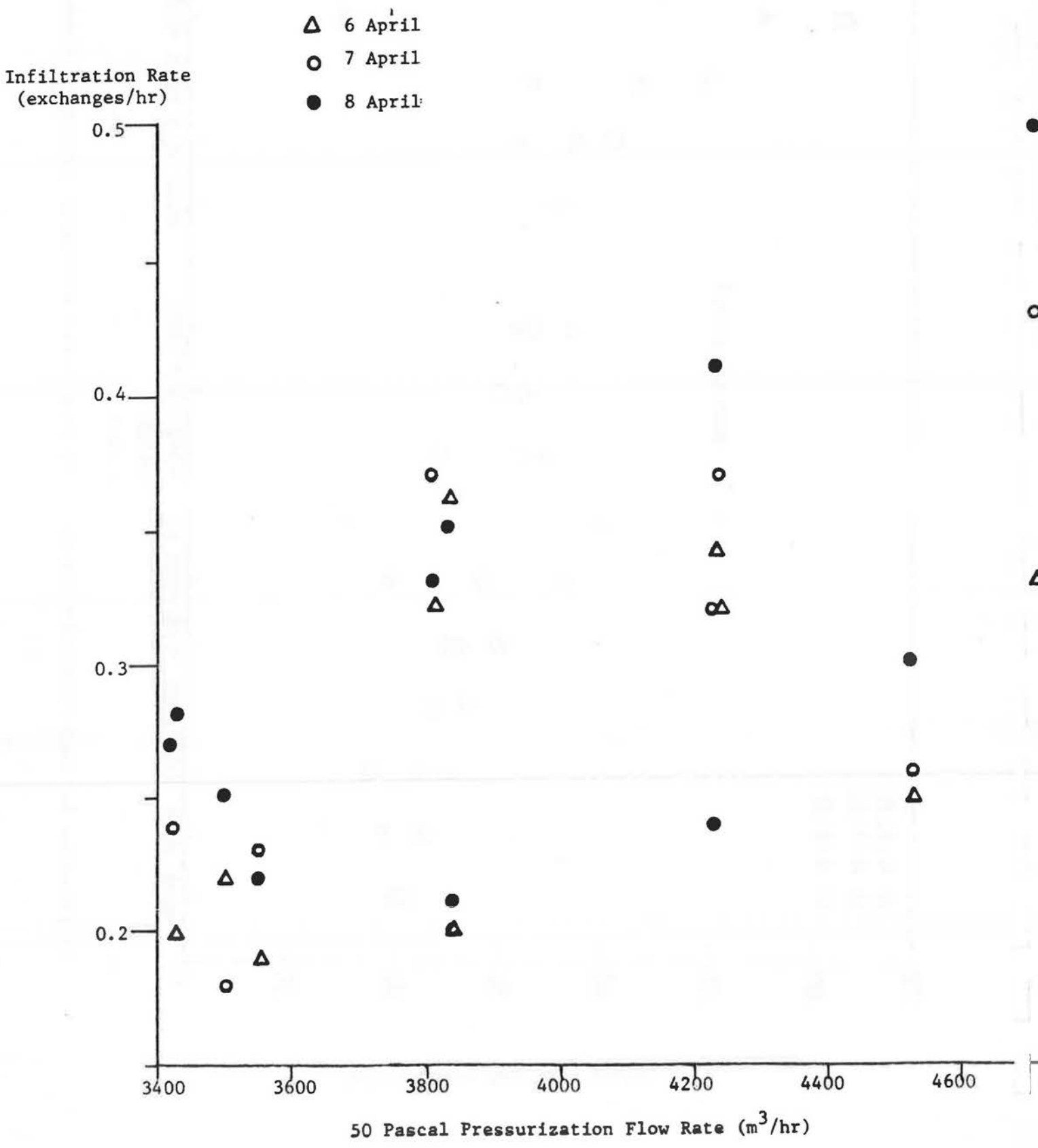

Figure 8.3

Infiltration vs 4 Pascal Flow Rate for the Freehold Homes

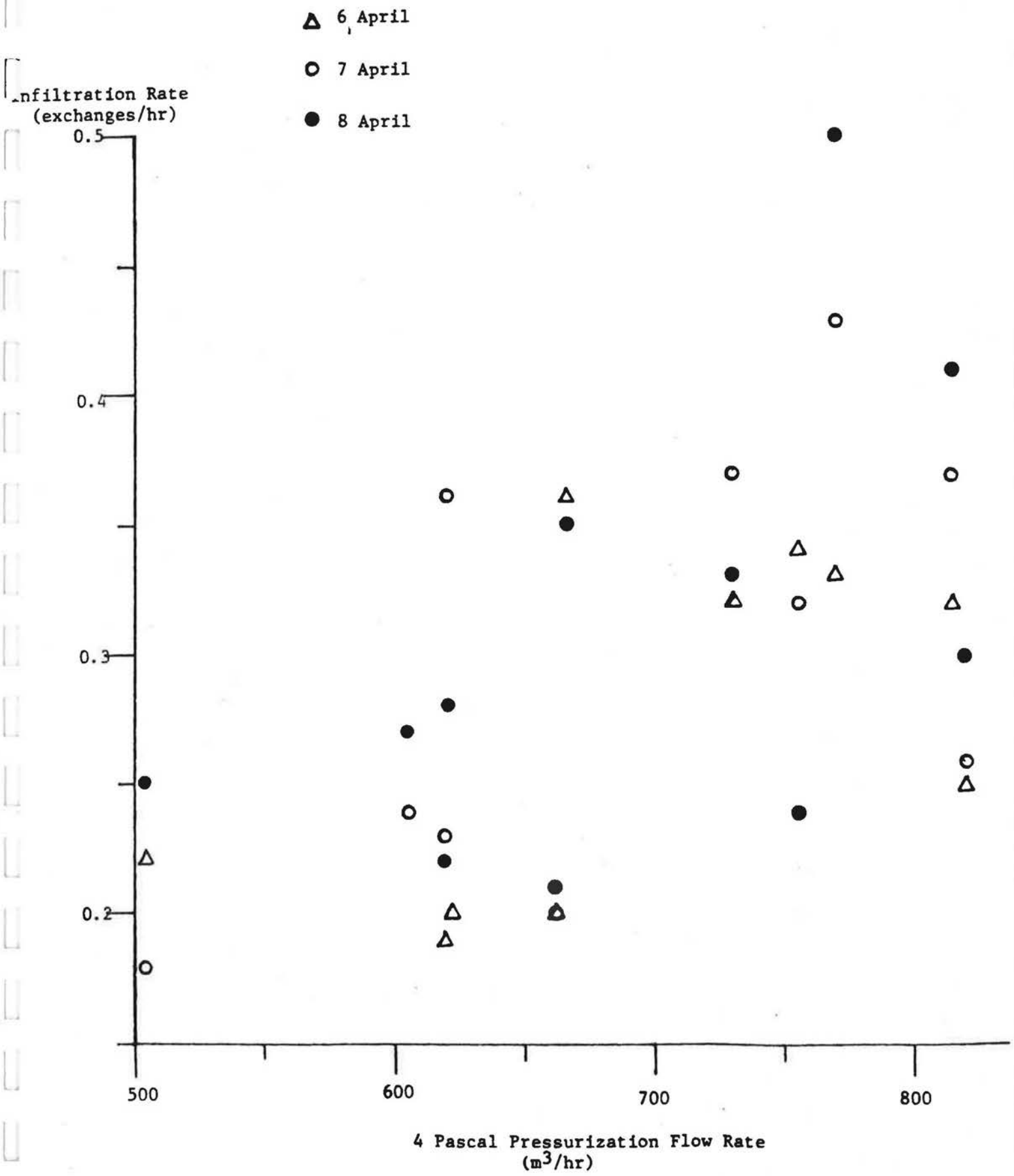

Chapter IX

REALISTIC TESTS OF AN AIR-TO-AIR HEAT EXCHANGER

Using the evaluation techniques discussed above we can determine if a house is too leaky so it may be tightened to save energy, or if it is so tight that indoor air pollution is a threat. In the latter case, one may employ various means to alleviate the problem such as cleaning the interior air or removing pollutants at their sources. Another solution is the use of mechanical ventilation with heat recovery, or air-to-air heat exchangers. Heat exchangers for houses are commercially available, and research into their design and performance is proceeding [1-5]. As these devices are developed it is important to evaluate their effectiveness for future designs and installations. Most of this research has involved experiments in laboratories which obscure the actual performance of the device. This chapter presents a realistic procedure to determine the efficiency of heat recovery of air-to-air heat exchangers and identifies several factors which may degrade their effectiveness.

We tested one particular heat exchanger, the Lossnay model VL-1500 manufactured by Mitsubishi Electric Industrial Products. This device was tested in a small building called the Test Chamber, used in the experiments in chapter VII and described in detail in appendix A. Because the Test Chamber is highly instru-

mented and well-controlled, we were able to precisely determine the Lossnay efficiency. In the efficiency measurements, the power consumed with the Lossnay running is compared to consumption expected without the Lossnay installed. The difference is related to the ventilation rate induced by the Lossnay to determine the efficiency of heat recovery. This chapter reports on experiments used to develop the ability to predict the Test Chamber heat loss, and presents the experiments evaluating the performance of the Lossnay.

9.1 THE HEAT LOSS OF THE TEST CHAMBER

Accurate measurements of the efficiency of the Lossnay require a precise knowledge of the conductive heat loss rate of the Test Chamber. Many complex and widely used methods for calculating the heat loss of a building exist. Generally, these techniques require very detailed knowledge of the construction of the building. Errors in these theoretical estimates will arise from the neglect of obscure and important construction anomalies such as gaps between building elements.

Rather than use a long-hand calculation approach to predicting the heat loss of the Test Chamber, we chose an empirical approach to the problem. The heat loss rate of the structure was carefully measured during several nights and then related to various physical effects. The tests were done at night in order to avoid the need to consider heat gains due to solar radiation. Since the Test Chamber is practically airtight, the heat loss is almost

totally due to conduction. This work on predicting the conductive heat loss rate of the Test Chamber is presented in detail in appendix D.

The heat loss rate of the Test Chamber was determined by measuring the heat input required to maintain the interior at a constant temperature. Figure (9.1) shows the experimental arrangement inside the structure. Energy is supplied by light bulbs connected to a thermostat which controls the inside temperature. The energy input is measured with a residential Watt-hour meter equipped with a photo-interrupter module to count revolutions of the Watt-hour meter disk. The air exchange rate of the Test Chamber with the outside is measured using the tracer gas decay technique. Ethane is used as the tracer gas, and a Wilks infrared gas analyzer measures the ethane concentration. Inside and outside temperatures are measured with thermistors, and the average wind speed with a cup anemometer. The level of infrared radiation from the night sky is monitored with an Eppley infrared radiometer. All of the instrumentation is discussed in detail in appendix B.

The conduction heat loss rate is characterized by the "lossiness" of the Test Chamber. The lossiness of a structure may be defined as the power required to maintain an inside-outside temperature difference, divided by that temperature difference. This definition is imperfect because the heat input rate will generally not be proportional to the instantaneous temperature difference due in part to the thermal inertia of the building. Because

of thermal storage effects, the heat input depends on the history of inside and outside temperatures. Alternatively, one defines the "overall" lossiness L as the heat input rate divided by the temperature difference when the inside and outside temperatures are constant. The overall lossiness is not a uniquely defined property of the structure, but is determined by effects discussed below. Although steady temperature conditions never exist for the Test Chamber, or any other structure, one may determine the overall lossiness by using the "trailing" temperature instead of the instantaneous temperature. The trailing temperature is a lagged temperature which accounts for the past temperature history. Appendix D presents a model of the heat transfer from the Test Chamber from which the trailing temperature is developed. To calculate the overall lossiness for a night, the trailing outside temperature is used instead of the actual outside temperature. Each lossiness measurement is an average from midnight to 6 a.m. From the power input $\overline{Q}$, and the trailing temperature difference ΔT^*, the overall lossiness $L = \overline{Q}/\Delta T^*$ is calculated. ΔT^* is the inside air temperature minus the trailing outside temperature. The overall lossiness varies by roughly ±10% about the mean value due to the effects outlined below and discussed in detail in appendix D.

Variations in the Test Chamber Lossiness

The variation in the overall lossiness of the Test Chamber is due to several physical effects. First, the coupling of infrared radiation from the sky and surroundings and the wind speed affect the overall lossiness by determining the outside surface temperature of the Test Chamber. On calm nights with clear skies, the outside surface gets significantly colder than the ambient air due to radiative heat loss to the sky. This cold surface leads to a large overall lossiness because the overall lossiness is related to the difference between the inside and outside air, not surface, temperatures. On clear nights with a strong wind blowing, the increase in the outdoor film coefficient causes the surface temperature to approach the outside air temperature, thereby decreasing the lossiness. On cloudy nights, the outside surface temperature is closer to, though seldom greater than, the outside air temperature and this causes a lower lossiness than on clear, calm nights. All of these infrared/wind conditions can occur at the same outside air temperature, and therefore do not affect the temperature difference ΔT^*, but do affect the heat loss $\bar{Q}$ and the lossiness L. The infrared/wind effect is described in more detail in Appendix D.

In general, the thermal resistance of a material depends on its temperature. It has been well documented that the thermal resistance of a wall section decreases as its average temperature increases [6]. To model this effect in the Test Chamber, we use the average of the interior air temperature T_i and the calculated outside surface temperature T_T.

Although the Test Chamber is extremely air tight, there is still a small amount of air infiltration. With the significant inside-outside temperature differences existing during the lossiness tests, from about 20 to 25 °C, the infiltration rate ranges from 0.05 to 0.10 X/hr depending on the wind speed. One expects that the heat loss associated with an air infiltration rate I is given by

$$Q_I = \rho c_p V I \Delta T_I \qquad (9.1)$$

ρc_p = Volumetric heat capacity of air (W-hr/m^3-°C)
V = Volume of the structure being heated or cooled (m^3)
I = Infiltration rate (hr^{-1})
ΔT_I = Instantaneous inside-outside temperature difference (°C)

There has been little experimental work to verify the accuracy of equation (9.1). While it is straightforward and seems appropriate to account for air infiltration heat loss, it may not be correct in all cases. For example, if air enters a building and then leaves before attaining the inside temperature, its heating will require less than the energy predicted by the above expression. Such infiltration will not be completely accounted for by tracer gas measurement since this short-lived air stream will not mix completely with the tracer gas. These questions of mixing complicate the application of equation (9.1), and point out the need for care in assigning a heat loss due to air infiltration.

By considering the three effects discussed above, i.e. the infrared/wind interaction, temperature effects on thermal resis-

tance and the wind dependence of the air infiltration rate, we were able to predict the overall lossiness of the Test Chamber within 1% based on empirically derived relations. Such precision is important when studying air infiltration heat loss in this or any other structure. A calculation approach to the heat loss would not have given us such precise results.

9.2 AIR INFILTRATION HEAT LOSS EXPERIMENTS

Before studying the Lossnay heat exchanger experiments were conducted in the Test Chamber to check the validity of equation (9.1) to account for the heat loss associated with air infiltration. In these tests, some air exchange between the inside and outside was allowed. The predicted heat loss due to conduction $\overline{Q}_C$ based on the work presented in appendix D was subtracted from the measured heat loss $\overline{Q}_M$, both in Watts. This difference, or the remaining heat loss $\overline{Q}_R$, was then compared to the calculated heat loss $\overline{Q}_I$ from equation (9.1).

The test results are shown in table (9.1). In the first test, the infiltration rate was low, only 0.10 X/hr above the leakage rate under the Test Chamber's normal tightness. The remaining power input $\overline{Q}_R$ after subtracting out conduction is very close to the expected power input $\overline{Q}_I$. In the next two tests an exhaust fan was used to induce a larger amount of infiltration. In both cases, the remaining heat loss $\overline{Q}_R$ is close to that predicted by equation (9.1). The results are even better than they appear because the power used by the exhaust fan, about 20 Watts, was to a

large degree lost to the outside. From these three tests, we conclude that equation (9.1) works well for quantifying the heat loss due to air infiltration. Also, our technique of using the predicted heat loss to study other heat loss effects gives good results.

9.3 TESTS OF THE HEAT EXCHANGER

This section describes experiments to test the effectiveness of the Lossnay air-to-air heat exchanger in the Test Chamber. The Lossnay is a cross-flow heat exchanger constructed of plates and fins made from treated paper capable of moisture transfer. An aluminum core is available if moisture transfer is not desired. Figure (9.2) is a sketch of the Lossnay showing an inlet and exhaust for both the inside and outside. An electric motor drives two centrifugal blowers which draw air into the heat exchanger. The model VL-1500 is the size of a small window air conditioner, requires no ductwork and has a capacity suited to one or two rooms. The Lossnay was chosen as an example of a commercially available residential heat exchnnger and not because of any unique design features.

In these experiments, the heat exchanger was installed in one of the Test Chamber's lower windows as seen in the photographs in figures (9.3) through (9.6). The photographs in figure (9.3) and (9.4) were taken from inside the Test Chamber. In the first photo the Lossnay is uncovered, revealing the centrifugal blower or "squirrel cage fan" intake and a triangular opening in the corner

through which the supply air flows. Figure (9.4) shows the Lossany with its plastic cover in place. The photos in figure (9.5) and (9.6) were taken from outside the Test Chamber. The close-up of the Lossnay in figure (9.5) shows two openings, one for exhausting the inside air and the other for drawing in outside air.

The Lossnay air-to-air heat exchanger was evaluated by running it in the Test Chamber and doing a heat balance on the structure. As in the air infiltration heat loss tests, the predicted energy consumption was subtracted from the measured energy use. The remainder was then related to the measured infiltration rate induced by the Lossnay to determine the efficiency of heat recovery. The Lossnay efficiency was also determined through measurements of the four temperatures in figure (9.2).

Results

The results of the tests involving a heat balance on the Test Chamber are summarized in table (9.2). The first two columns give the test number and the conditions during the experiment. The third column is the measured infiltration rate minus the rate expected under the normally tight conditions. The next three columns are the average measured wattage input to the Test Chamber $\overline{Q}_M$, the predicted wattage due to conduction $\overline{Q}C$, and the remaining wattage $\overline{Q}_R$ after subtracting $\overline{Q}_C$ from $\overline{Q}_M$. Next is the expected power consumed due to infiltration $\overline{Q}_I$ as calculated from equation (9.1). Since $\overline{Q}_I$ is the expected heat loss associated with the induced ventilation rate and $\overline{Q}_R$ is the actual heat loss, then the "overall" efficiency of heat recovery η_o is given by

$$\eta_o = 1 - (\bar{Q}_R/\bar{Q}_I). \qquad (9.2)$$

In the first three tests, tw64 through tw66, the Lossnay was installed but not operating. By installing the Lossnay in the Test Chamber, we are replacing many centimeters of insulated wall with a metal box, thereby increasing the conduction losses. These tests were made to measure this increase in conduction. All the inlet and outlet vents were sealed off with plastic and tape, and therefore the expected additional heat loss due to air infiltration $\bar{Q}_I$ is zero. But $\bar{Q}_R$ is clearly nonzero. Dividing $\bar{Q}_R$ by ΔT_I for each night, one obtains a value of the lossiness associated with conduction through the Lossnay, L_L. For the three nights L_L equals 0.8, 0.5, and 1.0 W/°C which average out to roughly 0.8 W/°C. This value is used to account for conduction through the Lossnay in subsequent analysis. The relevancy of this number for installations in homes depends on where the Lossnay is installed. If one puts the Lossnay in a window the conduction losses will not be increased significantly, but if one installs the device in a hole in the wall then this conduction increase is relevant.

After these preliminary tests, we were able to study the overall efficiency of the Lossnay itself. The tests were done at the low and medium fan settings of the heat exchanger. The tests with the fan on low were done under two conditions, (a) with the Lossnay as is, and (b) with any obvious leaks in the Lossnay case taped up to see if the sealing would increase the efficiency.

The tests with the fan on medium were done only in the retrofitted state. The last column in table (9.2) lists the overall efficiency η_o for each case. η_o is the efficiency of the device as it performs in the Test Chamber including degradations due to conduction through the Lossnay itself and the power consumed by the fan.

Table (9.2) shows an overall efficiency of 46% when the fan is on low and the heat exchanger is unretrofitted. Retrofitting the device increases η_o by about 6% to 52% at the low fan setting. The improvement in efficiency implies that there is some leakage in the unit between the incoming and outgoing air streams which bypasses the heat exchanger core. Turning up the fan speed to medium decreases the efficiency to about 49%. While these efficiencies seem reasonable, they are significantly less than the manufacturer's claim of 70%.

To further understand the Lossnay performance, two other factors were taken into account. We correct for conduction through the Lossnay and for the power used by the fans to move the air. Using a Watt-hour meter the fan was found to consume 18 W on low and 39 W on the medium setting. It is not clear how much of this fan power reaches the Test Chamber interior and how much is exhausted to the outside. Because the device is symmetrical, as shown in figure (9.2), it seems reasonable to assume that one-half of the fan power is lost to the outside while the other half stays within the Test Chamber.

In table (9.3) the six efficiency tests are reconsidered in detail by including fan power and conduction through the Lossnay case. Again, the predicted heat loss due to conduction through the Test Chamber is subtracted from the measured power $\overline{Q}_M$. In addition, one-half of the fan power and the conduction through the Lossnay are also subtracted from $\overline{Q}_M$. The power lost by conduction is obtained by multiplying the instantaneous temperature difference T_I by 0.8 W/°C. The remaining wattage $\overline{Q}'_R$ is the heat loss associated with the induced infiltration alone. In table (9.3), $\overline{Q}'_R$ is used to calculate the heat exchanger effciciency η_L similarly to the overall efficiency η_o using

$$\eta_L = 1 - (\overline{Q}'_R/\overline{Q}_I). \qquad (9.3)$$

The heat exchanger efficiencies η_L are larger than the corresponding overall efficiencies by about 7 to 10%. By accounting for the effects of fan power and conduction through the device, we have isolated the efficiency of the heat exchanger itself to be about 60% which is closer to but still lower than the manufacturer's claim of 70%. Experimental error leads to an uncertainty in the efficiency η_L of about ±2%, but this can not account for the 10% difference in the efficiencies.

The heat exchanger efficiency was also determined by measuring the four air temperatures in figure (9.2): the outside air, T_{OA}; the feed air into the interior, T_{SA}; the exhaust air, T_{EA}; and the return air from inside, T_{RA}. These four temperatures were measured with thermistors while the infiltration rate of the Test

Chamber was monitored. Doing a heat balance on the heat exchanger while assuming that the fan power is negligible and that the heat capacity for the four air streams are the same, one arrives at expressions for two efficiencies of the heat exchanger. The heat transfer to the incoming air, or the feed side efficiency, is

$$\eta = (T_{OA} - T_{SA})/(T_{OA} - T_{RA}). \tag{9.4}$$

The exhaust side efficiency or the efficiency of heat transfer from the outgoing air is

$$\eta' = (T_{EA} - T_{SA})/(T_{OA} - T_{RA}). \tag{9.5}$$

The four temperatures were monitored through several nights and days, and the efficiencies η and η' were calculated. For a typical night, the average feedside efficiency was $\eta = 72\%$ and the average exhaust side efficiency was $\eta' = 61\%$. From the design of the heat exchanger, one does not expect such a large difference between the two values. The discrepancy is due to the power from the fan which tends to warm both air streams. Warming the incoming air tends to make the feed side efficiency larger while warming the exhaust stream decrease the exhaust side efficiency.

Through a heat balance on the Lossnay one can estimate the power consumed by the fan $\bar{q}_f$ using the four measured temperatures. Equating the heat flows into the device to the heat flows out, one obtains

$$(\dot{m}c_p)_{OA}T_{OA} + (\dot{m}c_p)_{RA}T_{RA} + \bar{q}_f = (\dot{m}c_p)_{SA}T_{SA} + (\dot{m}c_p)_{EA}T_{EA}. \tag{9.6}$$

$\dot{m}c_p$ is the heat flow per unit of absolute temperature for the particular air stream noted, $\dot{m}$ being the mass flow rate and c_p the heat capacity. Assuming that $\dot{m}c_p$ is the same for each stream, basing its value on the measured infiltration rate at the medium fan setting, and making conservative estimates of the experimental errors, one obtains $\bar{q}_f = 46 \pm 10$ W. The value measured with a Watt-hour meter is 39 W.

During the day the feedside efficiency is as high as 85 or 90% due to solar heat gain of the Lossnay. In this way, the device acts as a solar collector.

The feedside efficiency determined by the four temperatures at night is close to the manufacturer's claim. This efficiency determination is crude due to errors in temperature measurement due to radiation and conduction along the thermistor stem. Even with a spread of ±5%, the feed side efficiency is significantly different from $\eta_L = 56\%$ as calculated from a heat balance on the Test Chamber. A possible explanation for this discrepancy is imperfect mixing of the air within the Test Chamber.

The Lossnay heat exchanger was designed with the interior supply and return vents only about 40 cm apart. This design eliminates the need for any additional ductwork in the home, but it may be a disadvantage because it makes the Lossnay basically a "local" device. The heat exchanger is predominantly involved with the air near the device and has less effect on the air at some distance. This effect may be more important in very tight homes where there is little air flow through the structure and

less internal mixing than in a leakier structure. The effect of internal mixing on the Lossnay is shown in appendix F in which the Test Chamber is modelled as two separate cells exchanging air with the outside at two different rates. One cell has a large infiltration rate induced by the heat exchanger and the other has only minimal infiltration through the shell. The net infiltration rate is determined from the tracer concentration of an equally blended mixture from both sections. Hunt [7] and others have pointed out that infiltration rates measured under these conditions may be lower than the actual rates. The development of this two cell model in the appendix also shows this effect.

While low internal mixing causes the measured infiltration rate to be lower than that induced by the Lossnay, the magnitude of the effect is not clear. The heat exchanger efficiency as measured with the thermistors at the medium fan estimated setting is about $\eta = 70\%$ with an estimated uncertainty of $\pm 5\%$. The efficiency calculated from the Test Chamber heat balance is about $\eta_L = 55\%$. One may assume that the heat exchanger works at 70% efficiency on the actual infiltration rate I'. The amount of heat recovered must equal the amount recovered with the measured value of I = 4.55 X/hr and the calculated efficiency of $\eta_L = 55\%$. Thus,

$$I'(1-\eta) = I(1-\eta_L) \tag{9.7}$$

or,

$$I' = I(1-\eta_L)/(1-\eta). \tag{9.8}$$

For $\eta = 70\pm5\%$ and $\eta_L = 55\pm2\%$, the actual infiltration rate according to equation (9.8) is $I' = 6.8\pm1.2$ X/hr which is about 50% higher than the measured rate. This difference seems large, but the uncertainty is also very high. Small changes in η and η_L have large effects on I'. Although it can not be said whether errors in the measured infiltration rate due to incomplete mixing account for all of the difference between η and η_L, the effect of mixing is certainly an important factor in the Lossnay performance.

9.4 ECONOMICS

It is difficult to estimate the economics of the Lossnay because of variable use patterns and other effects. We did some rough calculations for a 300 m^3 house which show that the heat exchanger is economical in some cases. The high fan setting of the Lossnay is about 70 cfm which corresponds to 0.4 X/hr in this house. Assuming that the house starts with an average infiltration rate of 1.0 X/hr, this correseponds to 22.9 million Btu for each 5000 °F-day winter. We then tighten the home so that its average infiltration rate is 0.2 X/hr, but install two Lossnays which operate continuously to yield a total ventilation rate of 1.0 X/hr. Assuming a 50% efficiency of heat recovery for the Lossnays, the house now consumes 13.8 million Btu for ventilation. Thus, we save 9.1 million Btu each winter.

The Lossnay presently costs about $300, and the amount of savings associated with the 9.1 million Btu depends on the type of

fuel used and its price. We assume prices for natural gas of 50¢ per therm (10^5 Btu_t), $1.20 per gallon for oil, and 9¢/Kwh for electricity. In addition we assume seasonal efficiencies of two-thirds for both gas and oil. Based on the above assumptions, the 9.1 million Btu savings corresponds to $68 for gas, $123 for oil and $236 for electricity. Of course the savings will vary with the patterns of use, the fuel price, house volume and the furnace efficiency. One should also consider the costs of tightening the house. Additional savings will be realized if one also airconditions the house with the Lossnay running. The above calculations are indeed crude, but they show that the Lossnay can make sense economically.

Conclusions

The Lossnay air-to-air heat exchanger has been tested in the Test Chamber. Through a heat balance on the structure the device was found to recover about 55 to 60% of the heat passing through it. This efficiency decreases to about 50% if one also considers the lost fan power and heat conduction through the metal case of the Lossnay. Both the manufacturer's claimed efficiency and the efficiency as measured by doing a heat balance on the device are close to 70%. We also found that retrofitting the device increases the efficiency significantly, implying that there is leakage between the two air streams within the Lossnay.

The discrepancy between the measured and the manufacturer's claimed efficiency is due in part to incomplete mixing of the air

within the Test Chamber. Because of imperfect mixing, the Lossnay tends to affect predominantly a localized volume within the structure. This finding may have important implications for the design of air-to-air heat exchangers, particularly for the placement of the interior supply and return vents.

Incomplete mixing is less of a problem in leakier houses, but it is impossible to control the ventilation rate of a leaky dwelling. Also, it is tighter housing which is more likely to have indoor air quality problems and to need an air-to-air heat exchanger.

We have learned two things from our tests of the Lossnay heat exchanger in the Test Chamber. First, we found that this device does recover significantly more heat than is required to run it. Thus, air-to-air heat exchangers may prove to be an economical way of ventilating homes without wasting energy. Also, we found that our realistic test method has enabled us to learn about effects that would not be apparent in a laboratory test facility. The conduction of heat through the Lossnay and the effects of imperfect mixing on the heat exchanger effectiveness would have been missed if the experiments were not done in the Test Chamber. Future work on evaluating heat exchangers and other conservation devices will benefit from such in-situ measurements of their performance.

REFERENCES

[1] Besant, R.W., Brooks, E.E., Schoenan, G.J., Dumont, R.S., "Design of Low Cost Ventilation Air Heat Exchangers," Energy Conservation in Heating, Cooling, and Ventilating Buildings, eds., Hoogendoorn, C.J., Afgan, N.H., Series in Thermal and Fluids Engineering, Hemisphere Publishing Corporation, 1978.

[2] Hand, A.J., "Blow Out Stale Air but Save the Heat," Popular Science, Vol. 217, No. 4, October 1980.

[3] Roseme, G.D., Hollowell, C.D., Meier, A., Rosenfeld, A., Turiel, I., "Air- to-Air Heat Exchangers: Saving Energy and Improving Indoor Air Quality," Report No. 9381, Lawrence Berkeley Laboratory, University of California, 1979.

[4] Shoukri, M., "The Use of a Regenerative Air-to-Air Rotary Heat Exchanger for Heat Recovery in Residential Ventilation Systems," American Society of Mechanical Engineers, Annual Meeting, New York, 1979.

[5] Shurcliff, W.A., Air-to-Air Heat Exchangers for Houses, published by the author, 19 Appleton St., Cambridge, Mass., 1981.

[6] Wilkes, K.E., "Thermophysical Properties, Data Base Activities at Owens- Corning Fiberglas," Proceedings of ASHRAE/DOE Conference on Thermal Performance of the Exterior Envelope of Buildings, Orlando, Florida, December 1979.

[7] Hunt, C.M., "Air Infiltration: A Review of Some Existing Measurement Techniques and Data," Building Air Change Rate and Infiltration Measurement, eds., Hunt, C.M., King, J.C., Trechsel, H.R., ASTM STP 719, American Society for Testing and Materials, 1980.

Table 9.1

Air Infiltration Heat Loss

Test Conditions	I(x/hr)	$\bar{Q}_M$	$\bar{Q}_C$	$\bar{Q}_R$	$\bar{Q}_I$
		(Watts)			
Natural Ventilation	0.10	503	484	19	17
Mechanical Ventilation	0.81	530	403	127	111
" "	0.46	460	385	75	62

Table 9.2

Effectiveness of the Lossnay

Test #	Test Conditions	Infiltration Rate (exchanges/hour)	$\overline{Q}_M$	$\overline{Q}_C$	$\overline{Q}_R = \overline{Q}_M - \overline{Q}_C$ (Watts)	$\overline{Q}_I$	$\eta_o = 1 - \frac{\overline{Q}_R}{\overline{Q}_I}$
tw64	Lossnay off; sealed	0.0	472	452	20	0	-
tw65	" ; "	0.0	433	420	13	0	-
tw66	" ; "	0.0	460	435	25	0	-
tw62	Lossnay on low; unretrofitted	2.37	490	339	151	279	46%
tw63		2.35	580	407	173	319	46%
tw70	Lossnay on low; retrofitted	2.29	415	301	114	243	53%
tw72		2.34	576	416	160	330	52%
tw74	Lossnay on medium; retrofitted	4.57	645	364	281	566	50%
tw75		4.55	710	388	322	629	49%

Table 9.3 Heat Exchanger Efficiency Calculations

Test Conditions

Lossnay on low; unretrofitted

	tw62	tw63
$\bar{Q}_M$	= 490	= 5
$-\bar{Q}_c$	= -339	= -4
-Fan Power	= - 9	= - 9
-Lossnay Conduction	= - 16	= -
$\bar{Q}'_R$	= 126	= 1
$\eta_L = 1 - \frac{\bar{Q}'_R}{\bar{Q}_I}$	= 55%	= 5%

Lossnay on low; retrofitted

	tw70	tw72
$\bar{Q}_M$	= 415	= 5
$-\bar{Q}_c$	= -301	= -416
-Fan Power	= - 9	= -
-Lossnay Conduction	= - 15	= - 20
$\bar{Q}'_R$	= 90	= 131
$\eta_L = 1 - \frac{\bar{Q}'_R}{\bar{Q}_I}$	= 63%	= 60%

Lossnay on medium; retrofitted

	tw74	tw75
$\bar{Q}_M$	= 645	= 7
$-\bar{Q}_c$	= -364	= -3
-Fan Power	= - 19	= - 19
-Lossnay Conduction	= - 17	= - 19
$\bar{Q}'_R$	= 245	= 2
$\eta_L = 1 - \frac{\bar{Q}'_R}{\bar{Q}_I}$	= 57%	= 5%

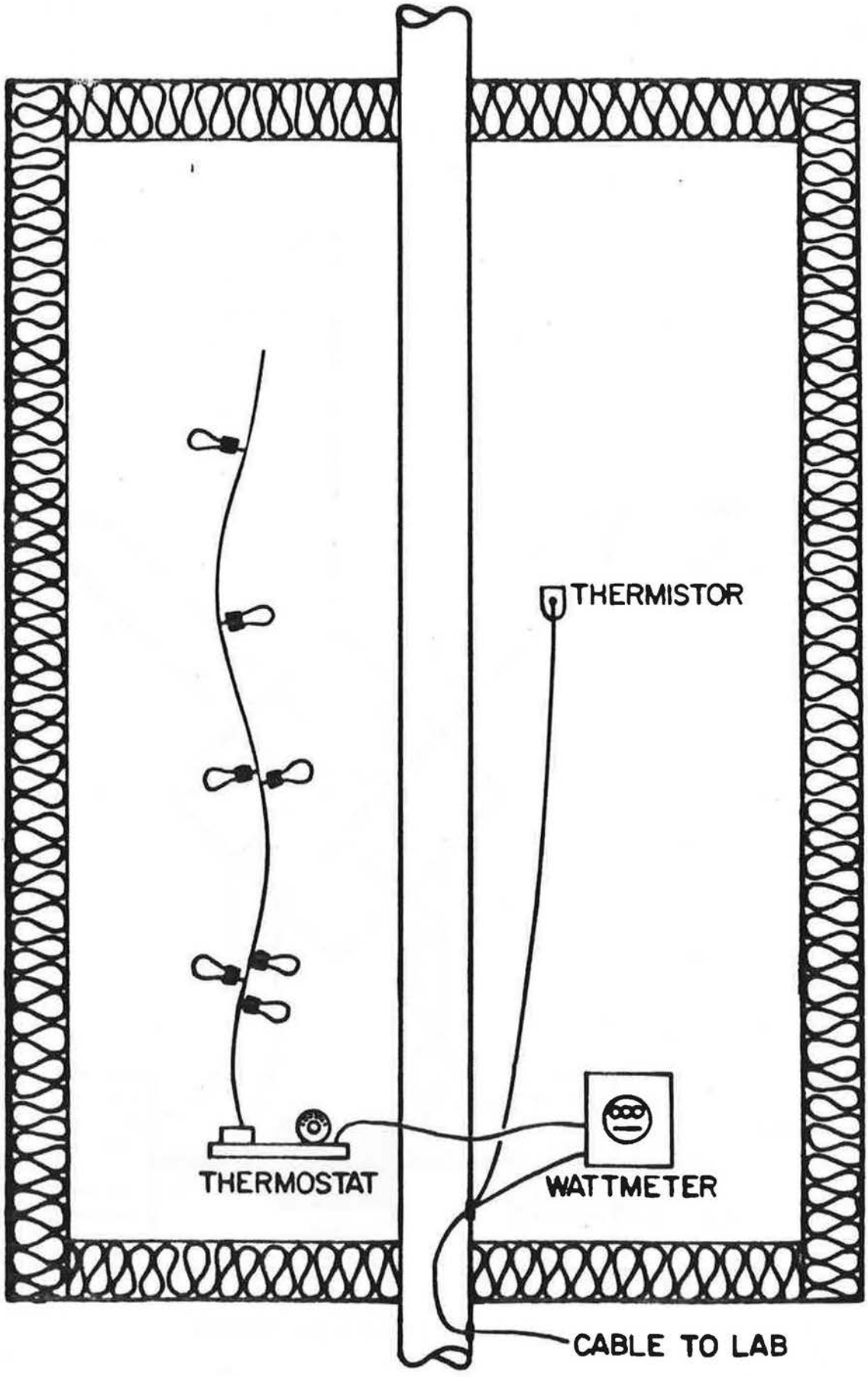

Figure 9.1 Instrumentation for Measuring Test Chamber Heat Loss

Figure 9.2

Schematic Diagram of Lossnay Heat Exchanger

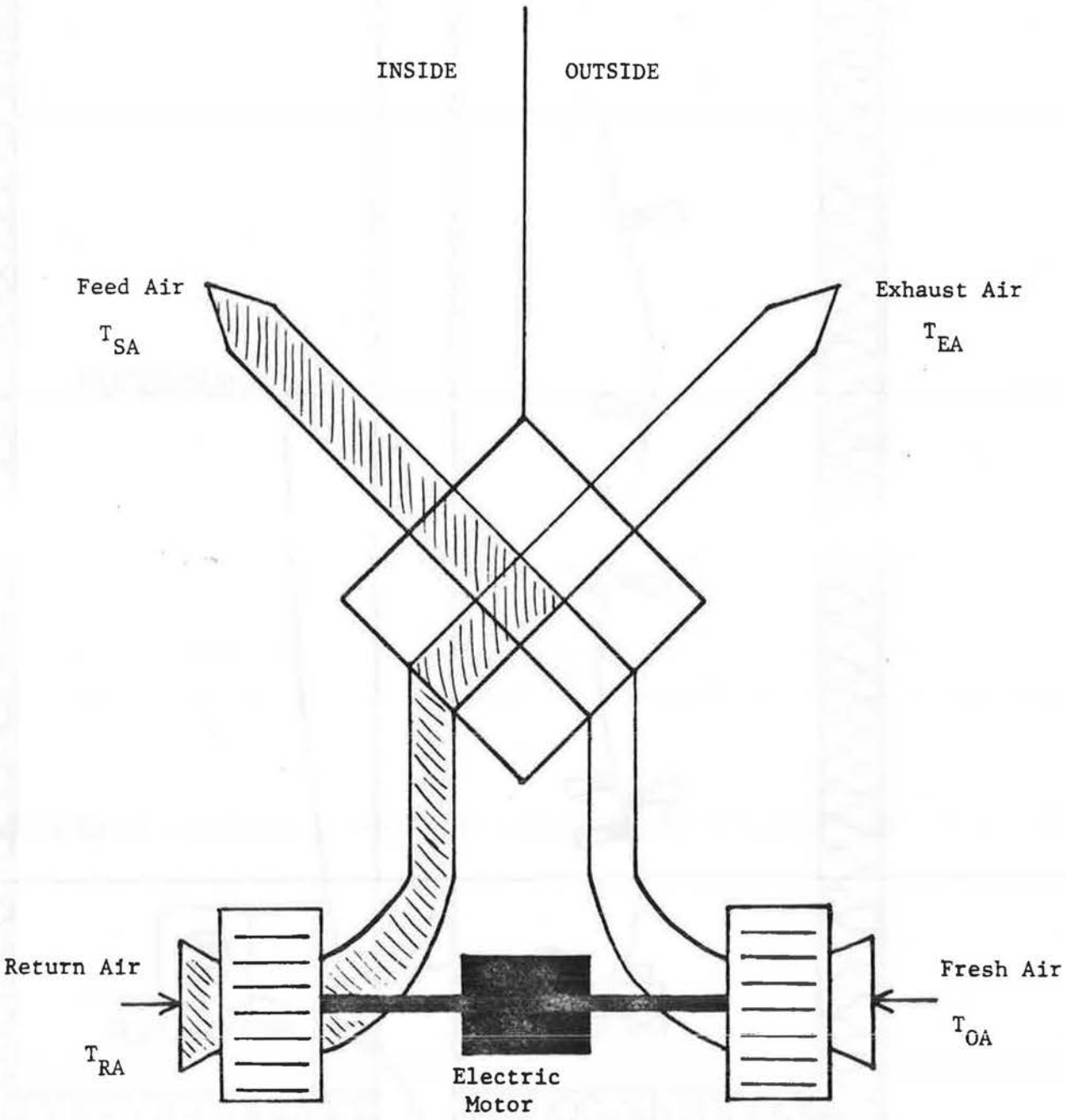

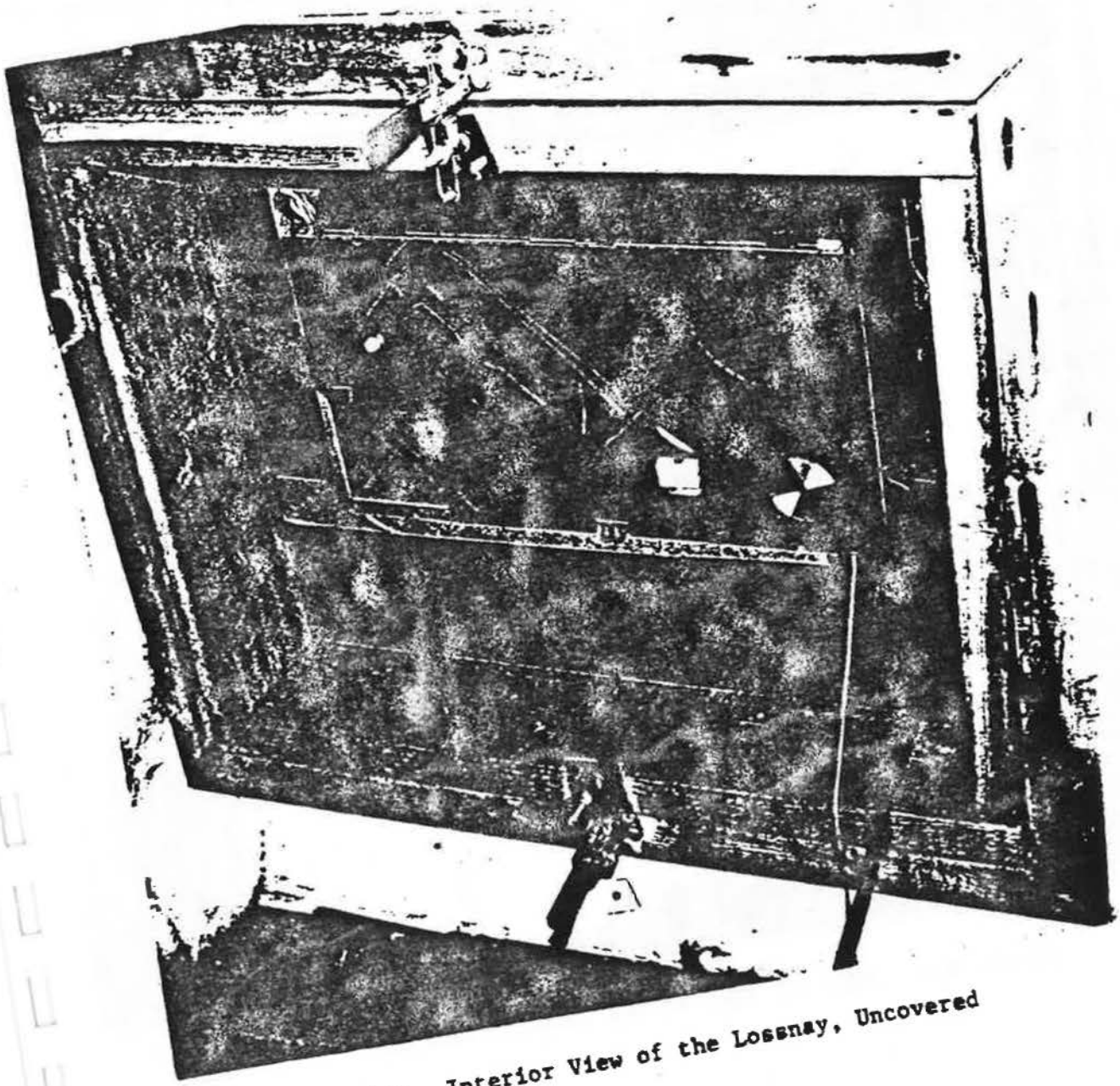

Figure 9.3 Interior View of the Lossnay, Uncovered

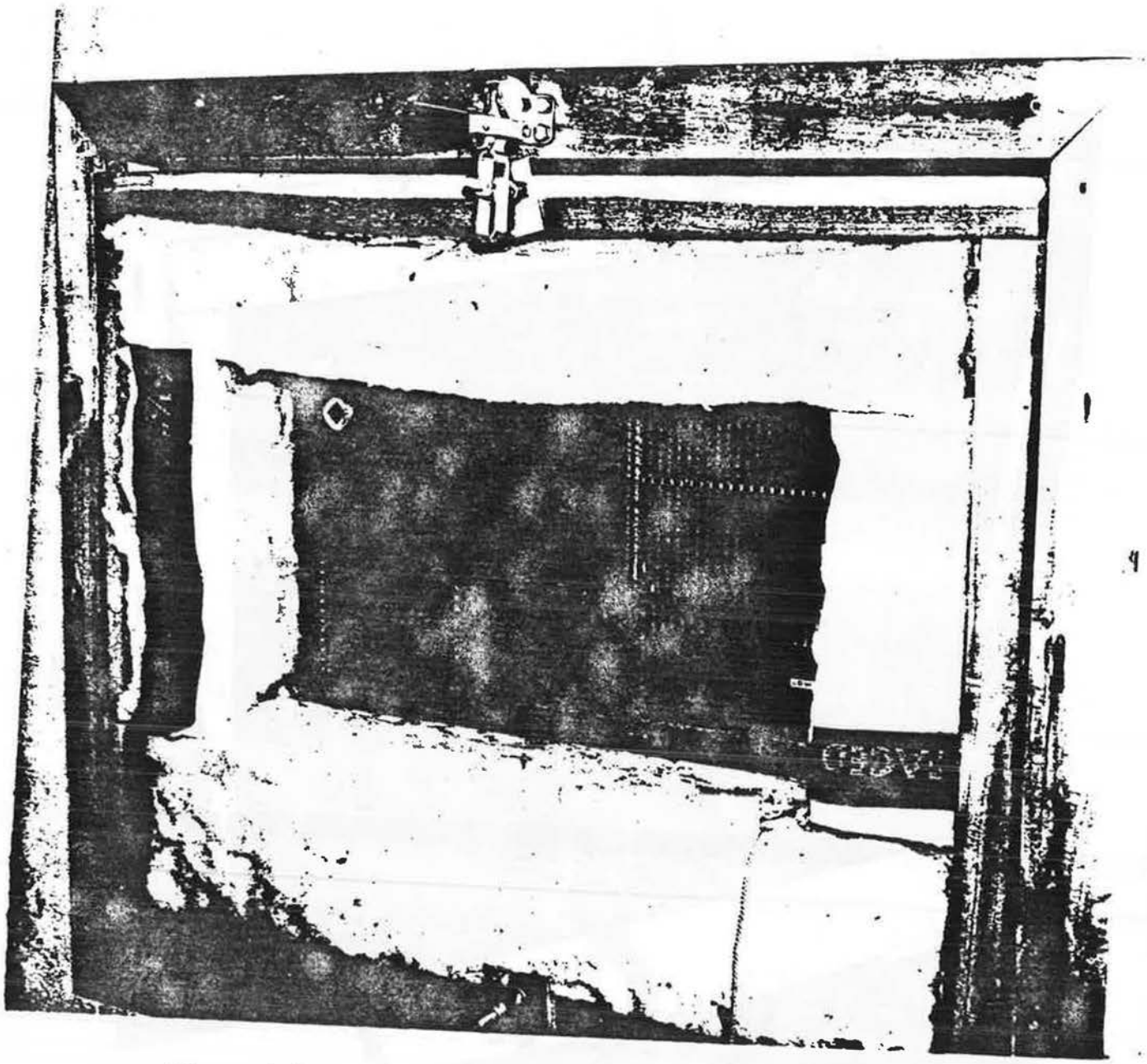

Figure 9.4 Interior View of the Lossnay, Covered

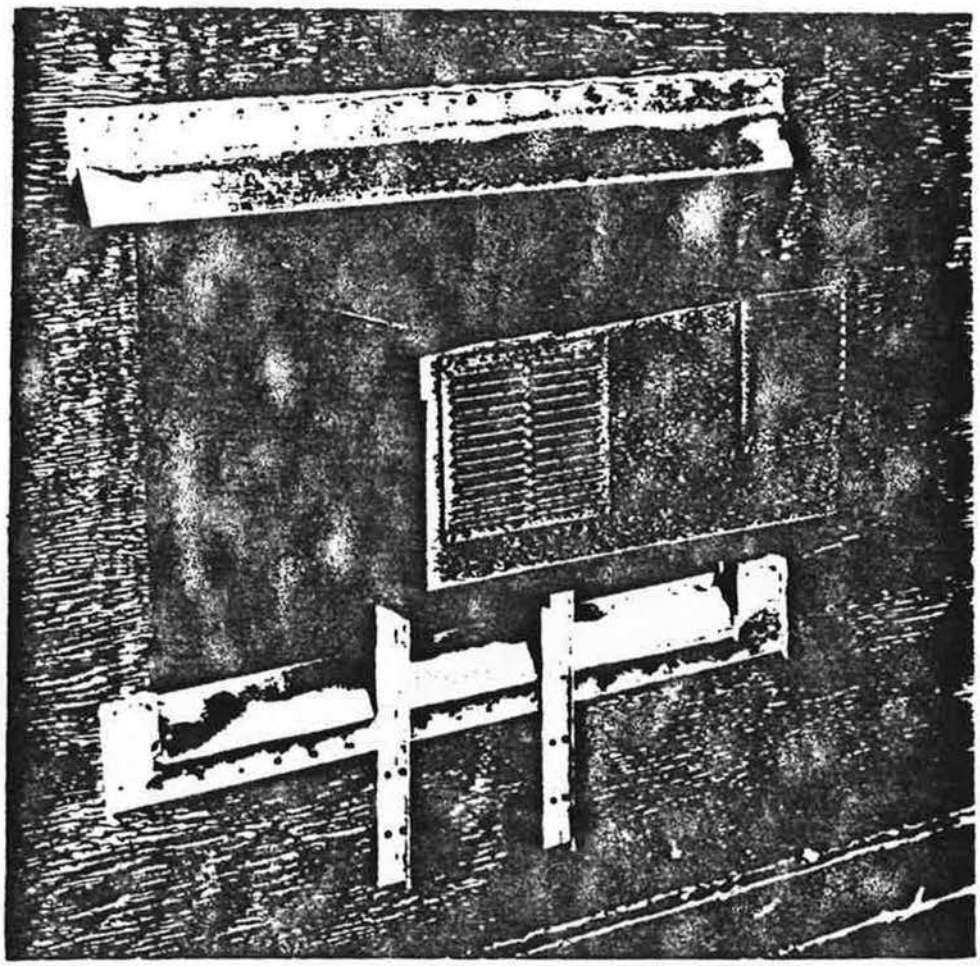

Figure 9.5 Exterior View of the Lossnay, Close-Up

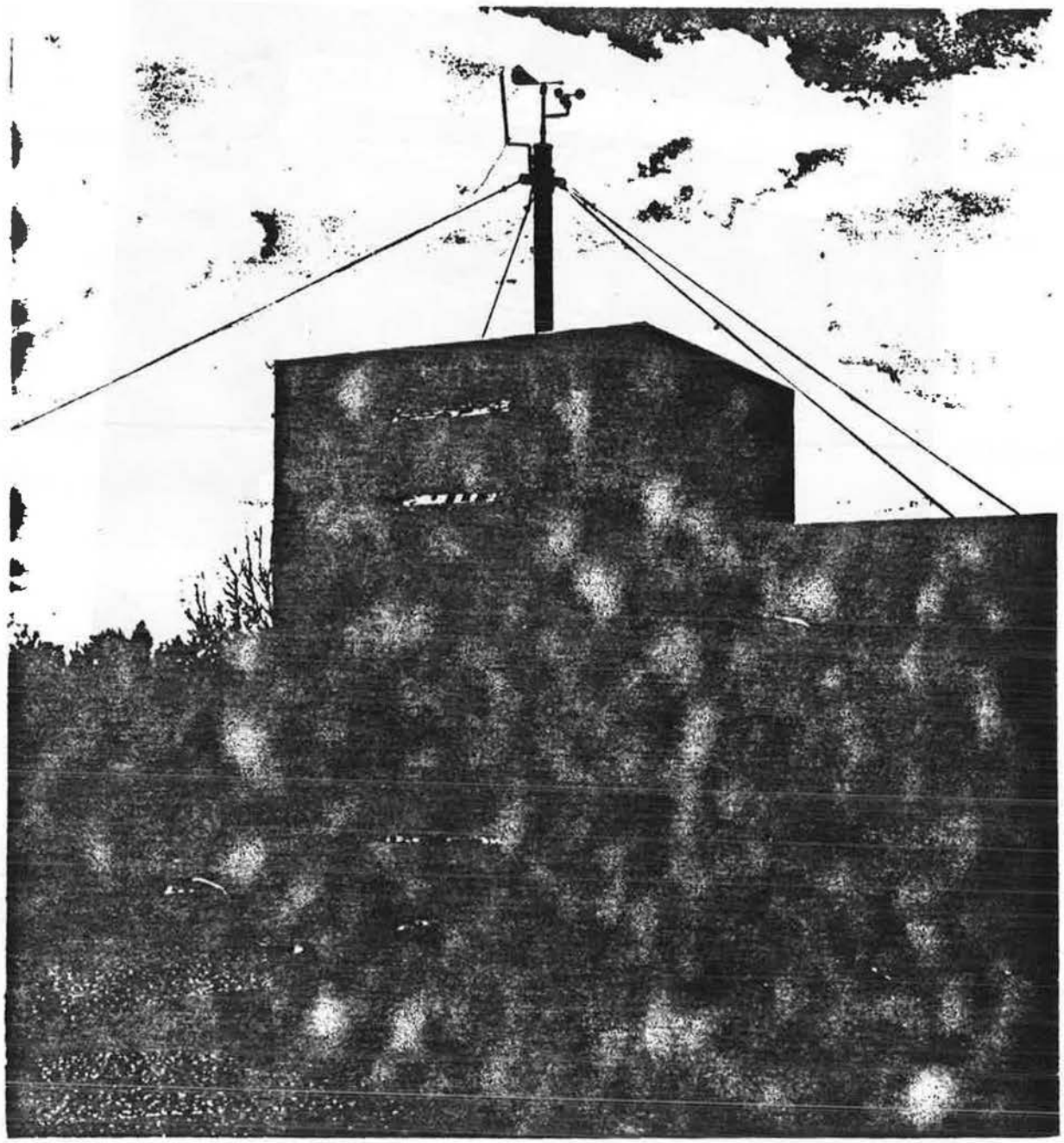

Figure 9.6 Test Chamber with Lossnay Installed

Chapter X

CONCLUSIONS

In this thesis we have studied the problem of tightness evaluation of homes. Our general motivation is the need to determine whether a house is excessively leaky such that its exchange rate with the outdoors should be reduced to save energy. We also need to determine if a house is so tight that the indoor air is unhealthy for the occupants. Our work has involved reviewing the past research into tightness evaluation of homes. This review has raised several important questions which our experimental work has investigated.

10.1 MEASUREMENT OF INFILTRATION RATES

There is presently no way to determine the infiltration rate of a home other than tracer gas measurement. Predictive models are not yet accurate enough. Subtracting the calculated conduction heat loss from the total measured heat loss of a home to determine the infiltration rate is inaccurate because of errors in the calculation methods for conduction. Tracer gas measurements of air infiltration rates are accurate when care is taken to avoid errors due to imperfect mixing of the interior air. But tracer gas measurements give the infiltration rate only for the weather conditions during the test and there are no general rules

for extrapolating to other weather conditions. For this reason, evaluating the tightness of a home using the tracer gas technique requires many measurements under a variety of weather conditions. It takes a long time to gather these data and ties up expensive tracer gas equipment for many months. Also, the tightness of a home can change over this time period making the determination of the relation of infiltration to weather impossible. To overcome some of these problems long-term, passive infiltration monitors are being developed to obtain an inexpensive measure of the infiltration rate of a home averaged over a long period of time. We have also demonstrated the inexpensive "bottle sample" technique in Freehold which yields reliable measurements of short-term infiltration rates. Efforts are also being directed towards multi-chamber infiltration to study the flow between the separate sections of a home.

10.2 PRESSURIZATION TESTING OF HOMES

To avoid the expense and time associated with tracer measurements for evaluating the tightness of homes, the technique of pressurization testing has been developed. Pressure testing a home is quick and inexpensive, but it does have some problems due to differences between the test conditions and those induced by weather. In chapter II we showed that weather induced pressure differences are on the order of 5 Pa, but homes are pressure tested from 10 to 60 Pa. The leakage characteristics of a home can be quite different at these high pressures than at the natu-

rally occuring pressure differences. Also, pressurization testing yields a global value for the leakage of a home with no information on the distribution of this leakage around the shell of the house. Finally, the test pressures are uniform over the building surface and constant in time, while weather induced pressures are variable in both time and position.

Our review of pressure testing has raised several questions. First, it is not clear how best to convert pressurization test results into a measure of tightness. The flow rate necessary to sustain a 50 Pa pressure difference between inside and outside is the most common measure, but others, such as the 4 Pa flow rate based on curve fits to the test data, have been proposed. The relative merits of these tightness measures have been discussed but never experimentally compared. Another important question is how reproducible are pressurization test results and how are they affected by the weather conditions during the test. The final, and perhaps most basic question, is how pressurization test results relate to infiltration rates induced by the weather.

10.3 THE RELATION BETWEEN PRESSURIZATION AND INFILTRATION

Theoretically, the relation between pressurization and infiltration is straightforward, but in reality a usable relation is difficult to obtain. Given the geometry of a home, the location and leakage function of each opening in the shell, and the relation between wind and the exterior pressure distribution of the house one can calculate the infiltration rate for any conditions

of weather. But, as mentioned above, pressurization testing gives only the global leakage function of a house at large pressure differences. Also, it is difficult to relate the wind speed to the exterior pressure distribution due to the great variablity in wind exposure among homes. Several models of the relation between pressurization and infiltration have been developed which replace these unknowns with assumptions in order to obtain a usable relation. These models vary in their complexity and their ability to deal with the differences among houses. Most of them predict infiltration rates within 30% of measurements, but they can be in error by as much as 100%. These models and the general relation between pressurization and infiltration are discussed in chapter V. Simple relations between the 50 Pa flow rate and measured infiltration rates are presented which predict infiltration as well as or better than the present models. Attempts to validate the models by their developers have employed a wide variety of houses, and it is impossible to determine whether their predictive successes and failures are due to the models or due to variation in the pressurization-infiltration relation for difference types of homes.

EXPERIMENTAL WORK

We have presented the conclusions of our review of past research into the tightness evaluation of homes. This review has raised several questions which prompted the experimental work described in this thesis. These questions, the experiments and the results are discussed below.

10.4 REPRODUCIBILITY OF PRESSURIZATION MEASUREMENTS

The Blower Door has been widely used for pressure testing homes in North America, but no work had been done on the reproducibility of the test results. Also, the effect of weather conditions during the test on the results was unknown. To answer both of these questions we pressure tested a home in the Princeton area about once a week for a year. We found the 50 Pa flow rate to be reproducible within 1 or 2%, and the 4 Pa flow within about 6%. This difference is to be expected because the 4 Pa flow is an extrapolation out of the range of measurements. We found the test results to be unaffected for local wind speeds less than 2.5 m/s which is close to the ASTM recommendation for conducting pressurization tests at wind speeds less than 2.2 m/s. Above 2.5 m/s the 50 Pa flow was found to be either indistinguishable from the calm wind results or as much as 15% higher. Wind errors are intermittent because even windy days have calm periods, and measurements made during these calm periods are not in error. These reproducibility experiments are unique in the field of pressure testing and the information obtained is important, but

the experiments on wind sensitivity need to be repeated in other homes with different wind exposures.

By pressure testing this house for a year we found a large seasonal variation in the leakiness of this wood-frame house. The roughly 25% variation from the minimum to the maximum is due to drying and shrinking of the wood in the cold, dry winter weather, and subsequent swelling in the spring and summer. This seasonal variation is important for the use of pressurization test results for comparison of the tightness of homes to each other or a tightness standard. Other homes should be checked for the magnitude of the seasonal variation in leakiness.

10.5 PREDICTING INFILTRATION FROM PRESSURIZATION TESTS

We have mentioned differences between pressure test conditions and weather induced conditions which make the use of pressurization test results for infiltration prediction questionable. Studying such prediction in a real home is difficult because it is practically impossible to know the location of the leakage for the house and the leakage function for each opening. Also, the variablity of the wind exposure of houses makes it difficult to relate the wind speed to the exterior pressure distribution. In order to study the relation of pressurization and infiltration without the unknowns associated with homes in the field, we conducted experiments in a simple structure called the Test Chamber for which we know the location of all significant leakage. The leakage functions for the openings were determined through pres-

surization tests and these functions were used with the calculated pressure differences to predict infiltration rates. The predicted and measured infiltration rates were very close for weather conditions in the stack regime and for cases with the wind blowing normal to the openings in the Test Chamber. The infiltration rates were generally underpredicted for the case of wind blowing across the openings in the structure. These errors in prediction are due to the fact that the wind does not blow consistently parallel to the walls with the openings, but constantly changes direction. Also, turbulence in the wind induces infiltration which is not accounted for by our simple steady state model. These fluctuations are important factors which must be studied to properly account for wind induced infiltration. But the fact that we were able to predict so well for the other cases show that pressurization test results can be successfully related to infiltration rates when we have detailed knowledge of the structure involved.

10.6 RELATING PRESSURIZATION TO INFILTRATION IN IDENTICAL HOMES

In reviewing models of the relation between pressurization and infiltration, we pointed out that the validation tests on the models have been done on many different types of homes. It is difficult to determine whether their predictive successes and failures are attributable to the models or to variations in the pressurization-infiltration relation among the homes due to differences in housing style, construction materials and age. In

order to separate the two possible sources of variation, we conducted pressurization and infiltration measurements on fourteen identical homes in Freehold, New Jersey. The infiltration rates of the houses were measured simulataneously on three nights to eliminate variablity due to weather. Straightforward regressions of measured infiltration rates against the 50 and 4 Pa flow rates yielded values of r^2 of about one-third. Thus, two-thirds of the variation in the infiltration rates of these homes is due to the different leakage distributions and wind exposures, as well as measurement error. Some of the pressurization-infiltration models presented in chapter V were applied to these data, and the predicted infiltration rates were within 25 to 100% of the measured rates. Several of the models require inputs which if chosen correctly improve the predictions, but there is no way to know which values of the inputs work best beforehand. The predictions are better in the stack regime than in the wind regime, as was the case for the Test Chamber experiments. Again we find that predicting infiltration from pressurization is complicated by the difficulty in characterizing wind induced pressures.

10.7 4 VS 50 PASCAL

At several points in this thesis we have mentioned the relative appropriateness of the 4 and 50 Pascal flow rates for characterizing the leakiness of homes. The extrapolation of the pressurization test data to 4 Pa is used because weather induced pressure differences are on the order of 4 Pa as opposed to the

larger pressures during the pressurization test. But because the 4 Pa flow rate is an extrapolation out of the range of measurements, it is a less certain measure than the 50 Pa flow. The greater variability of the 4 Pa flow is evident in the BRAT house experiments. In the Test Chamber and Freehold infiltration tests we compared the correlation of both the 4 and 50 Pa flows with measured infiltration rates and found no clear advantage in either. Since the 50 Pa flow rate is more commonly used and is more well-defined, we believe it should be used as a tightness measure unless evidence to the contrary is brought forth.

10.8 RESEARCH NEEDS IN TIGHTNESS EVALUATION

Our research into tightness evaluation has answered some questions in this field and raised some new ones. We will now review research needs in the field which future work must address. An area of weakness in the use of pressurization testing for predicting infiltration rates is the relation of wind to the exterior pressure distribution of a house. In our experiments in the Test Chamber and the Freehold houses, our predictions of infiltration were worse for wind-induced infiltration than for stack dominated conditions. We discussed past research into the determination of wind pressure coefficients in chapter II and stated that most research has involved isolated homes. Experiments into the effects of obstructions such as houses and trees on the values of C_p have considered only very simple cases, but did find that these obstructions affect C_p and infiltration rates signifi-

cantly. The wind exposure of homes is quite variable and we need to learn more about the effects of this exposure on wind-induced infiltration.

Our experiments on the reproducibility of pressurization test results and the effects of wind on these results are new and important contributions to the field. Many more homes with different wind exposures should be tested for wind speed effects on pressurization test results. This will enable the establishment of well-founded guidelines for test conditions, and quantify the magnitude of potential errors due to wind. Other homes should be studied to determine the extent of the seasonal variation of tightness which we measured in our test house. These studies should consider homes with different construction materials and in different climates. The pressurization tests should be accompanied by infiltration measurements to determine how the seasonal variation in pressurization test results converts to a variation of actual infiltration rates.

Pressurization testing also lacks a precise calibration technique for the Blower Door and other devices. New techniques will provide us with confidence in our test results and enable the verification of the temperature correction presented in appendix C.

More research is needed into the models relating pressurization test results to infiltration. The research into wind-induced infiltration mentioned above will improve these models, but additional studies verifying these models on homes in the field

are needed. Consideration should be given to the effects of housing style and age on the pressurization-infiltration relation. Factors such as the existence of basements and attics, building materials and heating systems have not been studied, and may be important for infiltration prediction from pressurization.

10.9 AIR-TO-AIR HEAT EXCHANGERS

Air-to-air heat exchangers provide mechanical ventilation to maintain a safe indoor environment while recovering some of the energy contained in the outgoing stream of indoor air. We tested one such device, the Lossnay, in the Test Chamber as opposed to a laboratory set-up to obtain a more realistic evaluation of its performance. We found that the Lossnay recovered about 50% of the heat normally associated with the induced ventilation rate. This efficiency is degraded by the fan power lost to the outside and by heat conducted through the Lossnay case to the outdoors. These two factors degrade the efficiency by about 10% for operation in the Test Chamber. We also found that sealing leaks within the device improves the efficiency significantly by minimizing cross-contamination of the incoming and outgoing air streams. The close proximity of the interior supply and return ducts causes some of the incoming air to be drawn out before it has a chance to mix with the rest of the interior air, and this lessens the effectiveness of the device. The effects of imperfect mixing and conduction through the Lossnay case would have been overlooked in laboratory tests of air-to-air heat exchangers. These

results justify the use of in-situ testing of heat exchangers, and suggest the need for such testing of other energy conserving devices.

10.10 AIRTIGHTNESS STANDARDS FOR HOMES

One may ask how our researh applies to real homes, and to the current efforts to tighten homes to save energy. We want to able to say how tight people can make homes before they encounter health hazards. Unfortunately, the health effects of indoor pollutants are not yet sufficiently understood to set ventilation standards for homes. Such standards must consider the volume of the house, the number of occupants, and the pollutant sources such as the cooking fuel and whether the occupants smoke. When indoor air pollution is more well understood, this and future research will be important in the formulation of ventilation standards for homes. Our research will be used to determine the form of the ventilation standards and the conditions under which the tests should be conducted.

Today, new, carefully constructed homes can have 50 Pa flow rates of 2 or 3 house volumes exchanged per hour, and this may be too tight. Air-to-air heat exchangers can then be used to ventilate the houses without wasting energy. Most existing homes are so leaky that significant tightening is possible before any problems will occur. There are so many potential leakage sites in obscure places, and they are so hard to find, it would be virtually impossible for most homeowners and contractors to make an

existing house too tight. Additional research into the health effects of indoor pollution and into air infiltration is needed for the formulation of ventilation standards.

Appendix A

TEST CHAMBER HANDBOOK

During the winter and spring of 1978, a "Test Chamber" was designed and constructed at Princeton University for research in building science. The structure is a miniature house with no internal partitions, built to be simple and uniform. The Test Chamber was also built to have minimal infiltration rates, and with versatility to facilitate experimentation. Due to the simplicity and controllability of the Test Chamber, experiments conducted with the structure reveal phenomena that would be obscured in real homes. Homes in the field have many unknown and uncontrollable variables, making precise experimentation difficult.

A.1 PHYSICAL DESCRIPTION

The Test Chamber is basically a boxlike structure with a square base and dimensions as shown in figure (A1). The structure is supported by a wooden frame of "two-by-fours" and a steel mast, 5.5 m (18 ft) high, running vertically through the center of the structure and extending about 1.5 m (5 ft) above the roof. The Test Chamber rests on four casters (one in each corner) which enable the entire structure to be rotated about the center mast. Thus, one can control the direction from which the wind or sun impinges on the structure. The casters sit on a wooden plat-

form which in turn rests on the roof of the von Neumann Building on the Princeton University campus.

A detailed sketch of a wall section is shown in figure (A2). From inside to outside, the walls are constructed as follows: 2.5 cm of rigid polystyrene insulation; a layer of 6 mil polyethylene; "two-by-four" studs 0.4 m on center, with 8.9 cm of fiberglass insulation between them; another layer of polyethylene; and finally a sheathing of 1.6 cm plywood. These walls have an R-value of about 15 in English units according to handbook calculations.

Two of the outside walls are painted flat black, while the other two are painted with aluminum paint. The roof is of almost identical construction as the walls, except it is painted with an aluminum roof coating with asbestos. Also, there is a 1.2 m square piece of 1.6 cm plywood on the inside of the roof. The floor of the Test Chamber is slightly different. From inside to out, there is a flooring of 0.6 cm masonite followed by 2.5 cm of polystyrene, 1.6 cm of plywood, a layer of polyethylene, a layer of "two-by-four" studs and fiberglass insulation, another layer of polyethylene, and finally 0.9 cm of plywood. In both the roof and the floor, the stud spacing is not uniform, as can be seen in figure (A1). There is a well weatherstripped door in the silver wall without windows. It is a solid wood door, 2.0 m by 0.8 m and 4.4 cm thick, and is insulated with 7.6 cm of rigid polystyrene so that it has an R-value similar to the rest of the structure. To the left of the door is a small opening for passing out

wires and gas lines. When necessary, this hole is filled with fiberglass insulation and covered with polyethylene.

Several features make flexible experimentation with the Test Chamber possible. At the base of the steel mast, below the floor of the Test Chamber, is a hole through which runs an electrical cable. One end of the cable is in the interior, passing through another hole in the mast, while the other end runs down into the von Neumann building to the data acquistion system. This cable is used to transmit data (temperatures, energy use, etc.) from the structure. The data acquistion system is described in the appendix on instrumentation. The two holes in the mast are also used to run an AC power cable into the Test Chamber.

The Test Chamber has four "windows," two each on opposite sides. As can be seen in the photographs in figure (A3), one window is high and the other low. These windows consist of a wooden frame in the wall into which a variety of panels can be easily installed. In figure (A3), masonite panels with small circular holes are in place. The panels are 0.76 m by 0.64 m, and are held tightly in place with metal clamps. (See figure (A4).) An air tight fit is assured by the placement of closed cell foam weatherstripping between the window panel and the wooden frame. When no openings are desired, panels of fiberglass insulation and masonite, with an R-value similar to the walls, are fitted into the windows.

A.2 HEAT LOSSES OF THE TEST CHAMBER

The heat losses (and gains) of the Test Chamber include conduction, air infiltration, and radiation to and from the environment. The calculations of these heat losses are presented below, except for radiation which will be discussed at length in appendix D. These calculations yield an estimate of the "lossiness" in units of Watts of internal power necessary for each degree Celsius of temperature difference between indoors and out.

The major portion of the heat loss is conduction through the shell. As shown below, the walls and roof have R-values of about 15 in English units, while the floor has a somewhat higher thermal resistance. By assuming predominantly one-dimensional heat flow and estimating losses at the corners and edges, one obtains a value of the lossiness due to conduction of 16 W/°C.

A second source of conduction heat loss is the steel mast running through the center of the structure. In order to minimize the mast's contribution to the heat loss, an attempt was made to isolate it from the inside of the Test Chamber. The mast was wrapped with batts of fiberglass insulation to minimize conduction, and then covered with aluminim foil to cut down radiative heat transfer. In addition, the mast was filled with vermiculite to eliminate convective within the pipe. As shown below, the losses due to the mast are estimated to be about 0.5 W/°C. This upper limit is only about 3% of the conduction through the shell.

Another source of heat loss is the infiltration of outside air into the Test Chamber. The structure was built to have very low

infiltration rates, and the measured rates are indeed small. For each tenth of a "house volume" exchanged in one hour there is a net loss of 0.5 W/°C. Since the measured rates are on the order of 0.1 exchanges per hour or less, infiltration losses are small compared to conduction losses.

Radiative heat gains and losses of the Test Chamber present a complex problem. Daytime solar gains are dependent on cloud cover and other factors, and the actual heat gain of the structure is a complicated, time-dependent problem. The radiative heat loss at night depends on the amount of longwave radiation from the sky and surroundings. Experiments studying nighttime radiative heat loss have been conducted in the Test Chamber and are discussed in appendix D.

Conduction through the Shell

The conduction of heat through the Test Chamber shell dominates its heat exchange with the surroundings. Conduction losses are determined by the building materials, and their arrangement and thicknesses. The calculations presented here employ standard techniques and numerical values in the literature [1-2].

Table (A1) lists the materials used in the Test Chamber, along with several physical and thermal properties including: density ρ; heat capacity per unit mass c_p; thermal conductivity k; amd material thickness in the direction of heat flow d. From these values, the conductance U and the capacitance C_s are calculated and are also listed in table (A1).

With the conductances and capacitances of table (A1), the U-values and capacitances of the walls, roof and floor are calculated using the following expressions,

$$U = [\sum_{i=1}^{N} (1/U_i)]^{-1} = [\sum_{i=1}^{N} R_i]^{-1} \qquad (A1)$$

$$C = \sum_{i=1}^{N} C_{si} \qquad (A2)$$

N is the number of layers in the surface. U_i and C_{si} are the conductance and capacitance of the ith layer. And $R_i = (U_i)^{-1}$ is the thermal resistance of the ith layer. The calculations of U and C for the walls, roof and floor are shown in table (A2).

Some comment on table (A2) is necessary concerning the stud/insulation layers. These layers were handled identically to the technique used in reference [1]. The heat transfer is assumed one-dimensional, which is quite reasonable in this case where the thickness of the studs and insulation are the same. Average values of U and C_s are determined by weighting the two components by the areas they occupy. The stud spacing in the floor and roof is not uniform, but an average of 0.3 m is used. The thermal resistance and the capacitance of the polyethylene sheets are so small that they are neglected. Also, in the roof calculation, the 1.2 m square piece of plywood on the inside is approximated as a thinner sheet of plywood which covers the entire ceiling. The door and window panels with insulation in place both have R-values larger than the walls, but due to the small area they occupy, the correction to the wall U-value results in less than a 1% effect on the total heat loss and these differences are ignored.

In most calculations of conduction losses, the structure is much larger than the Test Chamber. It is common practice in determining such losses for a home to multiply the area of each wall by its U-value and then add the contributions for each face of the building. This neglects the effects of corners and edges where the heat flow is not one-dimensional. The results of such a calculation for the Test Chamber is presented in table (A3), and gives a first order lossiness of 15.2 W/°C. In homes, the wall area is so large compared to its thickness, that corner effects are negligible and the first order lossiness is adequate. But in the Test Chamber, the wall area is much smaller and it is not clear whether corner effects can be ignored.

If the walls were of homogeneous construction, the heat losses at the corners and edges could have been easily calculated through the use of "shape factors" [3]. But the walls are constructed of several layers. If these layers continued uniformly to the edges where the walls meet, the calculations would have been more complex, but manageable. In the Test Chamber, at the edges the 8.9 cm stud/insulation layer is almost all stud. A cross section of the corner is shown in figure (A5.1). The effective "post" of wood in the corner would complicate the heat loss calculations, so instead we take the approach of calculating upper and lower limits for the corner effects.

The corner calculations are done considering a wall section 1 m high and extending from the center of the wall to the corner. (See figure (A5.2).) The lower limit on the lossiness of this

section is obtained by considering the corner to be a perfect insulator. Thus we need consider only one-dimensional heat flow through a wall section with a width equal to one-half the inside width of the Test Chamber, 1.09 m. The area of this section is 1.09 m^2, which when multiplied by the wall's U-value of 0.38 $W/m^2-°C$, yields a low value for the heat loss of 0.41 W/°C.

The upper limit is obtained by a more complex method based on an article by Langmuir, et al [4]. In this method, one assumes that a series of infinitely thin, perfectly conducting sheets are embedded parallel to the wall. The isotherms are therefore also parallel to the wall, and the heat flows perpendicularly to the wall. The wall section considered is shown in figure (A6). It extends from the middle of the wall to the corner, and it is 1 m high. As shown in the figure, the wall is divided into several sections. Each section is considered separately, but as a result of the assumptions made, the border between each section is an isotherm and the heat flow through each section is the same.

The first layer is the inside air film with an area of A_i = 1.09 m^2 and a heat transfer coefficient of h_i = 8.28 $W/m^2-°C$. This layer separates the Test Chamber interior at a temperature T_i from the inner surface of the wall at T_1. Thus the heat flow across this air layer is $Q = h_i A_i (T_i - T_1)$. The next layer in the wall is the 2.5 cm of polystyrene insulation. As shown in figure (A6), this layer separates temperatures T_1 from T_2. The heat flow across the polystyrene is given by $Q = k_1 S_1 (T_1 - T_2)$ where S_1 is the shape factor for this layer and

k_1 is the thermal conductivity of polystyrene. The shape factor for this layer is equal to its width of 1.09 m divided by its thickness 0.025 m plus 0.27 for the corner, all multiplied by its 1 m length. Thus, S_1 = 43.9 m.

The most complex layer in the wall is that of the studs and insulation shown in figure (A7). The dimensions are x_o = 1.12 m and y_o = 0.089 m, and it consists of two parts labeled α and β. The section of studs and insulation is treated as a uniform material with a thermal conductivity obtained from that of the studs and insulation by weighting their areas. That is, k = (.906)(0.047 W/m-°C) + (.094)(0.118 W/m-°C) = 0.054 W/m-°C. The β section is assumed to be all stud, which is on the safe side since this is a high estimate. k_β = 0.118 W/m-°C. To determine the heat flow across this layer, one considers an elemental section of thickness dy which is a distance y from the inside of the layer. The area of such an elemental section is $(x_o + y)$ 1 m, and the temperature across the section is dT. The heat flow across any such elemental section consists of two parts and is equal to:

$$Q = (k_\alpha/dy)(x_o \times 1m)\,dT + (k_\beta/dy)(y \times 1m)\,dT \qquad (A3)$$
$$= (k_\alpha x_o + k_\beta y) \times 1m \times dT/dy.$$

The temperature difference across the entire layer is $T_2 - T_3 = \Delta T = \int_{y=0}^{y=y_o} dT$. Thus,

$$\Delta T/Q = \left(\int_{y=0}^{y=y_o} dT\right)/Q = \int_0^{y_o} dy/[(x_o k_\alpha + y k_\beta)(1m)] \qquad (A4)$$
$$= (1/k_\beta \times 1m)\ \ln[1 + (y_o k_\beta / x_o k_\alpha)]$$

or,

$$Q = k_\beta [\ln(1 + (y_o k_\beta / x_o k_\alpha)]^{-1} \ (1m) \ \Delta T \qquad (A5)$$
$$= 0.737 \ W/°C \ (T_2 - T_3)$$

The next layer is the outer sheathing of plywood which is treated like the layer of polystyrene. The plywood separates T_3 and T_4 and has a thermal conducitivity of $k_3 = 0.115$ W/m-°C. Its shape factor is equal to $S_3 = (1.20m/0.016m + 0.27) \times 1m = 75.3$ m. Finally, there is the outside film coefficient which equals $h_o = 26.2$ W/m^2-°C and acts over an area of $A_o = 1.23$ m^2. This outside air layer separates T_4 from T_o as in figure (A6).

Thus, for the five separate layers, there are the five expressions for the heat flow through the wall Q:

Inside air	$Q = h_i A_i (T_i - T_1) = 9.03 \ W/°C (T_i - T_1)$	(A6)
Polystyrene	$Q = k_1 S_1 (T_1 - T_2) = 1.54 \ W/°C (T_1 - T_2)$	(A7)
Studs/Insulation	$Q = 0.737 \ W/°C (T_2 - T_3)$	(A8)
Plywood	$Q = k_3 S_3 (T_3 - T_4) = 8.66 \ W/°C (T_3 - T_4)$	(A9)
Outside Air	$Q = h_o A_o (T_4 - T_o) = 32.2 \ W/°C (T_4 - T_o)$	(A10)

From these five expressions, we can obtain the desired expression for Q in terms of only T_i and T_o, i.e. $Q = H_{net}(T_i - T_o)$. The results of this calculation is $H_{net} = 0.44$ W/°C, our desired upper limit.

Multiplying the upper and lower limits by the inside wall height, 3.53 m, one obtains 1.55 W/°C and 1.45 W/°C as limits on the heat loss rate of one-half of a wall. There is only a 7%

difference between these two numbers. We choose to use the average of these two numbers 1.50 W/°C.

Multiplying 1.50 W/°C by eight for all the half wall sections, one obtains 12.0 W/°C for the heat loss of the walls. One must add to this 1.8 W/°C for the roof and 1.7 W/°C for the floor as in the first order lossiness calculations. In addition, there are eight edges where the four walls meet the roof and floor. The inside length of the edges is 2.18 m, and therefore the shape factor for all eight of them is S = 8×0.54×2.18 m = 9.42 m. Using a value of the thermal conducitvity for the edges of k = 0.048 W/m-°C, one obtains a heat loss constant for the edges of kS = 0.5 W/°C. Adding all these contributions together, the net lossiness due to conduction alone is L = 12.0 + 1.8 + 1.7 + 0.5 = 16.0 W/°C. This value is 5% larger than the first order lossiness of 15.2 W/°C.

Air Infiltration

The Test Chamber was built to be very air tight, but there is still some air infiltration. The air infiltration rates are dependent on the outside weather and are therefore variable. Measured infiltration rates are on the order of 0.1 exchanges per hour or less. If one assumes the heat loss rate associated with air infiltration is equal to $\rho c_p VI\ T$, then the lossiness due to air infiltration is $L_A = \rho c_p VI$. If the infiltration rate is 0.1 X/hr, then $L_A = 0.5$ W/°C for $\rho c_p = 0.33$ W-hr/m^3-°C and V = 16.6 m^3. This lossiness will vary with the outside weather,

but since it is only a 3% correction to L_c = 16.0 W/°C, this variation will be neglected.

Losses Through the Steel Mast

The steel mast running through the center of the Test Chamber gives it extra support and enables the structure to be rotated. It also presents a complex heat transfer problem. To estimate the conduction losses through the mast, it is considered as three vertical sections, each at a single temperature T_1, T_2 and T_3. Thermal resistances between the sections are estimated, along with the resistances to the interior and exterior temperatures T_i and T_o. A sketch of the resistance network is shown in figure (A8). R_1 is the resistance between a pipe section and the interior. There are two resistances to the outside, one out the top R_2 and one through the bottom R_2'. R_3 is the resistance between each of the pipe sections. Once these resistances have been determined, one can compute an overall resistance of the pipe between T_i and T_o.

The important physical parameters of the mast and its insulation are as follows. The inner radius of the pipe is r_1 = 0.051 m, and the outer radius is r_2 = 0.057 m. The radius of the layer of insulation around the pipe is r_3 = 0.14 m. The steel has a thermal conducitivity of k_1 = 52 W/m-°C, while the compressed fiberglass insulation has an estimated thermal conductivity of k_2 = 0.066 W/m-°C.

The thermal resistance R_1, between the pipe and the Test Chamber interior consists of the sum of the resistances of the fiberglass insulation and the film layer. This sum takes the form

$$R_1 = [\ \ln(r_3/r_2)/2\pi k_2 L\ ] + (1/2\pi r_3 hL), \qquad (A11)$$

where L is one-third of the inside length of the mast, 1.18 m, and h is the film coefficient 8.28 W/m^2-°C. Thus,

$$R_1 = 1.84\ \ °C/W + 0.12\ °C/W = 1.96\ °C/W. \qquad (A12)$$

R_3 is the resistance of one-third the inside length of the mast in the direction parallel to the mast. Since the thermal conductivity of steel is so much larger than that of the vermiculite inside the pipe or the fiberglass around it, one may assume that this resistance is only due to the steel acting through an area of $\pi r_2^2 - \pi r_1^2 = 2.0\times10^{-3} m^2$. Thus,

$$R_3 = (1.18m)\ /\ (2\times10^{-3}\ m^2)(52\ W/m-°C) = 11.3\ °C/W. \qquad (A13)$$

Finally, there are the resistances between T_1 and the outside temperature T_o, R_2 and between T_3 and T_o, R_2'. In order to simplify the calculations, we assume that once the pipe reaches the outside through the roof or floor, it immediately reaches the outside temperature. This will cause the estimate of the pipe losses to be on the high side. Since the pipe is surrounded by fiberglass insulation as it passes through the roof and floor, these resistances are calculated as R_3, except the length of pipe

considered is the thickness of the roof and floor. These thicknesses are 0.14 m and 0.30 m respectively. Thus,

$$R_2 = (0.14\ m) / (2\times10^{-3}\ m^2)(52\ W/m\text{-}°C) = 1.35\ °C/W, \quad (A14)$$

and

$$R_2' = (0.30m) / (2\times10^{-3}\ m^2)(52\ W/m\text{-}°C) = 2.88\ °C/W. \quad (A15)$$

With the required resistances, we calculate the lossiness due to conduction through the pipe numerically by setting T_i = 20 °C and T_o = 10 °C. We require the heat flows at each node to add to zero, and solve for the temperatures T_1 and T_3. The sum of the calculated heat flows out of the top and bottom, divided by the 10 °C temperature difference is the desired lossiness. The result is a lossiness due to the steel mast of 0.5 W/°C.

Combining the computed heat losses due to conduction through the shell and the steel mast, and due to air infiltration, a net lossiness of 17.0 W/°C is obtained. There is some uncertainty in this value due to construction imperfections and the many assumptions. Also, air infiltration rates different from the assumed 0.1 exchanges per hour will cause a small amount of variation in the lossiness.

REFERENCES

[1] Socolow, R.H., ed., Saving Energy in the Home, Ballinger Publishing Co., 1978.

[2] ASHRAE Handbook of Fundamentals, American Society of Heating, Refrigerating and Air-Conditioning Engineers, Inc., New York, 1977.

[3] Karlekar, B.V., Desmond, R.M., Engineering Heat Transfer, West Publishing Co., 1977.

[4] Langmuir, I., Adams, E.Q., Meikle, G.S., "Flow of Heat Through Furnace Walls: The Shape Factor," American Electrochemical Society Transactions, Vol. 24, 1913.

Table A1 Properties of Test Chamber Materials from references [1] and [2]

Material	ρ (kg/m^3)	c (Wh/kg-°C)	k (W/m-°C)	d (m)	U (W/m^2-°C)	C_s Wh/m^2-°C)
Plywood	540	0.336	0.115	0.016	7.19	2.9
"	"	"	"	0.0095	12.1	1.7
Studs*	510	0.383	0.118	0.089	1.33	17.4
Fiberglass Insulation	14	0.210	0.047	0.089	0.528	0.3
"	"	"	"	0.152	0.309	0.4
Polystyrene Insulation	16	0.441	0.035	0.025	1.40	0.2
Door	510**	0.383**	0.118**	0.044	2.68	8.6
Masonite	800	0.360	0.106	0.0064	16.6	1.8
Indoor Film Coefficient (Vertical)					8.28	
Indoor Film Coefficient (Horizontal)					9.25	
Outdoor Film Coefficient (4.5m/s wind)					26.2	

* One dimensional heat transfer only
** Estimate
Conductance U = k/d
Capicitance (Capacity per unit area) $C_s = \rho cd$

ρ = Density
c = Specific Heat
k = Conductivity
d = Thickness

Table A2 Description, Overall U-Values and Overall Thermal Mass of Walls, Roof and Floor

Walls	U (W/m^2-°C)	R = 1/U	C_s (Wh/m^2-°C)
Indoor film coefficient	8.28	0.121	0.0
2.5 cm Polystyrene	1.40	0.714	0.2
R-11 Insulation/Studs*	0.605	1.653	1.9
1.6 cm Plywood	7.19	0.139	2.9
Outdoor film coefficient	26.2	0.038	0.0
		R = 2.665	5.0 Wh/m^2-°C
	U = 0.38 W/m^2 °C [R-14.9]		
Roof			
Indoor film coefficient	9.25	0.108	0.0
Plywood**	18.3	0.055	1.1
2.5 cm Polystyrene	1.40	0.714	0.2
R-11 Insulation/Studs*	0.624	1.603	2.4
1.6 cm Plywood	7.19	0.139	2.9
Outdoor film coefficient	26.2	0.038	0.0
		R = 2.657	6.6 Wh/m^2-°C
	U = 0.38 W/m^2 -°C [R-14.9]		
Floor			
Indoor film coefficient	9.25	0.108	0.0
0.6 cm Masonite	16.6	0.060	1.8
2.5 Polystyrene	1.40	0.714	0.2
1.6 cm Plywood	7.19	0.139	2.9
R-11 Insulation/Studs*	0.624	1.603	2.4
0.9 cm Plywood	12.1	0.083	1.7
Outdoor film coefficient	26.2	0.038	0.0
		2.745	9.0 Wh/m^2-°C
	U = 0.36 W/m^2 -°C [R-15.8]		

* Aggregated as described in text

** Estimated as described in text

Table A3 First Order Lossiness

U_{wall}	= 0.38 W/m^2 -°C	A_{wall}	= 7.70 m^2
U_{roof}	= 0.38 W/m^2 -°C	A_{roof}	= 4.69 m^{2*}
U_{floor}	= 0.36 W/m^2 -°C	A_{floor}	= 4.69 m^{2*}

$$\text{Lossiness} = 4\,U_w A_w + U_r A_r + U_f A_f$$

$$= 11.7 + 1.8 + 1.7$$

$$= 15.2 \ W/°C$$

---

*Does not include area of pipe and its insulation

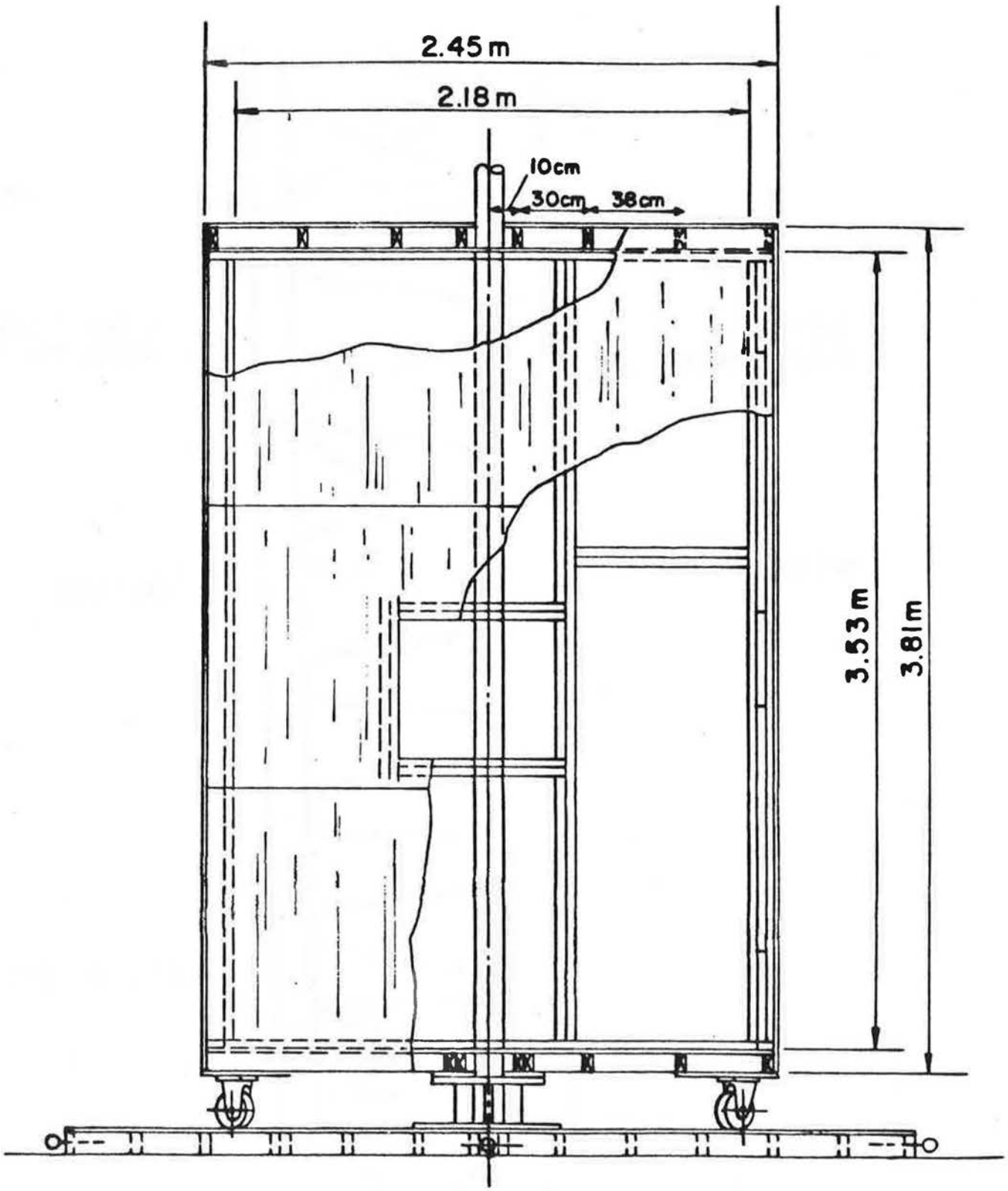

Figure A1 Dimensions of the Test Chamber

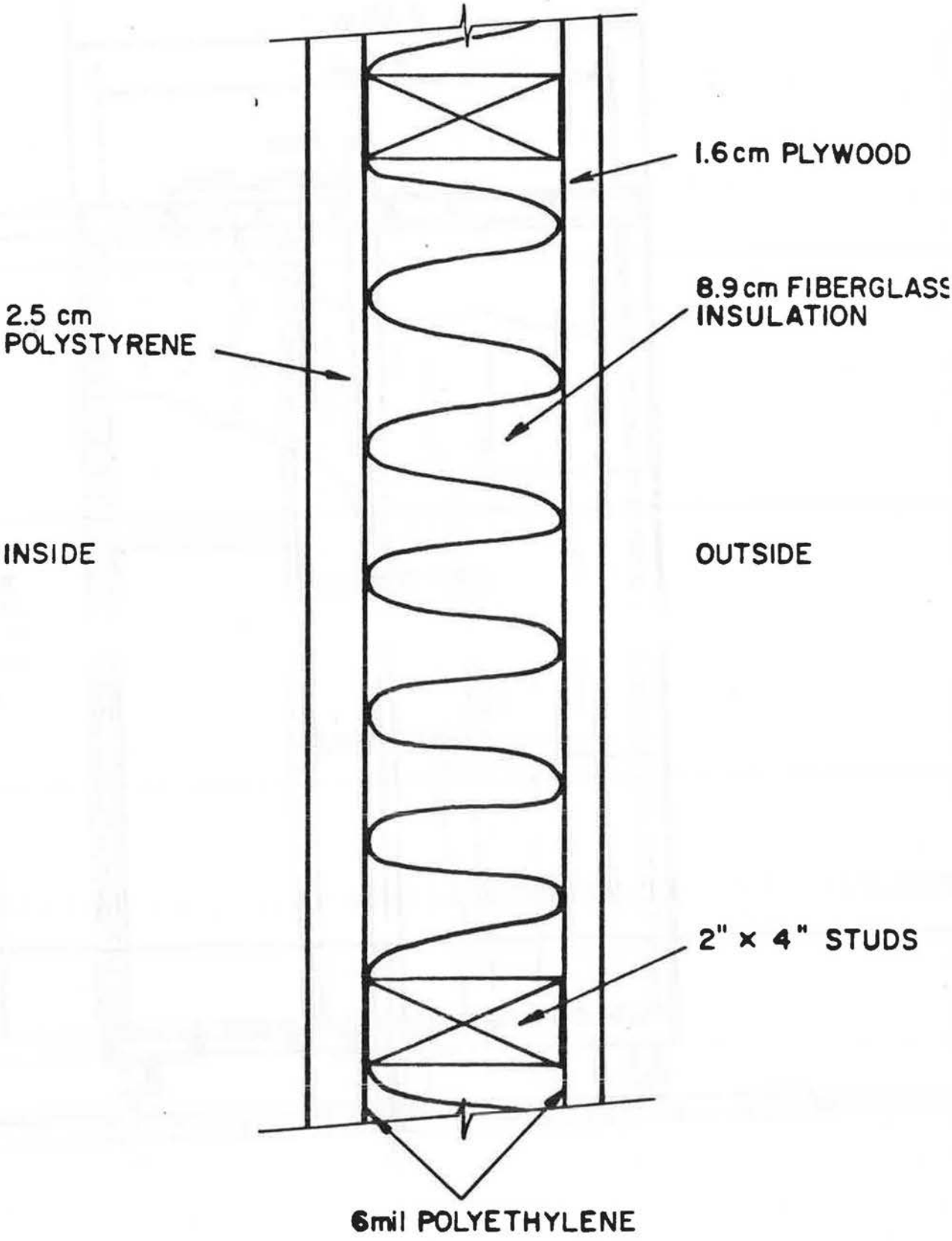

Figure A2 Cross-Section of Wall, from above

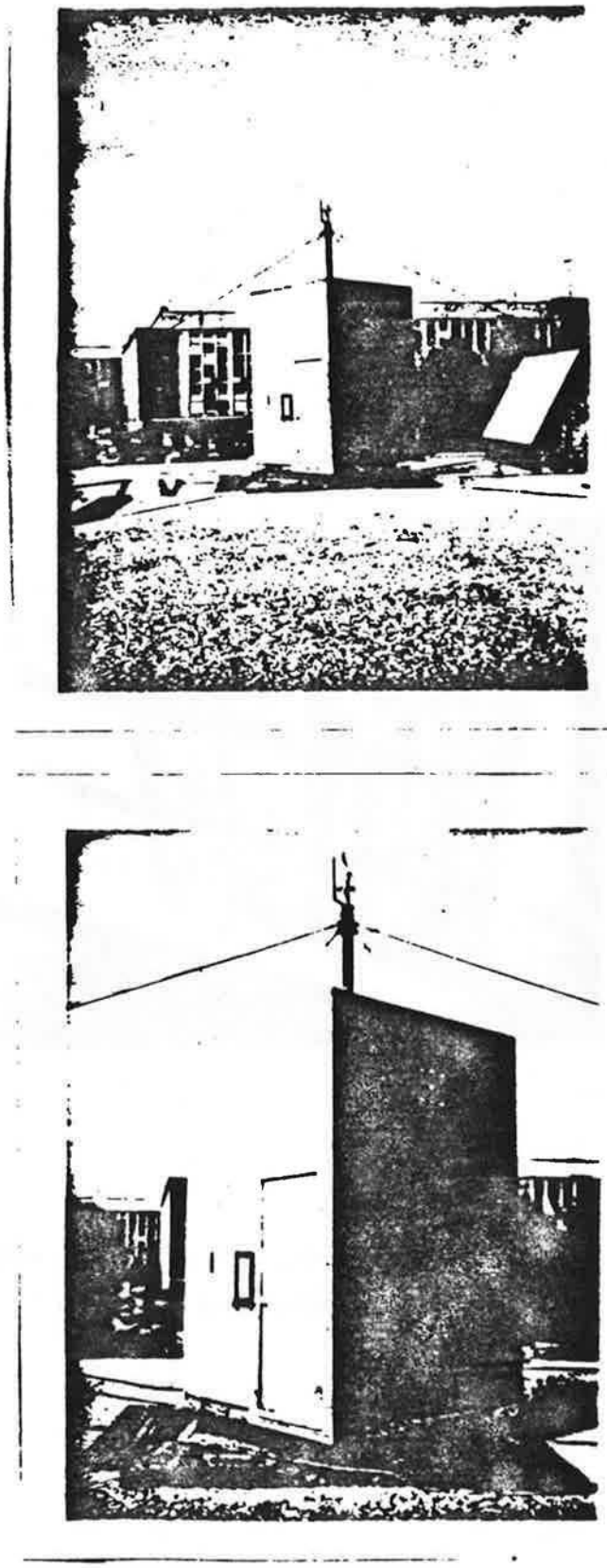

Figure A3 Photographs of the Test Chamber

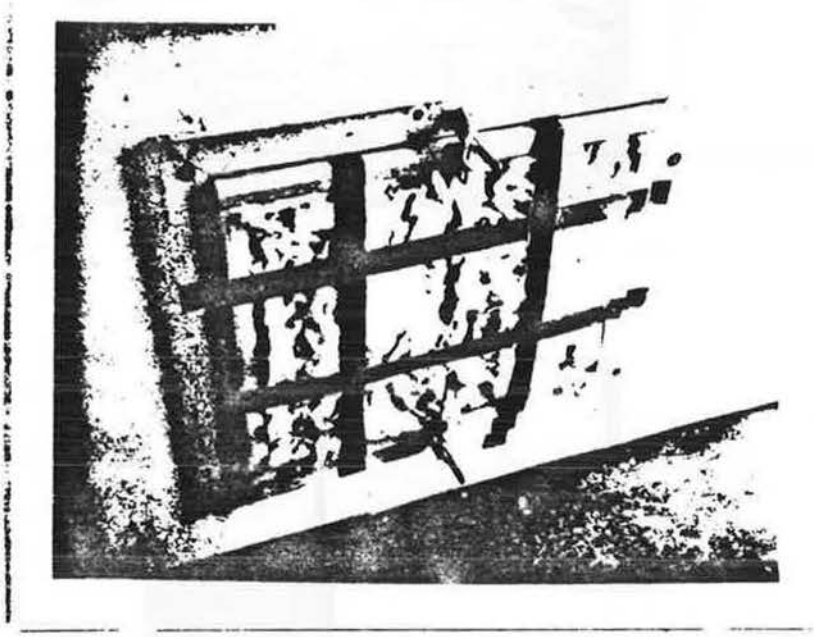

Figure A4 Photograph of Window with Insulation Panel in Place

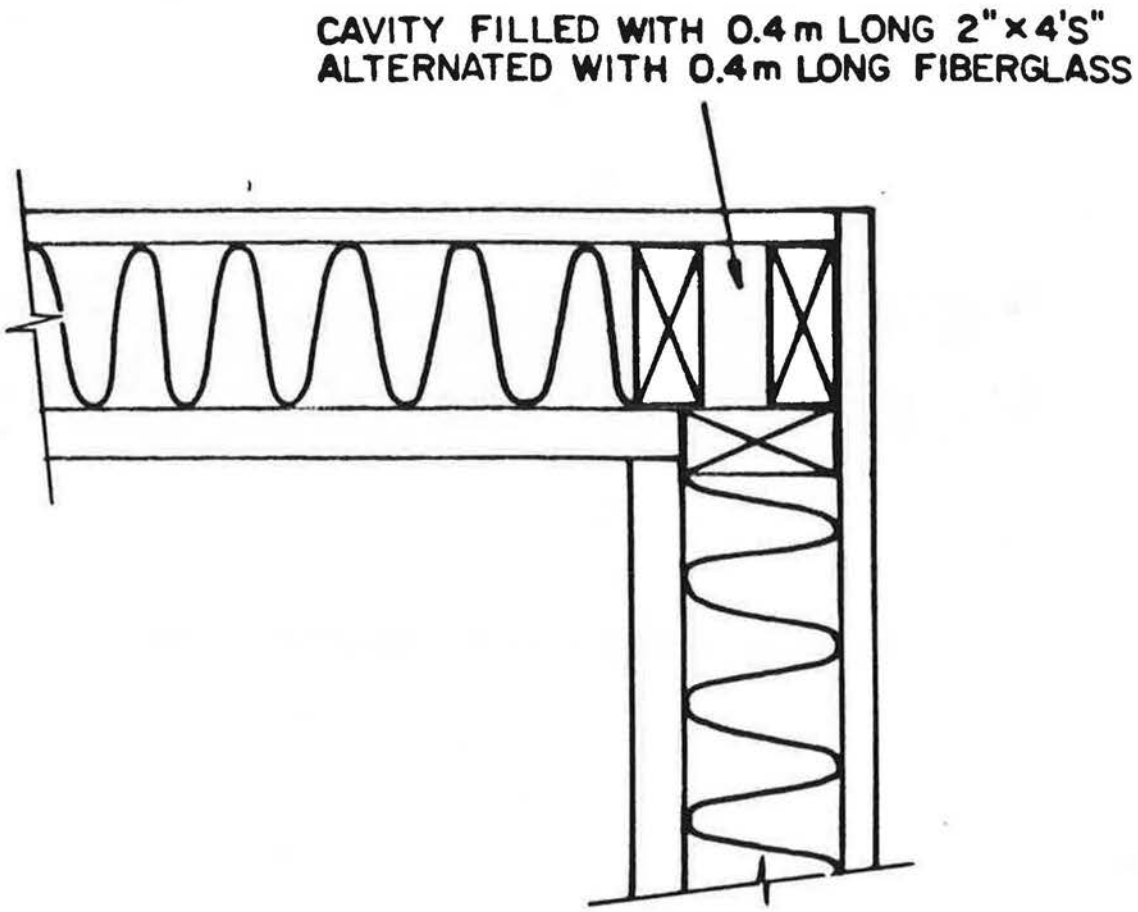

Figure A5.1 Top View of Corner

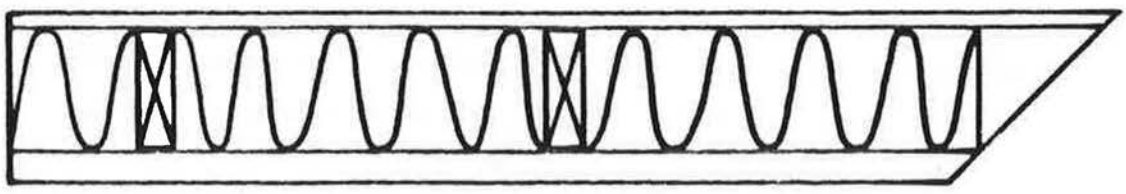

Figure A5.2 Top View of a Half Wall Section

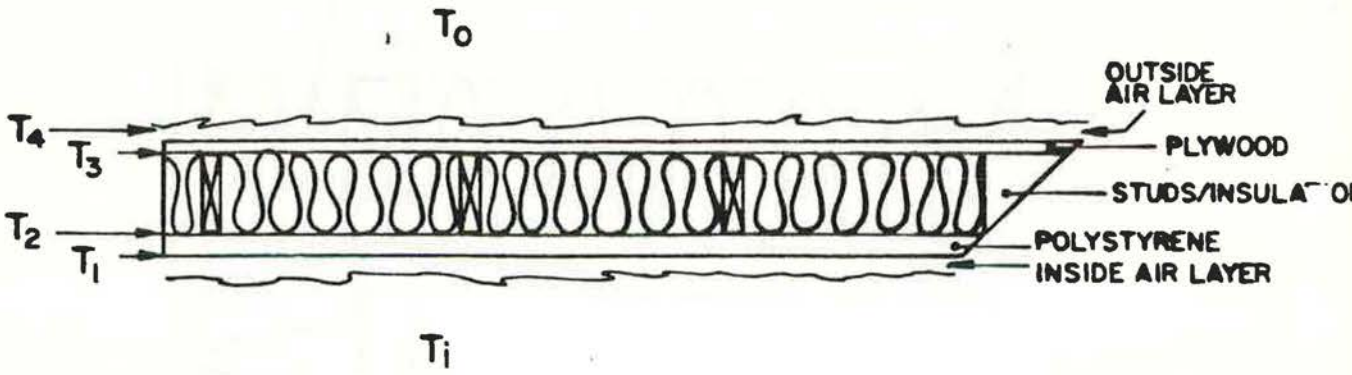

Figure A6 Wall Section for Corner Calculation

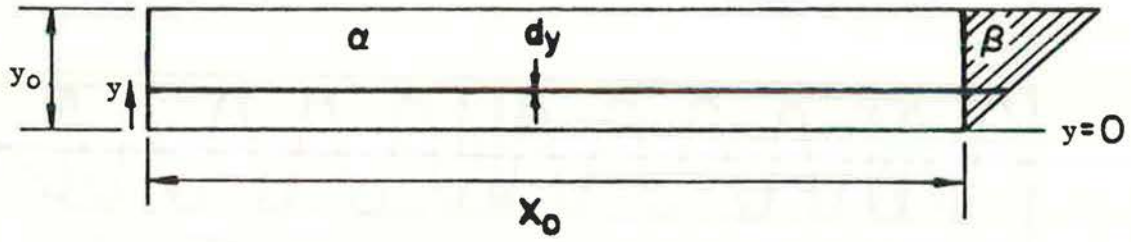

Figure A7 Stud/Insulation Layer

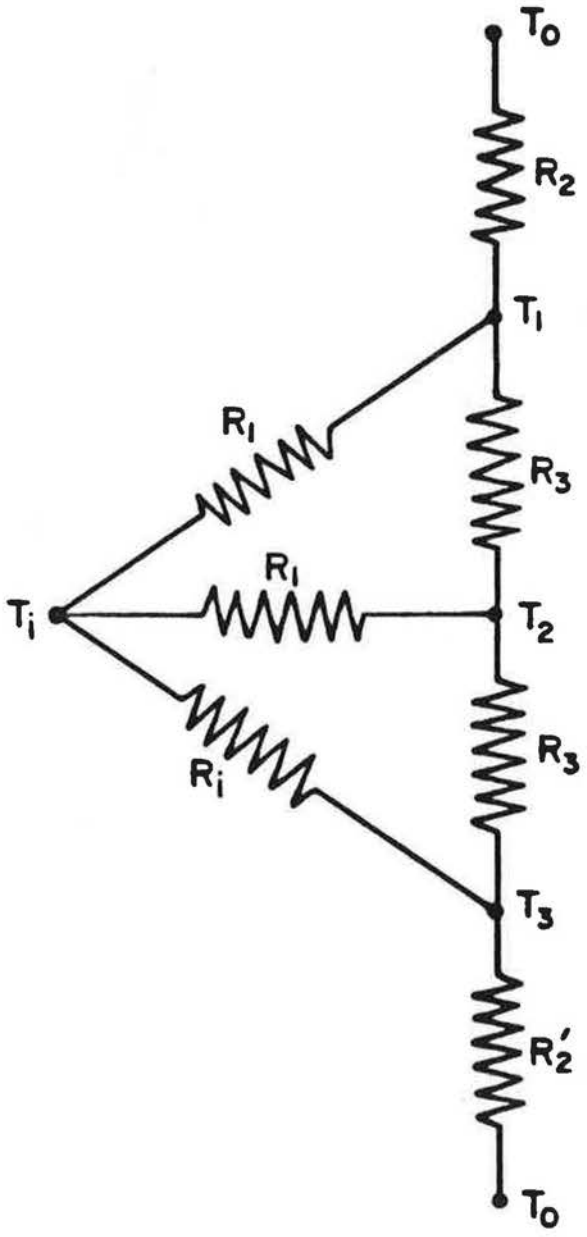

Figure A8 Resistance Network of Steel Mast

Appendix B

INSTRUMENTATION

B.1 DATA ACQUISITION SYSTEM AND WEATHER STATION

This section describes the devices used to monitor and record the conditions inside the Test Chamber and the outside weather. The Test Chamber variables include interior air temperature, energy consumption and ethane concentration. Ethane is used as a tracer gas to measure air infiltration rates as described in the second section of this appendix. The outside weather variables are air temperature, wind speed (average and instantaneous), wind direction and intensity of infrared radiation.

Measurements

Temperatures

Air temperatures, both inside and outside the Test Chamber, are measured using YSI Precision Thermistors. Probe No. 705 which contains the 44018 thermistor composite is used. The probes are wired according to figure (B1.1) to give a measurement range of -30 to +50°C and an accuracy of 0.15°C. The temperature T(°C) is related to the supply voltage V_s by,

$$T = (V_{out} - 0.34893V_s)/(0.0067966V_s) \qquad (B1.1)$$

where V_{out} is the output of the thermistor circuit.

The thermistors used to measure the outside air temperature are placed in an "aspirated instrument shelter." This shelter shields the thermistors from radiative exchange with the surroundings, but is mechanically ventilated at a rate of 115 cfm to yield a true air temperature. A similar instrument shelter was used to measure the Test Chamber interior temperature. These thermistors were placed in a 0.5 m length of 4 in. diameter PVC plumbing pipe which serves as a radiation shield. The thermistor is mounted in the center of the pipe. A fan ventilates the pipe at a rate of 50 cfm.

Wind

The instantaneous wind speed is measured with a Gill generator anemometer with a minature tachometer generator with a voltage output V_I linearly related to the speed. The relation between the instantaneous wind speed u_I in m/s and V_I is

$$u_I = V_I/0.107 \qquad \text{(B1.2)}$$

Because of internal friction, the device is not accurate at very low wind speeds.

One may also measure the average wind velocity over a time period Δt (minutes) with another cup anemometer. This 3-cup Gill photo-chopper anemometer produces a voltage pulse for each 10 meters of wind. These pulses are fed into the Data Conditioning System (DCS), described below, which integrates the pulses. Each pulse increases the integrated voltage by 0.01. The change

in voltage ΔV over a time period Δt is related to the average wind speed $\bar{u}$ (m/s) according to

$$\bar{u} = (\Delta V/\Delta t)\ 121.92 \qquad \text{(B1.3)}$$

Internal friction within the device also leads to errors at low wind speeds.

The wind direction is measured with a Gill microvane with a 1K-Ohm, low torque potentiometer. The voltage output V_θ is related to the wind direction θ in radians through the equation,

$$\theta = 3.560V_\theta - .3545. \qquad \text{(B1.4)}$$

$\theta = 0$ corresponds to a wind from the south, while $\pi = /2$ corresponds to a wind from the west. π is north, and $3\pi/2$ is east.

Energy and Radiation

Electric energy consumption within the Test Chamber is monitored with a modified version of the standard Watt-hour meter used by utilities in homes. The disk in the meter rotates at a rate proportional to the instantaneous power consumption. This disk is perforated by four small equally spaced holes close to the edge of the disk. Fixed to the meter is a photo-coupler, or a "photo-coupled interrupter module" built by General Electric, model no. H13B1. This device emits a light beam from E in figure (B1.2) toward the detector D. The beam is interrupted by the disk except when a hole in the disk passes by, and then a voltage pulse is produced. The DCS integrates the pulses, increasing the

voltage V_E by 0.01 volts for each pulse. One revolution of the disk (4 pulses) corresponds to 7.2 W-hr of energy consumed. Thus, the average Wattage $\overline{W}$ consumed over a time period Δt (minutes) is related to the change in voltage ΔV_E by

$$\overline{W} = (\Delta V_E/\Delta t)\times 10800. \qquad (B1.5)$$

The infrared radiation intensity from the night sky and the surroundings is measured with an Eppley Infrared Radiometer or Pyrgeometer, shown in figure (B1.3). This device, model PIR, measures the intensity from the hemisphere above the horizon, and is temperature compensated from -20 to +40 °C. The Eppley Laboratory calibrates the device using a blackbody reference and the result for the radiometer is that 4.65×10^{-6} volts corresponds to 1 W/m^2. Because the signal of the radiometer is so small, a Dana DC amplifier (Model no. 2200) is used to increase the signal by a factor of one-hundred.

Data Acquistion System

A system was designed to record the above variables easily and reliably. The base of this system is an Esterline Angus Model D-2020 Programmable Data Acquisition System. This device gathers data on up to 20 channels at preset time intervals from 20 seconds to 1 hour. Three different voltage ranges, ±100mV, ±1V and ±10V, can be used for each channel. Each data transmission includes the Julien day, the time and each channel number along with the corresponding voltage.

The Esterline Angus requires DC voltages as inputs. For some of the above variables, particularly temperatures and power supply voltages, no data conditioning is necessary. But in the other cases, a Data Conditioning System (DCS) is used. The DCS contains power supplies and voltage regulators for several of the instruments. It also contains "counter cards" to integrate the pulses for the average wind speed and energy consumption.

The output of the Esterline Angus is compatible with an ASR 33 Teletype. Instead of using this hard copy device, we convert the 20 milliamp current loop output from the Esterline Angus into an RS-232C signal using a Connecticut Microcomputer Adapter, ADA 400B. This signal is then transmitted to a Techtran Model no. 8410 Datacassette. The Techtran records the Esterline Angus output on magnetic tape. The tapes are later read from the Techtran into a PDP-11 minicomputer. The entire data system, except for the PDP-11, is shown in figure (B1.4).

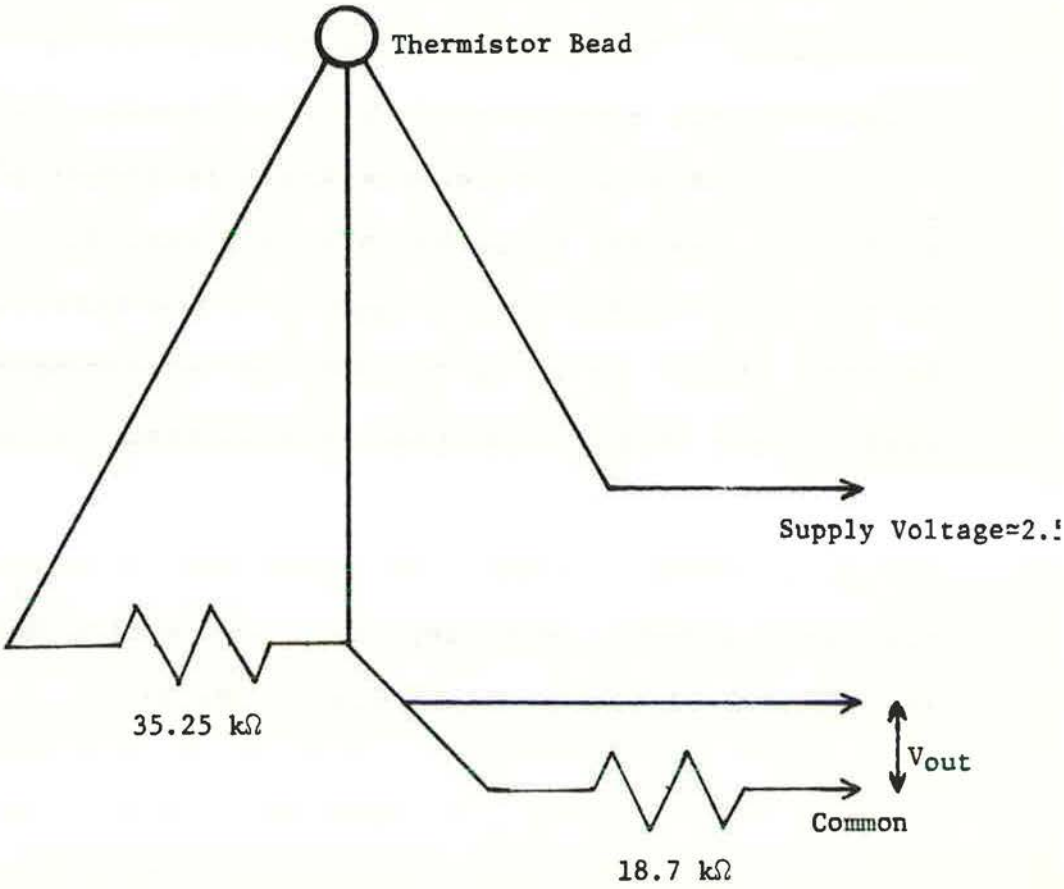

Figure B1.1 Thermistor Wiring Diagram

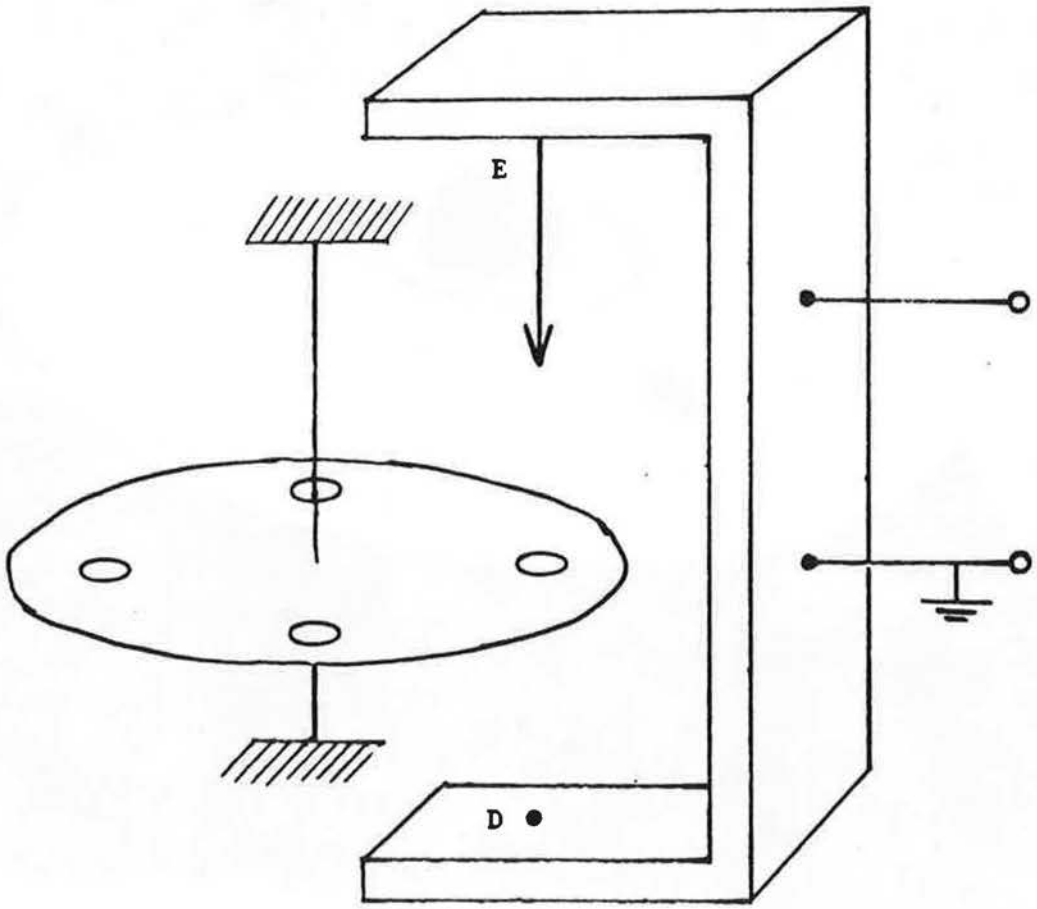

Figure B1.2 Photo-interrupter Module for Watt-hour Meter

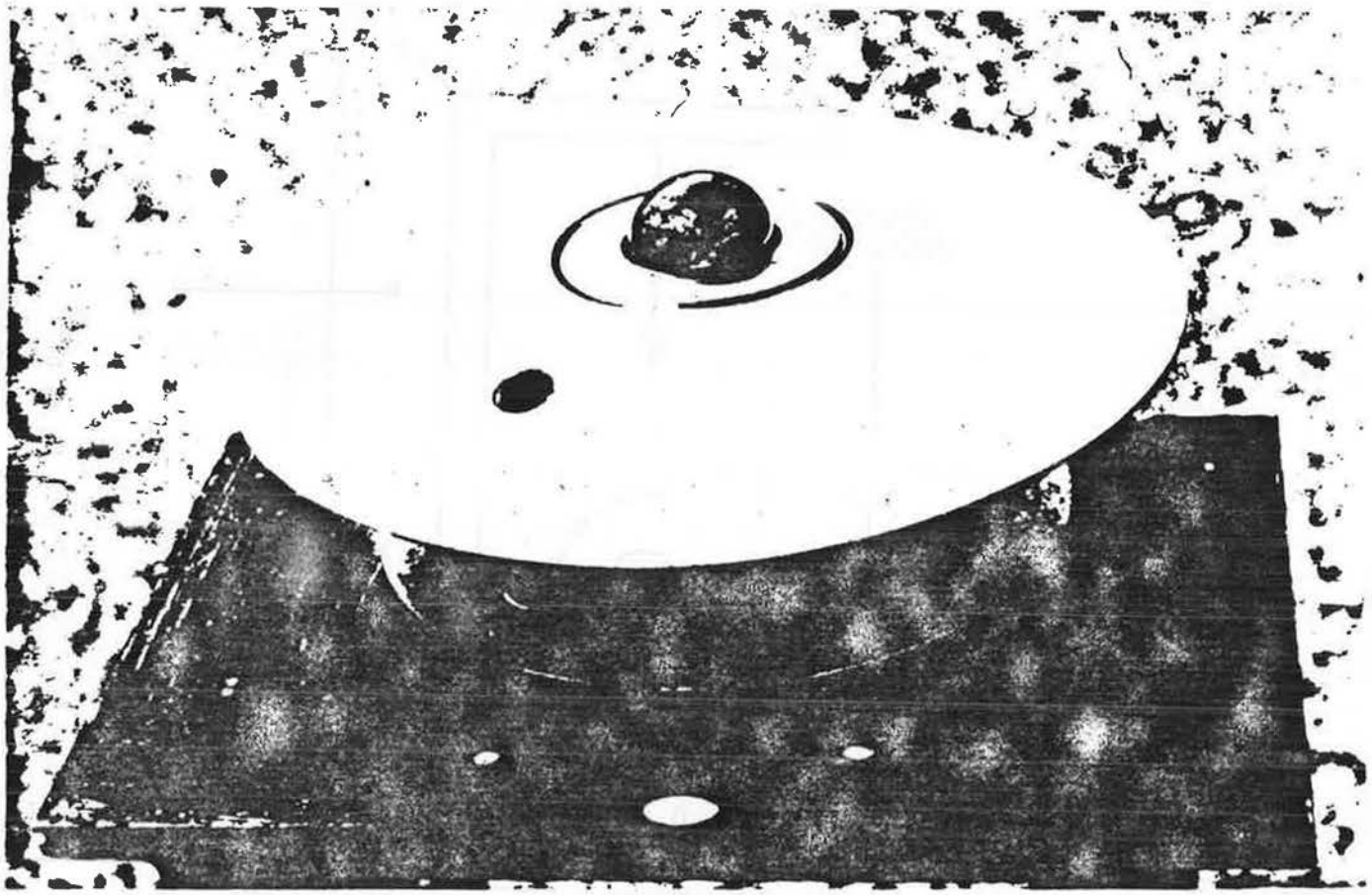

Figure B1.3 Infrared Radiometer

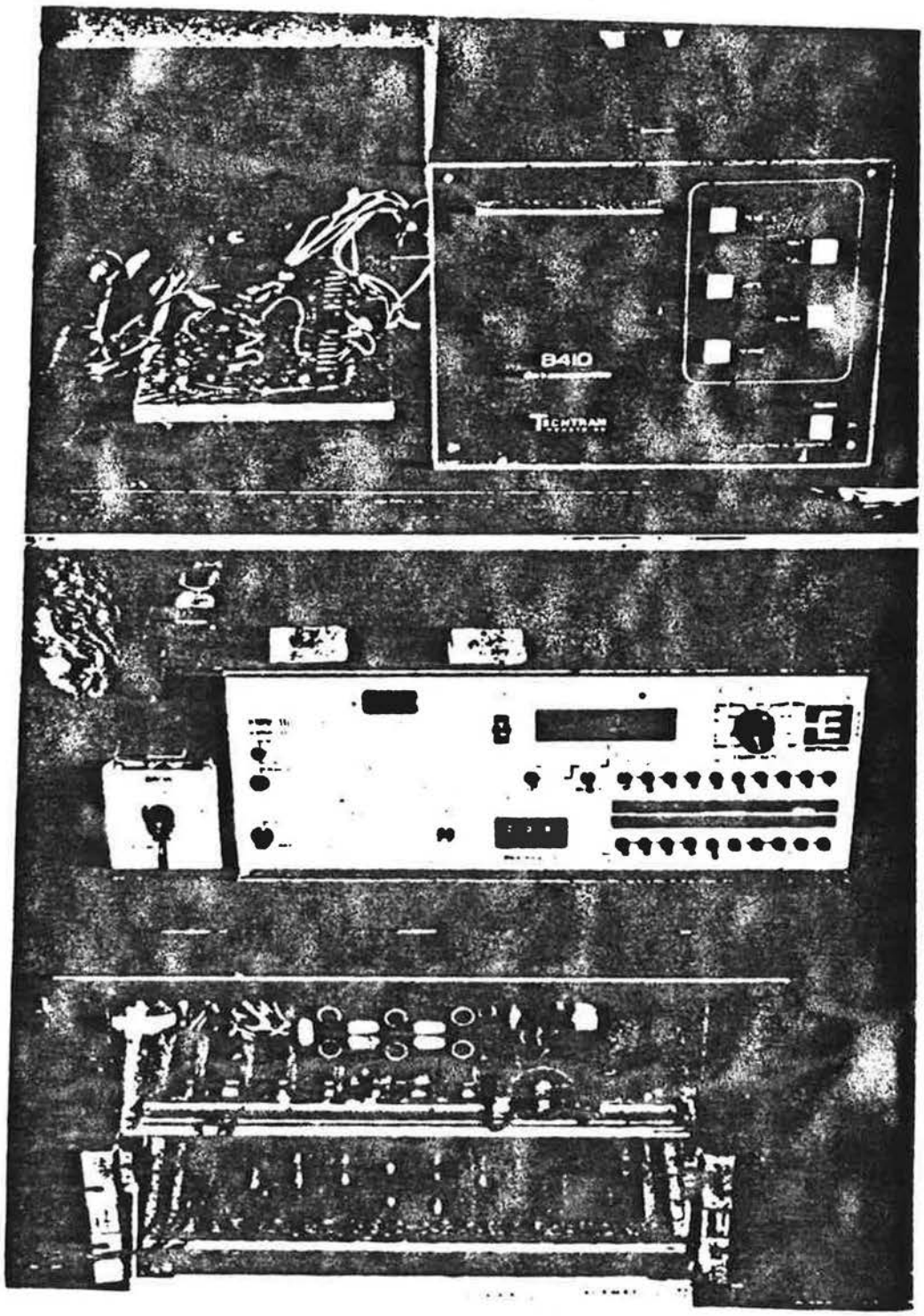

Figure B1.4 Data Acquisition System (from top to bottom: Techtran Datacassette, Esterline Angus, Data Conditioning System)

B.2 CALIBRATION AND USE OF THE WILKS ETHANE ANALYZER

A Miran-101 Specific Vapor Analyzer, built by the Wilks Infrared Center of Foxboro Amalytical, is used to measure ethane concentrations in the Test Chamber. Ethane is used as a tracer gas to measure air infiltration rates under various conditions. The Miran-101, or Wilks Ethane Analyzer (WEA), measures the ampunt of infrared radiation absorbed by the ethane at a factory selected wavelength of 3.4 μm using a single beam infrared spectrometer. The WEA is shown in figure (B2.1). This analyzer provides an immediate and continuous indication of concentration by drawing the air to be measured through a sample cell with an integral pump. The WEA directly displays parts per million (ppm) on a meter which is factory calibrated at one point on each of two scales. In addition, there is a DC output from 0 to 1 volts nonlinearly related to concentration. Researchers experienced with the device have done their own calibrations over the entire range of the WEA and their results were generally quite different from the meters readings [1]. Therefore, using methods recommended by these researchers, we calibrated our WEA and indeed the results were very different from the meter. This calibration yields the concentration in ppm as a function of the DC voltage output which is easily added to the data acquistion system for the Test Chamber. This section describes the calibration procedure of the WEA and its use in infiltration measurements.

Outline of the Calibration Technique

The WEA is calibrated by injecting small amounts of ethane into a known volume and recording the output of the analyzer. The calibration volume used is a closed loop obtained by connecting the exhaust of the WEA to the intake with a length of tygon tubing. The volume of the tygon is known, while the cell volume of the WEA is only roughly known to be about 2.5 liters. Therefore, the cell volume has to be determined before a calibration is obtained.

The cell volume V_w, is found by obtaining a profile of concentration versus volts for two different closed loops. This concentration is in units of μl of ethane per unknown volume V, where $V = V_T + V_w$. V_T is the volume of the tygon tubing. Two different lengths of tygon are used with volumes V_{T1} and V_{T2}. Thus, the closed loop volumes are $V_1 = V_{T1} + V_w$ and $V_2 = V_{T2} + V_w$. After several injections of ethane a relation is found between volts and concentration in units of $\mu l/V_i$ where i=1,2. Using the two relations, the cell volume V_w is found and the final result is an expression of the form

$$C = A + Be^{v} \qquad \text{(B2.1)}$$

where C is in ppm and v is the voltage output of the WEA.

Calibration Procedure

The WEA calibrations are done by injecting small amounts of ethane into the closed loops described above. Two different

closed loops are used, each with a different length of tygon tubing connecting the exhaust to the intake. The ethane is injected with a gas-tight Hamilton microsyringe with a total capacity of 100 µl.

Before the ethane is injected, the WEA must be allowed to warm up for several hours. After the unit is turned on, it runs for three hours drawing room air through a so-called "zero gas filter" (ZGF) of activated charcoal which filters out most organic vapors. During these three hours, the voltage output rises. At first the increase is rather steep, but then it flattens out. After this three hour warm up period on the ZGF, the tygon tubing is connected from the exhaust to the intake and again the unit runs for three hours. This second warm up is necessary because the gas in the closed loop is continually warmed by the machine itself. The rise in the gas temperature causes the voltage output to increase. During this second warm up period, the gas temperature reaches an equilibrium and the voltage flattens out. Figure (B2.2) shows the voltage profile during such a six hour period. Once the warm up is over and the WEA voltage has stabilized, the injection of ethane into the closed loop begins. Before the injections are made, the WEA voltage is set to 0 using the unit's zero adjustment control.

The ethane is injected into the closed loop in tiny amounts, normally 100 µl at a time. The 100 µl injections continue until the voltage output increases beyond 1.3 volts. This takes six or ten 100 µl injections, depending on which of the two lengths of

tygon is used. Two sets of such calibrations were done, one for each length of tygon. Table (B2.1) shows the results for hose no.1 with a volume of V_{T1} = 200 cc. Table (B2.2) shows the results for hose no.2 with V_{T2} = 1974 cc.

Calibration Analysis

The data in tables (B2.1) and (B2.2) were analyzed to determine the cell volume V_w. For each of the two hoses, an expression was obtained of the form

$$C_i = A_i v^{n_i}, \qquad (B2.2)$$

where

C_i = ethane concentration ($\mu l/V_i$)
A_i = constant
n_i = exponent
V^i = voltage output of the WEA $\times 10^3$.

This expression was obtained through linear regressions of $\ln(C_i)$ against $\ln(v \times 10^3)$. A good fit to the above expression was found by using two curves, one for v<0.9 and another for v>0.9. The regression coefficient or slope equals n_i, and the intercept is $\ln(A_i)$. The results for i=1,2 are as follows:

v<0.9

$$C_1 = 372v^{1.213} \qquad C_2 = 616v^{1.221} \qquad (B2.3)$$

v>0.9

$$C_1 = 349v^{1.636} \qquad C_2 = 648v^{1.635} \qquad (B2.4)$$

These expressions fit the data within ± 2% for voltages between 0.2 and 1.3.

The expressions for C_1 and C_2 are used to determine the cell volume V_w. Regardless of which tygon hose is used, and therefore whether one is measuring concentration on the C_1 or C_2 scale, the same concentration in ppm will produce the same voltage output v. Thus, to determine V_w one chooses several voltages within the calibration range and finds values of C_1 and C_2 which correspond to each value of voltage. By equating these two concentrations, one can calculate V_w. Several voltages were used in order to obtain some sense of the uncertainty involved.

The concentrations C_1 and C_2 may be expressed in terms of the volumes of ethane injected, μl, divided by the appropriate containment volume,

$$[(\mu l)_1/V_1] = [(\mu l)_2/V_2] \qquad \text{(B2.5)}$$

$V_1 = V_{T1} + V_w = 200$ cc $+ V_w$, and $V_2 = V_{T2} + V_w = 1974$ cc $+ V_w$. Using these definitions of V_1 and V_2, the equality of concentrations yields the following expression,

$$V_w = [(200cc)(\mu l)_2 - (1974cc)(\mu l)_1]/[(\mu l)_1 - (\mu l)_2] \qquad \text{(B2.6)}$$

Table (B2.3) presents values of voltage and concentration used to calculate V_w as well as the results of these calculations. The resulting value for the cell volume is $V_w = 2535 \pm 19$ cc.

Knowing the value of V_w permits one to obtain the absolute value of concentration in ppm. The relation between ppm and volts is as follows

$$C = = -79.14 + 82.20e^{V}. \qquad (B2.7)$$

This expression agrees with the measured concentration to within ±1% in the calibration range of voltages, 0.2 to 1.3.

The uncertainty in this expression for concentration is due partly to the uncertainty in the cell volume V_w. But this only affects whether the concentration in is ppm or in parts per some fixed fraction of a million. Since in tracer gas decay measurements of infiltration we use differences in logarithms of concentration, such a constant multiplier makes no difference.

The calibration was repeated four months after those shown in tables (B2.1) and (B2.2). There was no significant change in the calibration over this period of time.

Temperature Effects on the WEA

The voltage of the WEA, while related to the ethane concentration, is also affected by the temperature of the gas sample. If the WEA continuously samples gas with a constant ethane concentration, the voltage output will change as the temperature of the gas changes. This voltage drift with temperature presents serious problems in the Test Chamber where the interior temperature changes by as much as 20°C over a day due to solar gain. This section describes a method to account for this drift in air infiltration measurements.

In using the WEA to measure air infiltration rates in the Test Chamber, the WEA runs in the structure for several hours before any ethane is released inside. This time is necessary for the

machine to warm up and to reach a stable zero level. This voltage is converted to ppm and serves as a baseline from which to measure ethane concentrations. After ethane is injected into the Test Chamber, the measured voltage output is converted to ppm. The zero level concentration is subtracted from the measured concentration, and the result is used to compute the air infiltration rate. A drift in the zero level ppm will therefore affect the measured ethane concentrations, and may lead to the calculation of erroneous infiltration rates.

Measurement of the Drift

To determine the magnitude and behavior of the zero level drift, experiments were conducted to relate the drift to the Test Chamber interior temperature. In these experiments, the WEA continuously sampled the inside air with no ethane present. The zero level voltage and interior temperatures were monitored during these tests which lasted from several hours to several days. The results of one test are shown in figure (B2.3). Note that the maximums and minimums in the zero level voltage lag behind the corresponding maximums and minimums in the air temperature. This is because the temperature of the WEA itself affects the sampled gas temperature, and it takes time for the WEA to respond to changes in the interior temperature. This lag in voltage response means the interior air temperature by itself is not an appropriate predictor of the zero level voltage.

Predicting the Zero Level Voltage

The interior temperature of the Test Chamber is not a good predictor of the WEA zero level voltage. Instead, the temperature of the gas exhausted by the WEA T_{wo} is used to predict this voltage. T_{wo} is measured by placing a thermistor in the exhaust port of the device.

Figure (B2.4) is a plot of the zero level voltage V_{wo} with no ethane present versus the outlet temperature T_{wo}. Each point represents the hourly values of the two quantities over a period of about four days. The first point is noted, and a warming up period is evident. After about ten hours, the points fall on a line. The least squares fit to the line is given in the figure.

Similar data was collected in the Test Chamber for several such periods. In each case, the data fell on a line although the lines were not always the same for the different tests. Thus, for each air infiltration test a warm up period of at least one day is necessary for the Wilks voltage/outlet temperature relation to develop.

When analyzing infiltration test data one has long term records of the Wilks voltage V_w and the outlet temperature T_{wo}. T_{wo} is used to predict the zero level voltage V_{wo} and the ethane concentration C' is calculated using

$$C' = C(V_w) - C(V_{wo}). \qquad \text{(B2.8)}$$

After the infiltration measurement one should allow all the ethane to leak out of the Test Chamber in order to recheck the relation between T_{wo} and V_{wo}.

REFERENCES

[1] Personal communication with David Krinkel, Building Envelopes Group, Energy and Environment Division, Lawrence Berkeley Laboratory, University of California.

Table B2.1 Calibrations Using Hose #1

Concentration ($\mu l/V_1$)	WEA Voltage Output (volts x 1,000)								
	N07	N08	$N10_I$	$N10_{II}$	N11	$N12_I$	$N12_{II}$	$N12_{III}$	N13
0	0	0	0	0	0	0	0	0	0
50	-	-	-	-	-	185	184	-	18
100	338	339	342	343	340	345	341	347	34
150	-	-	-	-	-	487	481	-	483
200	603	606	608	610	606	614	608	616	6
250	-	-	-	-	-	727	722	-	725
300	820	824	826	828	825	831	826	836	8
350	-	-	-	-	-	927	921	-	9
400	1002	1006	1007	1010	1007	1014	1008	1019	101
450	-	-	-	-	-	1095	1088	-	10
500	1154	1159	1160	1163	1160	1168	1161	1172	1163
550	-	-	-	-	-	1233	1227	-	12
600	1278	1283	1284	1287	1285	1293	1285	1297	12

$V_1 = V_{T1} + V_W \approx 200\,cc + V_W$

Table B2.2 Calibrations Using Hose #2

Concentration ($\mu l/V_2$)	WEA Voltage Output (volts x 1,000)											
	014_I	015_{II}	030_I	031_I	$NO3_I$	$NO4_I$	$NO4_{II}$	$NO4_{III}$	$NO5_I$	$NO5_{II}$	$NO6_I$	$NO6_{II}$
0	0	0	0	0	0	0	0	0	0	0	0	0
100	222	219	222	222	223	219	219	218	220	223	219	218
200	411	407	409	408	412	404	402	403	406	406	404	402
300	576	572	571	571	577	564	561	562	567	566	565	562
400	720	716	713	714	721	706	701	704	710	706	707	704
500	848	840	840	841	849	833	828	829	835	831	833	830
600	962	955	953	954	964	945	940	943	946	943	946	942
700	1064	1058	1056	1054	1066	1047	1041	1044	1048	1044	1047	1043
800	1155	1150	1148	1146	1156	1138	1133	1135	1139	1133	1138	1134
900	1236	1232	1228	1227	1238	1219	1214	1216	1221	1215	1220	1216
1000	1305	1302	1299	1298	1307	1291	1286	1288	1292	1286	1291	1287

$V_2 = V_{T2} + V_W - 1974cc + V_W$

Table B2.3 Determination of Cell Volume

WEA Voltage Output (volts x 1000)	C_1* (μl)	C_2* (μl)	V_w (ml)
600	200	330	2529
700	241	399	2506
800	284	469	2523
1000	394	648	2552
1100	460	757	2548
1200	531	873	2554
		Mean	2535
		Standard Deviation	19

*These values are the number of μl of ethane necessary to produce the voltage output on the left. They are not strictly concentrations since they have units of volume.

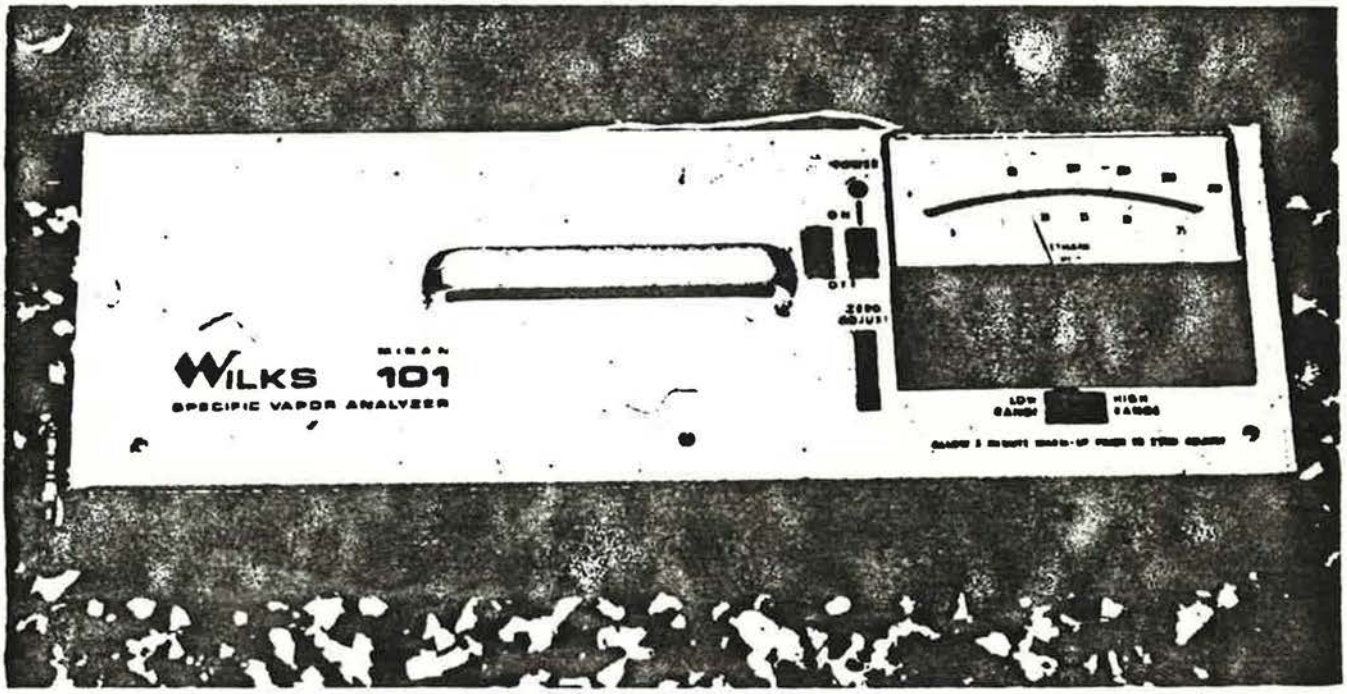

Figure B2.1 Wilks Ethane Analyzer

Figure B2.2 WEA Voltage Output During Calibration Warm-up

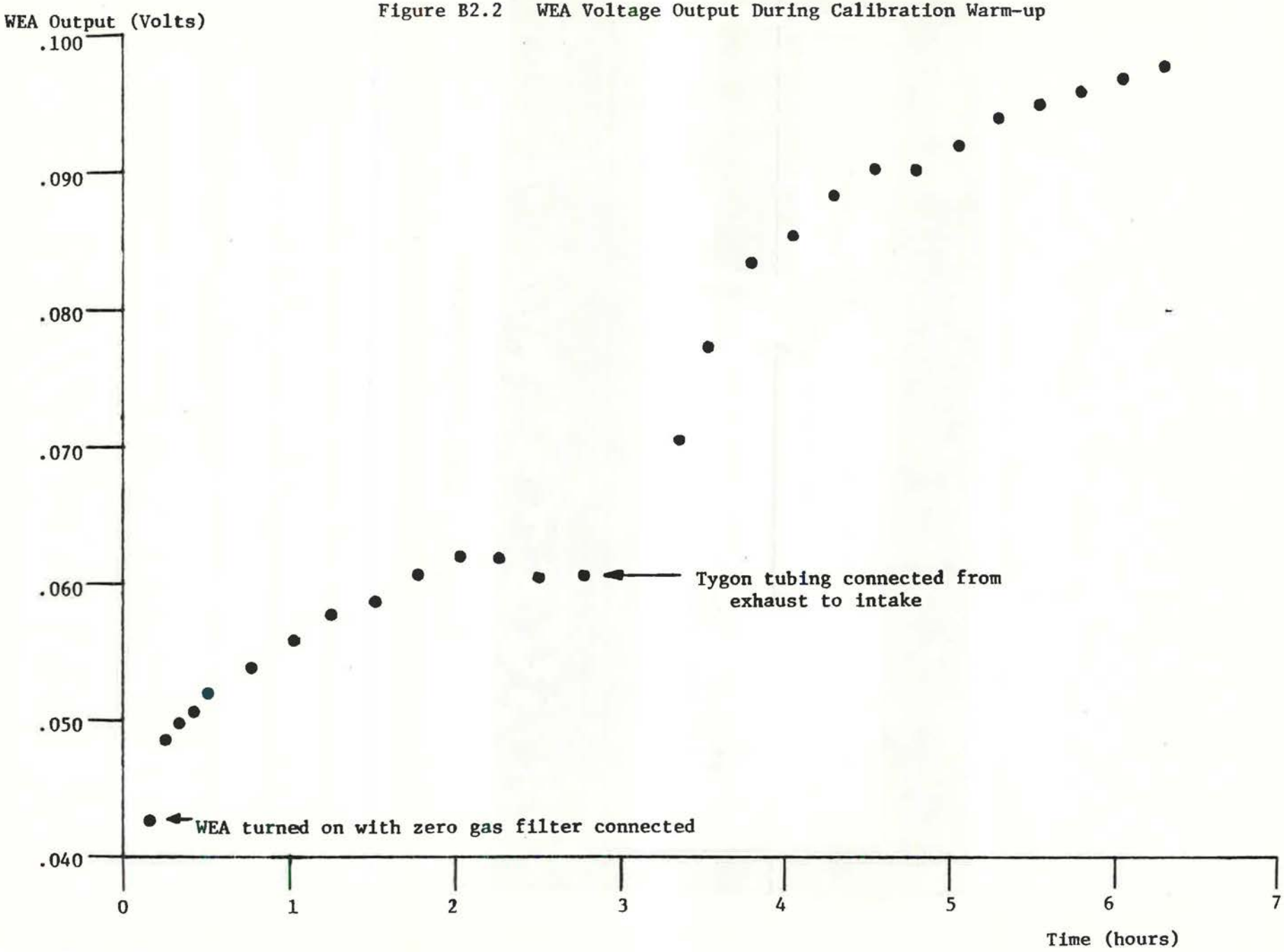

Figure B2.3 WEA Voltage Output and Inside Temperature vs Time

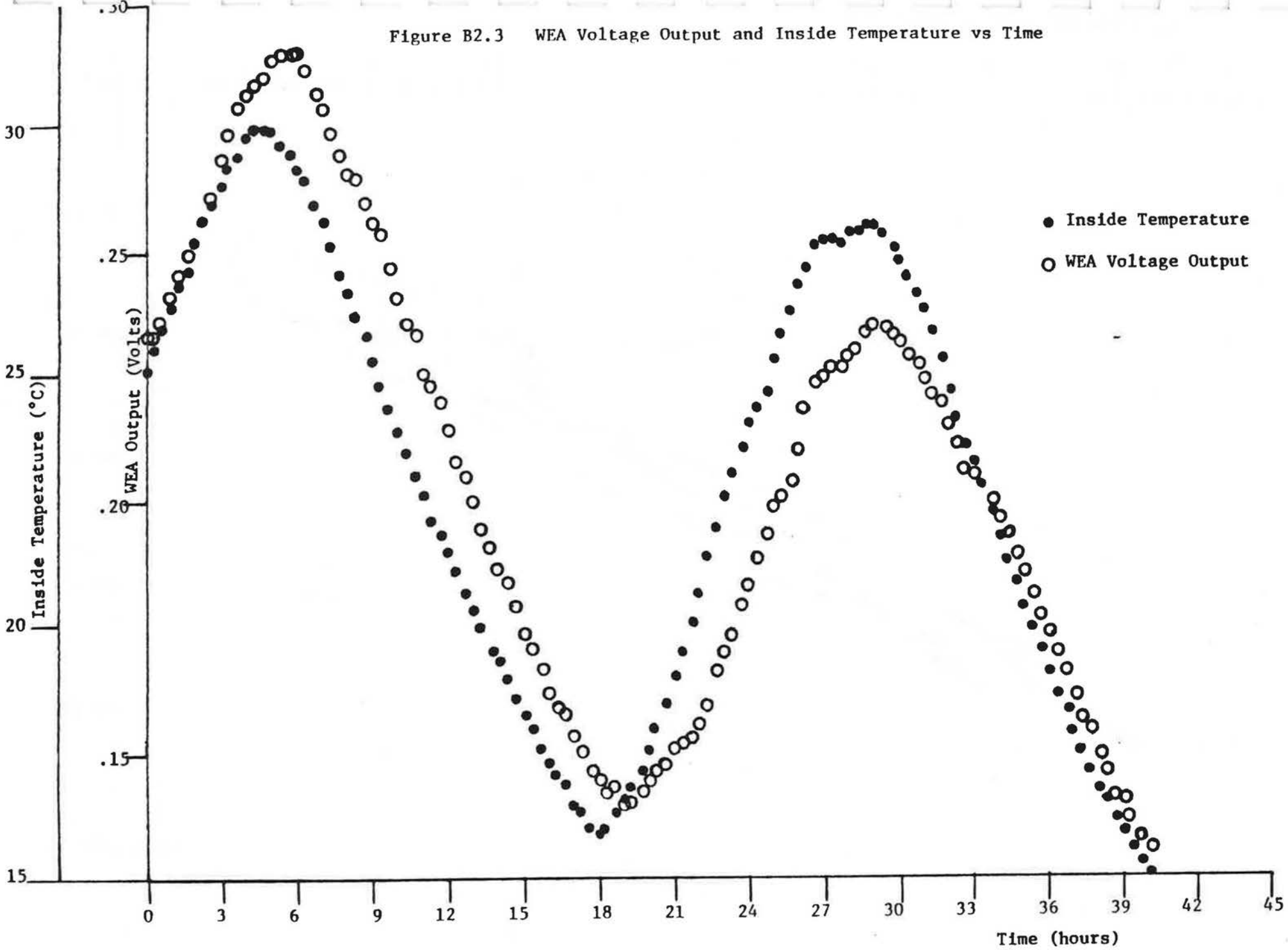

Figure B2.4 Wilks Voltage vs Outlet Temperature

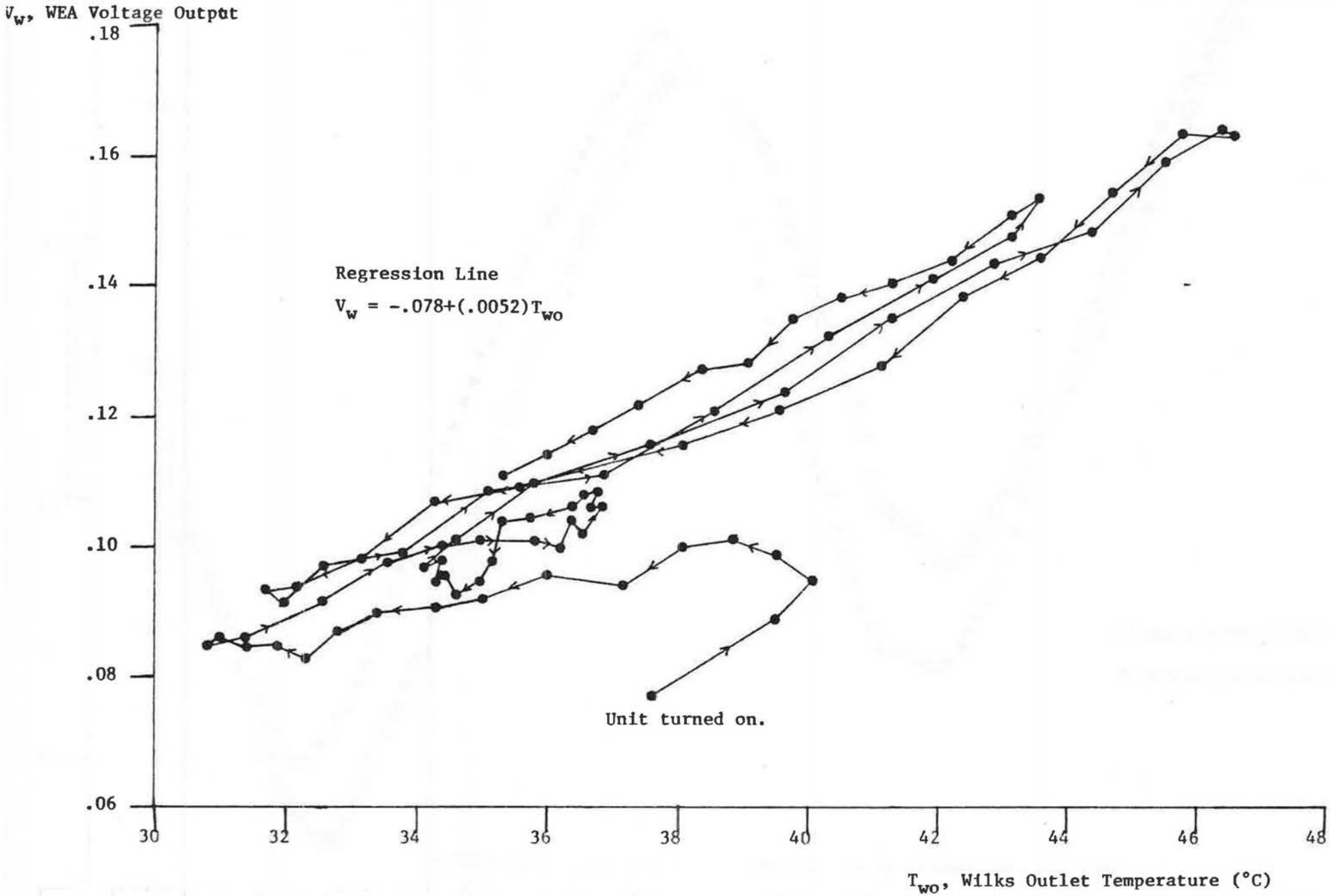

B.3 PRESSURIZATION DEVICE FOR THE TEST CHAMBER

In our studies of the relation between pressurization testing and natural infiltration measurements in the Test Chamber it was necessary to pressure test the structure. The Blower Door used in homes operates at flow rates much too large for the small Test Chamber. Therefore, we designed and built a low flow rate pressurization device with greater accuracy than the Blower Door. This device consists of a centrifugal blower to move the air and an orifice plate flowmeter to measure the air flow rate. This section describes the pressurization device that was built according to standard techniques [1-5].

Orifice Meters [1]

Orifices have been used to measure flow rates of fluids since the days of Caesar, and more recently for the flow of fluids in pipe lines. An orifice is simply a circular hole in a thin, flate plate clamped between two flanges at a joint in the pipe line. The plane of the orifice is perpendicular to the flow direction and the orifice is concentric with the pipe. The pressure difference Δp_m between the two sides of the orifice is measured and related to the flow rate. Figure (B3.1) is a sketch of an orifice meter along with a plot of the static pressure along the pipe. The static pressure increases on the upstream side of the orifice, reaching a maximum at the plate. There is a sharp pressure drop across the plate and the decrease continues past the orifice. After attaining a minimum value, the pressure in-

creases to a second maximum. The position of the minimum in static pressure, and the maximum in fluid velocity, is called the "vena contracta."

There are several possible locations for the pressure taps used to determine Δp_m. "Flange taps" are located 1 in. upstream and downstream of the orifice plate. In "vena contracta taps," the upstream tap is located between 1/2 and 2 pipe diameters from the plate and the downstream tap is at the vena contracta. In our device, we use pressure taps at 1 pipe diameter upsteam from the orifice and downstream at 1/2 pipe diameter from the plate.

From the theory of fluid mechanics one can show that the flow through the orifice q in m^3/s is equal to

$$q = aK\sqrt{2\Delta p_m/\rho}\ , \qquad (B3.1)$$

where

a = area of the orifice (m^2)
K = flow coefficient
Δp_m = pressure difference across the orifice (Pa)
ρ = fluid density (kg/m^3)

The flow coefficient K depends on β, the ratio of the orifice diameter d to the pipe diameter D, and the Reynold's number Re given by

$$Re = qD/A\nu\ . \qquad (B3.2)$$

A is the pipe area and ν is the kinematic viscosity of the fluid. The value of K also depends on the location of the pressure taps. Table (B3.1) shows the dependence of K on β and Re for the pipe

used in our device [1]. Note that as the Reynolds number increases, the flow coefficient approaches a constant for a given value of β. Above the solid line, the flow coefficient is accurate within ± 0.55 % while below the line, the uncertainty is twice this amount.

Description of the Test Chamber Orifice Meter

The flow meter used for pressurizing the Test Chamber is shown installed in the Test Chamber in figure (B3.2). Both the pipe and flanges are made of PVC with D = 0.102 m (4 in). The orifices are made of 1/16th in thick aluminum and seals of Garlock are used on both sides of the orifice. The orifices, primarily their edges, were built according to specifications in the references. Four orifice diameters were used to cover a large range of flow rates, i.e. d = 0.082 m (3.2 in), 0.064 m (2.5 in), 0.051 m (2.0 in) and 0.038 m (1.5 in). As mentioned earlier, the static pressure taps are located at 1 pipe diameter D upstream of the orifice and at 1/2 D downstream. Figure (B3.3) is a close-up photograph of the joint in the pipe line showing the flanges and the pressure taps. The pressure difference across the orifice Δp_m was measured with Dwyer inclined manometers. For low values of Δp_m the Model No. 215 was used, and for large values Model No. 202.5.

The air was moved using a centrifugal fan with a 6 in diameter wheel built by Dayton Electric Manufacturing Co., Model No. 1C791. The blower was powered by a Dayton DC motor, Model No.

22846. The induced pressure difference between inside and outside was measured with a Dwyer magnehelic gauge, Model No. 2000-00.

The entire device was installed in a 6 in hole in the side of the Test Chamber. An aluminum cone was built to connect the 6 in hole with the 4 in orifice pipe. The reduction in area occured over about 4 ft. In order to achieve fully developed flow at the orifice plate, the upstream length of pipe is fifteen pipe diameters long. The downstream section is about 13 diameters long. When pressurizing the Test Chamber the downstream section of pipe is connected to the cone through which the air flows into a flexible hose and then into the fan intake. During depressurization the flowmeter is turned around and the flexible hose is connected to the fan exhaust.

REFERENCES

[1] Fluid Meters, Their Theory and Application, Report of the ASME Research Committee on Fluid Meters, 5th ed., The American Society of Mechanical Engineers, 1959.

[2] Ower, E., Pankhurst, R.C., The Measurement of Air Flow, 4th ed., Pergamon Press Ltd., 1966.

[3] Daugherty, R.L., Franzini, J.B., Fluid Mechanics with Engineering Applications, 6th ed., McGraw-Hill Book Co., 1965.

[4] Clark, W.J., Flow Measrement by Square-edged Orifice Plate Using Corner Tapppings, Pergamon Press, 1965.

[5] Cox, G.N., Germano, F.J., Fluid Mechanics, D.Van Nostrand Co., Inc., 1941.

Table B3.1 (from reference [1])

TAPS AT 1 D AND ½ D

Values of the Flow Coefficient, K, Velocity of Approach Factor Included, as a Function of the Pipe Reynolds Number, R_D, and Diameter Ratio, β

For 4 In. Pipe, D = 4.026 In.

β \ R_D	500	1,000	2,000	3,000	4,000	5,000	6,000	8,000	10,000	15,000	20,000	30,000	50,000	100,000	500,000	10^6
0.100	0.6154	0.6087	0.6040	0.6019	0.6006	0.5998	0.5991	0.5982	0.5976	0.5967	0.5961	0.5955	0.5948	0.5941	0.5932	0.5930
.150	.6174	.6101	.6049	.6026	.6012	.6003	.5996	.5986	.5980	.5969	.5963	.5956	.5949	.5941	.5932	.5929
.200	.6208	.6126	.6068	.6042	.6026	.6016	.6008	.5997	.5990	.5978	.5972	.5963	.5955	.5947	.5936	.5933
.250	.6257	.6163	.6097	.6067	.6050	.6038	.6029	.6016	.6008	.5995	.5987	.5978	.5968	.5959	.5946	.5943
.300	.6322	.6215	.6138	.6104	.6084	.6070	.6060	.6046	.6036	.6021	.6012	.6001	.5991	.5980	.5966	.5962
.325	.6363	.6247	.6165	.6128	.6107	.6092	.6081	.6066	.6055	.6039	.6029	.6018	.6006	.5995	.5979	.5976
.350	.6408	.6284	.6196	.6157	.6134	.6118	.6106	.6090	.6078	.6061	.6050	.6038	.6026	.6013	.5997	.5993
.375	.6460	.6327	.6232	.6190	.6165	.6148	.6135	.6118	.6106	.6087	.6076	.6062	.6049	.6036	.6018	.6014
.400		.6375	.6274	.6229	.6202	.6184	.6170	.6151	.6138	.6118	.6106	.6092	.6077	.6063	.6044	.6039
.425		.6431	.6322	.6273	.6245	.6225	.6210	.6190	.6176	.6154	.6142	.6126	.6111	.6096	.6075	.6070
.450		.6494	.6377	.6325	.6294	.6273	.6257	.6235	.6220	.6197	.6183	.6167	.6151	.6134	.6112	.6107
.475		.6565	.6439	.6384	.6350	.6328	.6311	.6288	.6272	.6247	.6232	.6215	.6197	.6179	.6156	.6150
.500			.6510	.6451	.6415	.6391	.6373	.6348	.6331	.6304	.6288	.6270	.6251	.6232	.6206	.6200
.520			.6574	.6511	.6474	.6448	.6429	.6403	.6385	.6356	.6340	.6320	.6300	.6280	.6253	.6247
.540			.6644	.6578	.6538	.6512	.6491	.6463	.6444	.6414	.6397	.6376	.6355	.6334	.6305	.6299
.560			.6722	.6652	.6610	.6581	.6560	.6531	.6510	.6479	.6460	.6438	.6416	.6394	.6364	.6357
.580			.6808	.6733	.6689	.6659	.6637	.6605	.6584	.6551	.6531	.6508	.6484	.6460	.6429	.6421
.600				.6824	.6777	.6745	.6722	.6689	.6666	.6631	.6610	.6585	.6560	.6535	.6501	.6493
.620				.6926	.6876	.6842	.6816	.6781	.6757	.6720	.6697	.6671	.6644	.6618	.6582	.6573
.640				.7039	.6986	.6949	.6922	.6885	.6859	.6819	.6795	.6767	.6738	.6710	.6671	.6662
.660				.7168	.7110	.7071	.7042	.7001	.6973	.6930	.6904	.6874	.6843	.6812	.6771	.6761
.680				.7316	.7253	.7210	.7178	.7133	.7103	.7056	.7028	.6994	.6961	.6927	.6882	.6871
.700					.7418	.7370	.7335	.7285	.7252	.7199	.7168	.7131	.7094	.7056	.7006	.6994
.720					.7612	.7558	.7518	.7462	.7424	.7365	.7329	.7287	.7245	.7203	.7146	.7133
.740					.7847	.7784	.7737	.7672	.7628	.7559	.7518	.7469	.7420	.7371	.7305	.7289
.750					.7983	.7914	.7864	.7793	.7745	.7669	.7624	.7571	.7518	.7464	.7393	.7376
.760						.8059	.8004	.7926	.7873	.7790	.7741	.7683	.7624	.7566	.7487	.7468
.780						.8402	.8334	.8238	.8173	.8072	.8011	.7939	.7868	.7795	.7699	.7676
.800						.8837	.8751	.8630	.8548	.8420	.8343	.8253	.8162	.8070	.7948	.7919

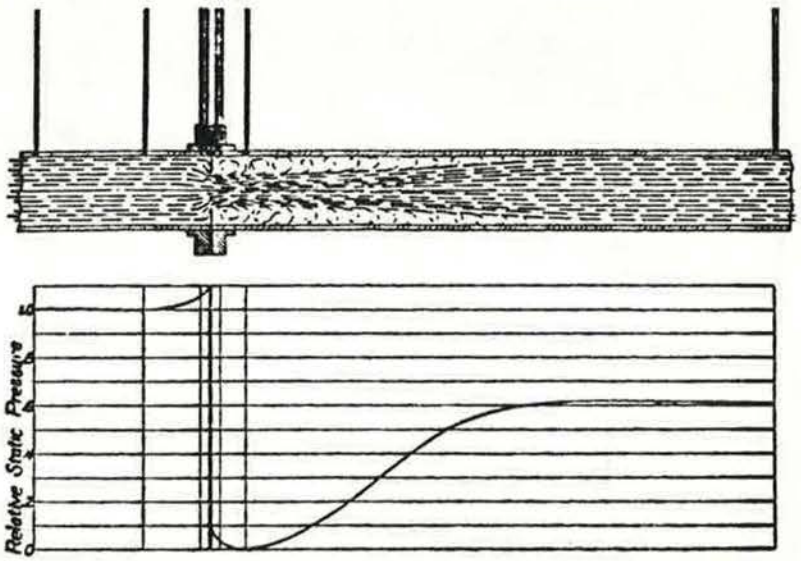

DIAGRAMMATIC REPRESENTATION OF FLUID FLOW THROUGH A THIN-PLATE ORIFICE SHOWING POSITIONS OF PRESSURE TAPS IN COMMON USE AND THE RELATIVE STATIC PRESSURE

(Flow is from left to right)

Figure B3.1 (from reference [3]).

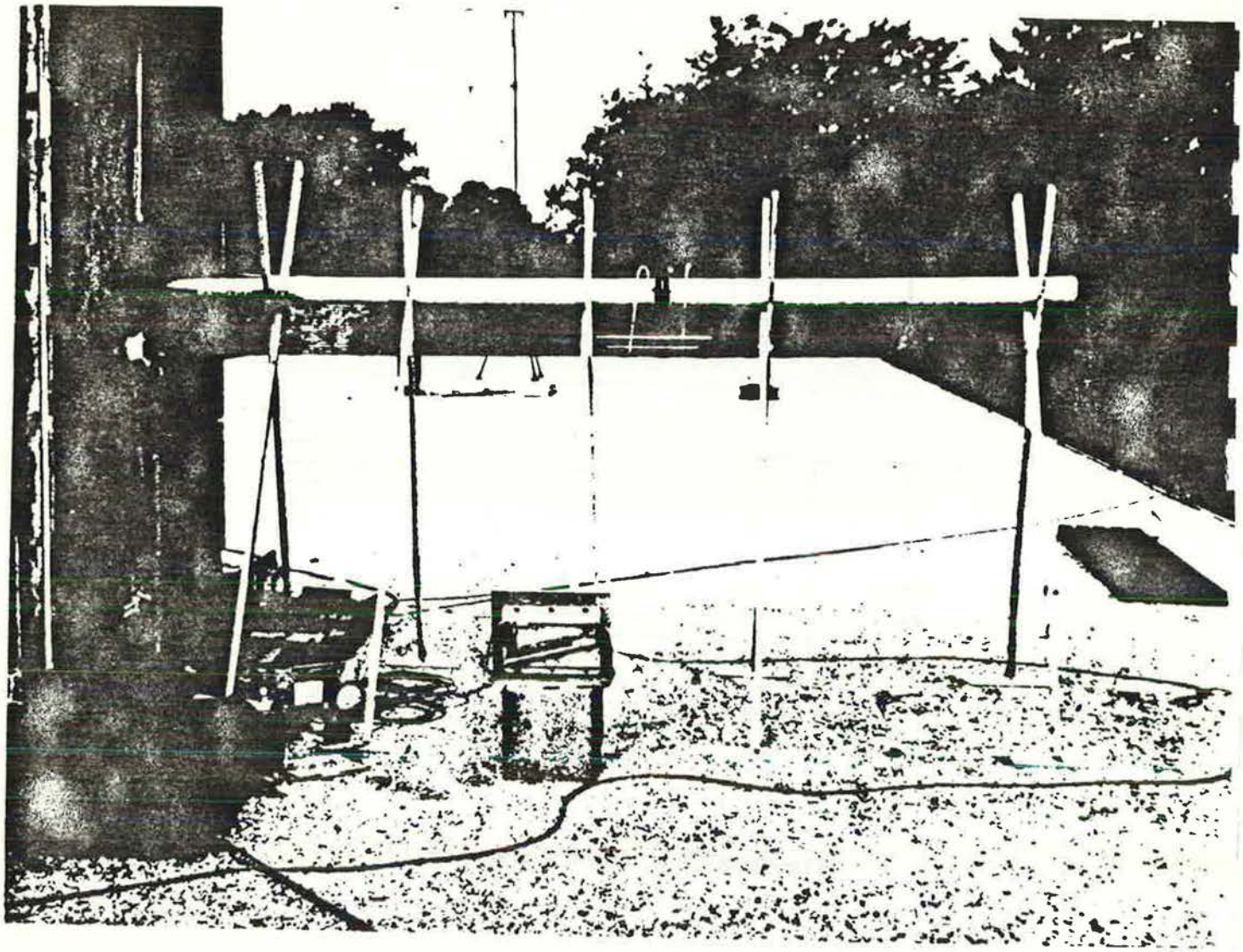

Figure B3.2 Pressurization Device for Test Chamber

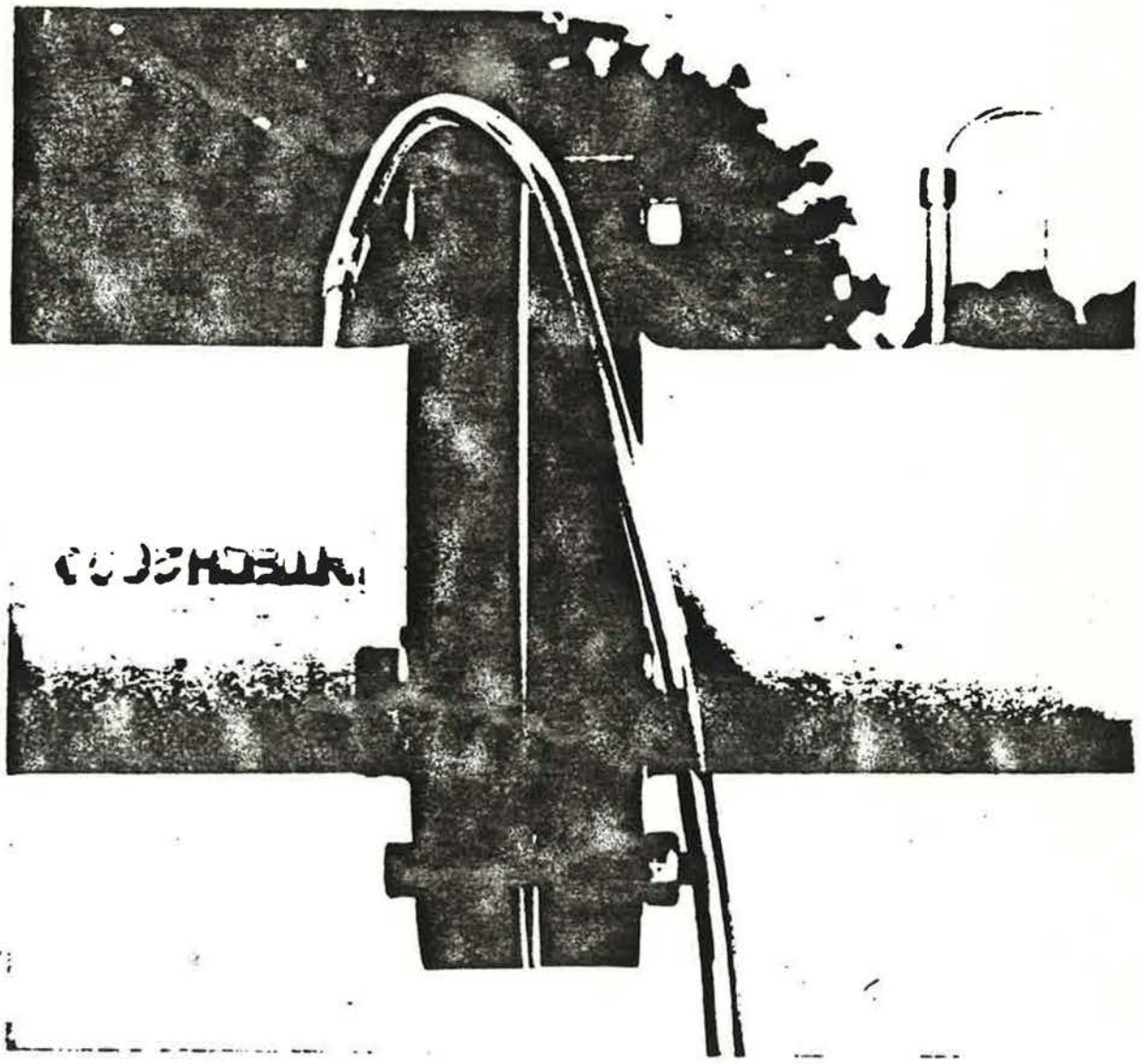

Figure B3.3 Orifice and Pressure Taps

Appendix C

TEMPERATURE CORRECTION FOR THE BLOWER DOOR

The Blower Door was calibrated by measuring the flow through the fan q (m^3/s) as a function of the fan RPM and the inside-outside pressure difference Δp (Pa). These calibrations were made at only a single air density of $\rho_T = 1.21$ kg/m^3. When Blower Door tests are made in the field, the air density is generally different from ρ_T. It is necessary to know the effect of air density on the Blower Door calibration. We know the flow rate q as a function of Δp and RPM at the calibration density, and we need to know how to find the flow rate at a different air density ρ. Fan laws exist to relate several aspects of fan performance under different conditions, but they are not applicable to our situation. One may use the fan laws only when the two conditions lie on the same point of the fan performance curve as described below.

Fan laws are derived through nondimensionalization. We are trying to relate the flow rate q to the fan speed in revolutions per second n, the fan diameter D = 0.46 m, the air density ρ and the pressure difference Δp. One uses these quantities to write expressions for a nondimensional flow rate Q/nD^3 and a nondimensional pressure difference $\Delta p/\rho(nD)^2$. Using the fan calibration from the Blower Door manual and setting $\rho = \rho_T = 1.21$ kg/m^3,

these two nondimensional quantities were calculated for a variety of Δp and n. Figure (C1) and (C2) are plots of Q/nD^3 against $\Delta p/\rho(nD)^2$ for the pressurization and depressurization calibrations respectfully. The fan laws apply only for two sets of conditions which lie on the same point of one of these curves. Our situation of constant Δp and n, but varying moves us along the curve, and the fan laws do not apply. These curves were used in chapter VI to correct the flow rate through the fan for temperature effects.

There needs to be a more precise calibration technique for the Princeton Blower Door and other pressurization devices. When such a technique is at hand, the calibrations should be done at several air densities in order to verify the above analysis.

REFERENCES

[1] Gadsby, K.J., Linteris, G.T., Dutt, G.S., Harrje, D.T., "The Blower Door," Report No. 124, Center for Energy and Environmental Studies, Princeton University, 1981.

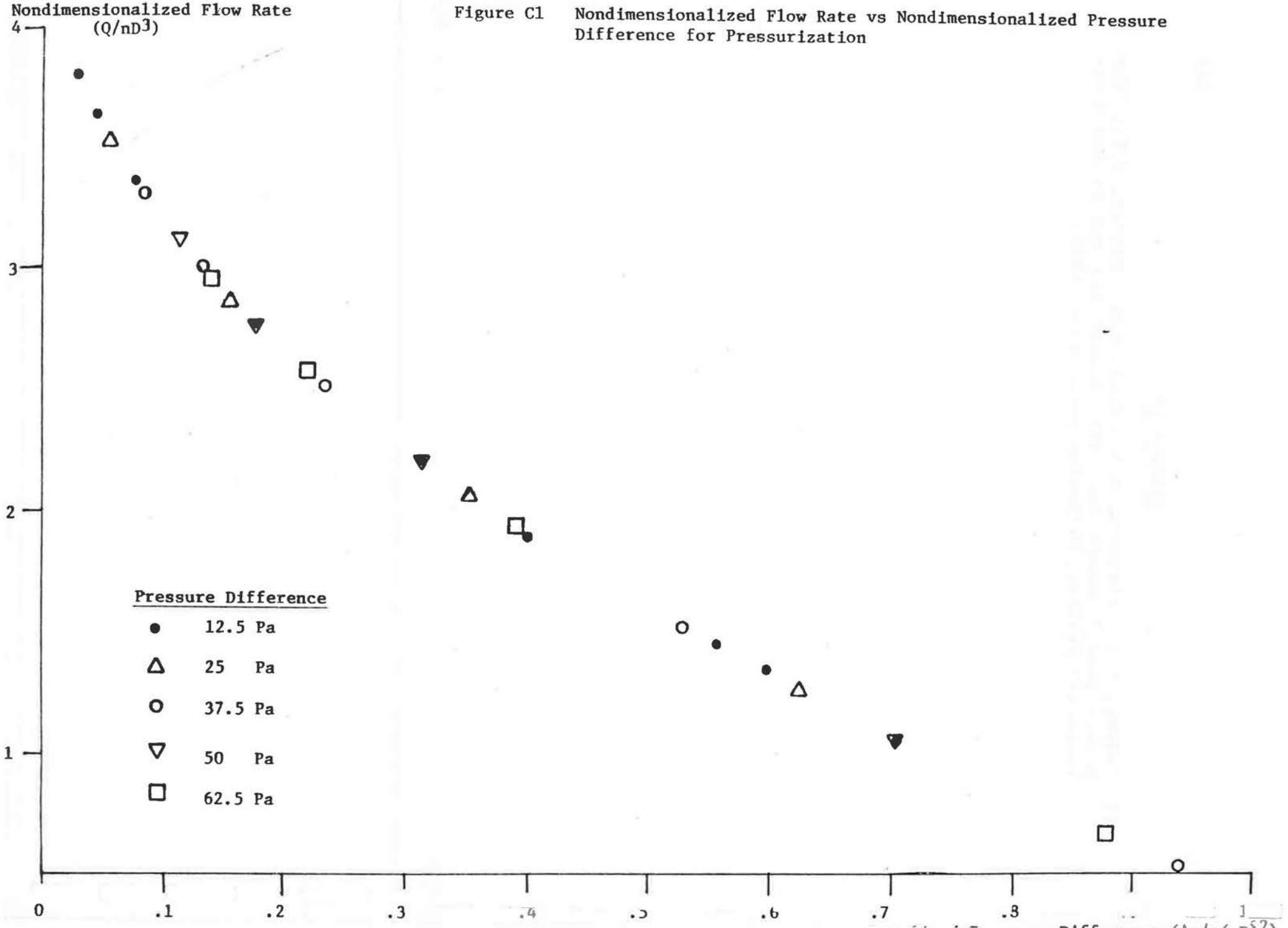

Figure C1 Nondimensionalized Flow Rate vs Nondimensionalized Pressure Difference for Pressurization

Figure C2

Nondimensionalized Flow Rate vs. Nondimensionalized Pressure Difference
for Depressurization

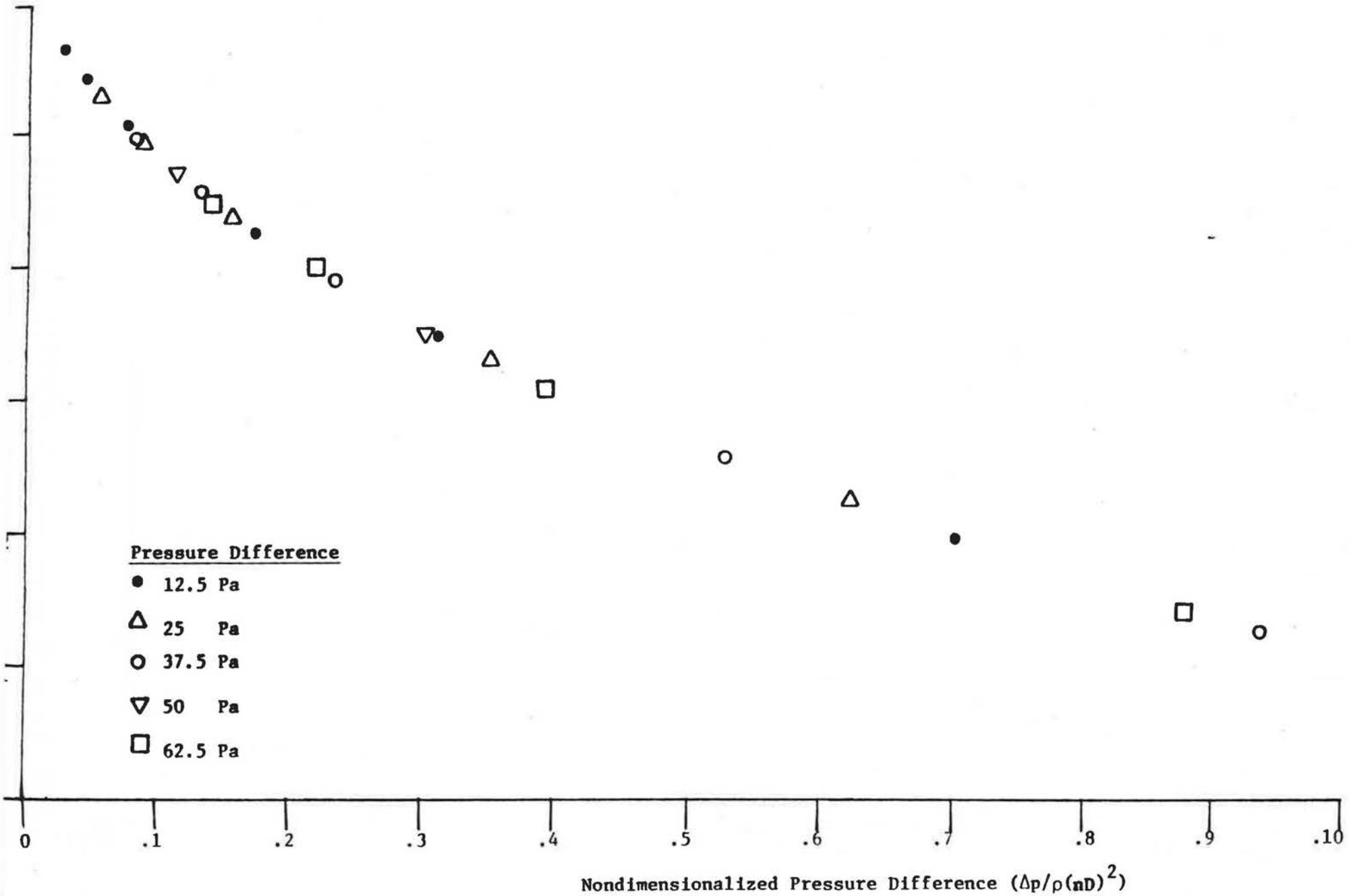

Appendix D

MEASURING THE TEST CHAMBER HEAT LOSS

D.1 TRAILING TEMPERATURE*

One method of experimentally determining a structure's heat loss rate is by relating the rate of heat flow across a wall to the temperature difference across the wall. Under steady state conditions this method is simple and reliable, and has formed the basis for measurement procedures such as the guarded hot box method [1]. In these procedures, the heat flow is measured under highly controlled conditions. However, a structure such as a home is not normally located in such a well-controlled environment, and its heat loss rate depends on the wind speed and the radiative environment in addition to the material properties of the structure.

If one intends the study the heat loss rate of a real building, the steady state heat flow equation is not generally valid, i.e.

---

* The author wishes to acknowledge the contributions of G.S.Dutt and F.W.Sinden to this work.

$$Q \neq L(T_i - T_o), \qquad \text{(D1.1)}$$

where

Q = heat input rate into the structure (W)
L = lossiness (W/°C)
T_i = inside temperature (°C)
T_o = outside temperature (°C)

A structure in the real world is never in steady state, and to determine the heat loss rate one must employ more complex techniques.

In this section, we propose a theoretical framework for evaluating the heat loss rate, or lossiness, of a structure from data on the heat input rate and the temperatures T_i and T_o. This technique is applied to determine the lossiness of the Test Chamber. Many experiments to measure the lossiness of this structure have been conducted, and they are described in detail later in this appendix. The experiments consist of heating the Test Chamber with light bulbs connected to a thermostat. The tests were conducted at night to eliminate the need for considering solar heat gain, though not the delayed effect of solar energy collected during the previous day. Each experiment consists of a night's history of T_i, T_o and the electric energy consumption Q.

The actual heat input rate to the interior of the structure will not always be proportional to the instantaneous temperature difference ($\Delta T_I = T_i - T_o$) primarily because of the thermal inertia of the building. We may calculate an "instantaneous" lossiness for an hour by dividing the average heat input by the average temperature difference, i.e.,

$$L_I = Q/\Delta T_I. \qquad \text{(D1.2)}$$

Figure (D1.1) shows the instantaneous lossiness, L_I, plotted over one night. This lossiness increases through the night as the stored solar heat from the day is dissipated and as the decrease in outside temperature is propagated into the Test Chamber interior. Towards the end of the night, as the outside temperature approaches a minimum, the lossiness flattens out at a maximum value.

We may define a "material" lossiness, a physical property of the structure, as the heat input rate divided by the difference between the interior and exterior surface temperatures under steady state conditions. Also, we define an "overall" lossiness for the structure as the heat input rate divided by the difference between the inside and outside air temperatures when these temperatures are constant. The overall lossiness is different from the material lossiness because of surface heat transfer phenomena. Wind and radiation affect the outside surface temperature of the structure, and therefore affect the rate of conduction. Thus, the overall lossiness will change under different wind and radiation conditions, but the material lossiness will remain the same. Although steady conditions never exist for the structure, the overall lossiness is useful in determining the effect on heat loss rate of wind and radiation. Under the unsteady conditions that do exist, one may determine the overall lossiness as described below.

The problem before us is to take the data which yields the instantaneous lossiness, Q, T_i, and T_o, and determine the overall

lossiness. There are numerous methods to predict the heating load of a building [2-9]. These techniques predict the heat load from the construction of the building, but neglect obscure but important deviations from the building plans. The heating load of the structure can also be experimentally determined using a simple empirical model. This second approach was used by Sonderegger to determine the so-called "equivalent thermal parameters" of a building [10]. To arrive at accurate values of the heat loss in order to evaluate relatively small effects like wind and radiation, we use an empirical approach.

Development of Trailing Temperature

It is possible to characterize the heat loss from the Test Chamber with a simple model shown in figure (D1.2). $\bar{c}$ is the effective heat capacity of the structure's thermal mass. U_i and U_o are the conductances of the thermal mass from the inside and to the outside respectively. Q is the heat input to the interior, and Q_o is the heat flow to the outside. T_i, T_c and T_o are the temperatures of the inside, thermal mass and outside. The equations for each of the three components are

$$\begin{aligned} Q &= U_i(T_i - T_c) \\ Q_o &= U_o(T_c - T_o) \\ \bar{c}\dot{T}_c &= Q - Q_o. \end{aligned} \tag{D1.3}$$

Eliminating T_c and Q_o from these equations yields,

$$\dot{Q} + (U_i+U_o)Q/\bar{c} = U_i\dot{T}_i + (T_i-T_o)U_iU_o/\bar{c}. \tag{D1.4}$$

In steady state with Q, T_i, and T_o constant, the heat flow Q is given by,

$$Q = [(U_i U_o/(U_i+U_o)](T_i-T_o) \qquad (D1.5)$$

This equation defines the overall lossiness L,

$$L = U_i U_o/(U_i+U_o) = 1/[(1/U_i)+(1/U_o)] \qquad (D1.6)$$

As a differential equation in Q, (D1.4) has the form,

$$\dot{Q} + Q/\tau = f(\ ) \qquad (D1.7)$$

where the time constant τ is

$$\tau = \bar{c}/(U_i+U_o) \qquad (D1.8)$$

and the driving function f(t) is,

$$f(t) = U_i\dot{T}_i + (U_i U_o/\bar{c})(T_i-T_o) \qquad (D1.9)$$

The solution of (D1.6) is,

$$Q(t) = \int_{-\infty}^{t} e^{-[(t-t')/\tau]} f(t')dt'. \qquad (D1.10)$$

Substituting (D1.8) into (D1.9),

$$Q(t) = U_i \int_{-\infty}^{t} e^{-[(t-t')/\tau]}\dot{T}_i(t')dt' \qquad (D1.11)$$

$$+ (U_i U_o/\bar{c}) \int_{-\infty}^{t} e^{-[(t-t')/\tau]}[T_i(t')-T_o(t')]dt'.$$

Integration of the first term by parts, and multiplication and division of the second term by τ gives,

$$Q(t) = U_i \int_{-\infty}^{t} \frac{1}{\tau} e^{-[(t-t')/\tau]} [T_i(t)-T_i(t')]dt' \qquad \text{(D1.12)}$$

$$+ (U_o U_o \tau/\bar{c}) \int_{-\infty}^{t} \frac{1}{\tau} e^{[(t-t')/\tau]} [T_i(t')-T_o(t')]dt'$$

Note that the coefficient in front of the second integral, $U_i U_o \tau/\bar{c}$ is equal to the lossiness L, by equations (D1.6) and (D1.8). Rewriting (D1.12),

$$Q(t) = U_i \int_{-\infty}^{t} \frac{1}{\tau} e^{-[(t-t')/\tau]} [T_i(t)-T_i(t')]dt' \qquad \text{(D1.13)}$$

$$+ L \int_{-\infty}^{t} \frac{1}{\tau} e^{-[(t-t')/\tau]} [T_i(t')-T_o(t')]dt'.$$

The first integral gives the effect on Q(t) of changes in interior temperature, while the second integral gives the weighted effect of past indoor-outdoor temperature differences.

The first integral in (D1.13) is zero if the inside temperature is constant, because in this case $T_i(t) = T_i(t')$ for all t and t'. If changes in $T_i(t)$ are small, then this integral can be regarded as a correction. For constant $T_i(t)$, $T_i(t')$ can be taken out of the second integral, and (D1.13) can be written as,

$$Q(t) = L[T_i - \int_{-\infty}^{t} \frac{1}{\tau} e^{-[(t-t')/\tau]} T_o(t')dt']. \qquad \text{(D1.14)}$$

For the more general case of non-constant T_i, L can be calculated by solving (D1.12),

$$L = \frac{Q(t) - U_i \int_{-\infty}^{t} \frac{1}{\tau} e^{-[(t-t')/\tau]} [T_i(t)-T_i(t')]dt'}{\int_{-\infty}^{t} \frac{1}{\tau} e^{-[(t-t')/\tau]} T_i(t')dt' - \int_{-\infty}^{t} \frac{1}{\tau} e^{-[(t-t')/\tau]} T_o(t')dt'.} \qquad \text{(D1.15)}$$

Equation (D1.15) can be simplified by removing $T_i(t)$ from the integral in t' and noting that,

$$\int_{-\infty}^{t} \frac{1}{\tau} e^{-[(t-t')/\tau]} dt' = 1. \qquad \text{(D1.16)}$$

Therefore,

$$L = \frac{Q(t) - U_i[T_i(t) - \int_{-\infty}^{t} \frac{1}{\tau} e^{-[(t-t')/\tau]} T_i(t') dt']}{\int_{-\infty}^{t} \frac{1}{\tau} e^{-[(t-t')/\tau]} T_i(t') dt' - \int_{-\infty}^{t} \frac{1}{\tau} e^{-[(t-t')/\tau]} T_o(t') dt'}. \qquad \text{(D1.17)}$$

We use equation (D1.17) to define the "trailing temperature" T^*,

$$T_*(t) = \int_{-\infty}^{t} \frac{1}{\tau} e^{-[(t-t')/\tau]} T(t') dt'. \qquad \text{(D1.18)}$$

The lossiness in expression (D1.17) can now be written as,

$$L = \frac{Q(t) - U_i[T_i(t) - T_i^*(t)]}{T_i^*(t) - T_o^*(t)} \qquad \text{(D1.19)}$$

Determining $T^*(t)$ requires knowledge of T(t) for all past time. But since past temepratures are weighted less and less as one moves further into the past, this lack of knowledge does not present a major problem. T(t) influences $T^*(t)$ minimally after several time constants τ into the past.

To enable easier use of the trailing temperature, one changes variables in (D1.18) to $x = t - t'$,

$$T^*(t) = \int_{0}^{\infty} \frac{1}{\tau} e^{-(x/\tau)} T(t-x) dx. \qquad \text{(D1.20)}$$

For small time steps Δ, this integral may be approximated by a summation,

$$T_*(t) \simeq \sum_{k=0}^{\infty} \frac{1}{\tau} e^{-(k\Delta/\tau)} T(t-k\Delta)\Delta . \qquad \text{(D1.21)}$$

Let,

$$\gamma = e^{-\Delta/\tau} \qquad \text{(D1.22)}$$

Then the sum in (D1.21) becomes,

$$(\Delta/\tau) \sum_{k=0}^{\infty} \gamma^k T(t-k\ ) \qquad \text{(D1.23)}$$

Note that for sufficiently small Δ/τ,

$$\Delta/\tau = \left(\sum_{k=0}^{\infty} \gamma^k\right)^{-1} \qquad \text{(D1.24)}$$

Therefore,

$$T^*(t) \simeq \left[\left(\sum_{k=0}^{\infty} \gamma^k T(t-k\Delta)\right)\right] \Big/ \left(\sum_{k=0}^{\infty} \gamma^k\right). \qquad \text{(D1.25)}$$

Using the Trailing Temperature

Equation (D1.25) defines the trailing temperature at time t in terms of the actual temperature history of T(t) and the weighting factor γ related to the time constant of the structure through equation (D1.22). Calculation of $T^*(t)$ can be greatly facilitated by noting that the expression in (D1.25) is a solution of the following difference equation,

$$T^*(t+\Delta) = \gamma T^*(t) + (1 - \gamma)T(t + \Delta) \qquad \text{(D1.26)}$$

In order to use the above expression to calculate $T^*(t)$ from $T(t)$ one needs to know the initial value of T^*, $T^*(0)$, and the parameter γ. γ was determined by reconsidering data such as that shown in figure (D1.1). Instead of using the hourly average of the instantaneous outside temperature to calculate the hourly lossiness, the trailing outside temperature was used. The instantaneous inside temperature changes very little due to the thermostat, so the trailing inside temperature was not used.

The hourly averages of the overall lossiness for a night were calculated using the trailing outside temperature. Because we do not know the time constant τ, and hence the weighting factor γ, several values of τ were used in an attempt to determine the most appropriate value. In addition, several values of the initial value of the trailing outside temperature $T_o^*(0)$ were used. Because the time constant is a physical property of the Test Chamber, its value is the same for every night. On the other hand, the difference between $T_o^*(0)$ and $T_o(0)$ will vary from night to night depending on the amount of solar radiation during the day and the history of outside temperature. By examining the overall lossiness calculated using T_o^*, one finds a region in $[T_o^*(0),\gamma]$ space which gives a relatively constant lossiness. Figure (D1.3) is a plot of the hourly lossiness for the same night as figure (D1.1) calculated with $\gamma = 0.965$ and $T_o^*(0) = T_o(0) + 6.0°C$. Note the constancy of the overall lossiness through the night.

Table (D1.1) compares the results obtained using several values of γ and $T_o^*(0)$ on the data from the night in figures (D1.1) and (D1.2). The hourly overall lossiness was calculated for each night for $\gamma = 0.955$ to 0.975. The values of $T_o^*(0)$ varied from 4.0 to 7.0 °C above $T_o(0)$. The difference between $T_o^*(0)$ and $T_o(0)$ is denoted by dtos. Each entry in the table is one-hundred times the standard deviation of the hourly lossiness for that combination of and dtos. The minimum value of the standard deviation occurs for $\gamma = 0.965$ and dtos = 6.0 °C. This minimum value of 8 is compared to a standard deviation times one-hundred of 122 for the instantaneous lossiness. Table (D1.2) shows the same information for a different night of data. Again, the standard deviation attains its minimum value at $\gamma = 0.965$.

Several nights of data were analyzed to find the value of γ which gave the minimum standard deviation of the hourly lossiness. The process requires other considerations in addition to the minimum standard deviation. Because infrared radiation and wind speed affect the overall lossiness, one can only expect constant lossiness through the night when the radiation and wind speed are also relatively stable. For example, if a night starts out cloudy and then clears up, the overall lossiness will increase during the night.

From the analysis of several nights of data, a value of $\gamma = 0.965 \pm 0.005$, for $\Delta = 5$ minutes, was obtained. According to equation (D1.22), this corresponds $\tau = 140 \pm 20$ minutes. The calculated lossiness over this range of τ varies by only about 1%.

With our knowledge of γ, we can use the trailing outside and inside temperatures to compute the Test Chamber lossiness. Since average values of the lossiness are desired, equation (D1.18) is rewritten as,

$$L = \frac{\bar{Q} - U_i(\bar{T}_i - \bar{T}_i^*)}{\bar{T}_i^* - \bar{T}_o^*} \qquad \text{(D1.27)}$$

In many cases one can replace T_i^* with T_i, thereby eliminating the need to know U_i.

After determining γ, one still needs an initial value of the trailing outside temperature. This quantity can not be known exactly, although dtos will be larger after a sunny day than a cloudy day. One determines a value of $T_o^*(0)$ by trying several and choosing the one which yields the most constant overall lossiness through the night. In the actual heat loss experiments in the Test Chamber, one begins collecting data at 6 p.m., but the overall lossiness value for the night is an average from midnight to 6 a.m. The six hour warm up period before midnight allows the effects of choosing a particular value of $T_o^*(0)$ to die out.

REFERENCES

[1] Standard Test Method for Thermal Conductance and Transmittance of Built-up Sections by Means of the Guarded Hot Box, ASTM designation C-236-66.

[2] Gupta, C.L., Spencer, J., Muncey, R., "A Conceptual Survey of Computer Oriented Thermal Calculation Methods," NBS Building Science Series, 39, 1971.

[3] Stephenson, D.G., Mitalas, G.P., "Cooling Load Calculations by Thermal Response Factor Method," ASHRAE Transactions, Vol. 73(I), 1967.

[4] Mitalas, G.P., Stephenson, D.G., "Room Thermal Response Factors," ASHRAE Transactions, Vol. 73(I), 1967.

[5] Kusuda, T., "Thermal Response Factors for Multi-Layer Structures of Various Heat Conduction Systems," ASHRAE Transactions, Vol. 75(I), 1969.

[6] Kusuda, T., "NBSLD, The Computer Program for Heating and Cooling Loads in Buildings," NBS Building Science Series, 69, 1976.

[7] Davies, M.G., "The Thermal Admittance of Layered Walls," Building Science, Vol. 8, No. 3, 1973.

[8] Mitalas, G.P., "Calulation of Transient Heat Flow Through Walls and Roofs," ASHRAE Transactions, Vol. 74(II), 1968.

[9] Stephenson, D.G., Mitalas, G.P., "Calculation of Heat Conduction Transfer Functions for Multi-layer Slabs," ASHRAE Transactions, Vol. 77(II), 1971.

[10] Sonderegger, R.C., "Dynamic Models of House Heating Based on Equaivalent Thermal Parameters," Report No. 57, Center for Environmental Studies, Princeton University, 1977.

Table D1.1 Standard Deviations of Lossiness for Combinations of γ and $T_o^*(0)$ for Test tw22

γ \ dtos	4.0	5.0	6.0	7.0	8.0	(°C)
0.955	47	34	25	19	21	
0.960	41	29	16	12	24	
0.965	38	22	(08)	17	23	
0.970	36	21	16	29	--	
0.975	37	25	28	--	--	

All standard deviations have been multiplied by one-hundred.

dtos = $T_o^*(0) - T_o(0)$.

Table D1.2 Standard Deviations of Lossiness for Combinations of γ and $T_o^*(0)$ for Test tw18

γ \ dtos	2.0	3.0	4.0	5.0	6.0	(°C)
0.955	45	28	14	18	37	
0.960	42	24	13	25	48	
0.965	45	25	(09)	29	57	
0.970	47	23	15	37	65	
0.975	51	25	16	46	81	

All standard deviations have been multiplied by one-hundred.

dtos = $T_o^*(0) - T_o(0)$.

Figure D1.1 Instantaneous Lossiness vs Time

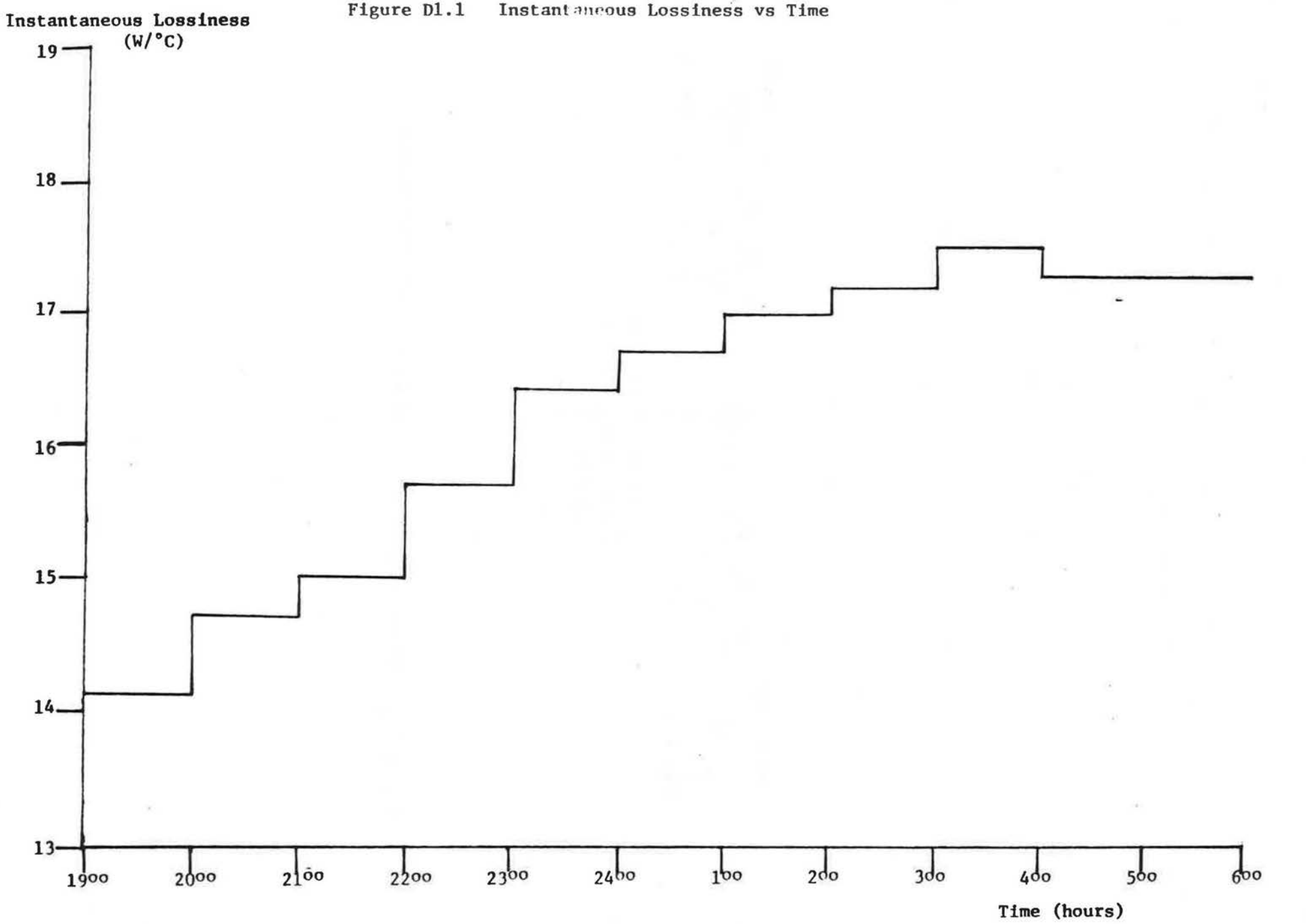

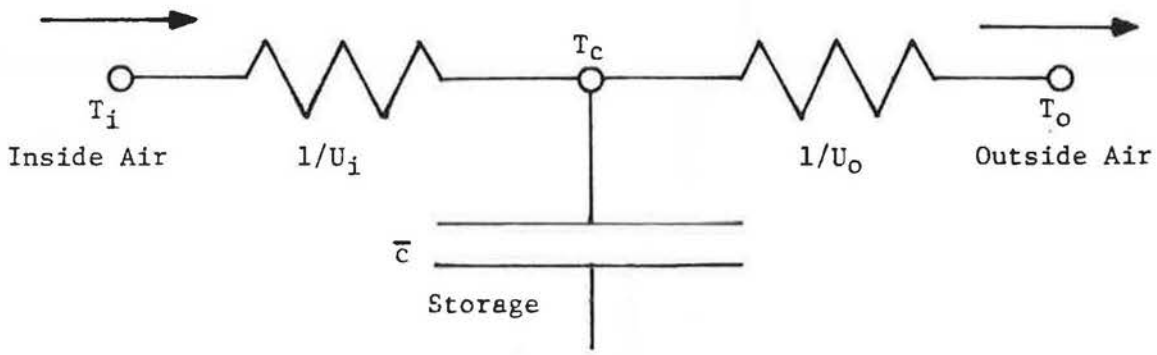

Figure D1.2 One-Capacitance Heat Flow Model of the Test Chamber

Figure D1.3 Overall Lossiness vs Time

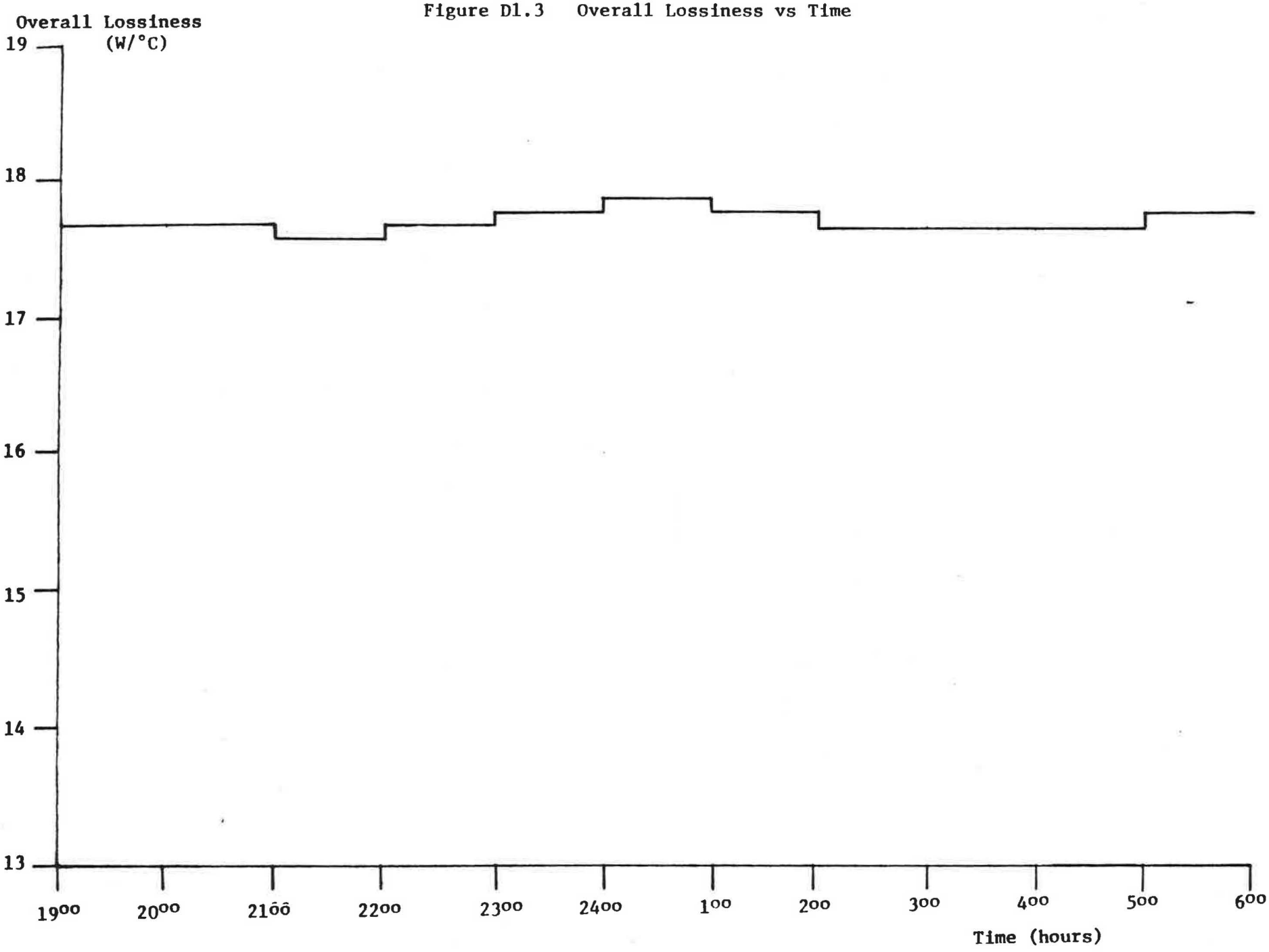

D.2 INFRARED/WIND INTERACTION

The infrared/wind interaction causes variations in the lossiness of a building depending on radiation levels from the sky and surroundings, and also on the wind speed. Gas molecules in the atmosphere, primarily carbon dioxide and water, emit infrared radiation at a level depending on their partial pressure and temperature. Building surfaces and the ground also emit radiation at levels determined by their surface temperatures and emissivities. This radiative exchange at the building surface, along with the outdoor film coefficient, determines the surface temperature of the structure. And it is this surface temperature which controls the rate of heat loss from the structure.

Infrared radiation levels from the sky and surroundings, and their effect on building heat loss have been discussed in the past [1-8]. Parmelee and Aubele also mention the part played by the wind speed in this interaction [7]. Kneubuhl and others have proposed alternative designs for the exterior surfaces of buildings which take into account infrared exchange with the sky [9]. Others have noted that the infrared radiation from the sky is not uniform and suggest taking advantage of "cold spots" to cool livestock [10].

To understand the infrared/wind interaction, consider the unit area of roof section with a heat flow Q through it, as shown in figure (D2.1). Given the U-value of the roof, and assuming reasonable values for T_i, T_o, the emissivity of the roof surface ε, the outside film coefficient h, and the "sky temperature" T_s, one

can calculate the temperature of the roof's surface T, and the heat flow Q, using the heat balance equation,

$$Q = U(T_i - T) = h(T-T_o) + \varepsilon\sigma(T^4 - T_s^4). \qquad (D2.1)$$

The sky temperature is the temperature of a blackbody which would radiate at the same level as the sky and surroundings. Since in all calculations, the sky temperature is converted back to radiation intensity, the fact that the sky does not radiate as a blackbody is not important. By varying the values of T_s, one considers clear or cold skies, about 30°K less than T_o, and cloudy or warm skies, about 5°K less than T_o. The windiness of a particular night affects the value of h, larger values corresponding to windy conditions. A linear relation between h and the average wind speed u is used,

$$h = 5.7 + 3.8u \quad [11]. \qquad (D2.2)$$

The outside film coefficient h has units of $W/m^2-°K$, and the average wind speed u is in m/s. The emissivity of the roof surface in the infrared range ε is set at 0.9. In this calculation $U = 0.37\ W/m^2-°K$, similar to the U-value of the Test Chamber roof. Also, for this example, $T_i = 293°K$ and $T_o = 263°K$.

The results of the calculation of the roof surface temperature are shown in figure (D2.2). The horizontal axis is the film coefficient h which is linearly related to the average wind speed u, given below h. Note that except for very warm skies, $T_s = 260°K$ (warmer than any measurements made), the roof sur-

face temperature is less than the outside air temperature. Ogunlesi reports measuring surface temperatures colder than the ambient air temperature [6]. When the wind speed increases, the wind will warm the surface and increase its temperature. An increase in the outside surface temperature means that the steady state heat flow through the roof Q is reduced. Since the lossiness is Q divided by T_i minus T_o, the lossiness also decreases with the increased surface temperature. As is evident in figure (D2.2), the rate of change of the roof temperature as the wind speed increases is larger for clear skies than for cloudy skies.

In figure (D2.3), these surface temperatures are converted into lossiness values for the unit area of roof section according to,

$$L = Q/\Delta T = U(T_i - T)/\Delta T$$
$$= (0.37\ W/°K)\ (293°K - T)/(293°K - 263°K). \qquad (D2.3)$$

In the upper two curves, which correspond to very cold skies, one notes 10% to 20% less heat transfer taking place on a windy night versus a calm night. Thus, as calculated previously by Parmelee and Aubele [7], the heat loss will be less on a clear windy night than on a clear calm one. Also, a similar reduction in heat loss occurs when there is a warm or cloudy sky as compared to a clear sky on a calm night.

A family of curves similar to those in figure (D2.3) exist for any roof section. T_s^* is the sky temperature which yields the line of constant surface temperature, $T = T_o$. When $T_s = T_s^*$, the

heat loss is independent of the wind speed. The value of T_s^* depends on the U-value of the wall and the inside and outside temperatures. Figure (D2.4) is a plot of T_s^* versus U-value for the values of T_i, T_o and ε used in the roof surface temperature calculations.

In summary, this calculation shows a 10 to 20% lossines reduction from a clear calm night to a clear windy night, and a similar reduction from a clear calm night to a cloudy one. Note that this calculation considers only conduction through the roof. Heat transfer due to air infiltration is neglected.

The surface temperature calculations for a roof section reveal an interesting source of variation of lossiness. But the roof "sees" only the sky, while the walls also see the ground which generally radiates at warmer temperatures than the sky. To determine the magnitude of the infrared/wind effect for the entire Test Chamber, one must also include the vertical walls. The radiative exchange for the floor is neglected. Table (D2.1) shows the appropriate heat balance equations for the walls, roof and floor. The walls are assumed to see half ground and half sky. A_w is the wall area, T_w its surface temperature, and ε_w the wall emissivity. ε_g is the average emissivity of the ground and T_g is an average ground surface temperature. Similar variables exist for the roof.

The lossiness of the structure is the sum of the heat flows for the roof, walls and floor divided by the inside-outside temperature difference. To simplify the calculations, the value of

ε = 0.9 used over the entire Test Chamber and the ground was assumed to radiate as a blackbody at the outside air temperature. In fact, the ground radiates at less than the air temperature for the same reason that the Test Chamber does, especially on clear, calm nights. These calculations are somewhat crude, but the intention is not to do an exact calculation; there are too many unknown parameters. Instead, the objective is to see if the effect is of measurable order.

The results of this calculation of the infrared/wind interaction effect on the lossiness of the Test Chamber are shown in table (D2.2). The lossiness of the structure is reduced by 6% on a clear windy night from a clear calm one. An increase in the wind on a clear night yields a 4% reduction in lossiness. The fact that the ground radiates at less than the outside air temperature, more so on clear calm nights, would make these reductions even larger. Thus, the infrared/wind effect causes a variation in the lossiness of the Test Chamber that should be measurable.

REFERENCES

[1] Bliss, R.W., "Atmospheric Radiation Near the Surface of the Ground: A Summary for Engineers," Solar Energy, Vol. 5, 1961.

[2] Brunt, D., "Notes on Radiation in the Atmosphere," Quarterly Journal of the Royal Meteorological Society, Vol 58, 1932.

[3] Cramer, R.D., Neubauer, L.W., "Diurnal Radiant Exchange with the Sky Dome," Solar Energy, Vol. 9, 1965.

[4] Hoglund, B.I., Mitalas, G.P., Stephenson, D.G., "Surface Temperatures and Heat Fluxes for Flat Roofs," Building Science, Vol. 2, 1967.

[5] Holden, T.S., "Calculation of Incident Low Temperature Radiation," ASHRAE Journal, April 1961.

[6] Ogunlei, O., "Solar Radiation and Thermal Gradients in Building Units," Building Science, Vol. 1, 1965.

[7] Parmelee, G.V., Aubele, W.W., "Radiant Energy Emission of Atmosphere and Ground," ASHRAE Transactions, Vol. 58, 1952.

[8] Swinbank, W.C., "Long-wave Radiation from Clear Skies," Quarterly Journal of the Royal Meteorological Society, Vol. 89, 1963.

[9] Kneubuhl, F.K., Zurcher, Ch., Thiebaud, F., Finger, G., Sagelsdorff, R., Frank, Th., "Thermal Radiation and Building Envelopes," CIB Symposium on Energy Conservation in the Built Environment, Copenhagen, Denmark, May 1979.

[10] Kelly, C.F., Bond, T.E., Ittrev, N.R., " 'Cold Spots' in the Sky May Help Cool Livestock," Agricultural Engineering," Vol. 38, 1957.

[11] McAdams, W., Heat Transmission, 3rd ed., McGraw Hill Book Company, Inc., New York, 1954.

Table D2.1 Heat Balance for Test Chamber

WALLS

$$Q_w = 4\ U_w\ A_w\ (T_i - T_w)$$

$$= 4\ h\ A_w\ (T_w - T_o) + 2\ \varepsilon_w\ \sigma\ A_w\ [(T_w^4 - T_s^4) + (T_w^4 - \varepsilon_g\ T_g^4)]$$

ROOF

$$Q_r = U_r\ A_r\ (T_i - T_r)$$

$$= h\ A_r\ (T_r - T_o) + \varepsilon_r\ \sigma\ A_r\ (T_r^4 - T_s^4)$$

FLOOR

$$Q_f = U_f\ A_f\ (T_i - T_o)$$

NET LOSSINESS

$$L = \frac{Q_w + Q_r + Q_f}{(T_i - T_o)}$$

Q_w,r,f = Heat flow through walls, roof, and floor.

U_w,r,f = U-value of walls, roof, and floor.

A_w,r,f = Area of walls, roof, and floor

T_w,r,f = Surface temperature of walls, roof, and floor.

ε_w,g,r = Emissivity of walls, ground, and roof.

T_i = Inside air temperature.

T_o = Outside air temperature.

Table D2.2 **Calculated Test Chamber Lossiness**

	Calm u = 0.9 m/sec	Windy u = 4.5 m/sec
T_s = 235 °K Cold Sky	16.2 W/°C	15.6 W/ °C
	6% ↓	4% →
T_s = 255 °K Warm Sky	15.2 W/°C	

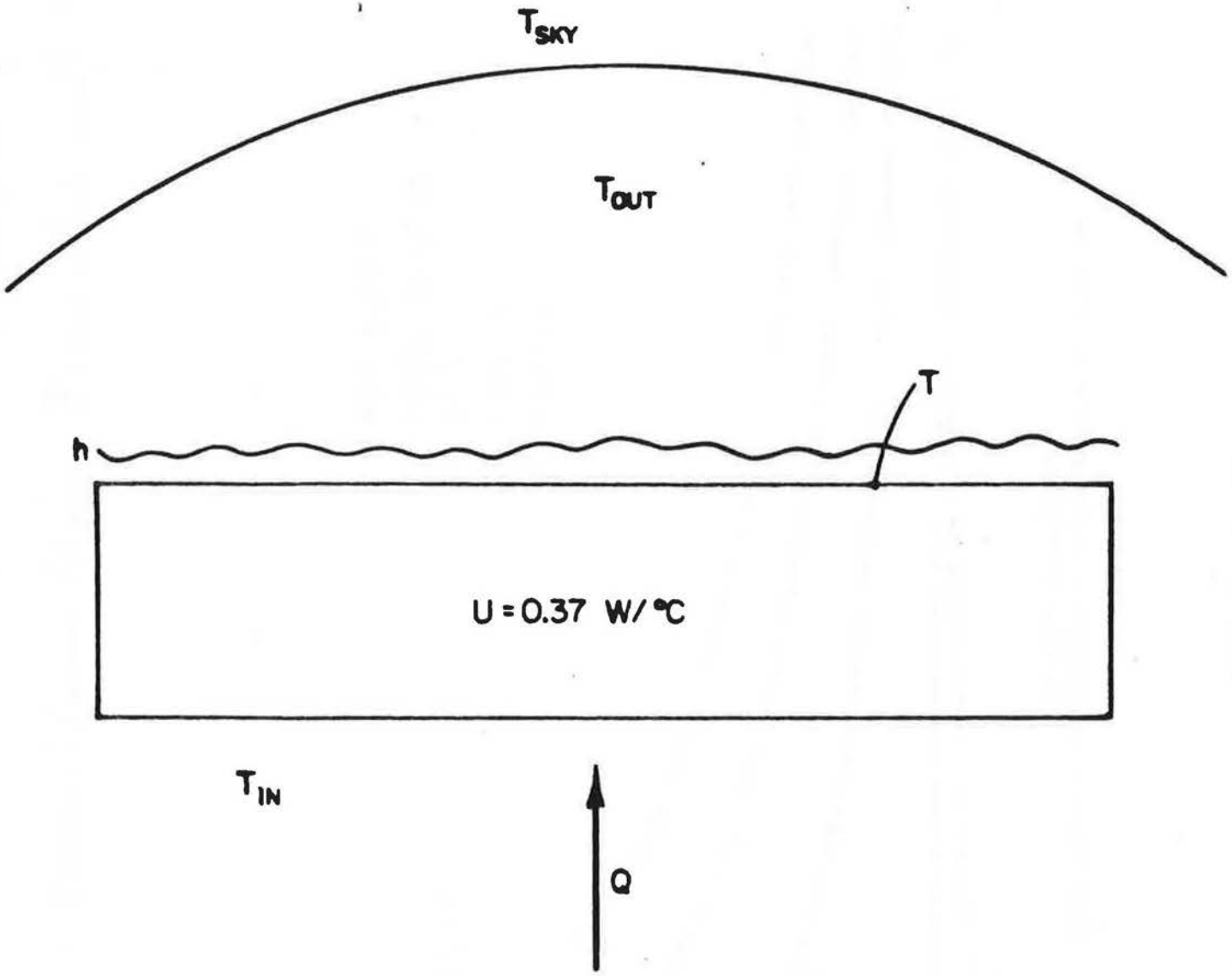

$$Q = U(T_{IN} - T) = h(T - T_{OUT}) + \epsilon\sigma(T^4 - T_S^4)$$

Figure D2.1 Unit Area of Roof Section

Figure D2.2 Roof Surface Temperature vs Outdoor Film Coefficient for Various Wind Conditions

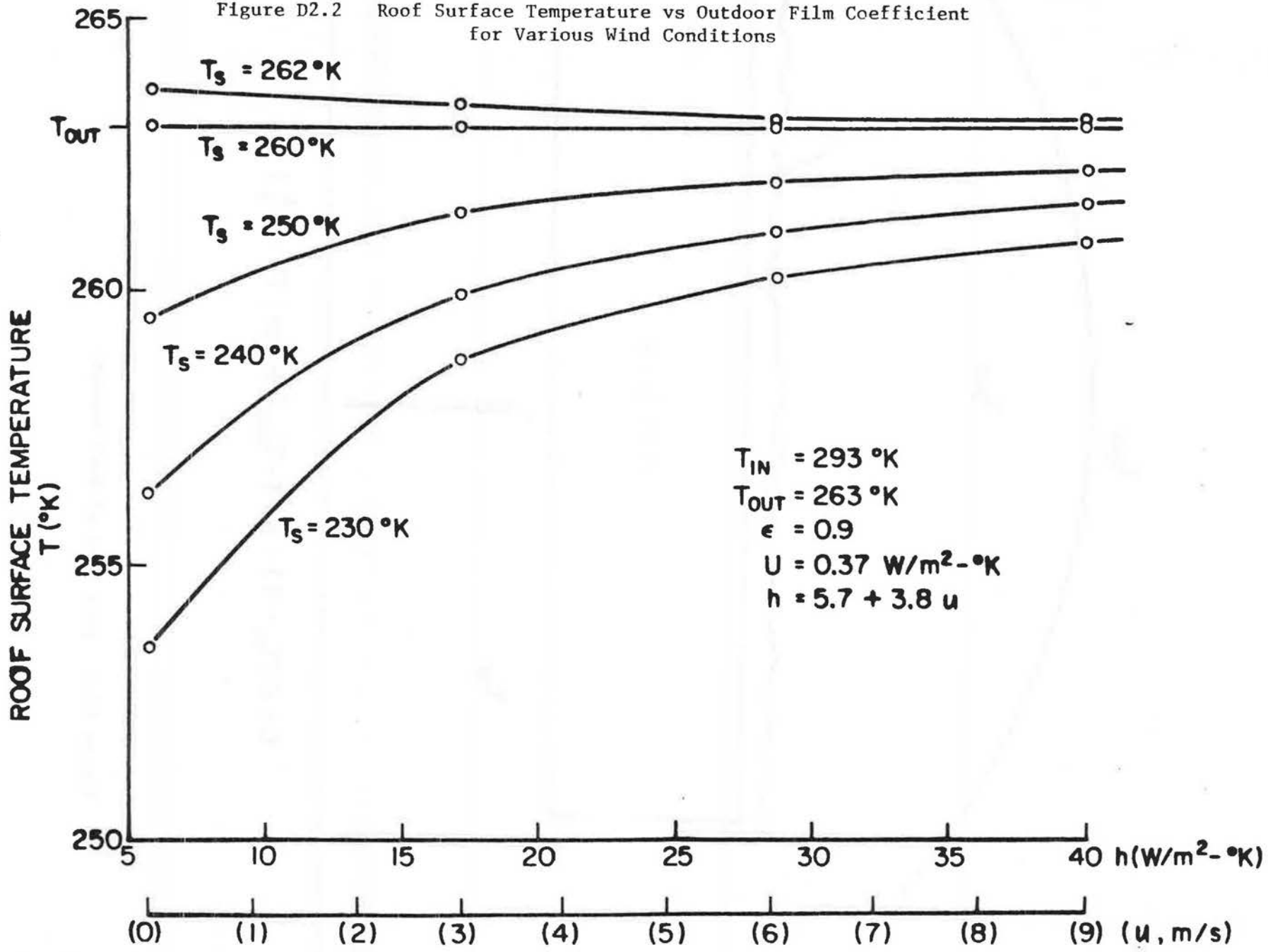

Figure D2.3 Lossiness of a Roof Section vs Outdoor Film Coefficient for Various Wind Conditions

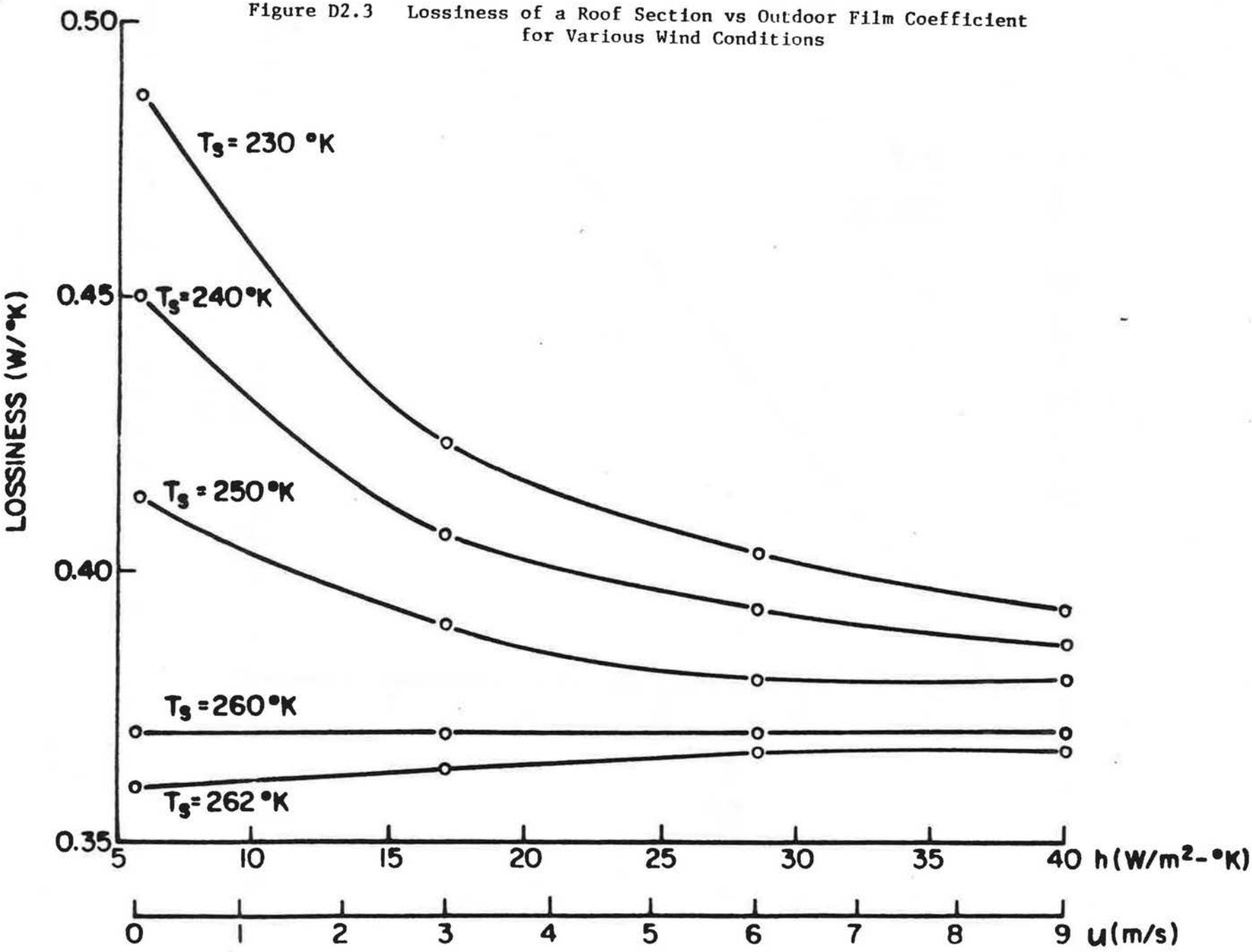

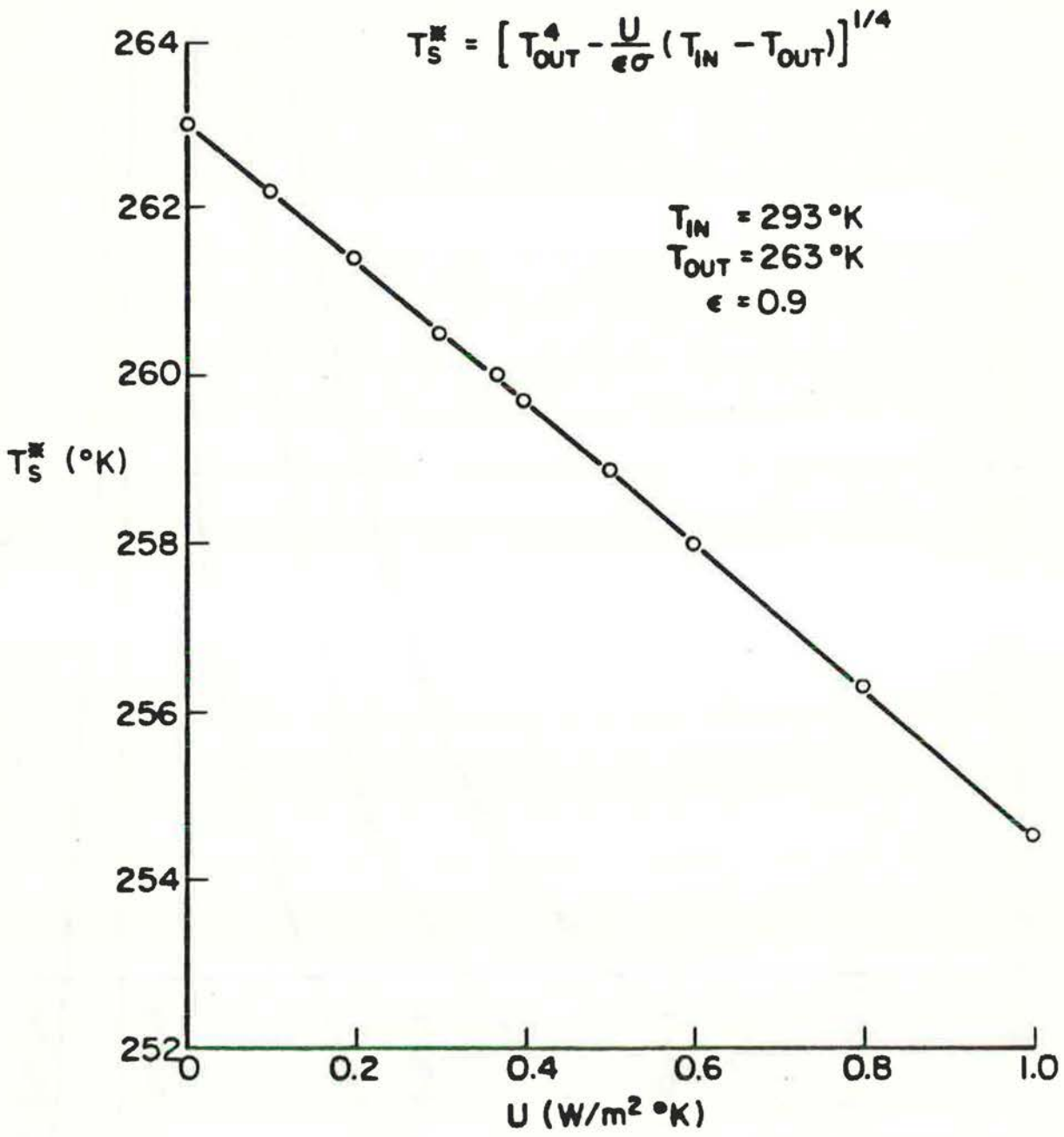

Figure D2.4 Sky Temperature which Yields a Constant Surface Temperature vs U-Value of Roof

D.3 HEAT LOSS EXPERIMENTS

Experimental Technique

The heat loss rate of the Test Chamber was determined by measuring the heat input required to maintain the interior at a constant temperature. The heat input divided by the inside-outside temperature difference is equal to the heat loss rate. Figure (D3.1) shows the experimental arrangement inside the structure. Energy is supplied by light bulbs connected to a thermostat which controls the inside temperature. The energy input is measured with a residential Watt-hour meter equipped with a photo-interrupter module to count revolutions of the Watt-hour meter disk. The air exchange rate of the Test Chamber with the outside is measured using the tracer gas decay technique. Ethane is used as the tracer gas, and a Wilks Specific Vapor Analyzer measures the ethane concentration. Inside and outside temperatures are measured with thermistors, and the average wind speed with a cup anemometer. The level of infrared radiation from the night sky is also monitored using an Eppley infrared radiometer. All instrumentation is described in detail in appendix B.

The outside weather variables and the interior conditions are recorded every five minutes on a magnetic tape for subsequent analysis. The data for each experiment is monitored from 6 p.m. in the evening until 7 a.m. the following morning. The heat loss rate of the Test Chamber for each night is an average value from midnight to 6 a.m. The six hour delay before midnight is necessary for the dissipation of stored solar heat from the day. Also

during this period, the effects of initial conditions of the trailing temperature die out.

Hourly averages of a typical night's data are shown in table (D3.1). The variables include the average wind speed u, and the inside and outside air temperatures T_i and T_o. Also given is the sky temperature T_s which is derived from the measurements of the level of infrared radiation (W/m^2) from the sky and surroundings. The last two columns in table (D3.1) are the hourly averages of the power input to the Test Chamber Q in Watts and the infiltration rate I in volumes exchanged per hour.

Data Analysis

Determining the interior temperature T_i and the power consumption Q are complicated by a peculiar measurement problem. The heat input to the Test Chamber is controlled by a thermostat and therefore the interior temperature oscillates between a maximum and a minimum. The period of the oscillation depends on the magnitude of the wattage supplied by the heaters and the inside-outside temperature difference. Therefore the period, or the length of the heating cycle, changes through the night. Since the inside temperature is recorded every five minutes, the inside temperature is measured at various points of the heating cycle. The difference between the heating and measurement frequency produces "beats" in the measurement of interior temperature. Measurements of the power input to the Test Chamber interior are similarly complicated by the on-off nature of the thermostat.

The fact that the heater is controlled by a thermostat requires some smoothing of the inside air temperature and energy input measurements. In both cases, a moving average is used. The first point in the smoothed series is obtained by averaging the first m values of the original series. One then drops the first of these m points and averages in the m+1 point of the original series, and so on. If the original series contains n points than the smoothed series will contain n-(m-1) points. In smoothing the interior temperature a value of m=9 was used, and therefore there are no hourly averages in table (D3.1) for the first and last hours. The power input was smoothed twice with m=13 each time, and again there are no averages for the first and last hours.

The lossiness of a structure may be defined as the power required to maintain an inside-outside temperature difference, divided by that temperature difference. This definition is lacking because the heat input rate will generally not be proportional to the instantaneous temperature difference. The inadequacy of the "instantaneous" lossiness L_I is due to the thermal inertia of a building. Because of thermal storage effects, the heat input depends on the history of the inside and outside temperatures. Alternatively, one defines the "overall" lossiness as the heat input rate divided by the temperature difference when the inside and outside temperatures are constant. The overall lossiness is not a uniquely defined property of the structure, but is determined by the amount of infrared radiation, the wind speed, temp-

erature effects on material properties and air infiltration as well as the thermal resistance of the building envelope. Although steady temperature conditions never exist for the Test Chamber, or any other structure, the overall lossiness is still useful. Under the unsteady conditions that do exist, one may determine the overall lossiness by using the trailing temperature T^* instead of the instantaneous temperature.

To calculate the overall lossiness, we use the trailing outside temperature T_o^*, but retain the instantaneous inside temperature because it changes very little through the night. The methods used in determining the trailing outside temperature are described earlier in this appendix. For each night's experiment, averages from midnight to 6 a.m. of the power input Q, the trailing temperature difference $\Delta T^* = T_i - T_o^*$, and the overall lossiness $L = Q/\Delta T^*$ were calculated. Table (D3.2) is a list of these three quantities for the eleven experiments done in 1981. The overall lossiness varies from 16.8 to 17.8 W/°C with an average of 17.4 W/°C. This is an unusually small variation in overall lossiness which occured because of the particular mix of weather conditions on the eleven nights. The variation in lossiness is generally greater as in 1980 when the lossiness varied from 16.4 to 18.7 W/°C. This variability in the overall lossiness is much too large to be accounted for by experimental error.

Heat Loss Prediction

The variation in the overall lossiness is due to several physical effects. First, the infrared radiation from the sky and surroundings coupled with the wind speed are important. Also, the thermal resistances of the building materials are affected by their temperature. And although the Test Chamber is very air tight, there is still a minute amount of air infiltration. By considering all three of these effects, one can develop a model to predict the overall lossiness of the Test Chamber on a given night.

The Infrared/Wind Interaction

The coupling of infrared radiation from the sky and surroundings and the wind speed affect the overall lossiness by determinign the outside surface temperature of the Test Chamber. This effect is discussed in detail earlier in this appendix. On calm nights with clear skies, the outside surface gets significantly colder than the ambient air. This cold surface leads to a large overall lossiness because the overall lossiness is derived from the difference between the inside and outside air temperatures. On clear nights with a significant wind blowing, the increase in the outdoor film coefficient causes the surface temperature to approach the outside air temperature, therefore decreasing the overall lossiness. On cloudy nights the outside surface is closer to, though seldom greater than the ambient air temperature and this also causes a low lossiness.

In developing a predictive model for the infrared/wind effect, one may assume that the power input divided by the temperature difference between the inside air and the outside surface is constant. One defines a constant "basic" lossiness as

$$L_T = Q/(T_i - T). \qquad \text{(D3.1)}$$

T is the average outside surface temperature. Thus the overall lossiness on a given night can be written as

$$\begin{aligned} L &= Q/\Delta T^* = (Q/T_i - T)\ [(T_i - T/\Delta T^*)] \\ &= L_T[(T_i - T)/\Delta T^*)]. \end{aligned} \qquad \text{(D3.2)}$$

To use this approach, an estimate of the average outside surface temperature T is necessary. This estimate is made using the heat balance equation

$$\begin{aligned} Q &= L_T(T_i - T) \\ &= hA_1(T - T_o^*) + \varepsilon\sigma A_2(T^4 - T_s^4) + \varepsilon\sigma A_3(T^4 - T_o^4). \end{aligned} \qquad \text{(D3.3)}$$

This equation states that the heat input to the Test Chamber equals the heat conducted to the outside surface, which equals the heat conducted across the outside boundary layer plus the heat loss by radiation. In equation (D3.3) h is the outdoor film coefficient (W/m^2-°K) related to the wind speed u (m/s) by

$$h = 5.7 + 3.8u \text{ [1]}. \qquad \text{(D3.4)}$$

ε is the average infrared emissivity of the outside surface, assumed equal to 0.9, and σ is the Stefan-Boltzmann constant,

5.67×10^{-8} W/m^2-°K^4. A_1 is the outside surface area of the Test Chamber equal to 48 m^2. A_2 is the outside area which exchanges radiation with the sky and surroundings. A_3 is the area which radiates to the ground, adjacent buildings and the roof surface on which the Test Chamber stands. It is assumed that these surfaces radiate as blackbodies at the trailing outside air temperature T_o^*. A_2 and A_3 are both set equal to $A_1/2 = 24$ m^2.

For each night's experiment. one calculates the average outside surface temperature T by solving equation (D3.3) rewritten as a quartic in T,

$$T^4 + (h/\varepsilon\sigma)T + [hA_1T_o^* + \varepsilon\sigma A_2(T_s^4 + T_o^{*4}) + Q] / \varepsilon\sigma A_1 = 0 \qquad (D3.5)$$

The trailing outside temperature is used in this expression, but instead of using a "trailing wind speed" and a "trailing sky temperature," we use the average values of u and T_s from 22:00 to 5:00 since these variables change slowly. Equation (D3.5) was solved to determine a value of T for each of the eleven nights. Table (D3.3) lists the values of u, h, T_o^*, T_s, Q, T, and L for each night.

From the calculated values of the average outside surface temperature T, one may form an independent variable to predict the overall lossiness L. Equation (D3.2) suggests the definition of the "sky factor"

$$S_{f,a} = (T_i - T)/\Delta T^* \qquad (D3.6)$$

The sky factor $S_{f,a}$ predicts the overall lossiness according to

$$L = L_T S_{f,a}. \qquad (D3.7)$$

Because $S_{f,a}$ is the ratio of two comparable differences in temperature, there is significant uncertainty in its value. In an attempt to avoid this problem one may rewrite $S_{f,a}$ as

$$S_{f,a} = 1 + (T_o^* - T)/\Delta T^* = 1 + S'_{f,a}/\Delta T^*, \qquad \text{(D3.8)}$$

where $S'_{f,a} = T_o^* - T$. Equation (D3.7) is rewritten as

$$L = L_T(1 + S'_{f,a}/\Delta T^*). \qquad \text{(D3.9)}$$

Another model of the infrared/wind effect on the overall lossiness can be developed by replacing the outside surface temperature T with the "infrared-air" temperature T_{IRA}. The infrared-air temperature is the nighttime version of the sol-air temperature [2], and is given by

$$T_{IRA} = T_o^* - \varepsilon \Delta R/h'. \qquad \text{(D3.10)}$$

h' is the outside convective-radiative film coefficient. ΔR is the difference between the infrared radiation from the sky and surroundings and the radiation emitted by a blackbody at T_o^*,

$$\Delta R = \varepsilon\sigma(T_o^{*4} - T_s^4). \qquad \text{(D3.11)}$$

In this model, one assumes that T_{IRA} is the driving temperature which determines the overall lossiness L,

$$L'_T = Q/(T_i - T_{IRA}) = \text{Constant}. \qquad \text{(D3.12)}$$

Thus, as in the case of $S_{f,a}$

$$L = L'_T[(T_i - T_{IRA})/\Delta T^*] = L'_T S_{f,b}. \qquad \text{(D3.13)}$$

And $S_{f,b}$ can be rewritten as

$$S_{f,b} = 1 + (T_o^* - T_{IRA})/\Delta T^* = 1 + S'_{f,b}/\Delta T^*. \qquad (D3.14)$$

Temperature Effects on Thermal Resistance

In general, the thermal resistance of a material depends on its temperature. This has been well documented in the case of wall sections [3]. The thermal resistance of a wall decreases as its average temperature increases. To model this effect in the Test Chamber, one may use the average of the interior air temperature T_i and the outside surface temperature T. One then defines the material temperature T_M as

$$T_M = (T_i - T)/2. \qquad (D3.15)$$

One may expect the basic lossiness, L_T or L'_T, to be linearly proportional to the material temperature T_M.

Air Infiltration Heat Loss

Although the Test Chamber is extremely airtight, there is still a small amount of air infiltration. With a significant temperature difference between inside and outside, from 20 to 25 °C, the infiltration rate ranges from 0.05 to 0.10 volumes per hour depending on the wind speed. One expects the heat loss associated with an air infiltration rate I is equal to

$$\rho c_p I V \Delta T_I. \qquad (D3.16)$$

ρc_p is the product of the air density ρ (kg/m^3) and the heat capacity c_p (W-hr/kg-°C) of air, roughly 0.35 W-hr/m^3-°C at a temperature of 280 K. V is the Test Chamber volume 16.6 m^3 and ΔT_I is the instantaneous inside-outside temperature difference. Therefore, the lossiness associated with air infiltration L_A is given by

$$L_A = [\ 5.8(W/°C)/(X/hr)]I. \qquad (D3.17)$$

For an air infiltration rate of 0.10 X/hr, the associated lossiness is 0.6 W/°C.

The air infiltration rate of the Test Chamber was measured during many of the lossiness measurements. Figure (D3.2) is a plot of the hourly average infiltration rate I against the wind speed u. At low wind speeds, less than about 2 m/s, the stack effect dominates the infiltration and little dependence on wind speed is evident. Beyond 2 m/s, the infiltration rate increases with the wind speed. Although this plot of infiltration rate against wind speed is nonlinear, the overall slope of the data is on the order of 0.02 (X/hr)/(m/s). Substituting this slope into equation (D3.17) leads one to expect that the overall lossiness is proportional to the wind speed multiplied by 0.12.

Models of Lossiness

Three factors affecting the overall lossiness on a given night have been presented. The infrared/wind interaction can be characterized by the sky factors. The material temperature T_M is

used to quantify the effect of temperature on the thermal resistance of the Test Chamber walls. The heat loss associated with air infiltration is modelled through the wind speed u'. u' is the average wind speed from midnight to 6 a.m. Table (D3.4) lists the values of the overall lossiness L, the material temperature T_M, the wind speed u', and the four sky factors for the eleven nights of measurement.

The simplest and most successful relation between the overall lossiness L and the independent variables has been a least squares, multiple regression against T_M, u' and a single sky factor. Although one might expect product terms, e.g. $T_M \times S_{f,a}$, using these terms actually reduces the goodness of fit of the regression equation. The four regression equations, one for each sky factor, are listed below:

$$L = -9.23 + (.0423)T_M + (.145)u' + (13.9)S_{f,a} \quad r^2=0.82 \qquad \text{(D3.18-A)}$$

$$L = 3.20 + (.0473)T_M + (.144)u' + (.534)S'_{f,a} \quad r^2=0.84 \qquad \text{(D3.18-B)}$$

$$L = -.482 + (.0355)T_M + (.218)u' + (6.61)S_{f,b} \quad r^2=0.84 \qquad \text{(D3.18-C)}$$

$$L = 3.49 + (.0451)T_M + (.208)u' + (.244)S'_{f,b} \quad r^2=0.89 \qquad \text{(D3.18-D)}$$

Equations (D3.9) and (D3.14) do not lead one to expect that $S'_{f,a}$ and $S'_{f,b}$ would be good predictors of L. The overall lossiness L was regressed against $S'_{f,a}$ and $S'_{f,b}$ because the previous winter's experiments showed a very high correlation between L and both of these sky factors. In this year's experiments, these sky

factors have the highest r^2 for each respective doublet althought the improvement in fit is small. Both $S_{f,a}$ and $S_{f,b}$ have the lowest r^2 in their doublet, possible due to the larger uncertainty in these parameters as mentioned earlier.

The models based on the average outside temperature make more physical sense that the "B" sky factor models. But the $S_{f,b}$ fits are as good if not slightly better than the "A" models. It is interesting to note that the coefficient of u' is roughly constant within each pair of regression equations. Also, the value of this coefficient is on the order of magnitude of the crudely calculated value of 0.12.

Table (D3.5) lists the overall lossiness L measured on each of the eleven nights plus the lossiness as calculated from the equations (D3.18-A) through (D3.18-D). In all four cases, the predicted lossiness is within 0.2 W/°C of the measured lossiness, i.e. within about 1%. From table (D3.5) it is clear that none of the four equations does a better job of prediction than any of the others.

It is interesting to compare this winter's and last winter's attempts to predict the overall lossiness. In the seven experiments of last winter the material temperature was not allowed to vary much. The lossiness was simply regressed against each of the four sky factors. The results were:

$$L = 3.30 + (12.7)S_{f,a},\ r^2=0.84 \qquad \text{(D3.19-A)}$$

$$L = 15.9 + (0.93)S'_{f,a},\ r^2=0.95 \qquad \text{(D3.19-B)}$$

$$L = 9.60 + (6.20)S_{f,b},\ r^2=0.79 \qquad \text{(D3.19-C)}$$

$$L = 15.6 + (0.45)S'_{f,b},\ r^2=0.97 \qquad \text{(D3.19-D)}$$

Note the high values of r^2 for $S'_{f,a}$ and $S'_{f,b}$. Besides these unexpectedly good fits, the others are on the order of those obtained from this winter's experiments. For last year's seven tests the average value of the material temperature was $T_M = 279°K$ and the average wind speed was $u' = 1.3$ m/s. Substituting these values into equations (D3.18-A) through (D3.18-D) yields:

$$L = 2.76 + (13.9)S_{f,a} \qquad \text{(D3.20-A)}$$

$$L = 16.6 + (.534)S'_{f,a} \qquad \text{(D3.20-B)}$$

$$L = 9.71 + (6.61)S_{f,b} \qquad \text{(D3.20-C)}$$

$$L = 16.3 + (.244)S'_{f,b} \qquad \text{(D3.20-D)}$$

The agreement between equations (D3.19-A) through (D3.19-D) and equations (D3.20-A) through (D3.20-D) is quite good. The only significant difference is between the coefficients of both $S'_{f,a}$ and $S'_{f,b}$ In both cases, this winter's coefficients are roughly twice as large as last winter's. The reason for this is not yet known. One difference between the two years is that the infrared radiometer was recalibrated by Eppley using a new technique. It is not clear why this would affect the primed sky factors more than the unprimed versions.

The attempts to predict the overall lossiness of the Test Chamber have been successful. By considering the infrared/wind interaction, temperature effects on thermal resisitance, and air infiltration one can predict the lossiness within 1% of its measured value. Four equations, (D3.18-A) and (D3.18-B) make the most physical sense. The ability to predict the lossiness of the Test Chamber is used in tests of the effectiveness of an air-to-air heat exchanger discussed in chapter IX.

REFERENCES

[1] McAdams, W., Heat Transmission, 3rd ed., McGraw Hill Book Company, Inc., New York, 1954.

[2] ASHRAE Handbook of Fundamentals, 1977.

[3] Wilkes, K.E., "Thermophysical Properties, Data Base Activities at Owens- Corning Fiberglas," Proceedings of ASHRAE/DOE Conference on Thermal Performance of the Exterior Envelope of Buildings, Orlando, Florida, December 1979.

Table D3.1 Hourly Averages for one Night's Experiment

Time	u (m/s)	T_i (°K)	T_o (°C)	T_s (°K)	Q (W)	I (exchanges/hour)
18-19	2.3	--	-4.6	241.0	--	0.08
19-20	2.4	19.7	-5.3	239.3	368	0.08
20-21	2.5	19.5	-6.0	237.7	393	0.08
21-22	2.7	19.4	-6.6	236.9	409	0.08
22-23	3.2	19.3	-7.4	237.0	427	0.10
23-24	3.4	19.2	-8.2	237.6	446	0.08
0-1	2.5	19.1	-9.0	237.7	457	0.07
1-2	2.3	19.0	-9.6	238.3	466	0.07
2-3	2.1	18.9	-9.7	239.2	474	0.06
3-4	1.2	18.9	-9.7	238.8	485	0.04
4-5	2.2	18.8	-9.7	238.5	493	0.06
5-6	1.3	18.8	-10.0	238.9	491	0.05
6-7	1.1	--	-10.0	239.3	--	0.04

Table D3.2 Heat Loss for all Nights

Test	Q(Watts)[1]	ΔT*(°C)[1]	L(W/°C)[2]
tw43	500	28.2	17.7
tw44	478	27.4	17.4
tw46	488	28.0	17.4
tw47	485	27.6	17.6
tw48	455	25.8	17.6
tw49	350	20.5	17.1
tw54	407	22.8	17.8
tw56	463	26.1	17.7
tw59	349	20.1	17.4
tw60	343	20.4	16.8
tw61	294	17.3	17.0

(1) Averaged from midnight to 6 a.m.

(2) $L = Q/\Delta T^*$

Table D3.3 Heat Loss Determinants for all Nights

Test	$u^{(1)}$ (m/s)	$h^{(2)}$ ($W/m^2-°K$)	$T_o^{*(3)}$ (°K)	$T_s^{(1)}$ (°K)	$Q^{(3)}$ (W)	$T^{(4)}$ (°K)	L (W/°C)
tw43	2.4	14.8	266.8	240.3	500	265.0	17.7
tw44	2.4	14.8	264.7	238.2	478	262.9	17.4
tw46	1.2	10.3	263.0	243.8	488	261.5	17.4
tw47	3.4	18.6	263.7	237.4	485	262.2	17.6
tw48	0.4	7.2	268.5	251.8	455	266.7	17.6
tw49	1.5	11.4	279.9	276.5	350	280.0	17.1
tw54	3.6	19.4	277.2	268.0	407	276.8	17.8
tw56	2.7	16.0	273.6	255.0	463	272.4	17.7
tw59	3.0	17.1	272.8	259.7	349	272.0	17.4
tw60	2.1	13.7	274.6	272.4	343	274.8	16.8
tw61	1.6	11.8	278.1	272.4	294	277.8	17.0

---

(1) Averaged from 22^{00} to 5^{00}.

(2) $h = 5.7 + 3.8u$

(3) Averaged from 0^{00} to 6^{00}.

(4) Calculated from equation (D3.3)

Table D3.4 Independent Variables for Lossiness Prediction

Test	T_M(°K)(1)	u'(m/s)(2)	$S_{f,a}$	$S'_{f,a}$	$S_{f,b}$	$S'_{f,b}$
tw43	280.0	2.3	1.064	1.8	1.167	4.7
tw44	277.5	1.9	1.066	1.8	1.168	4.6
tw46	276.3	1.2	1.054	1.5	1.164	4.6
tw47	276.8	3.4	1.054	1.5	1.138	3.8
tw48	280.5	0.3	1.070	1.8	1.209	5.4
tw49	290.2	1.6	0.995	-0.1	1.044	0.9
tw54	288.4	3.4	1.018	0.4	1.070	1.6
tw56	286.0	3.0	1.042	1.2	1.130	3.5
tw59	282.5	2.8	1.040	0.8	1.119	2.4
tw60	284.9	1.8	0.990	-0.2	1.025	0.5
tw61	286.6	1.6	1.017	0.3	1.087	1.5

---

(1) $T_M = 1/2\ (T_i + T)$.

(2) Averaged from 0^{oo} to 6^{oo}.

$S_{f,a} = (T_i - T)/\Delta T^*$ $\qquad$ $S_{f,b} = (T_i - T_{IRA})/\Delta T^*$

$S'_{f,a} = T^*_o - T$ $\qquad$ $S'_{f,b} = T^*_o - T_{IRA}$

Table D3.5 Measured vs Predicted Lossiness

Test	Measured Lossiness (W/°C)	Lossiness Predicted from:			
		$S_{f,a}$	$S'_{f,a}$	$S_{f,b}$	$S'_{f,b}$
tw43	17.7	17.7	17.7	17.7	17.7
tw44	17.4	17.6	17.6	17.5	17.5
tw46	17.4	17.3	17.2	17.3	17.3
tw47	17.6	17.6	17.6	17.6	17.6
tw48	17.6	17.6	17.5	17.5	17.5
tw49	17.1	17.1	17.1	17.1	17.1
tw54	17.8	17.6	17.5	17.6	17.6
tw56	17.7	17.8	17.8	17.8	17.9
tw59	17.4	17.6	17.4	17.6	17.4
tw60	16.8	16.8	16.8	16.8	16.8
tw61	17.0	17.3	17.1	17.2	17.1

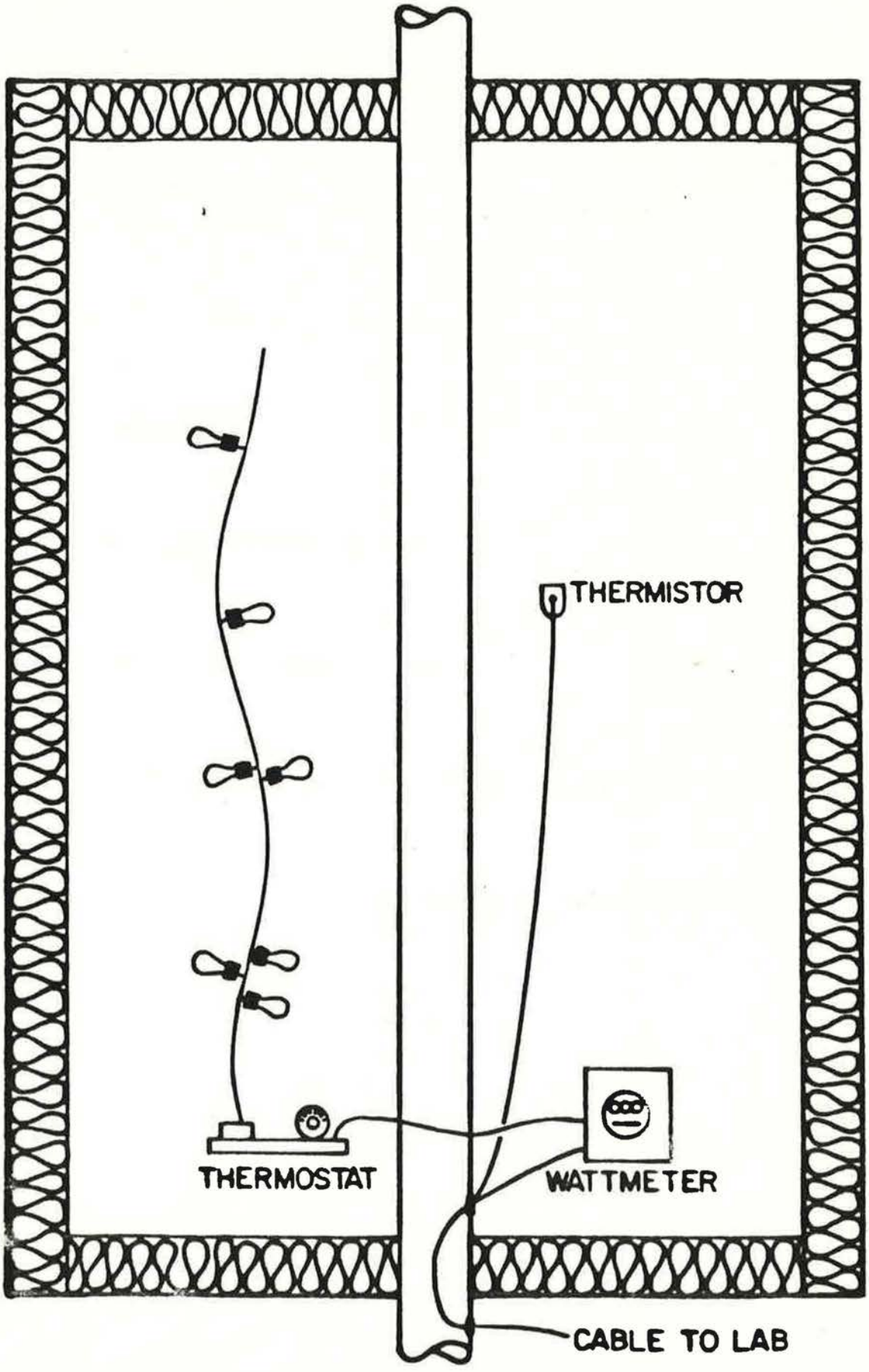

Figure D3.1 Experimental Set-up for Measuring Test Chamber Heat Loss

Figure D3.2 Hourly Average Infiltration Rate vs Wind Speed

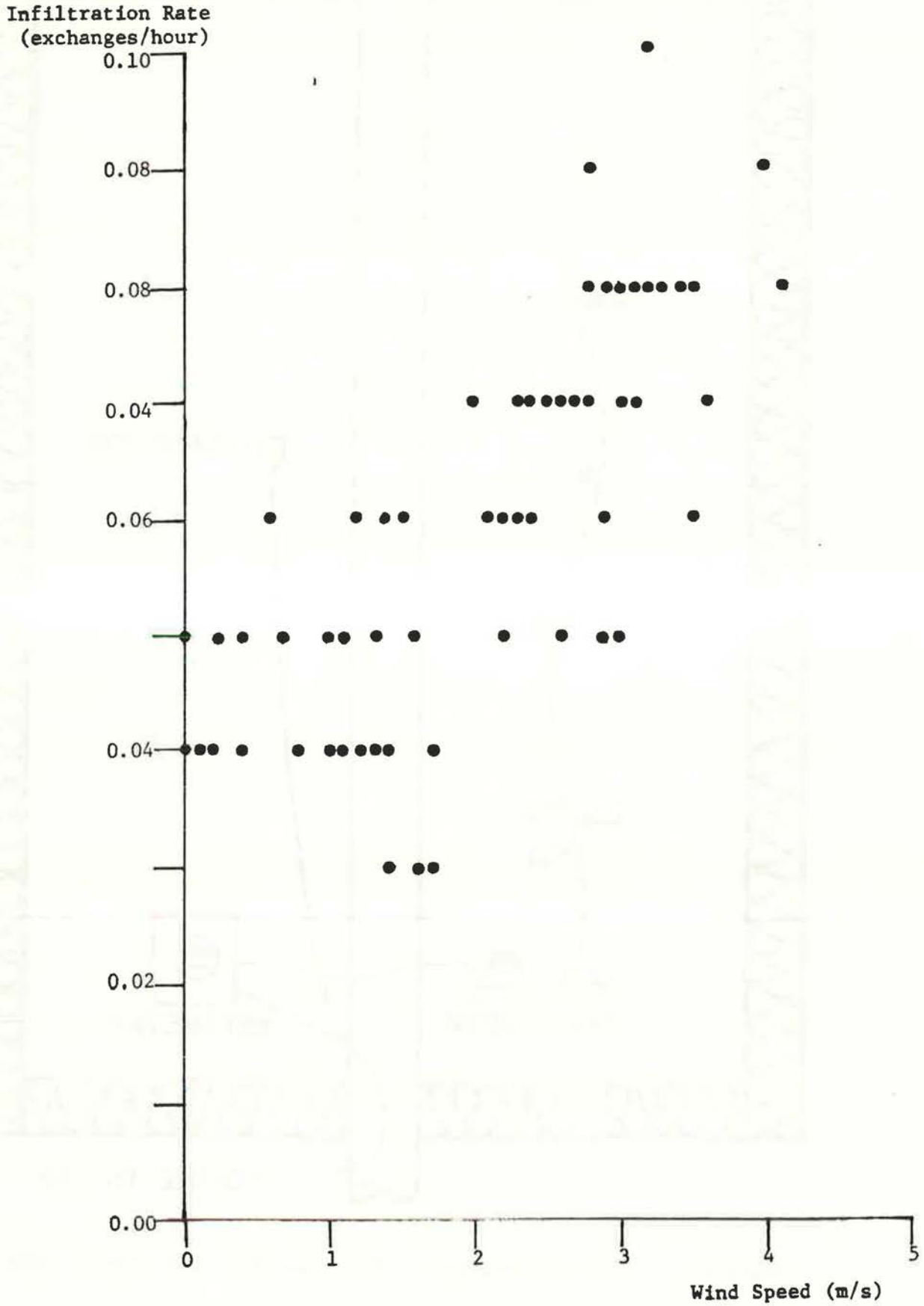

Appendix E

BLOWER DOOR TEST DESCRIPTION (BRAT)

In order to learn more about the repeatability and reliability of the Blower Door, a home in the Princeton area was subjected to intensive pressurization testing. The so-called "BRAT" house ia a two-story, wood frame structure built in the mid-60's with a gas-fired, forced-air heating system. The interior volume (less the basement) is about 450 m^3, and the floor area is roughly 185 m^2.

During each trip to the house, several pressurization tests were conducted. Each test included both pressurizing and depressurizing the house to several inside-outside pressure differences. The weather conditions during the test were monitored at the von Neumann weather station. The weather data includes averages of the outside temperature, wind speed and wind direction during the test. Table (E1) lists the tests in chronological order, along with the weather conditions. The table includes both the local wind speed measurement and a rougher value for the wind speed at the U.S. Weather Service station in Newark, about 40 miles from Princeton. An operator code is also given to specify which of eleven people conducted the test. The table also gives the average flow at 50 Pa of pressurization and the 4 Pa flow averaged over pressurization and depressuirzation. As of 9 September 1[illegible] eighty Blower Door tests had been made on this home.

The data from each Blower Door test is in the form of inside-outside pressure differences and a fan RPM for each pressure difference. The induced pressure differences are 12.5, 25, 37.5, 50 and 62.5 Pa, although on some days it was not possible to pressurize the house up to 62.5 Pa. The fan RPM are converted to flow rates (m^3/hr) using calibration formula [1].

The data from each test was read into a PET computer in the lab which calculated the flow rates and fit curves through the data points. Table (E2) depicts this process for test No. 2. For each test three curves are produced having the form

$$Q = C\Delta p^n \qquad \text{(E1)}$$

where

Q = flow coefficient ($m^3/hr\text{-}Pa^n$)
n = flow exponent

An equation of this form is found for the pressurization points alone, for the depressurization points and for both groups of points together. The PET also lists the calculated flow rate for each of the three curves at Δp = 4 and 50 Pa.

REFERENCES

[1] Gadsby, K.J., Linteris, G.T., Dutt, G.S., "The Blower Door," Report No. 127, Center for Energy and Environmental Studies, Princeton University, 1981.

Table E1 BRAT Files

Date	Operator	u (m/s)	$\hat{u}$ (1)	Outside Temperature (°C)	Wind Direction	Pressurization Flow Rate 50 Pa (2) (m^3/hr)	4 Pa (3)
8/21/79	K	--	--	--	--	3855	570
10/2/80	G A M	2.2	--	21.5	SSW	3755	617
10/7/80	M A	1.7	4	13.0	NNW	3765	589
10/8/80	A M	2.5	--	20.0	SW	4070	703
10/9/80	G A	2.5	6	18.0	N	3759	639
10/ 80	A G	1.0	4	17.0	SSW	3740	635
10/16/80	A M	1.9	2	15.0	SE	3674	640
10/22/80	M A H	2.5	7	14.5	NNW	3665	647
10/31/80	M G	2.7	8	14.2	W	3720	665
11/5/80	A M A M	4.0	8	11.0	NNW	3777	618
11/12/80	H C A	4.9	10	6.1	N	3698	619
11/26/80	A M	3.5	9	5.7	N	3922	553
12/3/80	M A	6.4	9	-2.1	NW	4251	642

(1) $\hat{u}$ recorded by U.S. Weather Service in Newark, N.J.

(2) Averaged over pressurization.

(3) Averaged over both pressurization and depressurization.

12/10/80	M A	1.8	4	5.4	NW	3802	707
12/17/80	A M	2.9	6	-4.4	N	3777	585
1/14/81	A D	0.7	1	-0.1	S	4422	791
1/22/81	M G	2.1	6	3.8	W	4550	787
1/29/81	M A	3.0	7	2.5	NNW	4448	759
2/5/81	M GA	2.3	6	-6.1	NW	4514	780
3/11/81	G A L	0.6	3	3.8	NW	4206	702
3/18/81	G J	3.7	9	-2.4	N	4332	709
3/26/81	A S	2.4	5	9.9	--	4374	733
4/2/81	G M	4.8	10	18.7	N	4396	715
4/8/81	A M	3.8	8	20.3	SW	4553	702
4/28/81	A A	2.7	5	21.6	WSW	4251	801
5/6/81	G A	1.4	5	18.5	--	4120	740
5/14/81	M A	0.4	3	15.0	NE	3778	672
5/20/81	A G	1.9	5	18.8	E	3856	716
5/27/81	A G	2.6	6	27.6	SW	4108	725
6/8/81	A G G	1.4	4	21.0	SSW	4049	722
6/18/81	M A	1.2	2	22.9	--	4001	735

7/2/81	A						
	A	2.5	7	21.7	ESE	4027	710
7/8/81	A						
	J	1.5	4	29.8	WNW	3975	701
7/17/81	A						
	A	1.3	3	25.4	SW	4132	756
7/28/81	A						
	A	1.7	4	21.8	ENE	4014	705
8/25/81	A						
	M	1.7	4	21.7	NW	4198	747
9/11/81	A						
	A	1.9	5	24.9	NW	4200	662

Table E2 Blower Door Data Treatment

Data Collected in the Field

	Pressurization	Depressurization
Δp	RPM	RPM
12.5	962	695
25	1402	1119
37.5	1810	1408
50	2211	1728
62.5	2512	2012

↓

P E T

↓

	Pressurization	Depressurization
Δp	Flow (m^3/hr)	Flow (m^3/hr)
12.5	1526	1327
25	2267	2399
37.5	3021	3082
50	3806	3951
62.5	4361	4725

Curve Fits

Pressurization	$Q = 280\ \Delta p^{.661}$	Q(4) = 701, Q(50) = 3724
Depressurization	$Q = 188\ \Delta p^{.779}$	Q(4) = 554, Q(50) = 3959
All points	$Q = 230\ \Delta p^{.720}$	Q(4) = 623, Q(50) = 3840

Appendix F

MIXING WITHIN THE TEST CHAMBER

During the discussion of the Lossnay experiments in chapter IX, we mentioned that if the air in the Test Chamber is poorly mixed, our infiltration measurement would be lower than the actual infiltration rate. To model the effect of internal mixing on tracer gas measurements of infiltration one may consider the Test Chamber to be two separate cells exchanging air with the outside at different rates. One cell has a large infiltration rate induced by the heat exchanger and the other has only minimal infiltration through the shell. The net infiltration rate is determined from the average tracer concentration of the two sections. Infiltration rates measured under these conditions will be lower than the actual rates. A development of this two cell model is presented below as an example of this effect.

Figure (F1) shows a sketch of the Test Chamber as two separate cells V_1 and V_2. Both V_1 and V_2 are equal to one-half the Test Chamber volume, i.e. $V_1=V_2=8.3m^3$. Considering the outside as a third cell with the subscript o, there are six separate air flows denoted by $\dot{V}_{ij}$. The subscript i refers to the cell from which the particular flow originates and j refers to the cell into which the flow enters. $\bar{c}_i$ denotes the concentration of tracer gas in the ith cell and $\bar{c}_o$ is assumed to be zero.

From the two cell model, one obtains two coupled differential equations in the concentrations $\bar{c}_1$ and $\bar{c}_2$,

$$\dot{\bar{c}}_1 = -(\dot{V}_{12}/V_1)\bar{c}_1 + (\dot{V}_{21}/V_1)\bar{c}_2 \qquad (F.1)$$

$$\dot{\bar{c}}_2 = (\dot{V}_{12}/V_2)\bar{c}_1 - (\dot{V}_{21}/V_2 + \dot{V}_{21}/V_2)\bar{c}_2 \qquad (F.2)$$

In writing these two equations, we have assumed that $\dot{V}_{01}=\dot{V}_{10}=0$, i.e. the top half V_1 exchanges no air with the outside. The exchange rate of the lower cell $\dot{V}_{20} = \dot{V}_{02}$ is the air flow induced by the heat exchanger. The magnitude of $\dot{V}_{12} = \dot{V}_{21}$ quantifies the amount of mixing between the two cells.

The purpose of this model is to show that the measured infiltration rate I can be significantly different from the actual rate $\dot{V}_{20}/V$. Of course, the model is only an approximation and requires several unknown inputs. First, we have assumed that V_1 and V_2 are equal to one-half the Test Chamber volume V. In fact, there are not two separate cells but a continuum of cells. The amount of mixing between the top and bottom cells is unknown and must also be input. The flow induced by the Lossnay is assumed to be $\dot{V}_{20}$=4.5 X/hr=75.0 m^3/hr.

By inputting several values of $\dot{V}_{12}=\dot{V}_{21}$, the measured infiltration rate can be calculated. The measured rate I is given by

$$I = -d\ \ln(\bar{c})/dt \qquad (F.3)$$

where

$$\bar{c} = (\bar{c}_1+\bar{c}_2)/2 \qquad (F.4)$$

The values of $\ln(\bar{c})$ from actual measurements show a linear decrease over time, thus we require the output of our model to show the same linearity. Several values of $\dot{V}_{12}$ were input and the concentration $\bar{c}$ was calculated. Initially the tracer concentrations are assumed to be 150 ppm in both V_1 and V_2. Values of $\dot{V}_{12}$ less than $\dot{V}_{20}$ exhibit noticable curvature in plots of $\ln(\bar{c})$ over the time of an infiltration measurement. Values of $\dot{V}_{12}$ greater than or equal to twice $\dot{V}_{20}$ result in a basically linear decrease in ln(c) over time.

For example, when $\dot{V}_{12}$=2 $\dot{V}_{20}$=150 m^3/hr, the solution of equations (F.3) and (F.4) is

$$\begin{pmatrix} c_1 \\ c_2 \end{pmatrix} = \begin{pmatrix} 167 \\ 130 \end{pmatrix} e^{-3.96t} + \begin{pmatrix} -16 \\ 20 \end{pmatrix} e^{-41.2t} \qquad \text{(F.5)}$$

The second term in this sum dies out very quickly compared to the first and thus the measured infiltration rate will be I=4.0 X/hr. Thus, there is a 0.5 X/hr or roughly 11% difference between the actual infiltration of 4.5 X/hr and the measured rate. As the value of $\dot{V}_{12}$ increases, the discrepancy between the measured and actual infiltration rate decreases. For $\dot{V}_{12}=4\times\dot{V}_{20}$=300 m^3/hr, the differen s 6%. At five times $\dot{V}_{20}$, the measured rate is 4% low.

This rcise shows that the measured infiltration rate can be lowe n the actual rate. During a tracer gas decay with the Los perating $\bar{c}_1$, $\bar{c}_2$ and $\bar{c}$ were monitored. As the model predict was consistently larger than $\bar{c}_2$. The fact that this differe ists shows that the internal mixing is not perfect

and that this could be a source of error in our determination of the efficieny of the Lossnay.

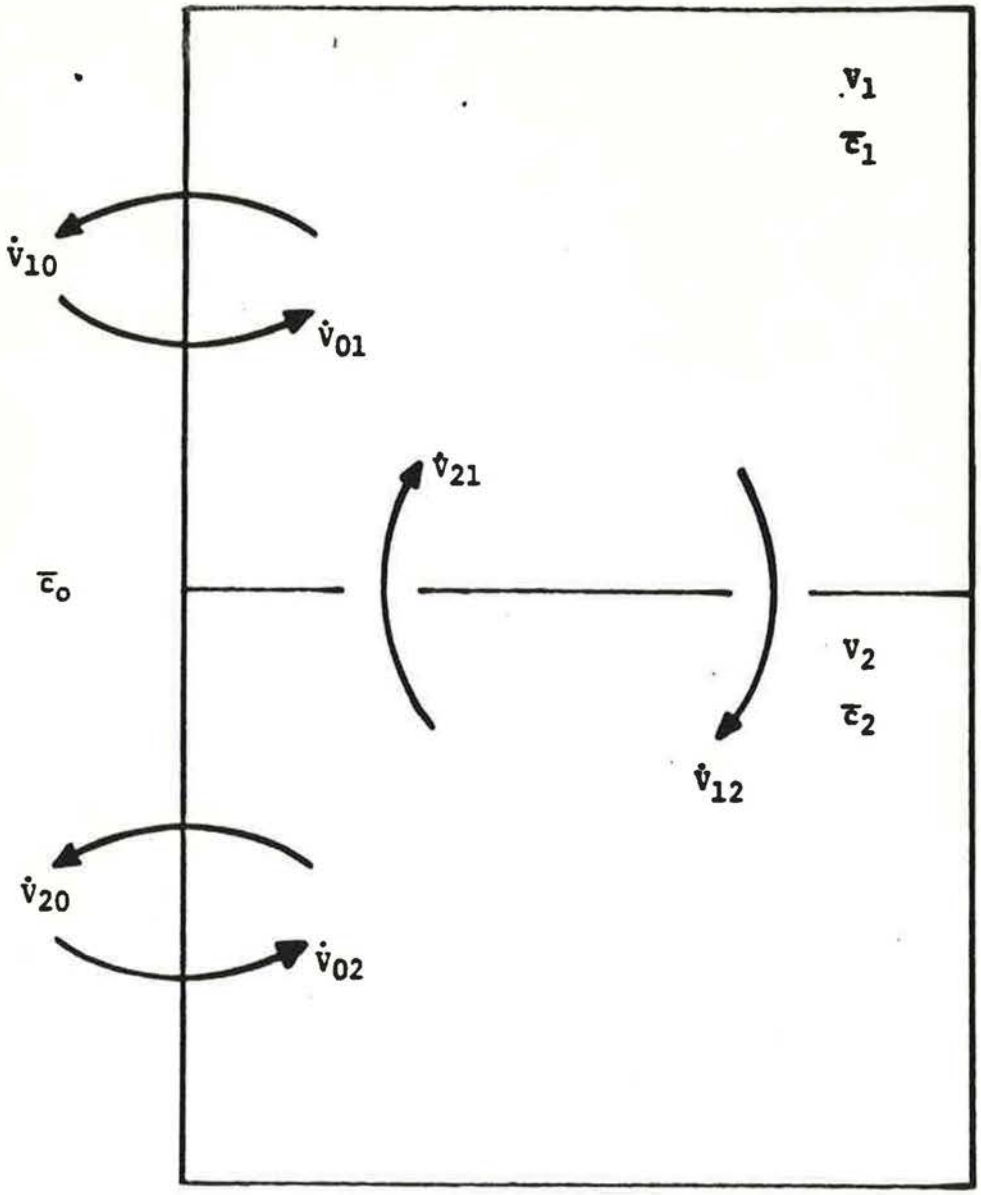

Figure F1 Two Cell Model of Mixing in the Test Chamber